NONLINEAR RESPONSE OF A PILE-SOIL-PILE INTERACTION MODEL TO A VERTICALLY INCIDENT WAVE

by

Hyung Suk Kim

A Dissertation Presented to the
FACULTY OF THE GRADUATE SCHOOL
UNIVERSITY OF SOUTHERN CALIFORNIA
In Partial Fulfillment of the
Requirements for the Degree
DOCTOR OF PHILOSOPHY
(CIVIL ENGINEERING)

May 2005

Acknowledgements

First of all, I sincerely appreciate the great guidance of my advisor, Prof. Mihailo Trifunac. He inspired and encouraged me to pursue career earthquake engineering and offered many valuable suggestions during my research and the preparation of this thesis. Without his supports this dissertation would not have been possible.

I am grateful to the committee members of my Defense and Qualifying exam, Prof. V. W. Lee, Prof. F. E. Udwadia, Prof. H. L. Wong, and Prof. L. C. Wellford. I want to thank Prof. M. I. Todorovska, who provided support and advice during my study, and I am grateful as well to my officemates Dr. G. Vlado and Dr. T. Y. Hao, who shared their memories and experiences over the years. I would also like to express thanks to the faculty and staff members of the Department of Civil Engineering at the University of Southern California and to all of my fellow graduate student friends for their concern and help during this work.

I especially wish to express my deep gratitude to my parents, sisters, and brothers for their unconditional love and support. Finally, I need to thank my beloved daughter Hyewon and wife Shinmin, who have unselfishly supported me for many years as I have pursued the goals of my career. I dedicate this dissertation to them.

Table of Contents

List of Tables

List of Figures

Abstract

A simple pile-soil-pile interaction model is presented to analyze the nonlinear response of the grouped piles to lateral movements. The model considers the nonlinear behavior of soil and gap formation at the soil-pile interface. The grouped pile effects are developed via friction force of the soil blocks located between piles. The proposed model is analyzed by solving differential equations using a fourth-order Runge-Kutta algorithm. Examples of the proposed model with different parameters are presented, and the energy flow and distribution during the response of the system are examined. Proportions of dissipated energy by nonlinear behavior of the soil near the piles and by the friction of soil blocks are presented for various conditions of the pile group and the input wave. The maximum displacement and bending moment of piles and gaps are computed for vertically propagating waves with different frequencies and velocities. In addition, the foundations with rigid mass that represent the building are analyzed to investigate the energy transferred into the super-structure for different geometries of the pile group, the number of piles, and the pile spacing ratio. It is shown that different responses of piles and amounts of transferred energy are generated in the system even though the same input energies transmitted into a foundation with same dimensions.

1. Introduction

1.1 General

The analysis of a laterally loaded single pile and pile groups has been the subject of considerable interest and research in foundation design for bridges, offshore structures, and machine foundations (Penzien et al., 1964; Matlock, 1970; O'Rourke and Dorby, 1979; Poulos and Davis, 1980; Kagawa and Kraft, 1980; Wolf and von Arx, 1982; Mylonakis et al., 1997; Ruesta and Townsend, 1997). When a pile foundation is subjected to ground excitation, it interacts with the surrounding soil. In addition, if piles in the grouped pile system are closely spaced, interactions between piles are generated because piles are connected via the soil and thus the movement of one pile contributes to the deflection of the others in group. These interactions (pile-soil-pile interactions) may change the motion of the ground and the response of the total foundation system.

This study presents a simple model of pile-soil-pile interaction for lateral response. The model includes the nonlinear behavior of the soil adjacent to the pile and creation of the gaps at the soil-pile interface. The *p*-multiplier has been commonly used in the analysis of pile groups. This method is based on the concept that the stiffness of the single pile is reduced in grouped pile foundations by modifying the single-pile p-y curve with a *p*-multiplier ($f_m < 1$) (Brown et al., 1988). However in this study, the grouped pile effects are directly developed via the interaction force of the soil blocks located between piles. The proposed model is analyzed by solving partial differential equations for the dynamic equilibrium equation of a grouped pile system, including the nonlinearity of the soil and pile group effects at the same time. The energy flow and its distribution

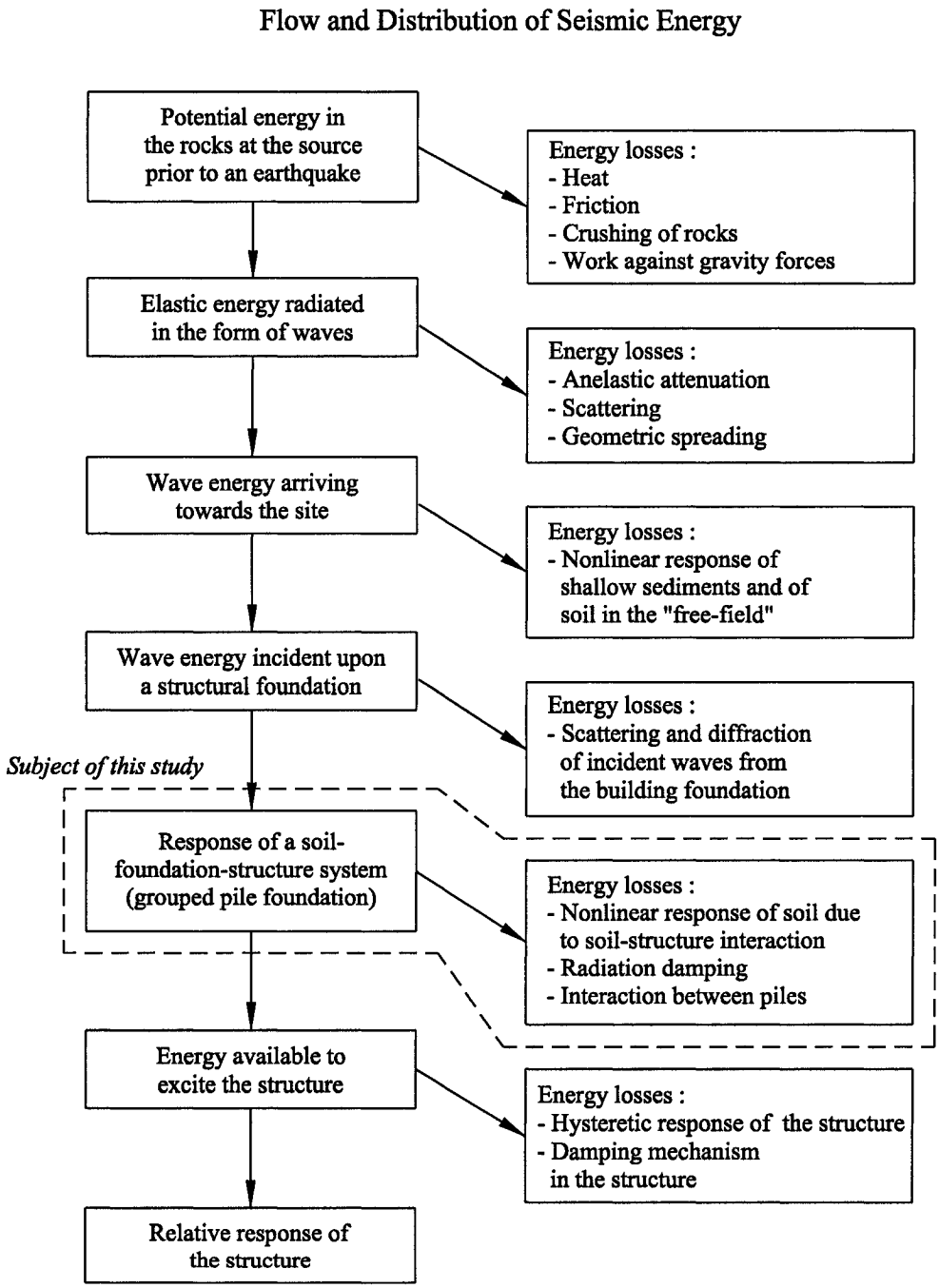

Fig. 1.1 An outline of principal stages in the flow of earthquake wave energy.

during the response of the foundation system are also analyzed using a vertically propagating wave.

Figure 1.1 outlines the principal stages in the flow of earthquake wave energy, from the earthquake source to a structure (Trifunac et al., 2001). This study focuses on the fifth stage, the energy flow and dissipation by the response of a soil-foundation-structure system. The pile-soil-pile system begins to respond when the incident earthquake waves propagate into the foundation. The transmitted incident wave energy is reduced by the nonlinear response of soil in the soil-pile interface (Luco et al., 1985; Todorovska and Trifunac, 1991; Trifunac et al., 1999, 2001) and by the interaction among piles. Figure 1.2 shows the problem under consideration. A pile foundation with a rigid pile cap is excited by a vertically incident wave. The wave propagates into the foundation system and induces the pile-soil-pile interaction.

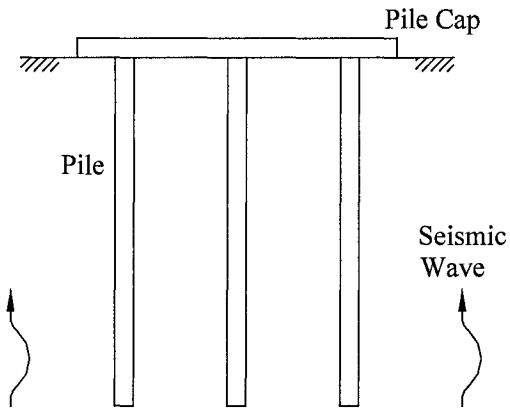

Fig. 1.2 Sketch of pile group in soil medium excited by a vertically incident wave.

1.2 Literature review

A number of numerical methods that can be used to analyze pile-soil-pile interaction have been developed in two ways: (1) approximate analysis based on the superposition of interaction factors where the interaction between piles is considered separately in forming the flexibility matrix of the entire group, and (2) direct analysis using techniques such as finite elements where all piles of the group are considered to interact at the same time.

Novak (1974) and Novak and Nogami (1977a, 1977b) considered a continuous model based on the Winkler assumption for the soil. They used a linear elastic model in which only horizontally propagating waves were considered in plane strain analysis. This work was extended by Novak and Aboul-Ella (1978a, 1978b) to the case of a layered medium. Novak and Sheta (1980) proposed including a cylindrical annulus of softer soil and inner weakened zone around the foundation in their plane strain analysis. Nonlinearity of soil, as well as the weakened bond and slippage, were presumed to be accounted for by a reduced shear modulus and increased material damping of the inner layer. This approach yields closed-form formulae for all vibration modes and is suitable for higher frequencies. However, the stiffness can be underestimated in the low frequency range because the soil stiffness approaches zero as the frequency tends toward zero. In this model, separation is not allowed between pile cylinder and soil medium.

Wolf and von Arx (1978, 1982) used numerical analysis to study the response of a large pile group for vertically and horizontally incident shear waves and Rayleigh waves. The soil was modeled with finite elements, and a transmitting boundary was

used to simulate the effects of the far field. This work was followed by Wass and Hartmann (1984).

The analytical methods used a linear soil model and showed that the response of the groups was frequency dependent. El Sharnouby and Novak (1985) described the static and low-frequency responses of a pile group. The method presented was to view the whole pile group with the soil as one composite continuum with conditions of equilibrium that were specified for a number of discrete points. Nogami (1985, 1988) presented a simple approach to analyzing the flexural vibration of a pile group in the frequency and time domains. In this approach, a pile group is replaced by a single pile for the evaluation of the pile-head flexibility matrix.

Han and Novak (1988) calculated the response of piles using the DYNA2 and PILAY2 computer codes and employed the theory of nonlinear vibration. They compared their results with dynamic experiments on large-scale models with horizontal and vertical vibrations. Novak and Han (1990) presented another approach using the program DYNA3, with a somewhat arbitrary reduction in shear modulus to account for nonlinear response. Their calculation of single pile stiffness and damping wasis based on the approach given in Novak and Aboul-Ella (1978). The interaction between two piles was used to formulate the group complex flexibility matrix from which the group stiffness and damping were deduced. An approximate account of nonlinearity can be taken by means of the weakened zone around the footing or pile by adjusting the values of soil shear modulus and internal damping according to the level of stress. The impedances of soil computed at $a_0 = 0.3$ were used over the entire frequency range from $a_0 = 0$ to $a_0 = 0.3$ due to the invalid value in the low frequency range. The dimensionless

frequency, a_0, was calculated by $a_0 = \omega d/V_s$, where ω, d, *and* V_s are excitation frequency, diameter of pile, and phase velocity, respectively.

Nogami (1992) accounted for the soil nonlinearity by introducing a multi-linear element for the inner field and a gap element to account for plastic deformation and gap opening at the pile-soil interface. He also accounted for the group effect and the wave propagation away from the pile by introducing a far field element. In aforementioned studies, integral formulation was solved as a boundary value problem involving Bessel functions with complex arguments.

Makris and Gazetas (1992, 1993) presented an approximate method based on a dynamic Winkler foundation method and a simplified wave interference analysis to account for pile-soil-pile interaction. They outlined a detailed multi-step procedure for a complete seismic soil-pile-foundation-structure interaction analysis. Makris (1994) presented a solution based on a dynamic Winker foundation model to compute the response of a solitary pile during the passage of a seismic Rayleigh wave and an oblique SH-wave. The impedance of soil was modeled with linear spring and dashpot.

El Naggar and Novak (1995, 1996) proposed a model of a pile for lateral response allowing for nonlinear soil behavior and discontinuity conditions at the pile-soil interface. They used the interaction coefficients to perform the group analysis using the superposition approach based on the model proposed by Gazetas and Dobry (1984a, 1984b, 1988). However, their model still led the complicated solution and underestimation of soil stiffness at low frequencies, in the range of practical interest.

Pender and Pranjoto (1996) considered a simple numerical model to monitor gap formation by pile head displacement and rotation. Wu and Finn (1997a, 1997b)

presented a quasi-three dimensional finite element method for nonlinear dynamic analysis of single piles and pile groups. This analysis was performed in the time domain and frequency domain using the computer program PILE-3D. To show the pile group effects, dynamic impedance of the pile group was normalized to the static stiffness of the pile group expressed as the stiffness of a single pile times the number of piles in the group. Mori and Hasegawa (2000) analyzed a pile-supported building using a hysteretic model that was able to consider the material nonlinearity of the soil, but the pile group was modeled as a single pile.

Ashour et al. analyzed the nonlinear behavior of an isolated pile (1998, 2002) and grouped piles (2004) based on the concept and assumptions of the strain wedge model for static lateral loading. By using the strain wedge model, the response parameters of a one-dimensional beam on an elastic foundation can be characterized in terms of three-dimensional soil-pile interaction behavior.

O'Neill and his colleague conducted a series of full-scale dynamic field tests as a point of reference with which to compare the results of numerical analyses (Dunnavant, 1986). Blaney and O'Neill (1983, 1986a, 1986b) used an instrumented steel pipe pile to compare measurements with a hysteretic subgrade reaction model. Brown, Reese, and O'Neill (1987, 1988) subjected a group of steel piles to cyclic lateral loading. They studied the nonlinear nature of the pile-soil-pile interaction by comparison with a test of an isolated single pile. Dunnavant and O'Neill (1989) used full-scale, cyclic, lateral load tests to investigate the effects of scale, including pile diameters, relative pile-soil stiffness, and the number of loading cycles on the p-y relationships.

Han and Vaziri (1992) also conducted dynamic experiments on a full-scale pile group subjected to lateral loading. They showed a reduction in stiffness and an increase in damping with increasing frequency. McVey et al. (1998) conducted centrifuge tests of a group of piles in sand. They presented p-y multipliers for laterally loaded pile groups based on experimental results. Curras et al. (2001) evaluated the BNWF(beam on a nonlinear Winkler foundation) analysis method against the recorded response of centrifuge experiments of pile-group-supported structures.

Trifunac et al. (2001) presented an alternative to the method of response spectrum in earthquake resistant design. They examined the flow of seismic energy from the earthquake source, along the propagation path, and the relative response of the structure. The method was verified by comparison with a model of buildings on rigid foundations that can experience nonlinear response.

1.3 Organization of this thesis

Chapter 2 deals with the presentation of the alternative pile-soil-pile interaction model. The proposed model is verified by comparison with dynamic compliance functions in previous studies. Examples of using the proposed model with different parameters are presented in Chapters 3 through 5. Chapter 3 presents properties of the soil and the pile and the characteristics of the propagating waves used in the examples. The transmitted energy by incident wave and the balance of all the energies associated with the response of the pile-soil-pile system are considered in Chapter 4. Proportions of dissipated energy by nonlinear behavior of the soil near the piles and by the friction of soil blocks located between piles for different pile-spacing ratios are presented. Chapter 5 describes the movements of piles when a vertically incident wave propagates into the system. The gaps caused by nonlinear behavior of the soil in soil-pile interface are computed for 6 x 6, 4 x 4, and 2 x 2 pile group systems. The maximum bending moment and total displacement of piles are also considered in this chapter. Finally, the grouped pile effects are investigated by analyzing the responses of different pile groups with the same dimensions. Chapter 6 presents a summary and conclusions of this study.

2. Dynamic pile-soil-pile interaction model

This chapter presents the dynamic pile-soil-pile interaction model and the derivation of energy equations. To model the behavior of piles embedded in a nonlinear layer of soil, the soil and pile are divided into segments. The soil around the pile shaft is divided into two different parts - the near-field element and the soil block. The near-field element, surrounding the pile shaft, models the nonlinear soil-pile interaction. Two components, spring and dashpot, are included in the element. The soil block models the grouped pile effect by the behavior of the soil that is located between piles. It accounts for the behavior of the soil outside the near-field element, which is the region of strong nonlinear behavior. Figure 2.1 shows the *i*th layer of the pile-soil-pile interaction model, which has three piles in the grouped pile system. Figure 2.2 shows the complete model, and the deformed shape from a vertically incident wave is illustrated in Figure 2.3.

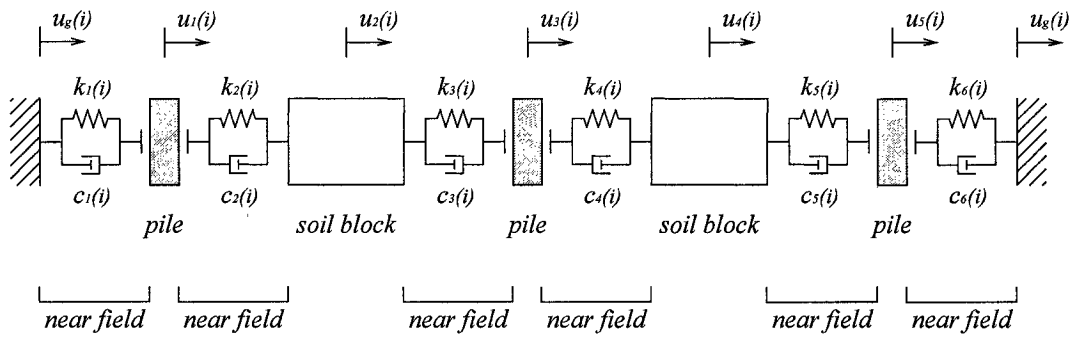

Fig. 2.1 Pile-soil-pile interaction model of *i*th layer.

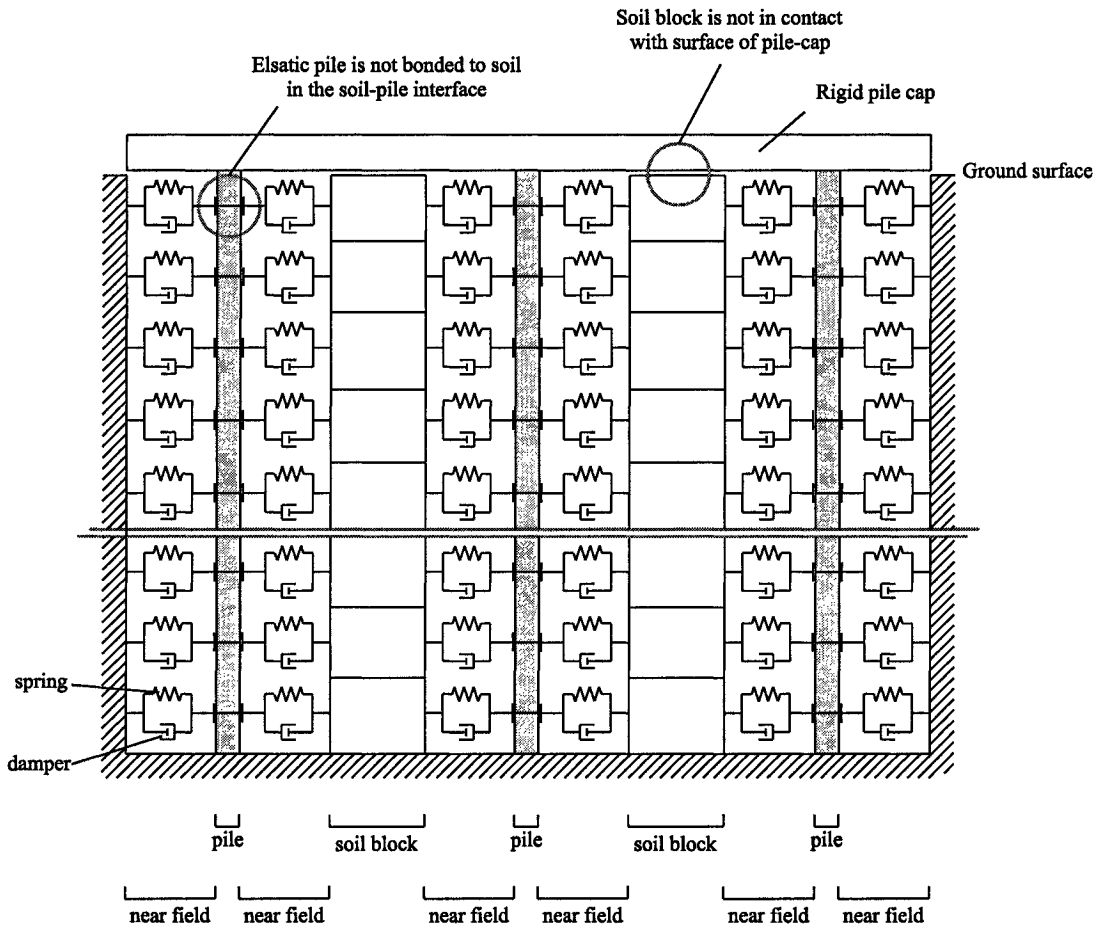

Fig. 2.2 Total system of proposed model.

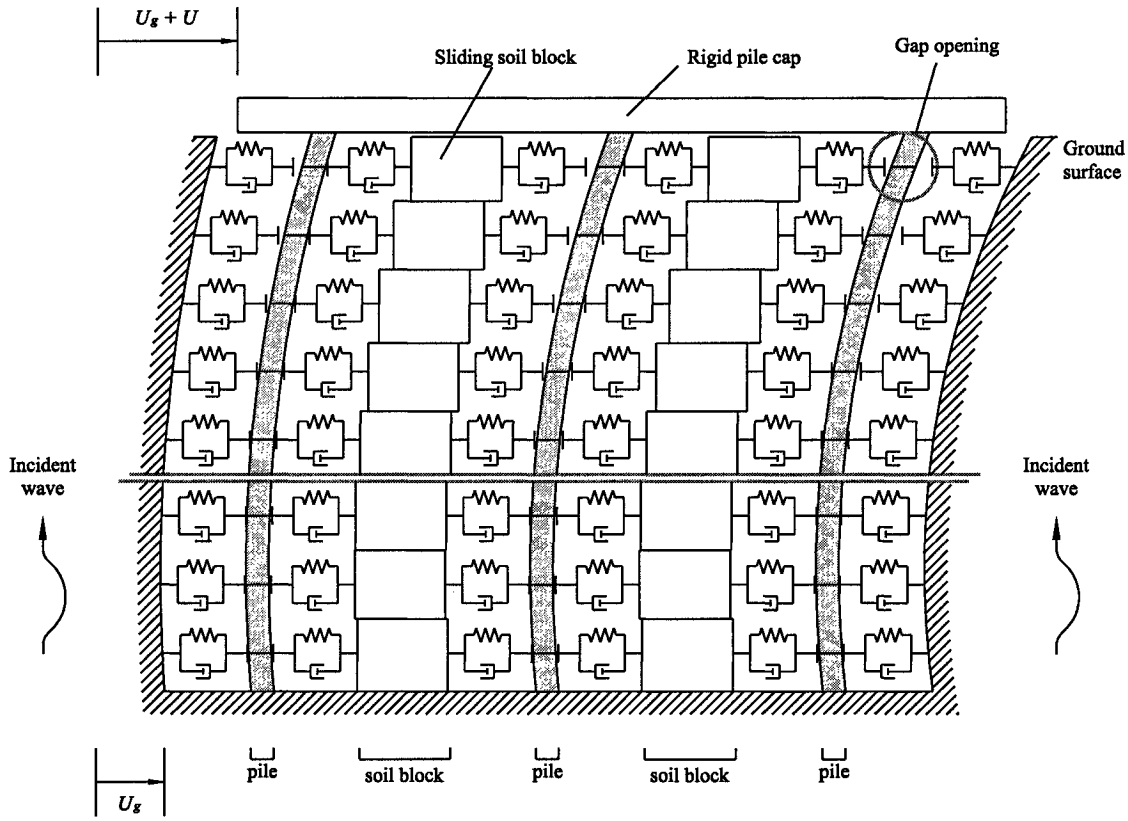

Fig. 2.3 Deformed shape of system from incident wave.

2.1 Pile

Piles are modeled as elastic Bernoulli-Euler beams and attached to soil medium. Vertical displacements are neglected, and pile-soil contact is assumed to be frictionless. The differential equation for the problem of the laterally loaded pile is governed by

$$E_p I_p \frac{\partial^4 u}{\partial z^4} + m_p \ddot{u} + P = 0, \tag{2.1}$$

where

$E_p I_p =$ bending stiffness of the pile

$u =$ lateral displacement of the pile

$\ddot{u} =$ lateral acceleration of the pile

$m_p =$ mass of the pile per unit length

$P =$ soil-pile interaction force

$z =$ distance along the pile (measured from the pile tip).

Equation (2.1) is solved numerically by discretizing the pile and the layered soil. The pile is subdivided into a number of elements, and every element is assumed to have a constant cross section (El Naggar and Novak, 1995). The spatial part of the nonlinear partial-differential equations is reduced to a set of ordinary-differential equations in time and then integrated in time using a fourth-order Runge-Kutta algorithm. The corresponding derivatives of u are represented by

$$\left.\frac{\partial^4 u}{\partial z^4}\right|_i = \frac{u_{i+2} - 4u_{i+1} + 6u_i - 4u_{i-1} + u_{i-2}}{\Delta z^4}, \qquad (2.2)$$

where u_i is a displacement of the pile at point i and Δz is an interval between two consecutive points, i, along the pile. Figure 2.4 shows the arrangement of the discretization points. The values u_1, u_2, u_{nx+3}, and u_{nx+4} are the auxiliary values.

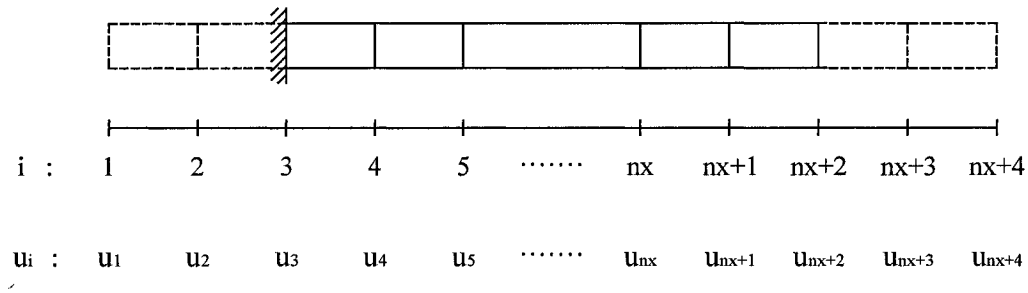

Fig. 2.4 Discretization of the pile element.

It is assumed that the pile is simply supported at the tip ($z = -L_p$) and fixed at the pile cap ($z = 0$). Piles are moving simultaneously with the movements of the incident wave at the tip and of the rigid pile cap at the top.

2.2 Soil model

The soil model is divided into two parts. The first part of the soil is the "near-field element", which accounts for the nonlinearity of the soil adjacent to the pile. Two separate components, spring and dashpot, model the behavior of soil in the near field of the system. The second part of soil is the "soil block" that accounts for the effects of soil movement within a group of piles. The frictional force is generated as the soil blocks move each other, and this force resists the motion induced by the spring force and the damping force of the soil in the near field.

2.2.1 Near-field element

The soil adjacent to a pile is modeled by springs, k, and dashpots, c. Vesic (1961) investigated the problem of infinite beam on an elastic foundation by comparing the results from numerical and approximate analyses with those obtained by means of subgrade reaction theory (Appendix A). Equation (2.3) presents the relationship between the stiffness of the soil and the soil characteristics, the flexural rigidity, and the diameter of the pile:

$$k_{initial} = \left(\frac{0.65}{d_p}\right) \cdot \sqrt[12]{\frac{E_s d^2}{E_p I_p}} \cdot \left(\frac{E_s}{1-\upsilon_s^{\,2}}\right), \tag{2.3}$$

where

$k_{initial}$ = initial stiffness of the soil

E_s = Young's modulus of the soil

E_p = Young's modulus of the pile

d_p = pile diameter

I_p = moment of inertia of pile section

υ_s = Poisson's ratio of the soil.

The dashpots model the energy loss due to hysteretic dissipation. The damping coefficient of the soil used in this model is shown in equation (2.4). The material damping of the soil is modeled in terms of the stiffness ($k_{initial}$) and the damping factor ratio of the soil (β_s):

$$c = \beta_s \cdot k_{initial}, \tag{2.4}$$

where

c = damping coefficients of the soil

$k_{initial}$ = initial stiffness of the soil

β_s = damping factor of the soil.

Under heavy cyclic loading, a pile embedded in cohesive soil can be separated from the surrounding soil, which may lead to a reduction in the lateral stiffness of the pile. Trifunac et al. (2001) suggested that a hysteretic slip model can simulate nonlinear behavior of the soil based on full-scale tests of a structure by Ivanović et al. (2000) and Trifunac et al. (2001a, b, c). This model leads to a separation, which is caused by soil compression. The gap between the pile shaft and the soil is modeled using an elastoplastic load-deflection curve (p-y curve), as shown in Figure 2.5. It is assumed

that the soil does not support tension. P_U is the ultimate resistance of the soil calculated using the standard relations given by the American Petroleum Institute (1991). The equations for the ultimate resistance of the soil are presented in Appendix A.

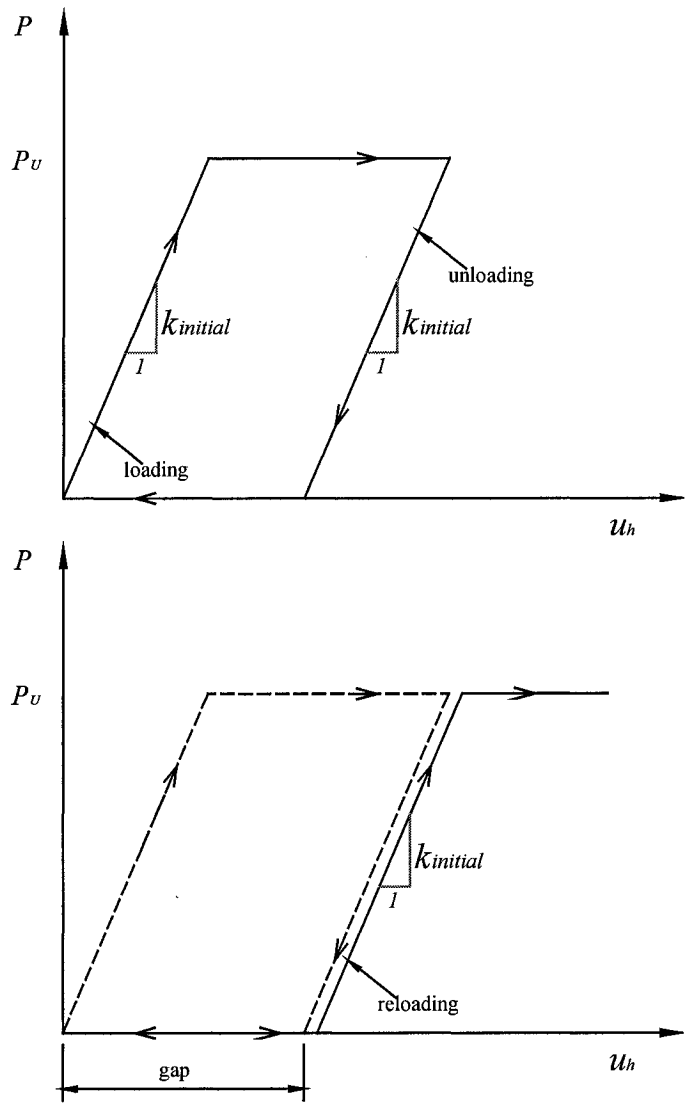

Fig. 2.5 Determination of gap using nonlinear p-y curve.

2.2.2 Soil block

The soil behavior between piles is modeled using sliding soil blocks. The "sliding block" concept was first proposed by Newmark (1965) to estimate the permanent displacement of slopes in earth structures under seismic loading. It was applied to embankments, dams, and retaining walls (Chopra et al., 1992; Gazetas et al., 1994; Cai et al., 1996; Rathje et al., 2000; Zeng et al., 2000). The presence of Coulomb friction at the interface of soil blocks yields a nonlinear response of the system to the forcing functions (Pratt and Williams, 1981). In the sliding block theory, soil is assumed to be rigid-plastic and sliding along a prescribed planer failure surface. If the forces transmitted into the soil block exceed the Coulomb friction, the soil block will start to move (Hundal, 1979; Westermo et al., 1983; Shaw, 1986). This representation is adopted in this model to account for the shear resistance of the soil between piles.

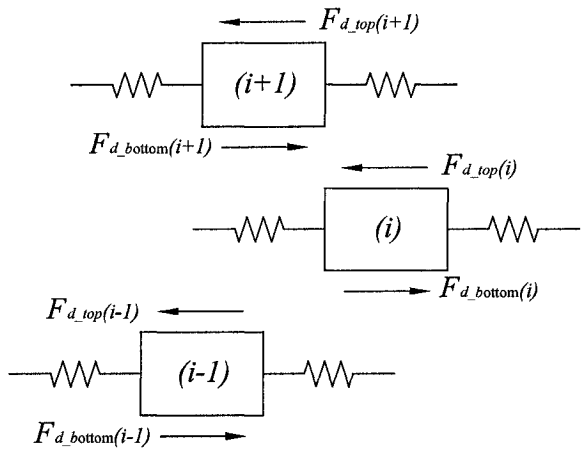

Fig. 2.6 Sliding soil blocks.

Figure 2.6 shows the sliding soil blocks in the (i-1)th, ith, and (i+1)th layer with friction force at the top surface and the bottom surface. The friction forces at the top and bottom surfaces of ith soil block are shown in equations (2.5) and (2.6), and the total friction force is calculated as the sum of the forces at both surfaces, as shown in equation (2.7):

$$F_{d\_top}(i) = \mu \cdot N_{top}(i), \quad \dot{u}(i) > \dot{u}(i+1) \tag{2.5}$$

$$F_{d\_top}(i) = -\mu \cdot N_{top}(i), \quad \dot{u}(i) < \dot{u}(i+1)$$

$$F_{d\_bottom}(i) = \mu \cdot N_{bottom}(i), \quad \dot{u}(i) > \dot{u}(i-1) \tag{2.6}$$

$$F_{d\_bottom}(i) = -\mu \cdot N_{bottom}(i), \quad \dot{u}(i) < \dot{u}(i-1)$$

$$F_d(i) = F_{d\_top}(i) + F_{d\_bottom}(i) \tag{2.7}$$

where

$F_d(i)$ = total friction force of the ith soil block

$F_{d\_top}(i)$ = friction force at the top surface of the ith soil block

$F_{d\_bottom}(i)$ = friction force at the bottom surface of the ith soil block

$\dot{u}(i)$ = velocity of the ith soil block

$\dot{u}(i-1)$ = velocity of the $(i-1)$th soil block

$\dot{u}(i+1)$ = velocity of the $(i+1)$th soil block

μ = friction coefficient of the soil

N_{top} = normal force on the top contact surface

N_{bottom} = normal force on the bottom contact surface.

$N_{top}(i)$ is determined as the sum of the total normal forces of soil blocks above the *i*th soil block. $N_{bottom}(i)$ is calculated as the sum of $N_{top}(i)$ and the normal force of the *i*th soil block. Figure 2.7 shows the plan view of the friction area of soil blocks, which is emphasized by shading. The angle α is determined by $\alpha = \phi/2$, where is ϕ the friction angle of the soil.

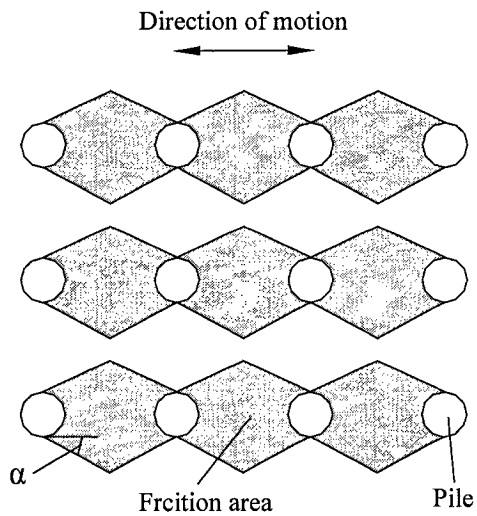

Fig. 2.7 Friction area of soil blocks.

2.3 Equations of motion

Next, we derive the equations of motion of the pile-soil-pile system for horizontal excitation. The scope of this study is limited to the consideration of only vertically incident waves. The general excitation and response of a foundation subjected to a non-vertically incident wave are also presented briefly.

2.3.1 Horizontal excitation and response

Figure 2.8 shows the free-body diagram of a typical element of the deformed model for $u_{i,j}$ and $u_{i,j+1}$, which are relative displacements of a pile and a soil block. The derivation of dynamic equilibrium equations uses the forces shown in Figure 2.8. Equation (2.8) shows the equilibrium equation of the horizontal motion for typical elements of a pile (i, j) and a soil block $(i, j+1)$.

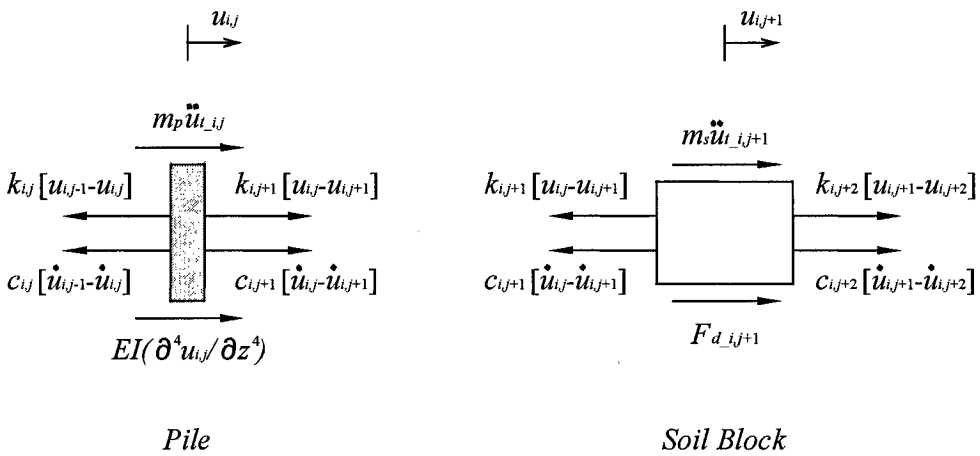

Fig. 2.8 Free-body diagram of the deformed model.

$$E_p I_p \frac{\partial^4 u_{i,j}}{\partial z^4} + m_p \ddot{u}_{t\_i,j} + \left[-c_{i,j}\dot{u}_{i,j-1} + (c_{i,j} + c_{i,j+1})\dot{u}_{i,j} - c_{i,j+1}\dot{u}_{i,j+1}\right] + \left[-k_{i,j}u_{i,j-1} + (k_{i,j} + k_{i,j+1})u_{i,j} - k_{i,j+1}u_{i,j+1}\right] = 0$$

$$m_s \ddot{u}_{t\_i,j+1} + \left[-c_{i,j+1}\dot{u}_{i,j} + (c_{i,j+1} + c_{i,j+2})\dot{u}_{i,j+1} - c_{i,j+2}\dot{u}_{i,j+2}\right] + \left[-k_{i,j+1}u_{i,j} + (k_{i,j+1} + k_{i,j+2})u_{i,j+1} - k_{i,j+2}u_{i,j+2}\right] + F_{d\_i,j+1} = 0' \quad (2.8)$$

where

$u_{t\_i,j} = u_{i,j} + u_{i,g}$

$u_{t\_i,j}$ = absolute displacement

$u_{i,i}$ = relative displacement

$u_{i,g}$ = ground displacement

$E_p I_p$ = flexural rigidity of pile

m_p = mass of pile

m_s = mass of soil

$k_{i,j}$ = stiffness of soil in the near field

$c_{i,j}$ = damping coefficient of soil in the near field

$F_{d\_i,j}$ = friction force of soil block located between piles.

Equation (2.9) shows the dynamic equilibrium equation of motion in the horizontal direction for the pile-soil-pile system in matrix form.

$$+\begin{bmatrix} m_p & 0 & 0 & \cdots & 0 & 0 \\ 0 & m_s & 0 & \cdots & 0 & 0 \\ 0 & 0 & m_p & \cdots & 0 & 0 \\ \vdots & \vdots & \vdots & \ddots & \vdots & \vdots \\ 0 & 0 & 0 & \cdots & m_s & 0 \\ 0 & 0 & 0 & \cdots & 0 & m_p \end{bmatrix} \begin{bmatrix} \ddot{u}_{t\_i,1} \\ \ddot{u}_{t\_i,2} \\ \ddot{u}_{t\_i,3} \\ \vdots \\ \ddot{u}_{t\_i,m-1} \\ \ddot{u}_{t\_i,m} \end{bmatrix}$$

$$+\begin{bmatrix} c_{i,1}+c_{i,2} & -c_{i,2} & 0 & \cdots & 0 & 0 \\ -c_{i,2} & c_{i,2}+c_{i,3} & -c_{i,3} & \cdots & 0 & 0 \\ 0 & -c_{i,3} & c_{i,3}+c_{i,4} & \cdots & 0 & 0 \\ \vdots & \vdots & \vdots & \ddots & \vdots & \vdots \\ 0 & 0 & 0 & \cdots & c_{i,m-1}+c_{i,m} & -c_{i,m} \\ 0 & 0 & 0 & \cdots & -c_{i,m} & c_{i,N}+c_{i,m+1} \end{bmatrix} \begin{bmatrix} \dot{u}_{i,1} \\ \dot{u}_{i,2} \\ \dot{u}_{i,3} \\ \vdots \\ \dot{u}_{i,m-1} \\ \dot{u}_{i,m} \end{bmatrix}$$

$$+\begin{bmatrix} k_{i,1}+k_{i,2} & -k_{i,2} & 0 & \cdots & 0 & 0 \\ -k_{i,2} & k_{i,2}+k_{i,3} & -k_{i,3} & \cdots & 0 & 0 \\ 0 & -k_{i,3} & k_{i,3}+k_{i,4} & \cdots & 0 & 0 \\ \vdots & \vdots & \vdots & \ddots & \vdots & \vdots \\ 0 & 0 & 0 & \cdots & k_{i,m-1}+k_{i,m} & -k_{i,m} \\ 0 & 0 & 0 & \cdots & -k_{i,m} & k_{i,m}+k_{i,m+1} \end{bmatrix} \begin{bmatrix} u_{i,1} \\ u_{i,2} \\ u_{i,3} \\ \vdots \\ u_{i,m-1} \\ u_{i,m} \end{bmatrix}$$

$$+ EI\begin{bmatrix} \partial^4 u_{i,1}/\partial z^4 \\ 0 \\ \partial^4 u_{i,3}/\partial z^4 \\ \vdots \\ 0 \\ \partial^4 u_{i,m}/\partial z^4 \end{bmatrix} + \begin{bmatrix} 0 \\ F_{d\_i,2} \\ 0 \\ \vdots \\ F_{d\_i,m-1} \\ 0 \end{bmatrix} = \begin{bmatrix} 0 \\ 0 \\ 0 \\ \vdots \\ 0 \\ 0 \end{bmatrix}.$$

(2.9)

2.3.2. General excitation and response

When the vertically incident waves excite a flat foundation on the ground surface, the foundation input motion $\{u_0\}$, corresponds to the free-field motion. However, in the case of an embedded foundation subjected to a non-vertically incident wave, the horizontal, vertical, and rotational motions are all present in the foundation motion. This motion is different from the free-field motion because the presence of the foundation modifies the free-field ground motion through diffracted and scattered waves. The differences between the above two cases are larger for short incident waves and for more deeply embedded foundations (Luco et al., 1975; Avilés et al., 2002).

Figure 2.9 shows the deformed shape of a pile foundation system considering horizontal, vertical, and rocking motions. The pile foundation is supposed to be located inside the "rigid massless box". The box is moving in the horizontal and vertical directions and rotating without deformation because the length of the input wave is assumed to be long (low-frequency wave). This figure shows the resultant forces inside the "box" $\{F_b\}$, acting at the point O' and the absolute displacements of the foundation $\{u_c\}$, which can be described as

$$\{F_b\} = \left[F_z^b,\ F_x^b,\ M_o^b\right]^T \tag{2.10}$$

$$\{u_c\} = \{u_b\} + \{u_0\} \tag{2.11}$$

$$\{u_c\} = \left[v_c,\ u_c,\ \phi_c\right]^T \tag{2.12}$$

$$\{u_b\} = \left[v_b,\ u_b,\ \phi_b\right]^T \tag{2.13}$$

$$\{u_0\} = \left[v_0,\ u_0,\ \phi_0\right]^T, \tag{2.14}$$

where

$\{u_c\}$= absolute displacement of the foundation

$\{u_b\}$= relative displacement of the foundation due to $\{F_b\}$

$\{u_0\}$= input motion of the foundation.

The resulting input motion, $\{u_0\}$, consists of the horizontal and vertical displacements u_0 and v_0 at the center of the base, respectively, and the rocking motion ϕ_0 about the transverse axis relative to the radial direction of the earthquake. The relative displacement vector of the foundation is given by

$$\{u_b\} = [C(\omega)] \cdot \{F_b\}, \tag{2.15}$$

where

$$[C(\omega)] = \begin{bmatrix} C_{VV}(\omega) & C_{VH}(\omega) & C_{VM}(\omega) \\ C_{HV}(\omega) & C_{HH}(\omega) & C_{HM}(\omega) \\ C_{MV}(\omega) & C_{MH}(\omega) & C_{MM}(\omega) \end{bmatrix} \tag{2.16}$$

is the compliance matrix of the foundation.

Figure 2.10 (a), (b), and (c) show the deformed shape of the pile foundation and the displacement of a typical element (*i, j*). The positions of the element are denoted as *(1)*, *(2)*, and *(3)* in this figure. The element moves from (1) to (2) due to the rigid body motion of the box (Figure 2.10 b and c). It is then deformed to (3) from (2) by the force

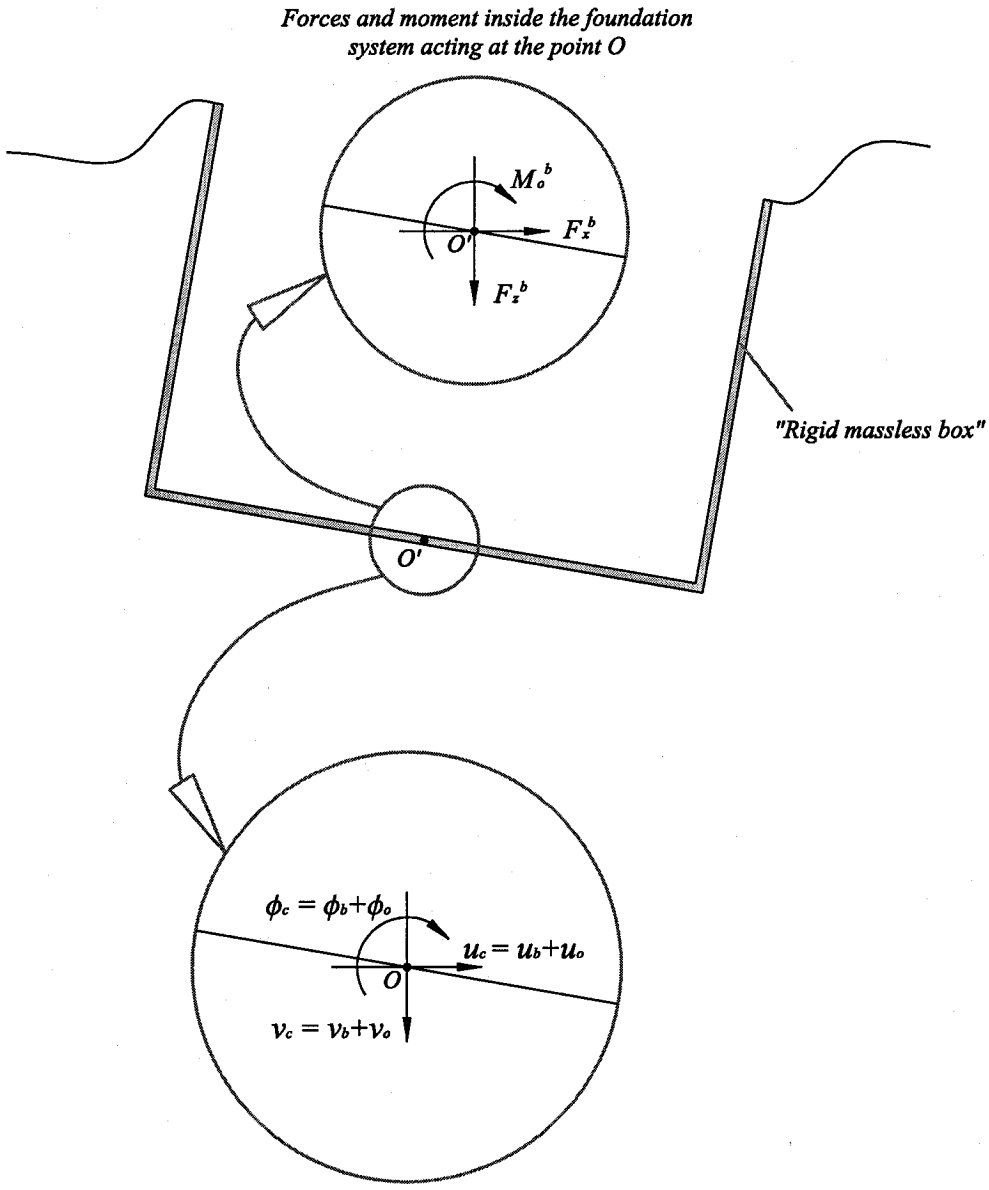

Fig. 2.9 Deformed shape of a pile foundation system.

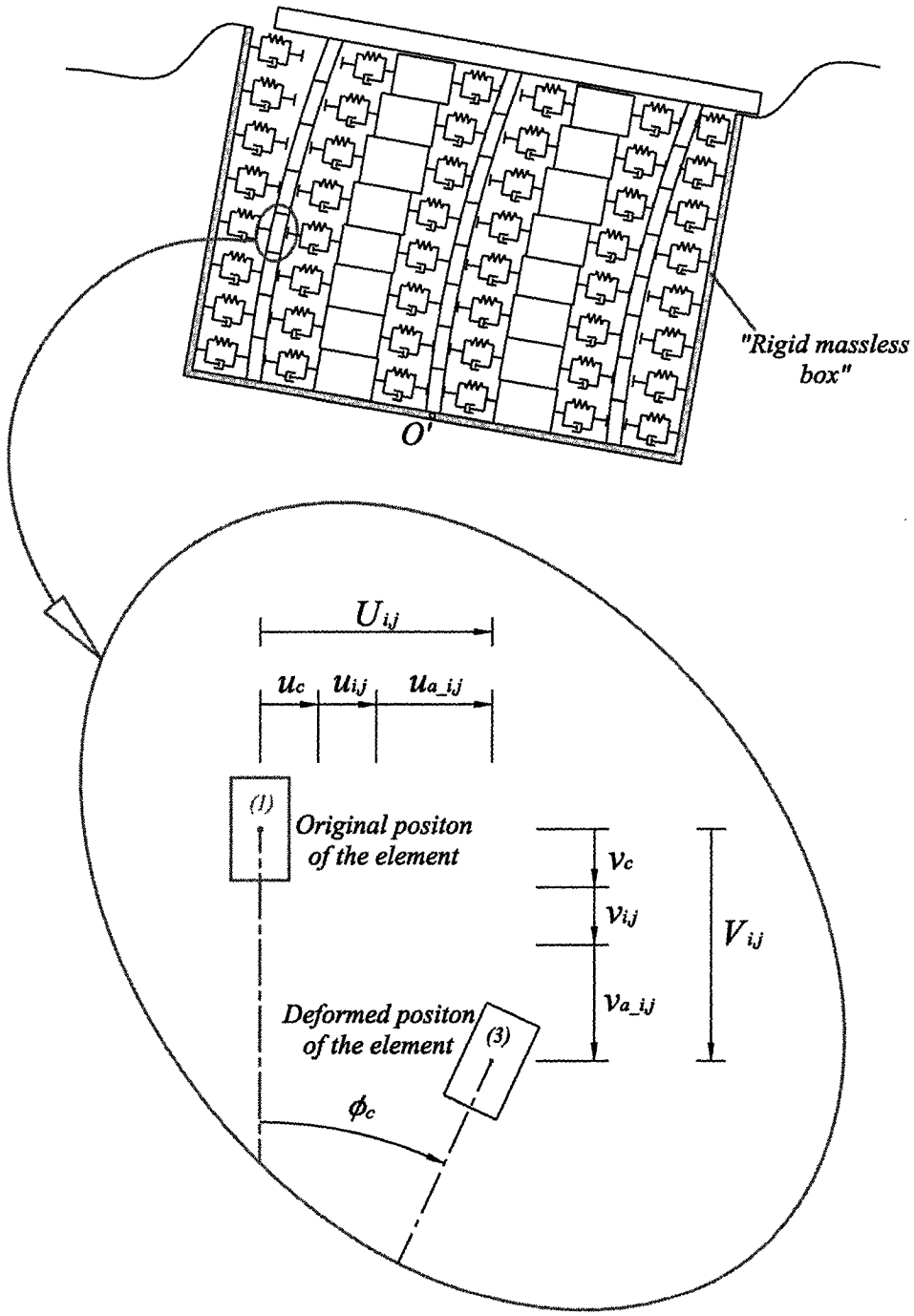

Fig. 2.10 (a) Deformed shape of the pile foundation and a typical element (*i, j*).

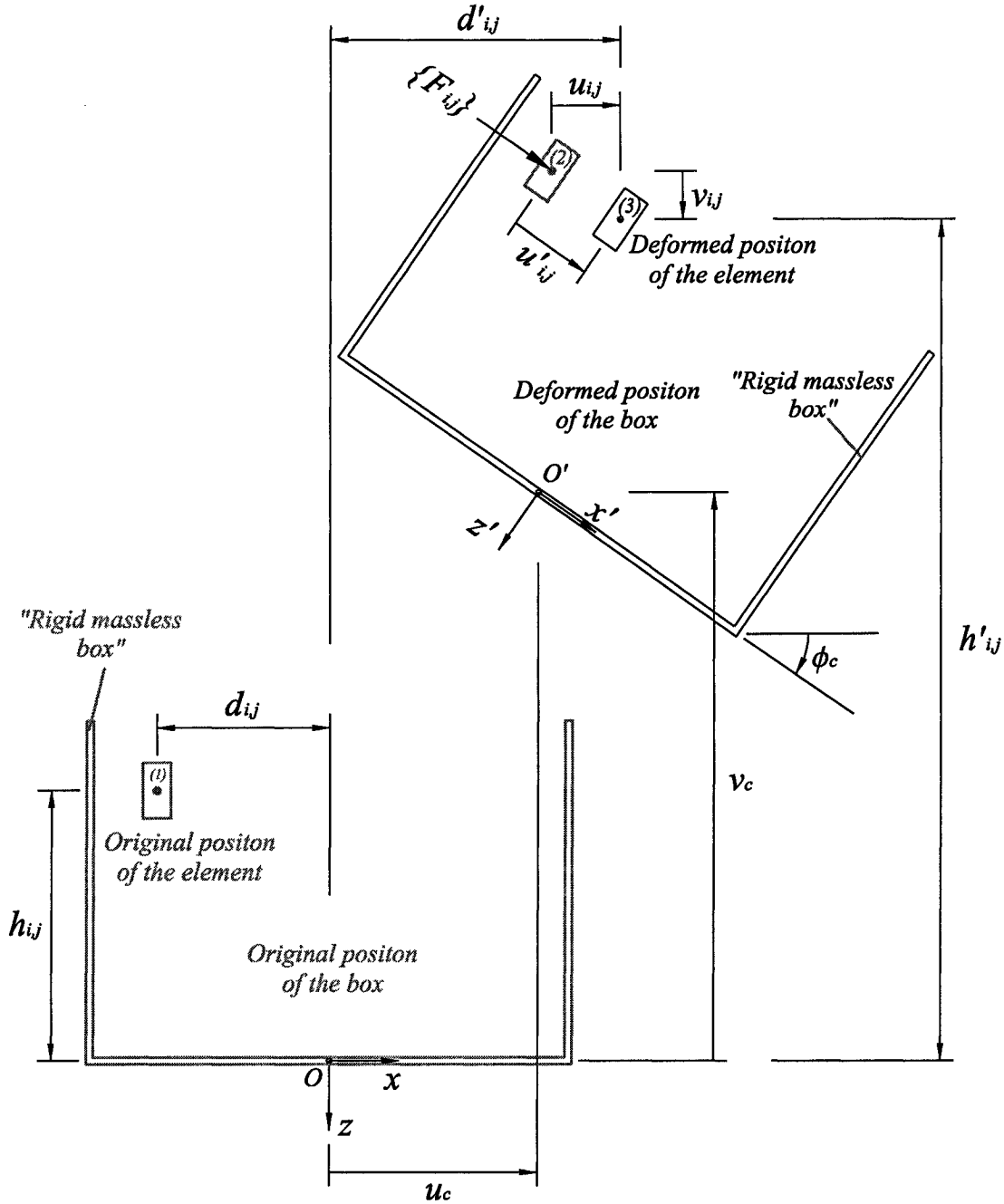

Fig. 2.10 (b) Deformed shape of the pile foundation and a typical element (*i, j*).

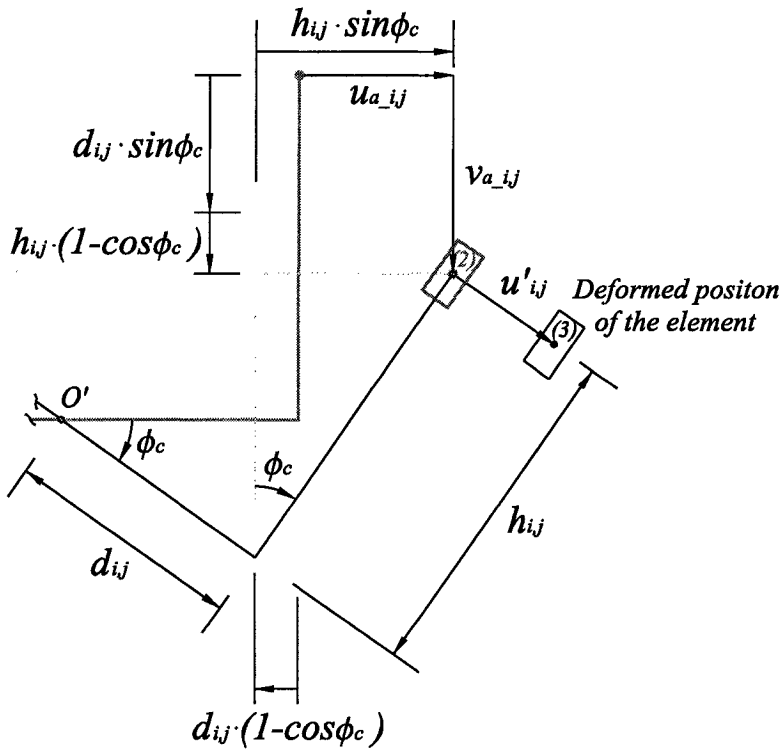

Displacement of the element due to rotation of the box

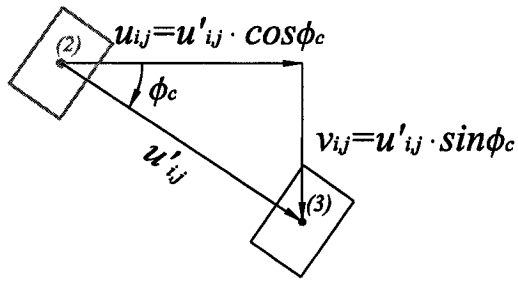

Relative displacement of the element respect to the box

Fig. 2.10 (c) Deformed shape of the pile foundation and a typical element (*i, j*).

$\{F_{b\_i,j}\}$ acting on the element. The displacements of the element shown in the figure are follows:

$$V_{i,j} = v_c + v_{i,j} + v_{a\_i,j} \tag{2.17}$$

$$U_{i,j} = u_c + u_{i,j} + u_{a\_i,j} \tag{2.18}$$

$$v_{i,j} = u'_{i,j} \cdot \sin\phi_c \tag{2.19}$$

$$u_{i,j} = u'_{i,j} \cdot \cos\phi_c \tag{2.20}$$

$$\ddot{V}_{i,j} = \ddot{v}_c + \ddot{v}_{i,j} + \ddot{v}_{a\_i,j} \tag{2.21}$$

$$\ddot{U}_{i,j} = \ddot{u}_c + \ddot{u}_{i,j} + \ddot{u}_{a\_i,j} \tag{2.22}$$

$$\ddot{v}_{i,j} = \ddot{u}'_{i,j} \cdot \sin\phi_c + \dot{u}'_{i,j} \cdot (2\dot{\phi}_c \cos\phi_c) + u'_{i,j} \cdot (\ddot{\phi}_c \cos\phi_c - \dot{\phi}_c^2 \sin\phi_c) \tag{2.23}$$

$$\ddot{u}_{i,j} = \ddot{u}'_{i,j} \cdot \cos\phi_c - \dot{u}'_{i,j} \cdot (2\dot{\phi}_c \sin\phi_c) - u'_{i,j} \cdot (\ddot{\phi}_c \sin\phi_c + \dot{\phi}_c^2 \cos\phi_c), \tag{2.24}$$

where

$V_{i,j}$ = total displacement of the element (i, j) in z direction

$U_{i,j}$ = total displacement of the element (i, j) in x direction

$u'_{i,j}$ = relative displacements with respect to the box in x' direction

due to forces $\{F_{i,j}\}$ acting on the element (i, j)

$v_{i,j}$ = z component of the relative displacement $u'_{i,j}$

$u_{i,j}$ = x component of the relative displacement $u'_{i,j}$

$v_{a\_i,j}$ = displacement in z direction due to rotation of the box (ϕ_c)

$u_{a\_i,j}$ = displacement in x direction due to rotation of the box (ϕ_c).

The displacements in the horizontal direction (x direction) and in the vertical direction (z direction) due to rotation of the box (ϕ_c) are

$$u_{a\_i,j} = h_{i,j} \cdot \sin\phi_c - d_{i,j} \cdot (1 - \cos\phi_c) \tag{2.25}$$

$$v_{a\_i,j} = h_{i,j} \cdot (1 - \cos\phi_c) + d_{i,j} \cdot \sin\phi_c \tag{2.26}$$

$$\ddot{u}_{a\_i,j} = h_{i,j} \cdot \left(\ddot{\phi}_c \cos\phi_c - \dot{\phi}_c^2 \sin\phi_c\right) - d_{i,j} \cdot \left(\ddot{\phi}_c \sin\phi_c + \dot{\phi}_c^2 \cos\phi_c\right) \tag{2.27}$$

$$\ddot{v}_{a\_i,j} = h_{i,j} \cdot \left(\ddot{\phi}_c \sin\phi_c + \dot{\phi}_c^2 \cos\phi_c\right) + d_{i,j} \cdot \left(\ddot{\phi}_c \cos\phi_c - \dot{\phi}_c^2 \sin\phi_c\right), \tag{2.28}$$

where $d_{i,j}$, $h_{i,j}$ are the distances from the reference point O to the original position of the element in the horizontal and vertical directions, respectively.

The equations of motion for the foundation then are derived for the typical elements of a pile (i, j) and a soil block (i, j+1). Figure 2.11 shows the free-body diagrams of the deformed pile and the soil block elements. The figure includes all horizontal (x-direction) and vertical (z-direction) forces and all of the moments. The axial-deformations of the pile and of the soil block are assumed to be small and will not be considered.

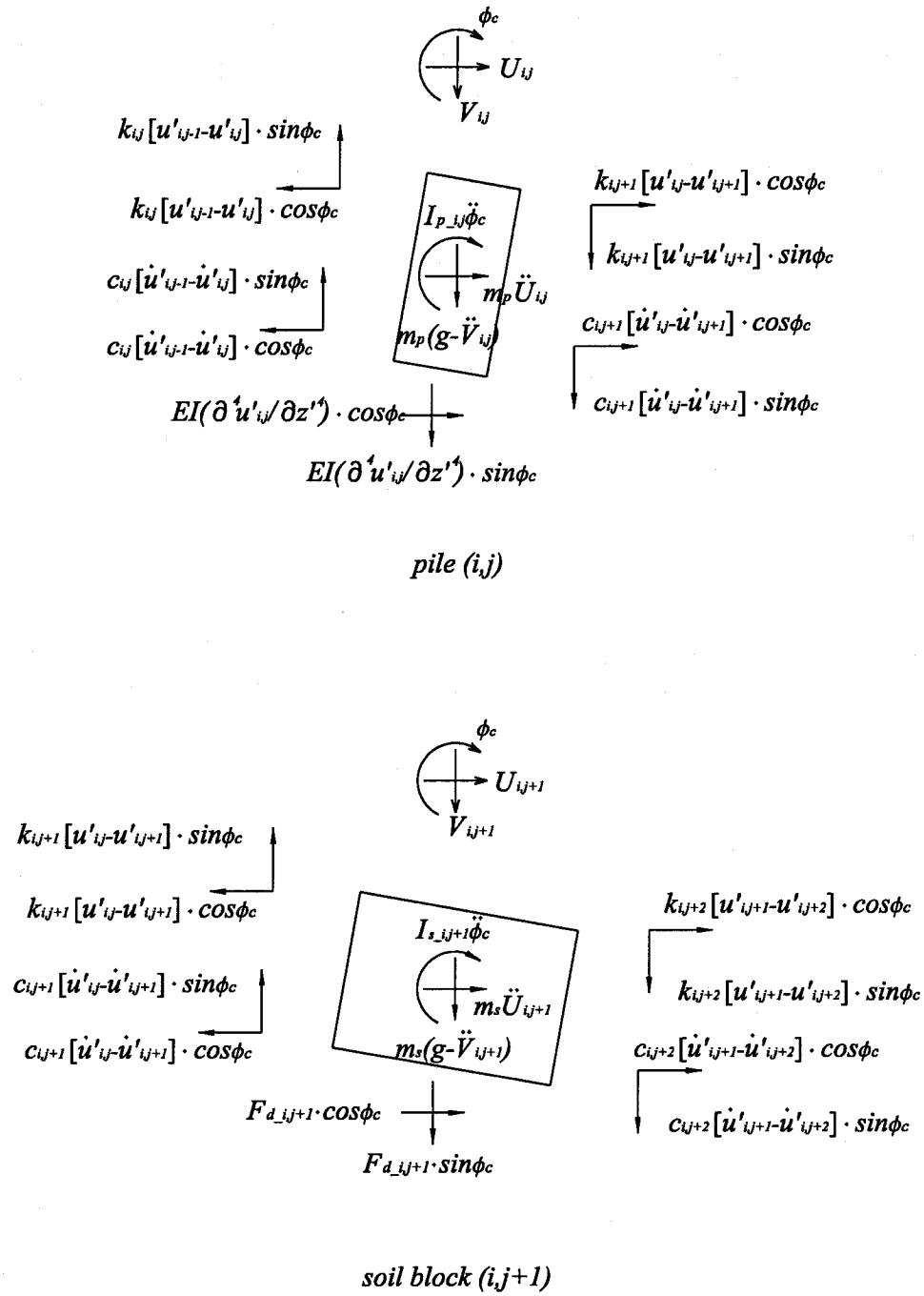

Fig. 2.11 Free-body diagram of the deformed model of the typical elements.

$F_{d\_i,j+1}$ is the friction force of the soil block in the i-th layer. Figure 2.12 shows the friction forces of sliding soil blocks. $F_{c\_i+1,j+1}$ and $F_{c\_i,j+1}$ are the compression forces at the top and bottom surfaces of the i-th soil block. Those are defined as

$$F_{c\_i+1,j+1} = F_{c\_i+2,j+1} - m_s \cdot \left(g - \ddot{V}_{i+1,j+1}\right) \tag{2.29}$$

$$F_{c\_i,j+1} = F_{c\_i+1,j+1} - m_s \cdot \left(g - \ddot{V}_{i,j+1}\right), \tag{2.30}$$

where

m_s = mass of a soil block

$\ddot{V}_{i,j+1}$ = total acceleration of the i-th soil block in z direction

g = acceleration of gravity (z direction).

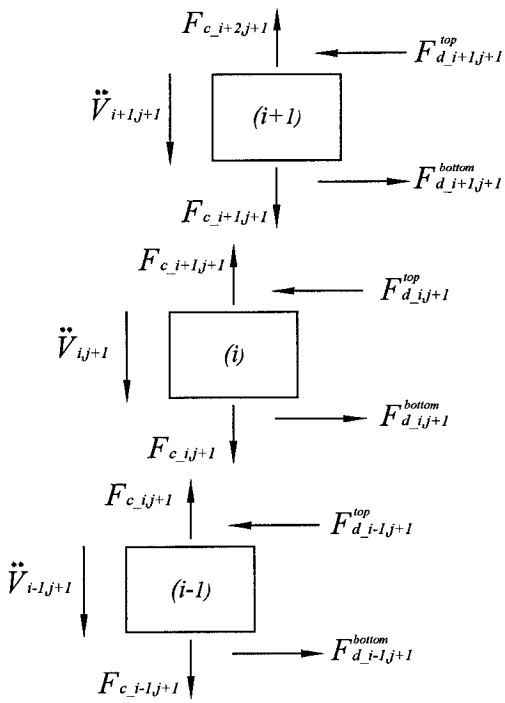

Fig. 2.12 Friction forces of sliding soil blocks.

The friction forces at the top and bottom surfaces of the soil blocks are

$$F_{d\_i,j+1}^{top} = +\mu \cdot F_{c\_i+1,j+1}, \qquad \dot{u}'_{i,j+1} > \dot{u}'_{i+1,j+1} \tag{2.31}$$

$$F_{d\_i,j+1}^{top} = -\mu \cdot F_{c\_i+1,j+1}, \qquad \dot{u}'_{i,j+1} < \dot{u}'_{i+1,j+1} \tag{2.32}$$

$$F_{d\_i,j+1}^{bottom} = +\mu \cdot F_{c\_i,j+1}, \qquad \dot{u}'_{i,j+1} > \dot{u}'_{i-1,j+1} \tag{2.33}$$

$$F_{d\_i,j+1}^{bottom} = -\mu \cdot F_{c\_i,j+1}, \qquad \dot{u}'_{i,j+1} < \dot{u}'_{i-1,j+1}, \tag{2.34}$$

where

$F_{d\_i,j+1}^{top}$ = friction force at the top surface of the i-th soil block

$F_{d\_i,j+1}^{bottom}$ = friction force at the bottom surface of the i-th soil block

μ = friction coefficient of the soil.

The total friction force acting on the soil block is the sum of the friction forces at both surfaces.

$$F_{d\_i,j+1} = F_{d\_i,j+1}^{top} + F_{d\_i,j+1}^{bottom}, \tag{2.35}$$

where $F_{d\_i,j+1}$ is the total friction force of the i-th soil block.

The equations of motion are derived based on the displacements shown in Figure 2.10 and in terms of the forces shown in Figure 2.11. The dynamic equilibrium equation of a typical element of the pile (i, j) in the horizontal direction (x direction) is

$$
\begin{aligned}
&EI\frac{\partial^4 u'_{i,j}}{\partial z'^4}\cos\phi_c + m_p\ddot{U}_{i,j} \\
&\quad + \left[k_{i,j}(u'_{i,j} - u'_{i,j-1})\cos\phi_c + k_{i,j+1}(u'_{i,j} - u'_{i,j+1})\cos\phi_c\right] \\
&\quad + \left[c_{i,j}(\dot{u}'_{i,j} - \dot{u}'_{i,j-1})\cos\phi_c + c_{i,j+1}(\dot{u}'_{i,j} - \dot{u}'_{i,j+1})\cos\phi_c\right] = 0.
\end{aligned} \tag{2.36}
$$

The equation of motion for a typical element of the soil block (i, j+1) in the horizontal direction is

$$
\begin{aligned}
&F_{d\_i,j+1}\cos\phi_c + m_s\ddot{U}_{i,j+1} \\
&\quad + \left[k_{i,j+1}(u'_{i,j+1} - u'_{i,j})\cos\phi_c + k_{i,j+2}(u'_{i,j+1} - u'_{i,j+2})\cos\phi_c\right] \\
&\quad + \left[c_{i,j+1}(\dot{u}'_{i,j+1} - \dot{u}'_{i,j})\cos\phi_c + c_{i,j+2}(\dot{u}'_{i,j+1} - \dot{u}'_{i,j+2})\cos\phi_c\right] = 0.
\end{aligned} \tag{2.37}
$$

The dynamic equilibrium equations of typical elements of a pile (i, j) and of a soil block (i, j+1) in the vertical direction (z direction) are shown in equations (2.38) and (2.39):

$$
\begin{aligned}
&EI\frac{\partial^4 u'_{i,j}}{\partial z'^4}\sin\phi_c + m_p(g - \ddot{V}_{i,j}) \\
&\quad + \left[k_{i,j}(u'_{i,j} - u'_{i,j-1})\sin\phi_c + k_{i,j+1}(u'_{i,j} - u'_{i,j+1})\sin\phi_c\right] \\
&\quad + \left[c_{i,j}(\dot{u}'_{i,j} - \dot{u}'_{i,j-1})\sin\phi_c + c_{i,j+1}(\dot{u}'_{i,j} - \dot{u}'_{i,j+1})\sin\phi_c\right] = 0
\end{aligned} \tag{2.38}
$$

$$
\begin{aligned}
&F_{d\_i,j+1}\sin\phi_c + m_s(g - \ddot{V}_{i,j+1}) \\
&\quad + \left[k_{i,j+1}(u'_{i,j+1} - u'_{i,j})\sin\phi_c + k_{i,j+2}(u'_{i,j+1} - u'_{i,j+2})\sin\phi_c\right] \\
&\quad + \left[c_{i,j+1}(\dot{u}'_{i,j+1} - \dot{u}'_{i,j})\sin\phi_c + c_{i,j+2}(\dot{u}'_{i,j+1} - \dot{u}'_{i,j+2})\sin\phi_c\right] = 0.
\end{aligned} \tag{2.39}
$$

The moments of inertia of the pile and soil block elements about the reference point O are

$$I_{p\_i,j} = I_{p0} + \sqrt{h'^2_{i,j} + d'^2_{i,j}} \tag{2.40}$$

$$I_{s\_i,j+1} = I_{s0} + \sqrt{h'^2_{i,j+1} + d'^2_{i,j+1}}\,, \tag{2.41}$$

where

$I_{p\_i,j}$ = moment of inertia of the typical pile element (i, j) about the reference point O

I_{p0} = moment of inertia of a pile element (i, j) about the center of mass of the element

$I_{s\_i,j+1}$ = moment of inertia of the typical soil block element $(i, j+1)$ about the reference point O

I_{s0} = moment of inertia of a soil block element $(i, j+1)$ about the center of mass of the element

$h'_{i,j}$ = distance from the point O to the deformed position of the element (i, j) in the vertical direction

$d'_{i,j}$ = distance from the point O to the deformed position of the element (i, j) in the horizontal direction

The displacement of an element is assumed to be much smaller than the distance from the reference point O to the undeformed position of the element $(h_{i,j}, d_{i,j})$. Thus, the distances and the moment of inertia of the pile element and the soil block can be defined approximately as

$$h'_{i,j} \approx h_{i,j}, \quad d'_{i,j} \approx d_{i,j} \tag{2.42}$$

$$I_{p\_i,j} = I_{p0} + \sqrt{h_{i,j}^2 + d_{i,j}^2} \tag{2.43}$$

$$I_{s\_i,j+1} = I_{s0} + \sqrt{h_{i,j+1}^2 + d_{i,j+1}^2}\,. \tag{2.44}$$

The equilibrium equation of the moments acting with respect to the point O is shown in equations (2.45) and (2.46). The equations for a typical element of the pile (i, j) and a typical element of the soil block (i, $j+1$) are

$$\begin{aligned}
&I_{p_i,j}\ddot{\phi}_c + \\
&[\ EI\frac{\partial^4 u'_{i,j}}{\partial z'^4}\cos\phi_c + m_p\ddot{U}_{i,j} \\
&\quad + k_{i,j}(u'_{i,j} - u'_{i,j-1})\cos\phi_c + k_{i,j+1}(u'_{i,j} - u'_{i,j+1})\cos\phi_c \\
&\quad + c_{i,j}(\dot{u}'_{i,j} - \dot{u}'_{i,j-1})\cos\phi_c + c_{i,j+1}(\dot{u}'_{i,j} - \dot{u}'_{i,j+1})\cos\phi_c\ ]\times h_{i,j} + \\
&[\ EI\frac{\partial^4 u'_{i,j}}{\partial z'^4}\sin\phi_c + m_p(g - \ddot{V}_{i,j}) \\
&\quad + k_{i,j}(u'_{i,j} - u'_{i,j-1})\sin\phi_c + k_{i,j+1}(u'_{i,j} - u'_{i,j+1})\sin\phi_c \\
&\quad + c_{i,j}(\dot{u}'_{i,j} - \dot{u}'_{i,j-1})\sin\phi_c + c_{i,j+1}(\dot{u}'_{i,j} - \dot{u}'_{i,j+1})\sin\phi_c\ ]\times d_{i,j} = 0
\end{aligned} \tag{2.45}$$

$$\begin{aligned}
&I_{s_i,j+1}\ddot{\phi}_c + \\
&[\ F_{d_i,j+1}\cos\phi_c + m_s\ddot{U}_{i,j+1} \\
&\quad + k_{i,j+1}(u'_{i,j+1} - u'_{i,j})\cos\phi_c + k_{i,j+2}(u'_{i,j+1} - u'_{i,j+2})\cos\phi_c \\
&\quad + c_{i,j+1}(\dot{u}'_{i,j+1} - \dot{u}'_{i,j})\cos\phi_c + c_{i,j+2}(\dot{u}'_{i,j+1} - \dot{u}'_{i,j+2})\cos\phi_c\ ]\times h_{i,j+1} + \\
&[\ F_{d_i,j+1}\sin\phi_c + m_s(g - \ddot{V}_{i,j+1}) \\
&\quad + k_{i,j+1}(u'_{i,j+1} - u'_{i,j})\sin\phi_c + k_{i,j+2}(u'_{i,j+1} - u'_{i,j+2})\sin\phi_c \\
&\quad + c_{i,j+1}(\dot{u}'_{i,j+1} - \dot{u}'_{i,j})\sin\phi_c + c_{i,j+2}(\dot{u}'_{i,j+1} - \dot{u}'_{i,j+2})\sin\phi_c\ ]\times d_{i,j+1} = 0\,.
\end{aligned} \tag{2.46}$$

The dynamic equilibrium equation for the *i*-th layer is expressed in matrix form as follows:

$$\begin{bmatrix} \ddots & \vdots & \vdots & \vdots & \\ \cdots & M_{11} & M_{12} & M_{13} & \cdots \\ \cdots & M_{21} & M_{22} & M_{23} & \cdots \\ \cdots & M_{31} & M_{32} & M_{33} & \cdots \\ & \vdots & \vdots & \vdots & \ddots \end{bmatrix} \begin{bmatrix} \vdots \\ \ddot{u}'_{i,j-1} \\ \ddot{u}'_{i,j} \\ \ddot{u}'_{i,j+1} \\ \vdots \end{bmatrix} + \begin{bmatrix} \ddots & \vdots & \vdots & \vdots & \\ \cdots & D_{11} & D_{12} & D_{13} & \cdots \\ \cdots & D_{21} & D_{22} & D_{23} & \cdots \\ \cdots & D_{31} & D_{32} & D_{33} & \cdots \\ & \vdots & \vdots & \vdots & \ddots \end{bmatrix} \begin{bmatrix} \vdots \\ \dot{u}'_{i,j-1} \\ \dot{u}'_{i,j} \\ \dot{u}'_{i,j+1} \\ \vdots \end{bmatrix}$$

$$+ \begin{bmatrix} \ddots & \vdots & \vdots & \vdots & \\ \cdots & K_{11} & K_{12} & K_{13} & \cdots \\ \cdots & K_{21} & K_{22} & K_{23} & \cdots \\ \cdots & K_{31} & K_{32} & K_{33} & \cdots \\ & \vdots & \vdots & \vdots & \ddots \end{bmatrix} \begin{bmatrix} \vdots \\ u'_{i,j-1} \\ u'_{i,j} \\ u'_{i,j+1} \\ \vdots \end{bmatrix} + \begin{bmatrix} \vdots \\ A_1 \\ A_2 \\ A_3 \\ \vdots \end{bmatrix} = \begin{bmatrix} \vdots \\ F_1 \\ F_2 \\ F_3 \\ \vdots \end{bmatrix}, \tag{2.47}$$

where the components of the matrices are

$$M_{11} = m_s \cdot (h_{i,j-1} \cos\phi_c + d_{i,j-1} \sin\phi_c)$$

$$M_{12} = 0$$

$$M_{13} = 0$$

$$M_{21} = 0$$

$$M_{22} = m_p \cdot (h_{i,j} \cos\phi_c + d_{i,j} \sin\phi_c)$$

$$M_{23} = 0$$

$$M_{31} = 0$$

$$M_{32} = 0$$

$$M_{33} = m_s \cdot (h_{i,j+1}\cos\phi_c - d_{i,j+1}\sin\phi_c)$$

$$D_{11} = (c_{i,j-1} + c_{i,j}) \cdot (h_{i,j-1}\cos\phi_c + d_{i,j-1}\sin\phi_c) - 2\dot{\phi}_c m_p \cdot (h_{i,j-1}\sin\phi_c + d_{i,j-1}\cos\phi_c)$$

$$D_{12} = -c_{i,j} \cdot (h_{i,j-1}\cos\phi_c + d_{i,j-1}\sin\phi_c)$$

$$D_{13} = 0$$

$$D_{21} = -c_{i,j} \cdot (h_{i,j}\cos\phi_c + d_{i,j}\sin\phi_c)$$

$$D_{22} = (c_{i,j} + c_{i,j+1}) \cdot (h_{i,j}\cos\phi_c + d_{i,j}\sin\phi_c) - 2\dot{\phi}_c m_p \cdot (h_{i,j}\sin\phi_c + d_{i,j}\cos\phi_c)$$

$$D_{23} = -c_{i,j+1} \cdot (h_{i,j}\cos\phi_c + d_{i,j}\sin\phi_c)$$

$$D_{31} = 0$$

$$D_{32} = -c_{i,j+1} \cdot (h_{i,j+1}\cos\phi_c + d_{i,j+1}\sin\phi_c)$$

$$D_{33} = (c_{i,j+1} + c_{i,j+2}) \cdot (h_{i,j+1}\cos\phi_c + d_{i,j+1}\sin\phi_c) - 2\dot{\phi}_c m_s \cdot (h_{i,j+1}\sin\phi_c + d_{i,j+1}\cos\phi_c)$$

$$K_{11} = (k_{i,j-1} + k_{i,j}) \cdot (h_{i,j-1}\cos\phi_c + d_{i,j-1}\sin\phi_c) - m_p \cdot \left[(\ddot{\phi}_c \sin\phi_c + \dot{\phi}^2{}_c \cos\phi_c) \cdot h_{i,j-1} + (\ddot{\phi}_c \cos\phi_c - \dot{\phi}^2{}_c \sin\phi_c) \cdot d_{i,j-1}\right]$$

$$K_{12} = -k_{i,j} \cdot (h_{i,j-1}\cos\phi_c + d_{i,j-1}\sin\phi_c)$$

$$K_{13} = 0$$

$$K_{21} = -k_{i,j} \cdot (h_{i,j}\cos\phi_c + d_{i,j}\sin\phi_c)$$

$$K_{22} = (k_{i,j} + k_{i,j+1}) \cdot (h_{i,j}\cos\phi_c + d_{i,j}\sin\phi_c) - m_p \cdot \left[(\ddot{\phi}_c \sin\phi_c + \dot{\phi}^2{}_c \cos\phi_c) \cdot h_{i,j} + (\ddot{\phi}_c \cos\phi_c - \dot{\phi}^2{}_c \sin\phi_c) \cdot d_{i,j}\right]$$

$$K_{23} = -k_{i,j+1} \cdot (h_{i,j}\cos\phi_c + d_{i,j}\sin\phi_c)$$

$$K_{31} = 0$$

$$K_{32} = -k_{i,j+1} \cdot (h_{i,j+1} \cos\phi_c + d_{i,j+1} \sin\phi_c)$$

$$K_{33} = (k_{i,j+1} + k_{i,j+2}) \cdot (h_{i,j+1} \cos\phi_c + d_{i,j+1} \sin\phi_c) - m_p \cdot \left[(\ddot{\phi}_c \sin\phi_c + \dot{\phi}^2{}_c \cos\phi_c) \cdot h_{i,j+1} + (\ddot{\phi}_c \cos\phi_c - \dot{\phi}^2{}_c \sin\phi_c) \cdot d_{i,j+1} \right]$$

$$A_1 = \left[F_{d\_i,j-1} \cos\phi_c \right] \cdot h_{i,j-1} + \left[F_{d\_i,j-1} \sin\phi_c \right] \cdot d_{i,j-1}$$

$$A_2 = \left[EI \frac{\partial^4 u'_{i,j}}{\partial z'^4} \cos\phi_c \right] \cdot h_{i,j} + \left[EI \frac{\partial^4 u'_{i,j}}{\partial z'^4} \sin\phi_c \right] \cdot d_{i,j}$$

$$A_3 = \left[F_{d\_i,j+1} \cos\phi_c \right] \cdot h_{i,j+1} + \left[F_{d\_i,j+1} \sin\phi_c \right] \cdot d_{i,j+1}$$

$$F_1 = -I_{s\_i,j-1} \cdot \ddot{\phi}_c - m_s \left[\ddot{u}_c + h_{i,j-1} \cdot \left(\ddot{\phi}_c \cos\phi_c - \dot{\phi}_c^2 \sin\phi_c \right) - d_{i,j-1} \cdot \left(\ddot{\phi}_c \sin\phi_c + \dot{\phi}_c^2 \cos\phi_c \right) \right] \cdot h_{i,j-1} - m_s \left[g - \ddot{v}_c - h_{i,j-1} \cdot \left(\ddot{\phi}_c \sin\phi_c + \dot{\phi}_c^2 \cos\phi_c \right) - d_{i,j-1} \cdot \left(\ddot{\phi}_c \cos\phi_c - \dot{\phi}_c^2 \sin\phi_c \right) \right] \cdot d_{i,j-1}$$

$$F_2 = -I_{p\_i,j} \cdot \ddot{\phi}_c - m_p \left[\ddot{u}_c + h_{i,j} \cdot \left(\ddot{\phi}_c \cos\phi_c - \dot{\phi}_c^2 \sin\phi_c \right) - d_{i,j} \cdot \left(\ddot{\phi}_c \sin\phi_c + \dot{\phi}_c^2 \cos\phi_c \right) \right] \cdot h_{i,j} - m_p \left[g - \ddot{v}_c - h_{i,j} \cdot \left(\ddot{\phi}_c \sin\phi_c + \dot{\phi}_c^2 \cos\phi_c \right) - d_{i,j} \cdot \left(\ddot{\phi}_c \cos\phi_c - \dot{\phi}_c^2 \sin\phi_c \right) \right] \cdot d_{i,j}$$

$$F_3 = -I_{s\_i,j+1} \cdot \ddot{\phi}_c - m_s \left[\ddot{u}_c + h_{i,j+1} \cdot \left(\ddot{\phi}_c \cos\phi_c - \dot{\phi}_c^2 \sin\phi_c \right) - d_{i,j+1} \cdot \left(\ddot{\phi}_c \sin\phi_c + \dot{\phi}_c^2 \cos\phi_c \right) \right] \cdot h_{i,j+1} - m_s \left[g - \ddot{v}_c - h_{i,j+1} \cdot \left(\ddot{\phi}_c \sin\phi_c + \dot{\phi}_c^2 \cos\phi_c \right) - d_{i,j+1} \cdot \left(\ddot{\phi}_c \cos\phi_c - \dot{\phi}_c^2 \sin\phi_c \right) \right] \cdot d_{i,j+1}.$$

In the above equations, terms involving $\dot{\phi}_c^2$ have been neglected because the rotation is assumed to be relatively small. Then, the vector $\{F\}$, can be expressed as

$$\begin{bmatrix} \vdots \\ F_1 \\ F_2 \\ F_3 \\ \vdots \end{bmatrix} = \begin{bmatrix} \vdots & \vdots & \vdots \\ N_{11} & N_{12} & N_{13} \\ N_{21} & N_{22} & N_{23} \\ N_{31} & N_{32} & N_{33} \\ \vdots & \vdots & \vdots \end{bmatrix} \begin{bmatrix} \ddot{v}_c \\ \ddot{u}_c \\ \ddot{\phi}_c \end{bmatrix} + \begin{bmatrix} \vdots \\ B_1 \\ B_2 \\ B_3 \\ \vdots \end{bmatrix}, \tag{2.48}$$

where

$$N_{11} = m_s \cdot d_{i,j-1}$$

$$N_{12} = -m_s \cdot h_{i,j-1}$$

$$N_{13} = -I_{s\_i,j-1} - m_s\left[h_{i,j-1}^2 \cdot \cos\phi_c - 2h_{i,j-1}d_{i,j-1} \cdot \sin\phi_c - d_{i,j-1}^2 \cdot \cos\phi_c\right]$$

$$N_{21} = m_p \cdot d_{i,j}$$

$$N_{22} = -m_p \cdot h_{i,j}$$

$$N_{23} = -I_{p\_i,j} - m_p\left[h_{i,j}^2 \cdot \cos\phi_c - 2h_{i,j}d_{i,j} \cdot \sin\phi_c - d_{i,j}^2 \cdot \cos\phi_c\right]$$

$$N_{31} = m_s \cdot d_{i,j+1}$$

$$N_{32} = -m_s \cdot h_{i,j+1}$$

$$N_{33} = -I_{s\_i,j+1} - m_s\left[h_{i,j+1}^2 \cdot \cos\phi_c - 2h_{i,j+1}d_{i,j+1} \cdot \sin\phi_c - d_{i,j+1}^2 \cdot \cos\phi_c\right]$$

$$B_1 = -m_s \cdot g \cdot d_{i,j-1}$$

$$B_2 = -m_p \cdot g \cdot d_{i,j}$$

$$B_3 = -m_s \cdot g \cdot d_{i,j+1}.$$

The forces inside the "box", and their resultant $\{F_b\}$ acting at the point O' are shown in Figure 2.13.

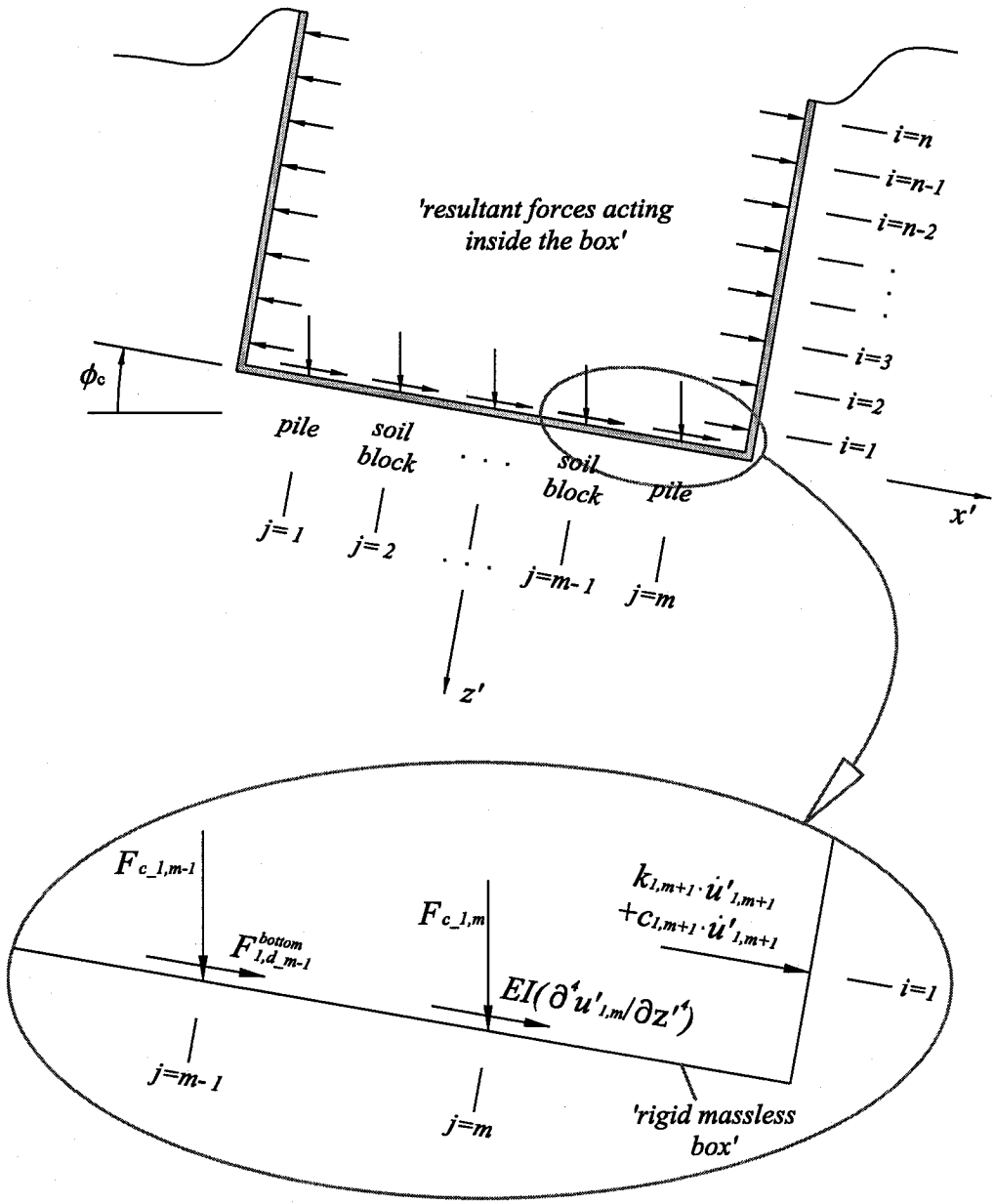

Fig. 2.13 Resultant forces acting on the "box".

The forces are defined in terms of the forces and displacements shown in Figures 2.9, 2.10, 2.11, and 2.13.

$$\{F_b\} = \left[F_z^b,\ F_x^b,\ M_o^b\right]^T\ , \tag{2.49}$$

where

$$F_z^b = \sum_{j=1}^{(m+1)/2} EI\frac{\partial^4 u'_{1,2j-1}}{\partial z'^4}\sin\phi_c + \sum_{j=1}^{(m+1)/2-1} F_{d\_1,2j}^{bottom}\sin\phi_c + \sum_{j=1}^{m} F_{c\_1,j}$$
$$+ \sum_{i=1}^{n}\left[k_{i,1}\cdot u'_{i,1} + c_{i,1}\cdot \dot{u}'_{i,1} + k_{i,m+1}\cdot u'_{i,m+1} + c_{i,m+1}\cdot \dot{u}'_{i,m+1}\right]\sin\phi_c$$

$$F_x^b = \sum_{j=1}^{(m+1)/2} EI\frac{\partial^4 u'_{1,2j-1}}{\partial z'^4}\cos\phi_c + \sum_{j=1}^{(m+1)/2-1} F_{d\_1,2j}^{bottom}\cos\phi_c$$
$$+ \sum_{i=1}^{n}\left[k_{i,1}\cdot u'_{i,1} + c_{i,1}\cdot \dot{u}'_{i,1} + k_{i,m+1}\cdot u'_{i,m+1} + c_{i,m+1}\cdot \dot{u}'_{i,m+1}\right]\cos\phi_c$$

$$M_o^b = F_z^b\cdot d_{i,j} + F_x^b\cdot h_{i,j}\,.$$

The equilibrium equation of the "massless foundation" is

$$\{F_s\} = \{F_b\}, \tag{2.50}$$

where $\{F_s\}$ is the resultant force with which the half space acts on the foundation. This equation does not have an inertial force term because the foundation is assumed to be a massless box. The resultant force $\{F_b\}$, shown in equation (2.49) is next transformed into matrix form as,

$$\begin{bmatrix} F_z^b \\ F_x^b \\ M_o^b \end{bmatrix} = \begin{bmatrix} \quad D^* \quad \end{bmatrix}_{3\times 2n} \begin{bmatrix} \ddot{u}'_{1,1} \\ \ddot{u}'_{2,1} \\ \vdots \\ \ddot{u}'_{n,1} \\ \ddot{u}'_{1,m} \\ \ddot{u}'_{2,m} \\ \vdots \\ \ddot{u}'_{n,m} \end{bmatrix}_{2n\times 1} + \begin{bmatrix} \quad K^* \quad \end{bmatrix}_{3\times 2n} \begin{bmatrix} u'_{1,1} \\ u'_{2,1} \\ \vdots \\ u'_{n,1} \\ u'_{1,m} \\ u'_{2,m} \\ \vdots \\ u'_{n,m} \end{bmatrix}_{2n\times 1} + \begin{bmatrix} G \end{bmatrix}_{3\times 1},$$

(2.51)

where

$$[D^*] = \begin{bmatrix} c_{1,1}\sin\phi_c & c_{2,1}\sin\phi_c & \cdots & c_{n,1}\sin\phi_c & c_{1,m+1}\sin\phi_c & c_{2,m+1}\sin\phi_c & \cdots & c_{n,m+1}\sin\phi_c \\ c_{1,1}\cos\phi_c & c_{2,1}\cos\phi_c & \cdots & c_{n,1}\cos\phi_c & c_{1,m+1}\cos\phi_c & c_{2,m+1}\cos\phi_c & \cdots & c_{n,m+1}\cos\phi_c \\ c_{1,1}(d_{1,1}\sin\phi_c + h_{1,1}\cos\phi_c) & c_{2,1}(d_{2,1}\sin\phi_c + h_{2,1}\cos\phi_c) & \cdots & c_{n,1}(d_{n,1}\sin\phi_c + h_{n,1}\cos\phi_c) & c_{1,m+1}(d_{1,m}\sin\phi_c + h_{1,m}\cos\phi_c) & c_{2,m+1}(d_{2,m}\sin\phi_c + h_{2,m}\cos\phi_c) & \cdots & c_{n,m+1}(d_{2,1}\sin\phi_c + h_{n,m}\cos\phi_c) \end{bmatrix}$$

$$[K^*] = \begin{bmatrix} k_{1,1}\sin\phi_c & k_{2,1}\sin\phi_c & \cdots & k_{n,1}\sin\phi_c & k_{1,m+1}\sin\phi_c & k_{2,m+1}\sin\phi_c & \cdots & k_{n,m+1}\sin\phi_c \\ k_{1,1}\cos\phi_c & k_{2,1}\cos\phi_c & \cdots & k_{n,1}\cos\phi_c & k_{1,m+1}\cos\phi_c & k_{2,m+1}\cos\phi_c & \cdots & k_{n,m+1}\cos\phi_c \\ k_{1,1}(d_{1,1}\sin\phi_c + h_{1,1}\cos\phi_c) & k_{2,1}(d_{2,1}\sin\phi_c + h_{2,1}\cos\phi_c) & \cdots & k_{n,1}(d_{n,1}\sin\phi_c + h_{n,1}\cos\phi_c) & k_{1,m+1}(d_{1,m}\sin\phi_c + h_{1,m}\cos\phi_c) & k_{2,m+1}(d_{2,m}\sin\phi_c + h_{2,m}\cos\phi_c) & \cdots & k_{n,m+1}(d_{2,1}\sin\phi_c + h_{n,m}\cos\phi_c) \end{bmatrix}$$

$$\{G\} = \begin{bmatrix} EI\frac{\partial^4 u'_{1,1}}{\partial z'^4}\sin\phi_c + EI\frac{\partial^4 u'_{1,3}}{\partial z'^4}\sin\phi_c + \cdots + EI\frac{\partial^4 u'_{1,m}}{\partial z'^4}\sin\phi_c \\ + F^{bottom}_{d\_1,2}\sin\phi_c + F^{bottom}_{d\_1,4}\sin\phi_c + \cdots + F^{bottom}_{d\_1,m-1}\sin\phi_c + F_{c\_1,1} + F_{c\_1,2} + \cdots + F_{c\_1,m} \\ \\ EI\frac{\partial^4 u'_{1,1}}{\partial z'^4}\cos\phi_c + EI\frac{\partial^4 u'_{1,3}}{\partial z'^4}\cos\phi_c + \cdots + EI\frac{\partial^4 u'_{1,m}}{\partial z'^4}\cos\phi_c \\ + F^{bottom}_{d\_1,2}\cos\phi_c + F^{bottom}_{d\_1,4}\cos\phi_c + \cdots + F^{bottom}_{d\_1,m-1}\cos\phi_c \\ EI\frac{\partial^4 u'_{1,1}}{\partial z'^4}d_{1,1}\sin\phi_c + EI\frac{\partial^4 u'_{1,3}}{\partial z'^4}d_{1,3}\sin\phi_c + \cdots + EI\frac{\partial^4 u'_{1,m}}{\partial z'^4}d_{1,m}\sin\phi_c \\ + F^{bottom}_{d\_1,2}d_{1,2}\sin\phi_c + F^{bottom}_{d\_1,4}d_{1,4}\sin\phi_c + \cdots + F^{bottom}_{d\_1,m-1}d_{1,m-1}\sin\phi_c + F_{c\_1,1}d_{1,1} + F_{c\_1,2}d_{1,2} + \cdots + F_{c\_1,m}d_{1,m} \end{bmatrix}.$$

From equations (2.11) and (2.15), the absolute displacements of the foundation $\{u_c\}$, and its second derivative with respect to the time $\{\ddot{u}_c\}$, become

$$\begin{bmatrix} v_c \\ u_c \\ \phi_c \end{bmatrix} = \begin{bmatrix} v_0 \\ u_0 \\ \phi_0 \end{bmatrix} + \begin{bmatrix} C_{VV}(\omega) & C_{VH}(\omega) & C_{VM}(\omega) \\ C_{HV}(\omega) & C_{HH}(\omega) & C_{HM}(\omega) \\ C_{MV}(\omega) & C_{MH}(\omega) & C_{MM}(\omega) \end{bmatrix} \begin{bmatrix} F_z^b \\ F_x^b \\ M_o^b \end{bmatrix} \tag{2.52}$$

$$\begin{bmatrix} \ddot{v}_c \\ \ddot{u}_c \\ \ddot{\phi}_c \end{bmatrix} = \begin{bmatrix} \ddot{v}_0 \\ \ddot{u}_0 \\ \ddot{\phi}_0 \end{bmatrix} + \begin{bmatrix} C_{VV}(\omega) & C_{VH}(\omega) & C_{VM}(\omega) \\ C_{HV}(\omega) & C_{HH}(\omega) & C_{HM}(\omega) \\ C_{MV}(\omega) & C_{MH}(\omega) & C_{MM}(\omega) \end{bmatrix} \begin{bmatrix} \ddot{F}_z^b \\ \ddot{F}_x^b \\ \ddot{M}_o^b \end{bmatrix}. \tag{2.53}$$

The second derivative of the resultant force $\{\ddot{F}_b\}$ is developed from equation (2.51) as follows:

$$\begin{bmatrix} \ddot{F}_z^b \\ \ddot{F}_x^b \\ \ddot{M}_o^b \end{bmatrix} = [\ddot{K}^*] \begin{bmatrix} u'_{1,1} \\ \vdots \\ u'_{n,m} \end{bmatrix} + [[\ddot{D}^*] + [\dot{K}^*]] \begin{bmatrix} \dot{u}'_{1,1} \\ \vdots \\ \dot{u}'_{n,m} \end{bmatrix} + [2 \cdot [\dot{D}^*] + [K^*]] \begin{bmatrix} \ddot{u}'_{1,1} \\ \vdots \\ \ddot{u}'_{n,m} \end{bmatrix}$$

$$+ [D^*] \begin{bmatrix} \partial^3 u'_{1,1} / \partial t^3 \\ \vdots \\ \partial^3 u'_{n,m} / \partial t^3 \end{bmatrix} + [\ddot{G}]. \tag{2.54}$$

The matrices in the above equation are obtained from the first and second derivatives of the matrices defined in equation (2.51):

$$\left[\ddot{D}^*\right]=\begin{bmatrix} c_{1,1}\ddot{\phi}_c\cos\phi_c & \cdots & c_{n,m+1}\ddot{\phi}_c\cos\phi_c \\ -c_{1,1}\ddot{\phi}_c\sin\phi_c & \cdots & -c_{n,m+1}\ddot{\phi}_c\sin\phi_c \\ c_{1,1}\ddot{\phi}_c(d_{1,1}\cos\phi_c & \cdots & c_{n,m+1}\ddot{\phi}_c(d_{n,m}\cos\phi_c \\ -h_{1,1}\sin\phi_c) & & -h_{n,m}\sin\phi_c) \end{bmatrix}_{3\times 2n} \tag{2.55}$$

$$\left[\ddot{K}^*\right]=\begin{bmatrix} k_{1,1}\ddot{\phi}_c\cos\phi_c & \cdots & k_{n,m+1}\ddot{\phi}_c\cos\phi_c \\ -k_{1,1}\ddot{\phi}_c\sin\phi_c & \cdots & -k_{n,m+1}\ddot{\phi}_c\sin\phi_c \\ k_{1,1}\ddot{\phi}_c(d_{1,1}\cos\phi_c & \cdots & k_{n,m+1}\ddot{\phi}_c(d_{n,m}\cos\phi_c \\ -h_{1,1}\sin\phi_c) & & -h_{n,m}\sin\phi_c) \end{bmatrix}_{3\times 2n} \tag{2.56}$$

$$\left[\dot{D}^*\right]=\begin{bmatrix} c_{1,1}\dot{\phi}_c\cos\phi_c & \cdots & c_{n,m+1}\dot{\phi}_c\cos\phi_c \\ -c_{1,1}\dot{\phi}_c\sin\phi_c & \cdots & -c_{n,m+1}\dot{\phi}_c\sin\phi_c \\ c_{1,1}\dot{\phi}_c(d_{1,1}\cos\phi_c & \cdots & c_{n,m+1}\dot{\phi}_c(d_{n,m}\cos\phi_c \\ -h_{1,1}\sin\phi_c) & & -h_{n,m}\sin\phi_c) \end{bmatrix}_{3\times 2n} \tag{2.57}$$

$$\left[\dot{K}^*\right]=\begin{bmatrix} k_{1,1}\dot{\phi}_c\cos\phi_c & \cdots & k_{n,m+1}\dot{\phi}_c\cos\phi_c \\ -k_{1,1}\dot{\phi}_c\sin\phi_c & \cdots & -k_{n,m+1}\dot{\phi}_c\sin\phi_c \\ k_{1,1}\dot{\phi}_c(d_{1,1}\cos\phi_c & \cdots & k_{n,m+1}\dot{\phi}_c(d_{n,m}\cos\phi_c \\ -h_{1,1}\sin\phi_c) & & -h_{n,m}\sin\phi_c) \end{bmatrix}_{3\times 2n} \tag{2.58}$$

$$\{\ddot{G}\}=\begin{bmatrix} EI\frac{\partial^2}{\partial t^2}\left(\frac{\partial^4 u'_{1,1}}{\partial z'^4}\right)\sin\phi_c+2EI\frac{\partial}{\partial t}\left(\frac{\partial^4 u'_{1,1}}{\partial z'^4}\right)\dot{\phi}_c\cos\phi_c \\ +EI\frac{\partial^4 u'_{1,1}}{\partial z'^4}\ddot{\phi}_c\cos\phi_c+\cdots \\ +\ddot{F}^{bottom}_{d\_1,2}\sin\phi_c+2\dot{F}^{bottom}_{d\_1,2}\dot{\phi}_c\cos\phi_c+F^{bottom}_{d\_1,2}\ddot{\phi}_c\cos\phi_c\cdots \\ +\ddot{F}_{c\_1,1}+\cdots+\ddot{F}_{c\_1,m} \\ \\ EI\frac{\partial^2}{\partial t^2}\left(\frac{\partial^4 u'_{1,1}}{\partial z'^4}\right)\cos\phi_c-2EI\frac{\partial}{\partial t}\left(\frac{\partial^4 u'_{1,1}}{\partial z'^4}\right)\dot{\phi}_c\sin\phi_c \\ -EI\frac{\partial^4 u'_{1,1}}{\partial z'^4}\ddot{\phi}_c\sin\phi_c+\cdots \\ +\ddot{F}^{bottom}_{d\_1,2}\cos\phi_c-2\dot{F}^{bottom}_{d\_1,2}\dot{\phi}_c\sin\phi_c-F^{bottom}_{d\_1,2}\ddot{\phi}_c\sin\phi_c\cdots \\ \\ EI\frac{\partial^2}{\partial t^2}\left(\frac{\partial^4 u'_{1,1}}{\partial z'^4}\right)d_{1,1}\sin\phi_c+2EI\frac{\partial}{\partial t}\left(\frac{\partial^4 u'_{1,1}}{\partial z'^4}\right)d_{1,1}\dot{\phi}_c\cos\phi_c \\ +EI\frac{\partial^4 u'_{1,1}}{\partial z'^4}d_{1,1}\ddot{\phi}_c\cos\phi_c+\cdots \\ +\ddot{F}^{bottom}_{d\_1,2}d_{1,2}\sin\phi_c+2\dot{F}^{bottom}_{d\_1,2}d_{1,2}\dot{\phi}_c\cos\phi_c+F^{bottom}_{d\_1,2}d_{1,2}\ddot{\phi}_c\cos\phi_c\cdots \\ +\ddot{F}_{c\_1,1}d_{1,1}+\cdots+\ddot{F}_{c\_1,m}d_{1,m} \end{bmatrix}_{3\times 1}. \tag{2.59}$$

The absolute rotation of the foundation is calculated from equation (2.52):

$$\phi_c=\phi_0+C_{MV}(\omega)\cdot F_z^b+C_{MH}(\omega)\cdot F_x^b+C_{MM}(\omega)\cdot M_o^b. \tag{2.60}$$

This equation is expanded by equation (2.51):

$$\begin{aligned}\phi_c = \phi_0 &+ C_{MV}(\omega)\cdot\left[c_{1,1}\sin\phi_c\cdot\dot{u}'_{1,1}+\cdots+k_{1,1}\sin\phi_c\cdot u'_{1,1}+\cdots\right.\\ &\left.+EI(\partial^4 u'_{1,1}/\partial z'^4)\sin\phi_c+\cdots+F^{bottom}_{d\_1,2}\sin\phi_c+\cdots+F_{c\_1,1}+\cdots\right]\\ &+C_{MH}(\omega)\cdot\left[c_{1,1}\cos\phi_c\cdot\dot{u}'_{1,1}+\cdots+k_{1,1}\cos\phi_c\cdot u'_{1,1}+\cdots+EI(\partial^4 u'_{1,1}/\partial z'^4)\cos\phi_c+\cdots\right]\\ &+C_{MM}(\omega)\cdot\left[c_{1,1}(d_{1,1}\sin\phi_c+h_{1,1}\cos\phi_c)\cdot\dot{u}'_{1,1}+\cdots+k_{1,1}(d_{1,1}\sin\phi_c+h_{1,1}\cos\phi_c)\cdot u'_{1,1}+\right.\\ &\left.\cdots+EI(\partial^4 u'_{1,1}/\partial z'^4)d_{1,1}\sin\phi_c+\cdots+F^{bottom}_{d\_1,2}d_{1,2}\sin\phi_c+\cdots+F_{c\_1,1}d_{1,1}+\cdots\right].\end{aligned} \tag{2.61}$$

For the small rotation of the foundation, the sine and cosine terms can be approximated as

$$\sin\phi_c \approx \phi_c,\quad \cos\phi_c \approx 1\ . \tag{2.62}$$

Then, equation (2.61) can be simplified as

$$\phi_c = \frac{\left[\begin{array}{l}\phi_0+C_{MV}(\omega)\cdot\left[F_{c\_1,1}+\cdots\right]\\ +C_{MH}(\omega)\cdot\left[c_{1,1}\dot{u}'_{1,1}+\cdots+k_{1,1}u'_{1,1}+\cdots+EI(\partial^4 u'_{1,1}/\partial z'^4)+\cdots\right]\\ +C_{MM}(\omega)\cdot\left[c_{1,1}h_{1,1}\dot{u}'_{1,1}+\cdots+k_{1,1}h_{1,1}u'_{1,1}+\cdots+F_{c\_1,1}d_{1,1}+\cdots\right]\end{array}\right]}{\left[\begin{array}{l}1-C_{MV}(\omega)\cdot\left[c_{1,1}\dot{u}'_{1,1}+\cdots+k_{1,1}u'_{1,1}+\cdots+EI(\partial^4 u'_{1,1}/\partial z'^4)+\cdots+F^{bottom}_{d\_1,2}+\cdots\right]\\ -C_{MM}(\omega)\cdot\left[c_{1,1}d_{1,1}\dot{u}'_{1,1}+\cdots+k_{1,1}d_{1,1}u'_{1,1}+\cdots\right.\\ \qquad\left.+EI(\partial^4 u'_{1,1}/\partial z'^4)d_{1,1}+\cdots+F^{bottom}_{d\_1,2}d_{1,2}+\cdots\right]\end{array}\right]}. \tag{2.63}$$

The terms of absolute displacement of the foundation (v_c, u_c, ϕ_c) in the dynamic equilibrium equation (2.47) are eliminated by using equations (2.54) and (2.63). Equation (2.47) becomes

$$\begin{bmatrix} \ddots & \vdots & \vdots & \vdots & \\ \cdots & M_{11}^{**} & M_{12}^{**} & M_{13}^{**} & \cdots \\ \cdots & M_{21}^{**} & M_{22}^{**} & M_{23}^{**} & \cdots \\ \cdots & M_{31}^{**} & M_{32}^{**} & M_{33}^{**} & \cdots \\ & \vdots & \vdots & \vdots & \ddots \end{bmatrix} \begin{bmatrix} \vdots \\ \ddot{u}'_{i,j-1} \\ \ddot{u}'_{i,j} \\ \ddot{u}'_{i,j+1} \\ \vdots \end{bmatrix} + \begin{bmatrix} \ddots & \vdots & \vdots & \vdots & \\ \cdots & D_{11}^{**} & D_{12}^{**} & D_{13}^{**} & \cdots \\ \cdots & D_{21}^{**} & D_{22}^{**} & D_{23}^{**} & \cdots \\ \cdots & D_{31}^{**} & D_{32}^{**} & D_{33}^{**} & \cdots \\ & \vdots & \vdots & \vdots & \ddots \end{bmatrix} \begin{bmatrix} \vdots \\ \dot{u}'_{i,j-1} \\ \dot{u}'_{i,j} \\ \dot{u}'_{i,j+1} \\ \vdots \end{bmatrix}$$

$$+ \begin{bmatrix} \ddots & \vdots & \vdots & \vdots & \\ \cdots & K_{11}^{**} & K_{12}^{**} & K_{13}^{**} & \cdots \\ \cdots & K_{21}^{**} & K_{22}^{**} & K_{23}^{**} & \cdots \\ \cdots & K_{31}^{**} & K_{32}^{**} & K_{33}^{**} & \cdots \\ & \vdots & \vdots & \vdots & \ddots \end{bmatrix} \begin{bmatrix} \vdots \\ u'_{i,j-1} \\ u'_{i,j} \\ u'_{i,j+1} \\ \vdots \end{bmatrix} + \begin{bmatrix} \vdots \\ A_1^{**} \\ A_2^{**} \\ A_3^{**} \\ \vdots \end{bmatrix} = \begin{bmatrix} \vdots \\ F_1^{**} \\ F_2^{**} \\ F_3^{**} \\ \vdots \end{bmatrix},$$

(2.64)

where the vector $\{F^{**}\}$ is

$$\begin{bmatrix} \vdots \\ F_1^{**} \\ F_2^{**} \\ F_3^{**} \\ \vdots \end{bmatrix} = \begin{bmatrix} \vdots & \vdots & \vdots \\ N_{11}^{**} & N_{12}^{**} & N_{13}^{**} \\ N_{21}^{**} & N_{22}^{**} & N_{23}^{**} \\ N_{31}^{**} & N_{32}^{**} & N_{33}^{**} \\ \vdots & \vdots & \vdots \end{bmatrix} \left\{ \begin{bmatrix} \ddot{v}_0 \\ \ddot{u}_0 \\ \ddot{\phi}_0 \end{bmatrix} + \begin{bmatrix} C_{VV}(\omega) & C_{VH}(\omega) & C_{VM}(\omega) \\ C_{HV}(\omega) & C_{HH}(\omega) & C_{HM}(\omega) \\ C_{MV}(\omega) & C_{MH}(\omega) & C_{MM}(\omega) \end{bmatrix} \begin{bmatrix} \ddot{F}_z^b \\ \ddot{F}_x^b \\ \ddot{M}_o^b \end{bmatrix} \right\} + \begin{bmatrix} \vdots \\ B_1 \\ B_2 \\ B_3 \\ \vdots \end{bmatrix}.$$

(2.65)

The matrices ($[M^{**}]$, $[D^{**}]$, $[K^{**}]$, and $[N^{**}]$), and the vectors ($\{A^{**}\}$ and $\{\ddot{F}_b\}$) are functions of $\partial^3 u'_{i,j}/\partial t^3$, $\ddot{u}'_{i,j}$, $\dot{u}'_{i,j}$ and $u'_{i,j}$. Therefore, if the compliance matrix for the foundation is known, the whole problem can be solved by using equations (2.64) and (2.65). These equations can be solved by a numerical method rather than by classical methods because they are highly nonlinear equations.

In this study, only vertically incident waves will be considered for analysis. The input wave is assumed to be the same as the free-field motion, and the diffracted and scattered waves will be ignored. The deformations will be assumed to be small, and therefore the geometric nonlinearity will not be considered. The vertical and rocking motions of the system will be the subjects of future studies. With those restrictions, equation (2.65) becomes

$$\begin{bmatrix} \vdots \\ F_1^{**} \\ F_2^{**} \\ F_3^{**} \\ \vdots \end{bmatrix} = \begin{bmatrix} \vdots \\ -m_s \cdot h_{i,j-1} \\ -m_p \cdot h_{i,j} \\ -m_s \cdot h_{i,j+1} \\ \vdots \end{bmatrix} \left\{ \ddot{u}_0 + C_{HH}(\omega) \cdot \ddot{F}_x^b \right\}, \tag{2.66}$$

where the second derivative of the resultant horizontal force $\ddot{F}_x^b$ is

$$\ddot{F}_x^b = \begin{bmatrix} k_{1,1}, & \cdots, & k_{n,1}, & k_{1,m+1}, & \cdots, & k_{n,m+1} \end{bmatrix} \begin{bmatrix} \ddot{u}'_{1,1} \\ \vdots \\ \ddot{u}'_{n,1} \\ \ddot{u}'_{1,m} \\ \vdots \\ \ddot{u}'_{n,m} \end{bmatrix}$$

$$+ \begin{bmatrix} c_{1,1}, & \cdots, & c_{n,1}, & c_{1,m+1}, & \cdots, & c_{n,m+1} \end{bmatrix} \begin{bmatrix} \partial^3 u'_{1,1} / \partial t^3 \\ \vdots \\ \partial^3 u'_{n,1} / \partial t^3 \\ \partial^3 u'_{1,m} / \partial t^3 \\ \vdots \\ \partial^3 u'_{n,m} / \partial t^3 \end{bmatrix}$$

$$+\begin{Bmatrix} EI\dfrac{\partial^2}{\partial t^2}\left(\dfrac{\partial^4 u'_{1,1}}{\partial z'^4}\right)+EI\dfrac{\partial^2}{\partial t^2}\left(\dfrac{\partial^4 u'_{1,3}}{\partial z'^4}\right)+\cdots+EI\dfrac{\partial^2}{\partial t^2}\left(\dfrac{\partial^4 u'_{1,m}}{\partial z'^4}\right) \\ +\ddot{F}^{bottom}_{d\_1,2}+\ddot{F}^{bottom}_{d\_1,4}+\cdots+\ddot{F}^{bottom}_{d\_1,m-1} \end{Bmatrix} .$$

(2.67)

By using equation (2.66) and neglecting the rotational and vertical displacement, equation (2.64) can be simplified as

$$\begin{bmatrix} \ddots & \vdots & \vdots & \vdots & \\ \cdots & m_s\cdot h_{i,j-1} & 0 & 0 & \cdots \\ \cdots & 0 & m_p\cdot h_{i,j} & 0 & \cdots \\ \cdots & 0 & 0 & m_s\cdot h_{i,j+1} & \cdots \\ & \vdots & \vdots & \vdots & \ddots \end{bmatrix}\begin{bmatrix} \vdots \\ \ddot{u}'_{i,j-1} \\ \ddot{u}'_{i,j} \\ \ddot{u}'_{i,j+1} \\ \vdots \end{bmatrix}$$

$$+\begin{bmatrix} \ddots & \vdots & \vdots & \vdots & \\ \cdots & (c_{i,j-1}+c_{i,j})\cdot h_{i,j-1} & -c_{i,j}\cdot h_{i,j-1} & 0 & \cdots \\ \cdots & -c_{i,j}\cdot h_{i,j} & (c_{i,j}+c_{i,j+1})\cdot h_{i,j} & -c_{i,j+1}\cdot h_{i,j} & \cdots \\ \cdots & 0 & -c_{i,j+1}\cdot h_{i,j+1} & (c_{i,j+1}+c_{i,j+2})\cdot h_{i,j+1} & \cdots \\ & \vdots & \vdots & \vdots & \ddots \end{bmatrix}\begin{bmatrix} \vdots \\ \dot{u}'_{i,j-1} \\ \dot{u}'_{i,j} \\ \dot{u}'_{i,j+1} \\ \vdots \end{bmatrix}$$

$$+\begin{bmatrix} \ddots & \vdots & \vdots & \vdots & \\ \cdots & (k_{i,j-1}+k_{i,j})\cdot h_{i,j-1} & -k_{i,j}\cdot h_{i,j-1} & 0 & \cdots \\ \cdots & -k_{i,j}\cdot h_{i,j} & (k_{i,j}+k_{i,j+1})\cdot h_{i,j} & -k_{i,j+1}\cdot h_{i,j} & \cdots \\ \cdots & 0 & -k_{i,j+1}\cdot h_{i,j+1} & (k_{i,j+1}+k_{i,j+2})\cdot h_{i,j+1} & \cdots \\ & \vdots & \vdots & \vdots & \ddots \end{bmatrix}\begin{bmatrix} \vdots \\ u'_{i,j-1} \\ u'_{i,j} \\ u'_{i,j+1} \\ \vdots \end{bmatrix}$$

$$+\begin{bmatrix} \vdots \\ F_{d\_i,j-1}\cdot h_{i,j-1} \\ EI(\partial^4 u'_{i,j}/\partial z'^4)\cdot h_{i,j} \\ F_{d\_i,j+1}\cdot h_{i,j+1} \\ \vdots \end{bmatrix}+\begin{bmatrix} \vdots \\ m_s\cdot h_{i,j-1} \\ m_p\cdot h_{i,j} \\ m_s\cdot h_{i,j+1} \\ \vdots \end{bmatrix}\left\{C_{HH}(\omega)\cdot \ddot{F}^b_x\right\}=\begin{bmatrix} \vdots \\ -m_s\cdot h_{i,j-1}\cdot \ddot{u}_0 \\ -m_p\cdot h_{i,j}\cdot \ddot{u}_0 \\ -m_s\cdot h_{i,j+1}\cdot \ddot{u}_0 \\ \vdots \end{bmatrix}.$$

(2.68)

The vertical distance of the above equation $h_{i,j}$, can be canceled out, and by using equation (2.67) the equilibrium equation (2.68) becomes

$$\begin{bmatrix} \ddots & \vdots & \vdots & \vdots & \\ \cdots & m_s & 0 & 0 & \cdots \\ \cdots & 0 & m_p & 0 & \cdots \\ \cdots & 0 & 0 & m_s & \cdots \\ & \vdots & \vdots & \vdots & \ddots \end{bmatrix} \begin{bmatrix} \vdots \\ \ddot{u}'_{i,j-1} \\ \ddot{u}'_{i,j} \\ \ddot{u}'_{i,j+1} \\ \vdots \end{bmatrix}$$

$$+ \begin{bmatrix} \ddots & \vdots & \vdots & \vdots & \\ \cdots & (c_{i,j-1}+c_{i,j}) & -c_{i,j} & 0 & \cdots \\ \cdots & -c_{i,j} & (c_{i,j}+c_{i,j+1}) & -c_{i,j+1} & \cdots \\ \cdots & 0 & -c_{i,j+1} & (c_{i,j+1}+c_{i,j+2}) & \cdots \\ & \vdots & \vdots & \vdots & \ddots \end{bmatrix} \begin{bmatrix} \vdots \\ \dot{u}'_{i,j-1} \\ \dot{u}'_{i,j} \\ \dot{u}'_{i,j+1} \\ \vdots \end{bmatrix}$$

$$+ \begin{bmatrix} \ddots & \vdots & \vdots & \vdots & \\ \cdots & (k_{i,j-1}+k_{i,j}) & -k_{i,j} & 0 & \cdots \\ \cdots & -k_{i,j} & (k_{i,j}+k_{i,j+1}) & -k_{i,j+1} & \cdots \\ \cdots & 0 & -k_{i,j+1} & (k_{i,j+1}+k_{i,j+2}) & \cdots \\ & \vdots & \vdots & \vdots & \ddots \end{bmatrix} \begin{bmatrix} \vdots \\ u'_{i,j-1} \\ u'_{i,j} \\ u'_{i,j+1} \\ \vdots \end{bmatrix} + \begin{bmatrix} \vdots \\ F_{d\_i,j-1} \\ EI(\partial^4 u'_{i,j}/\partial z'^4) \\ F_{d\_i,j+1} \\ \vdots \end{bmatrix}$$

$$+ C_{HH}(\omega) \cdot \begin{bmatrix} \vdots \\ m_s \\ m_p \\ m_s \\ \vdots \end{bmatrix} \begin{Bmatrix} k_{1,1}\ddot{u}'_{1,1} + \cdots + k_{n,1}\ddot{u}'_{n,1} + k_{1,m+1}\ddot{u}'_{1,m} + \cdots + k_{n,m+1}\ddot{u}'_{n,m} \\ + c_{1,1}\dfrac{\partial^3 u'_{1,1}}{\partial t^3} + \cdots + c_{n,1}\dfrac{\partial^3 u'_{n,1}}{\partial t^3} + \cdots + c_{1,m+1}\dfrac{\partial^3 u'_{1,m}}{\partial t^3} + \cdots + c_{n,m+1}\dfrac{\partial^3 u'_{n,m}}{\partial t^3} \\ + EI\dfrac{\partial^2}{\partial t^2}\left(\dfrac{\partial^4 u'_{1,1}}{\partial z'^4}\right) + \cdots + EI\dfrac{\partial^2}{\partial t^2}\left(\dfrac{\partial^4 u'_{1,m}}{\partial z'^4}\right) \\ + \ddot{F}^{bottom}_{d\_1,2} + \cdots + \ddot{F}^{bottom}_{d\_1,m-1} \end{Bmatrix}$$

$$= \begin{bmatrix} \vdots \\ -m_s \cdot \ddot{u}_0 \\ -m_p \cdot \ddot{u}_0 \\ -m_s \cdot \ddot{u}_0 \\ \vdots \end{bmatrix}. \qquad (2.69)$$

If the soil in the half space is assumed to be infinitely stiff, the terms of compliance matrix are zero - i.e., the soil-structure interaction of the box is ignored. Then equation (2.69) becomes (2.70), which is same as equation (2.9) and which will be used in all computations in this dissertation.

$$\begin{bmatrix} \ddots & \vdots & \vdots & \vdots & \\ \cdots & m_s & 0 & 0 & \cdots \\ \cdots & 0 & m_p & 0 & \cdots \\ \cdots & 0 & 0 & m_s & \cdots \\ & \vdots & \vdots & \vdots & \ddots \end{bmatrix} \begin{bmatrix} \vdots \\ \ddot{u}'_{i,j-1} \\ \ddot{u}'_{i,j} \\ \ddot{u}'_{i,j+1} \\ \vdots \end{bmatrix}$$

$$+ \begin{bmatrix} \ddots & \vdots & \vdots & \vdots & \\ \cdots & (c_{i,j-1}+c_{i,j}) & -c_{i,j} & 0 & \cdots \\ \cdots & -c_{i,j} & (c_{i,j}+c_{i,j+1}) & -c_{i,j+1} & \cdots \\ \cdots & 0 & -c_{i,j+1} & (c_{i,j+1}+c_{i,j+2}) & \cdots \\ & \vdots & \vdots & \vdots & \ddots \end{bmatrix} \begin{bmatrix} \vdots \\ \dot{u}'_{i,j-1} \\ \dot{u}'_{i,j} \\ \dot{u}'_{i,j+1} \\ \vdots \end{bmatrix}$$

$$+ \begin{bmatrix} \ddots & \vdots & \vdots & \vdots & \\ \cdots & (k_{i,j-1}+k_{i,j}) & -k_{i,j} & 0 & \cdots \\ \cdots & -k_{i,j} & (k_{i,j}+k_{i,j+1}) & -k_{i,j+1} & \cdots \\ \cdots & 0 & -k_{i,j+1} & (k_{i,j+1}+k_{i,j+2}) & \cdots \\ & \vdots & \vdots & \vdots & \ddots \end{bmatrix} \begin{bmatrix} \vdots \\ u'_{i,j-1} \\ u'_{i,j} \\ u'_{i,j+1} \\ \vdots \end{bmatrix}$$

$$+ \begin{bmatrix} \vdots \\ F_{d\_i,j-1} \\ EI(\partial^4 u'_{i,j}/\partial z'^4) \\ F_{d\_i,j+1} \\ \vdots \end{bmatrix} = \begin{bmatrix} \vdots \\ -m_s \cdot \ddot{u}_0 \\ -m_p \cdot \ddot{u}_0 \\ -m_s \cdot \ddot{u}_0 \\ \vdots \end{bmatrix}. \qquad (2.70)$$

2.4 Dynamic compliance of proposed model to horizontal excitation

The properties of the proposed model are studied by comparison with compliance functions presented by Luco et al. (1971, 1972) for horizontal oscillation of a rigid disc placed on an elastic half space. When the horizontal force $F_0 \cdot e^{i\omega t}$ acts on the footing, the response is given as

$$u(t) = F_0 \cdot C_{HH}(i\omega) \cdot e^{i\omega t} = F_0 \cdot \left|C_{HH}(i\omega)\right| \cdot e^{i(\omega t + \delta)} \quad , \tag{2.71}$$

where $\left|C_{HH}(i\omega)\right| = \sqrt{[\mathrm{Re}(C_{HH})]^2 + [\mathrm{Im}(C_{HH})]^2}$ and (2.72)

$$\delta = \tan^{-1}\left[\frac{\mathrm{Im}(C_{HH})}{\mathrm{Re}(C_{HH})}\right] \quad , \tag{2.73}$$

where

$\mathrm{Re}(C_{HH})$ = real part of horizontal compliance function

$\mathrm{Im}(C_{HH})$ = imaginary part of horizontal compliance function

F_0 = amplitude of input force

ω = circular frequency of input force

u = displacement.

Figure 2.14 is a plot of the normalized compliance function for the horizontal translation for different amplitudes of input force ($F_0 = 10$ kN, 20 kN, 30 kN, 40 kN, 50 kN, and 60 kN) and for different damping factors in the soil ($\beta_s = 0.02$, 0.03, 0.04, and 0.06). The compliance function by Luco et al. is shown by a thick gray line.

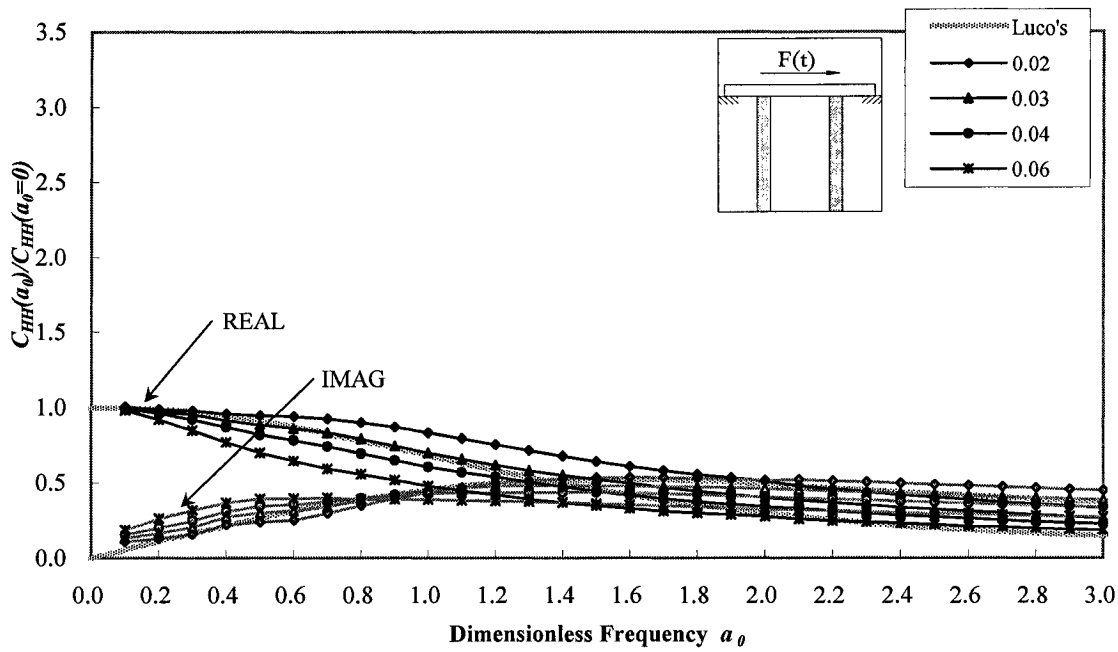

(a) F_0 = 10 kN

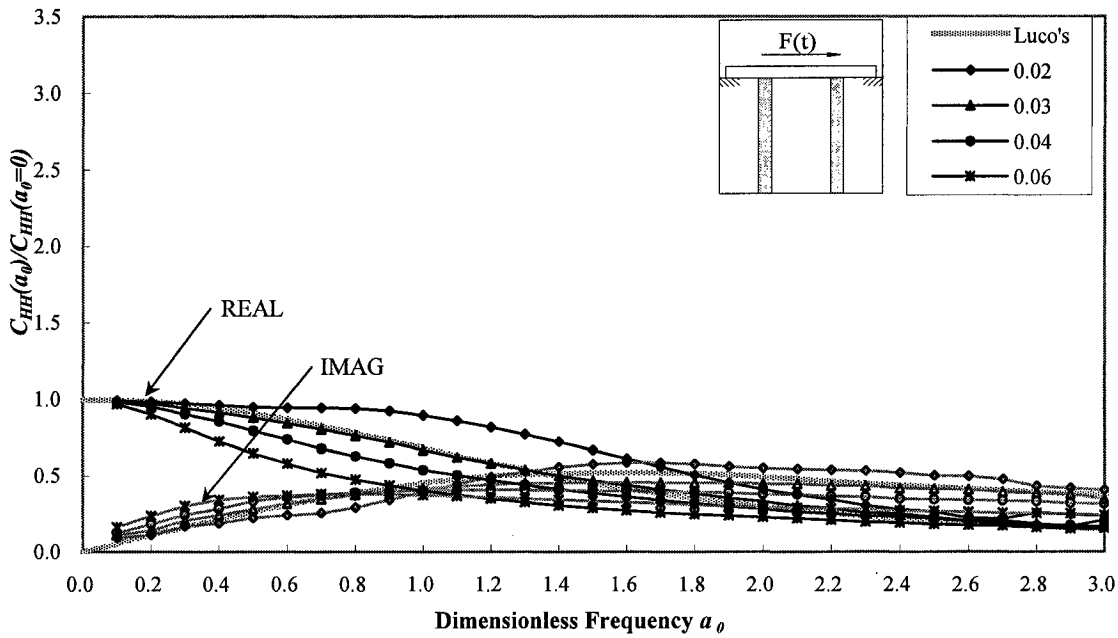

(b) F_0 = 20 kN

Fig. 2.14 Dynamic compliance function of proposed model for different amplitudes of input force.

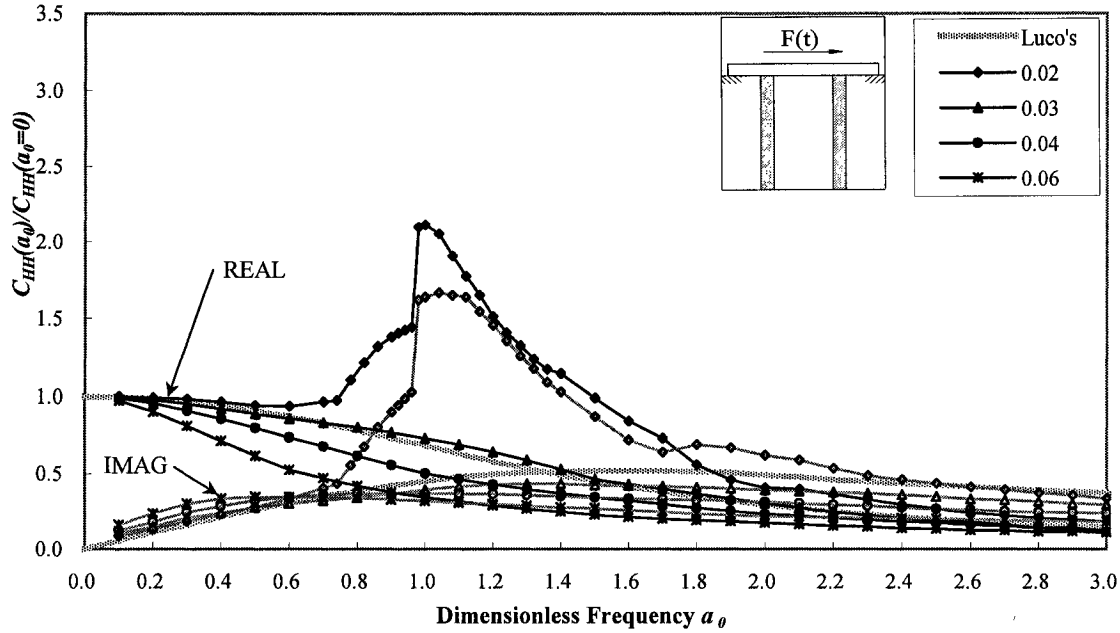

(c) F_0 = 30 kN

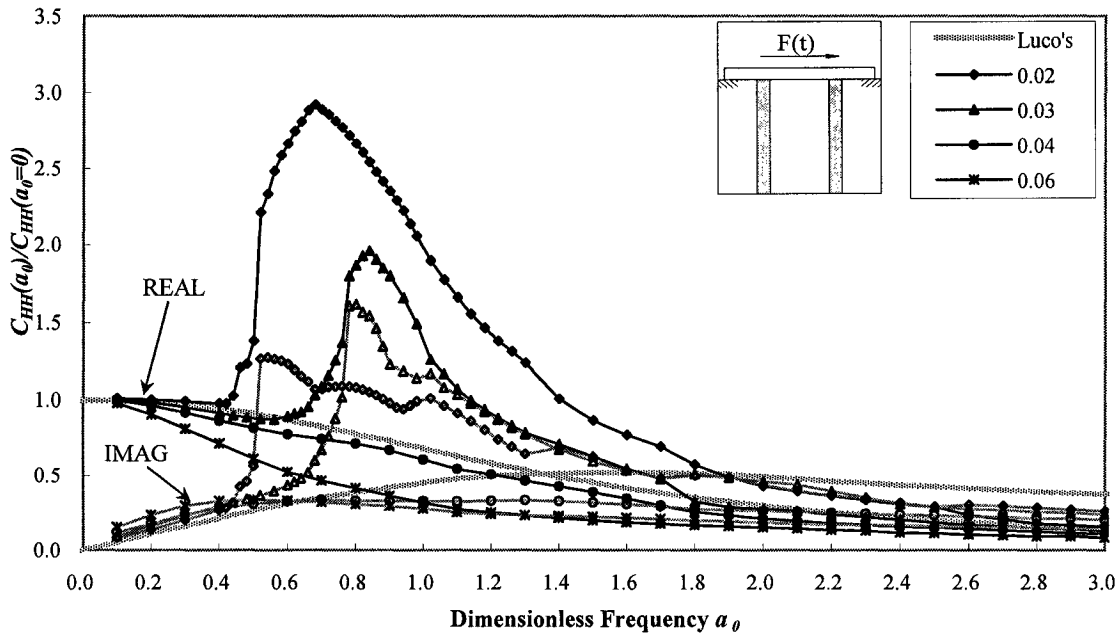

(d) F_0 = 40 kN

Fig. 2.14 Dynamic compliance function of proposed model for different amplitudes of input force. (continued)

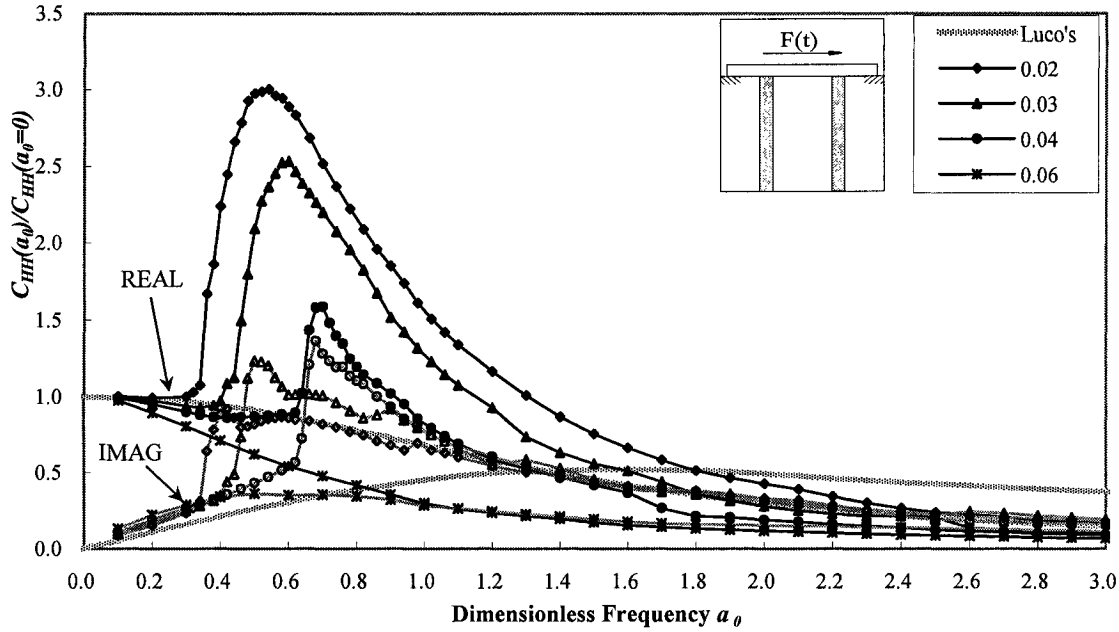

(e) F_0 = 50 kN

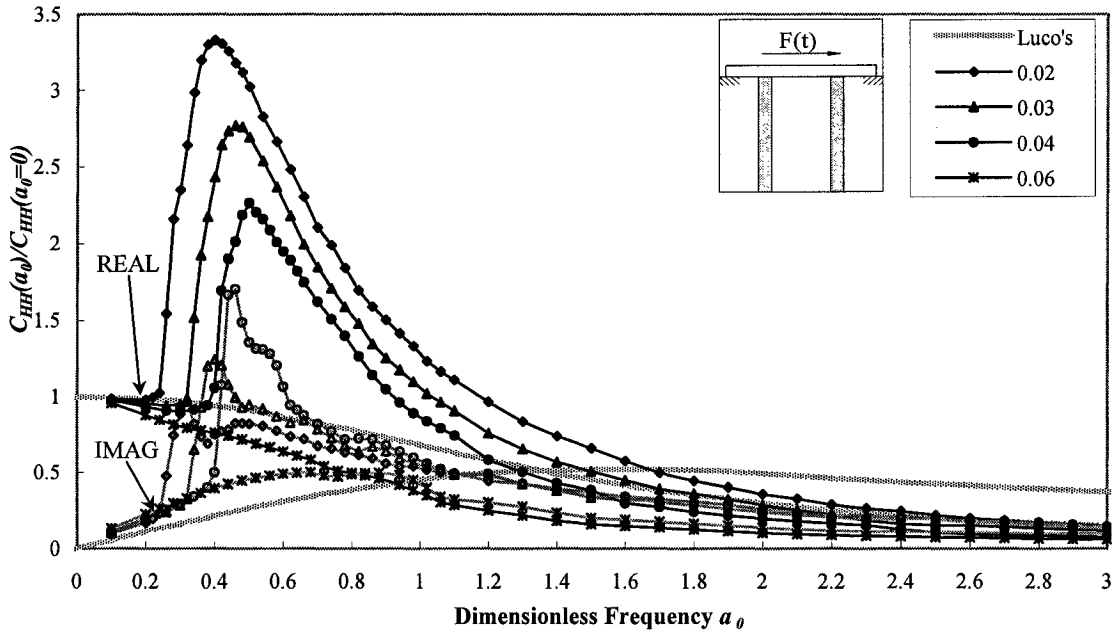

(f) F_0 = 60 kN

Fig. 2.14 Dynamic compliance function of proposed model for different amplitudes of input force. (continued)

Computed compliance functions for $\beta_s = 0.02$, 0.03, 0.04, and 0.06 are plotted by black lines (real part) and gray lines (imaginary line) with rhombus, triangle, circle, and star, respectively. The x axis shows the dimensionless frequency $a_0 = \omega \cdot B / V_s$, where ω is the circular frequency of the input force, B is the length of foundation, and V_s is the velocity of the shear waves. The y axis represents the compliance function that is normalized to its static case (at $a_0 = 0$).

When the amplitude of horizontal force is small ($F_0 = 10\,\text{kN}$), the computed compliance function is very close to the results of Luco et al. (1971, 1972). The total system behaves in the linear elastic range because the input force is not large enough to generate a nonlinear response in the foundation. However, if large amplitudes of force are applied to the system ($F_0 = 30\,\text{kN} \sim 60\,\text{kN}$), the real part of the compliance function can increase significantly. Sudden increases in the imaginary part of the compliance function are also found to the near peak in the real part of compliance.

Duffing presented the response curve for the system with a nonlinear restoring-force function (Jacobsen and Ayre, 1958; Meirovitch, 1986). Equation (2.74) shows the Duffing equation for an undamped system with a nonlinear restoring-force function:

$$m\ddot{x} + k\left(x \pm \kappa^2 x^3\right) = F\cos\omega t \quad , \tag{2.74}$$

where $\left(x \pm \kappa^2 x^3\right)$ is the nonlinear restoring force and κ^2 is a nonlinear factor. If the sign of the restoring force is *plus*, the system has a hardening spring, while a *minus* sign means that the system is restored by a softening spring (Jacobsen and Ayre, 1958).

Figure 2.15 shows the response curve for the Duffing equation model with damping and a softening spring. For a softening-spring system, the vertical resonance axis (plotted by gray line) bends toward from ω_0 to a value of low frequency, where ω_0 is the frequency of the system. In contrast, the parabola of the response curve bends to the right in the hardening-spring system. The x axis represents the frequency of force, and the y axis shows the absolute amplitude of response. The curve has a sudden increase in amplitude, which is similar to the results of this study. As the frequency of force increases from a small value, the amplitude increases until it reaches point 2 and jumps to point 3, from which it decreases with an increase in the frequency. On the other hand, if the frequency decreases form a large value, the amplitude increases until point 4 and experiences a sudden jump to point 1 on the response curve, from which it decreases with a decrease in the frequency.

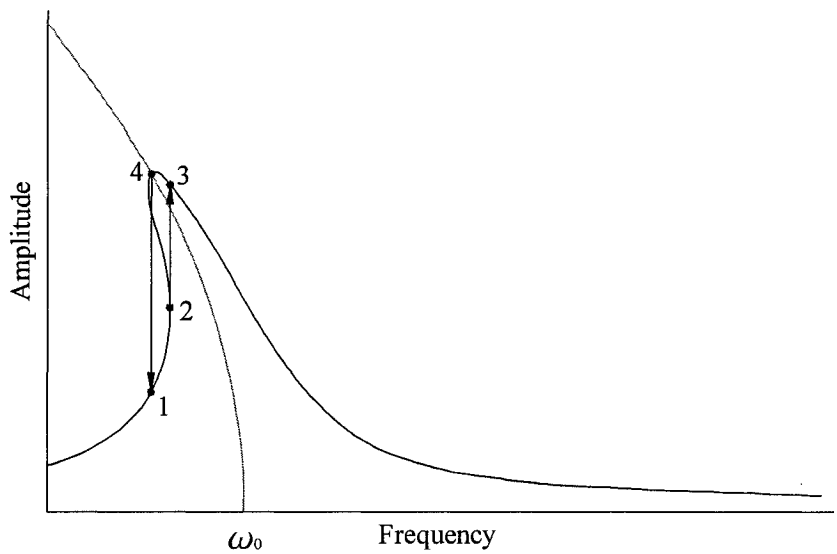

Fig. 2.15 Response curve for Duffing equation model with damping and softening spring.

2.5 Wave excitation

A single pulse is used as the input wave in this study, and the incident wave is assumed to propagate vertically toward the ground surface. When the disturbance strikes the ground surface, the wave is reflected and propagates back (downward). It is assumed that the incident wave is completely reflected, and so the maximum amplitude of the incident wave is doubled at the ground surface. The wave motion can be represented by a pulse as shown in equation (2.75). The velocity of the shear wave depends upon the properties of the soil. Equation (2.76) shows the velocity of the incident wave, and Figure 2.16 illustrates the wave motion in time.

$$u_g(z,t) = U_{g0} \cdot e^{i\omega\left(t-\frac{z}{V_s}\right)}, \quad 0 \le t - \frac{z}{V_s} \le \frac{\pi}{\omega} \quad , \tag{2.75}$$

where

U_{g0} = amplitude of the wave

ω = circular frequency

V_s = velocity of shear wave , and

$$V_s = \sqrt{\frac{G_s}{\rho}} \quad , \tag{2.76}$$

where

G_s = shear modulus of soil

ρ = mass density of soil.

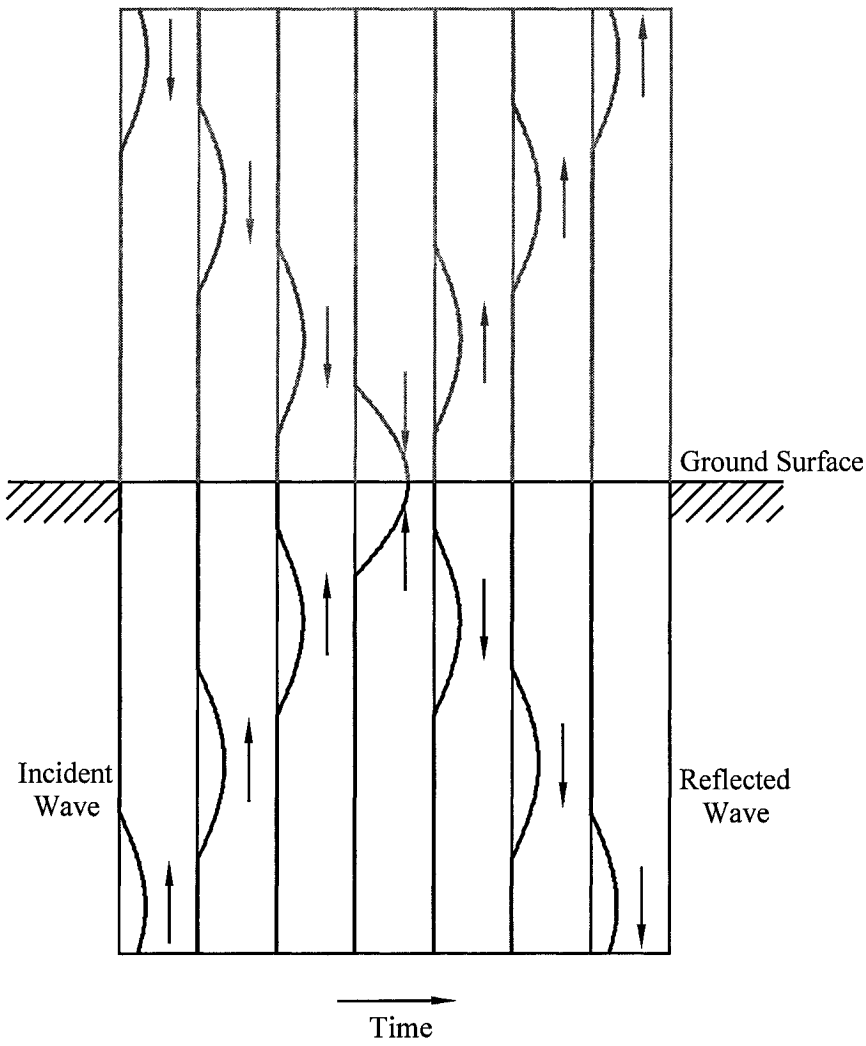

Fig. 2.16 Ground motion caused by vertically propagating wave.

2.6 Derivation of energy equations

As the incident waves propagate into the system, a portion of the incident wave energy is lost by scattering, while the rest is transmitted into the system. To derive the equations of energy balance, the dynamic equilibrium equation of the system (equation (2.9)) is integrated with respect to u from the time that the ground motion starts. Integrating the inertial force term in equation (2.9) gives

$$\begin{aligned}
&\int m_p \cdot \ddot{u}_{t_1} du_1 + \int m_s \cdot \ddot{u}_{t_2} du_2 + \cdots + \int m_p \cdot \ddot{u}_{t_m} du_m \\
&= \int m_p \cdot \ddot{u}_{t_1} \left(du_{t_1} - du_g\right) + \int m_s \cdot \ddot{u}_{t_2} \left(du_{t_2} - du_g\right) + \cdots + \int m_p \cdot \ddot{u}_{t_m} \left(du_{t_m} - du_g\right) \\
&= \left[\int m_p \cdot \frac{d\dot{u}_{t_1}}{dt} du_{t_1} - \int m_p \cdot \ddot{u}_{t_1} du_g\right] + \left[\int m_s \cdot \frac{d\dot{u}_{t_2}}{dt} du_{t_2} - \int m_s \cdot \ddot{u}_{t_2} du_g\right] + \\
&\qquad \cdots + \left[\int m_p \cdot \frac{d\dot{u}_{t_m}}{dt} du_{t_m} - \int m_p \cdot \ddot{u}_{t_m} du_g\right] \\
&= \left[\frac{1}{2} m_p \cdot \dot{u}_{t_1}{}^2 - \int m_p \cdot \ddot{u}_{t_1} du_g\right] + \left[\frac{1}{2} m_s \cdot \dot{u}_{t_2}{}^2 - \int m_s \cdot \ddot{u}_{t_2} du_g\right] + \\
&\qquad \cdots + \left[\frac{1}{2} m_p \cdot \dot{u}_{t_m}{}^2 - \int m_p \cdot \ddot{u}_{t_m} du_g\right] \\
&= \left[\frac{1}{2} m_p \cdot \dot{u}_{t_1}{}^2 + \frac{1}{2} m_s \cdot \dot{u}_{t_2}{}^2 + \cdots + \frac{1}{2} m_p \cdot \dot{u}_{t_m}{}^2\right] \\
&\qquad - \left[\int m_p \cdot \ddot{u}_{t_1} du_g + \int m_s \cdot \ddot{u}_{t_2} du_g + \cdots + \int m_p \cdot \ddot{u}_{t_m} du_g\right].
\end{aligned} \tag{2.77}$$

The first term in the above equation is the absolute kinetic energy E_K, while the second term is the energy that gets into the system, E_I. This gives

$$E_K = \frac{1}{2}\left[m_p \cdot \dot{u}_{t\_1}^2 + m_s \cdot \dot{u}_{t\_2}^2 + \cdots + m_p \cdot \dot{u}_{t\_m}^2\right] \tag{2.78}$$

$$E_I = \int\left[m_p \cdot \ddot{u}_{t\_1}^2 + m_s \cdot \ddot{u}_{t\_2}^2 + \cdots + m_p \cdot \ddot{u}_{t\_m}^2\right] du_g, \tag{2.79}$$

where

$u_{t\_j} = u_j + u_g$

u_{t_j} = absolute displacement

u_j = relative displacement

u_g = ground displacement

m_p = mass of pile

m_s = mass of soil.

The elastic strain energy of the pile E_S^{pile} can be evaluated by integrating with respect to the time the first term in equation (2.9):

$$\begin{aligned}&\int E_p I_p \frac{\partial^4 u_1}{\partial z^4} du_1 + \int E_p I_p \frac{\partial^4 u_3}{\partial z^4} du_3 + \cdots + \int E_p I_p \frac{\partial^4 u_m}{\partial z^4} du_m \\ &= \int E_p I_p \frac{\partial^4 u_1}{\partial z^4} \frac{du_1}{dt} dt + \int E_p I_p \frac{\partial^4 u_3}{\partial z^4} \frac{du_3}{dt} dt + \cdots + \int E_p I_p \frac{\partial^4 u_m}{\partial z^4} \frac{du_m}{dt} dt,\end{aligned} \tag{2.80}$$

$$E_S^{pile} = \int E_p I_p \frac{\partial^4 u_1}{\partial z^4} \cdot \dot{u}_1 dt + \int E_p I_p \frac{\partial^4 u_3}{\partial z^4} \cdot \dot{u}_3 dt + \cdots + \int E_p I_p \frac{\partial^4 u_m}{\partial z^4} \cdot \dot{u}_m dt, \tag{2.81}$$

where u_j = relative displacement

$\dot{u}_j$ = relative velocity

$E_p I_p$ = flexural rigidity of pile

The damping energy dissipated by the dashpots E_D^{soil}, and the strain energy E_S^{soil} of the soil in the near field are derived from integrating the third and fourth terms in equation (2.9) as

$$\int c_1 \cdot (\dot{u}_1)(du_1) + \int c_2 \cdot (\dot{u}_2 - \dot{u}_1)(du_2 - du_1) + \cdots + \int c_{m+1} \cdot (-\dot{u}_m)(-du_m)$$
$$= \int c_1 \cdot (\dot{u}_1)\left(\frac{du_1}{dt}\right) + \int c_2 \cdot (\dot{u}_2 - \dot{u}_1)\left(\frac{du_2}{dt} - \frac{du_1}{dt}\right) + \cdots + \int c_{m+1} \cdot (-\dot{u}_m)\left(-\frac{du_m}{dt}\right)$$

(2.82)

$$E_D^{soil} = \int c_1 \cdot (\dot{u}_1)(\dot{u}_1)dt + \int c_2 \cdot (\dot{u}_2 - \dot{u}_1)(\dot{u}_2 - \dot{u}_1)dt + \cdots + \int c_{m+1} \cdot (-\dot{u}_m)(-\dot{u}_m)dt,$$

(2.83)

where $\dot{u}_j$ = relative velocity

c_j = damping coefficient of soil in the near field.

$$\int k_1 \cdot (u_1)(du_1) + \int k_2 \cdot (u_2 - u_1)(du_2 - du_1) + \cdots + \int k_{m+1} \cdot (-u_m)(-du_m)$$
$$= \int k_1 \cdot (u_1)\left(\frac{du_1}{dt}\right) + \int k_2 \cdot (u_2 - u_1)\left(\frac{du_2}{dt} - \frac{du_1}{dt}\right) + \cdots + \int k_{m+1} \cdot (-u_m)\left(-\frac{du_m}{dt}\right)$$

(2.84)

$$E_S^{soil} = \int k_1 \cdot (u_1)(\dot{u}_1)dt + \int k_2 \cdot (u_2 - u_1)(\dot{u}_2 - \dot{u}_1)dt + \cdots + \int k_{m+1} \cdot (-u_m)(-\dot{u}_m)dt,$$

(2.85)

where u_j = relative displacement

$\dot{u}_j$ = relative velocity

k_j = stiffness of soil in the near field.

The energy dissipated by the friction of soil blocks E_F^{soil} is derived as

$$\begin{aligned} &\int F_{d\_2} du_2 + \int F_{d\_4} du_4 + \cdots + \int F_{d\_m-1} du_4 \\ &= \int F_{d\_2} \frac{du_2}{dt} dt + \int F_{d\_4} \frac{du_4}{dt} dt + \cdots + \int F_{d\_m-1} \frac{du_{m-1}}{dt} dt \end{aligned} \tag{2.86}$$

$$E_F^{soil} = \int F_{d\_2} \cdot \dot{u}_2 dt + \int F_{d\_4} \cdot \dot{u}_4 dt + \cdots + \int F_{d\_m-1} \cdot \dot{u}_{m-1} dt\,, \tag{2.87}$$

where

$\dot{u}_j$ = relative velocity

F_{d_j} = friction force of soil blocks.

Thus, the energy balance equation with all components included can be written as

$$E_K(t) + E_S^{pile}(t) + E_D^{soil}(t) + E_S^{soil}(t) + E_F^{soil}(t) = E_I(t)\,, \tag{2.88}$$

where

$E_K(t)$ = system kinetic energy

$E_S^{pile}(t)$ = strain energy of the piles

$E_S^{soil}(t)$ = strain energy of the soil in the near field

$E_D^{soil}(t)$ = energy dissipated by dashpots of the soil in the near field

$E_F^{soil}(t)$ = energy dissipated by friction of the soil block

$E_I(t)$ = energy that gets into the system.

3. Application of proposed pile-soil-pile interaction model

The proposed model will be used to analyze the nonlinear dynamic response of a pile-soil-pile system considering the nonlinearity of the soil and the interaction between piles. The steel piles are used in computation. The soil is modeled by distributed nonlinear springs and viscous dashpots along the pile length to resist the lateral motion. Piles and soil are divided into segments with the same number and length, and a vertically propagating pulse is used as input wave. The shape of the pulse depends upon velocity, frequency, and amplitude of the wave. The characteristics of the input wave are presented in section 3.2.

3.1 Properties of the piles and soil

The piles are assumed to be steel pipes with a circular cross section that behave in a linear elastic range. The properties of the piles are shown in Table 3.1. Piles in the grouped pile foundation are connected with a massless rigid pile cap, which is allowed to translate only in the horizontal direction and is not in contact with the soil layer. The arrangement of piles in 2 x 2, 4 x 4, and 6 x 6 pile group systems is shown in figure 3.1. Piles are named as 1st pile to 6th pile by their position. The space between piles(s) is determined by the pile-spacing ratio (s/d), which will be variable from 1.5 to 10.5.

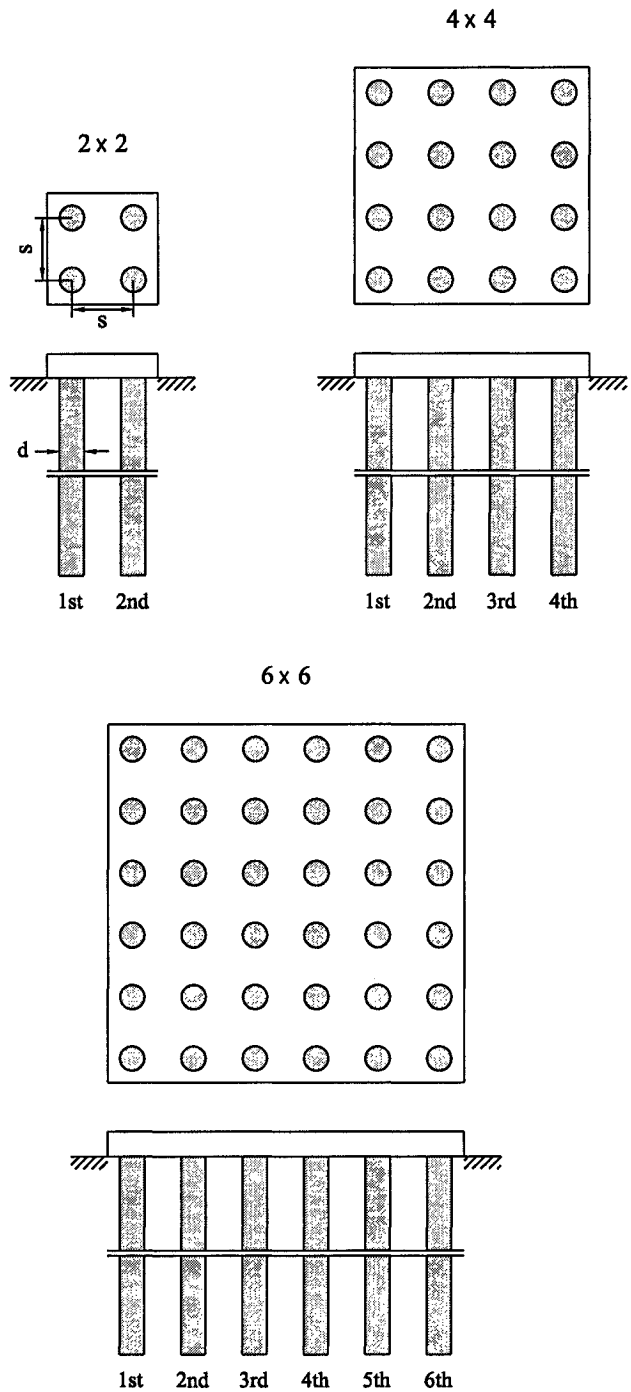

Fig. 3.1 Arrangement of piles in 2 x 2, 4 x 4, and 6 x 6 grouped pile systems.

Table 3.1 Properties of the piles*

L_p (m)	10.0
d_p (m)	0.254
t_p (m)	0.00556
E_p (kN/m^2)	2.00E+08
I_p (m^4)	3.35E-05
A_p (m^2)	4.40E-03

*

L_p = total length (m),

d_p = outside diameter (m),

t_p = wall thickness (m),

E_p = Young's modulus (kN/m^2),

I_p = moment of inertia (m^4),

A_p = cross-section area (m^2).

The grouped pile system is assumed to be placed in 3 types of soil - stiff, medium, and soft. Table 3.2 shows the properties of each soil. Poisson's ratio of the soil is assumed to be $\nu = 0.4$.

Table 3.2 Properties of the soil*

soil type	E_s (kN/m^2)	G_s (kN/m^2)	Vs (m/s)
stiff	402789	143853	280.0
medium	100697	35963	140.0
soft	25174	8991	70.0

*

E_s = Young's modulus of soil (kN/m^2),

G_s = shear modulus of soil (kN/m^2),

V_s = velocity of shear wave (m/s) $= \sqrt{\frac{G_s}{\rho}}$,

ρ = mass density of soil.

3.2 Input wave

The characteristics of the input wave are summarized in Table 3.3. The velocities of incident waves that depend upon Young's modulus of soil are 280.0 m/s in stiff soil, 140.0 m/s in medium soil, and 70.0 m/s in soft soil. The amplitude of the wave is assumed to be 0.5 m ($U_{g0} = 0.5\,\text{m}$), and three kinds of periods ($T_g = 0.2\,\text{s}$, $0.4\,\text{s}$, and $0.8\,\text{s}$) are used in the computation.

Table 3.3. Characteristics of the input wave*

V_s (m/s)	T_g (s)	ω (rad/s)	f (Hz)
280.00	0.2	31.42	5.00
	0.4	15.71	2.50
	0.8	7.85	1.25
140.00	0.2	31.42	5.00
	0.4	15.71	2.50
	0.8	7.85	1.25
70.00	0.2	31.42	5.00
	0.4	15.71	2.50
	0.8	7.85	1.25

*

T_g = period (s),

ω = circular frequency (rad/s),

f = frequency (Hz),

V_s = velocity of wave (m/s) $= \sqrt{\frac{G_s}{\rho}}$.

Figure 3.2 illustrates the movements of a vertically incident wave by plotting the motion for 8 time points. The *y* axis shows the depth below the ground surface to the position of the pile tip. Figure 3.2 (a) shows the movements for a short pulse ($T_g = 0.2\,\text{s}$) that propagates in soft soil ($V_s = 70.0\,\text{m/s}$). The movement of the incident wave is plotted at *t = 0.0325* s, *0.085* s, *0.1375* s, *0.19* s, *0.2425* s, *0.295* s, *0.3475* s, *and 0.4* s. At the beginning of motion (at *t = 0.0325* s, *0.085* s), the upper part of the foundation does not move. The ground surface begins to move around *t = 0.1375* s, and the motion of the reflected wave is seen at *t = 0.19* s. The total amplitude of wave is doubled at the ground level due to reflection of the wave (at *t = 0.2425* s). The incident wave is assumed to reflect totally, without energy loss. The reflected wave moving down form the ground surface is shown in plots at *t = 0.295* s, *0.3475* s, and *0.4* s. The relative motion by wave passage is clearly seen in this case of a high-frequency wave with low velocity.

In Figure 3.2 (b), the movement of the incident wave is plotted at *t = 0.0625* s, *0.175* s, *0.2875* s, *0.4* s, *0.5125* s, *0.625* s, *0.7375* s, *and 0.85* s. Because this incident wave is a long pulse with high velocity ($T_g = 0.8\,\text{s}$, $V_s = 280.0\,\text{m/s}$), the relative motion between the top and bottom parts of the foundation is not big compared with Figure 3.2 (a). The total amplitude of wave motion is again doubled by reflection near *t = 0.4* s.

The movements during vertically incident waves for 9 cases ($V_s = 280.0\,\text{m/s}$, 140.0 m/s, 70.0 m/s, and $T_g = 0.2\,\text{s}$, 0.4 s, 0.8 s) are summarized in Appendix B.

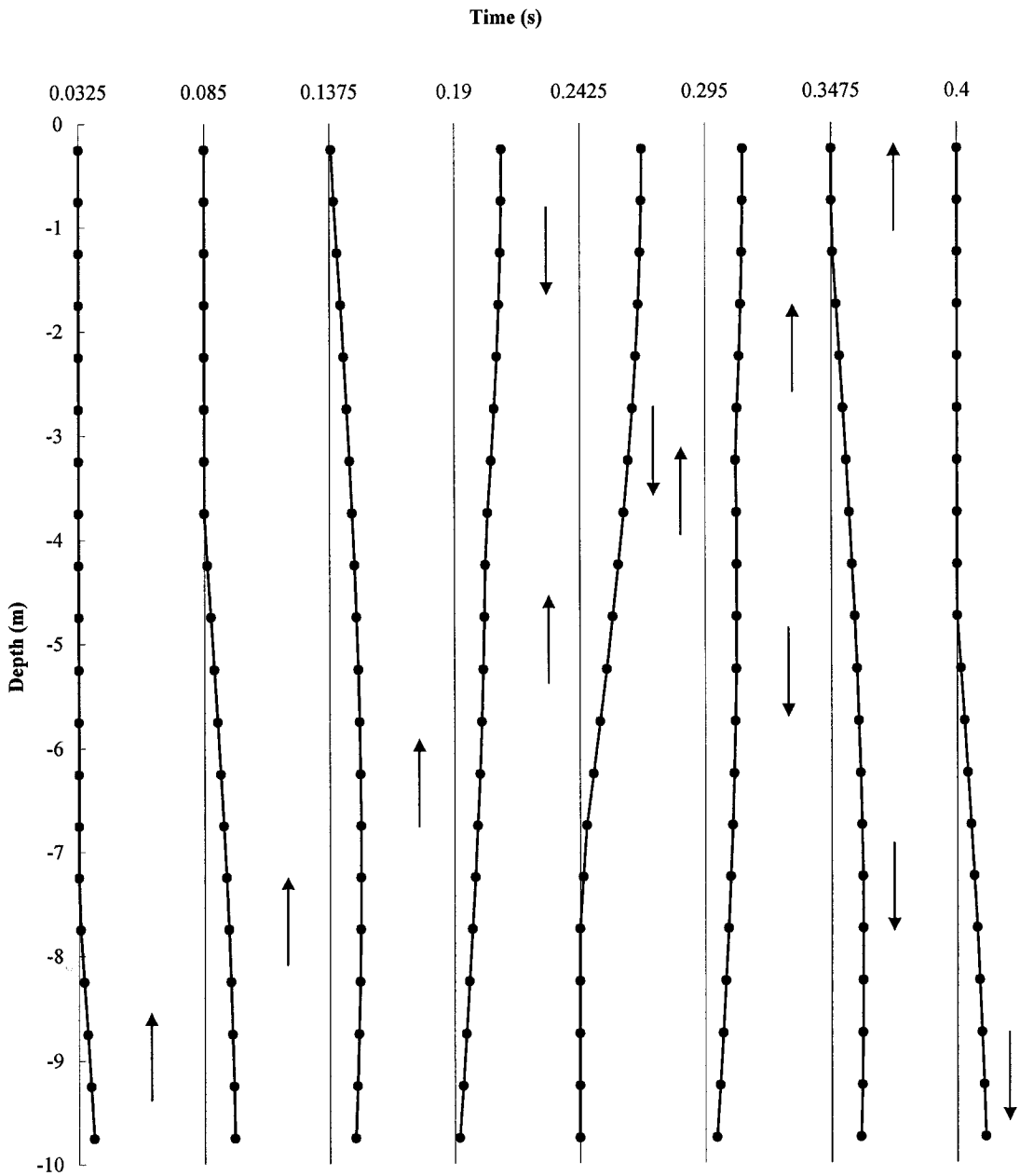

(a) V_s=70.0 m/s, T_g=0.2 s

Fig. 3.2 Movements of a vertically incident wave.

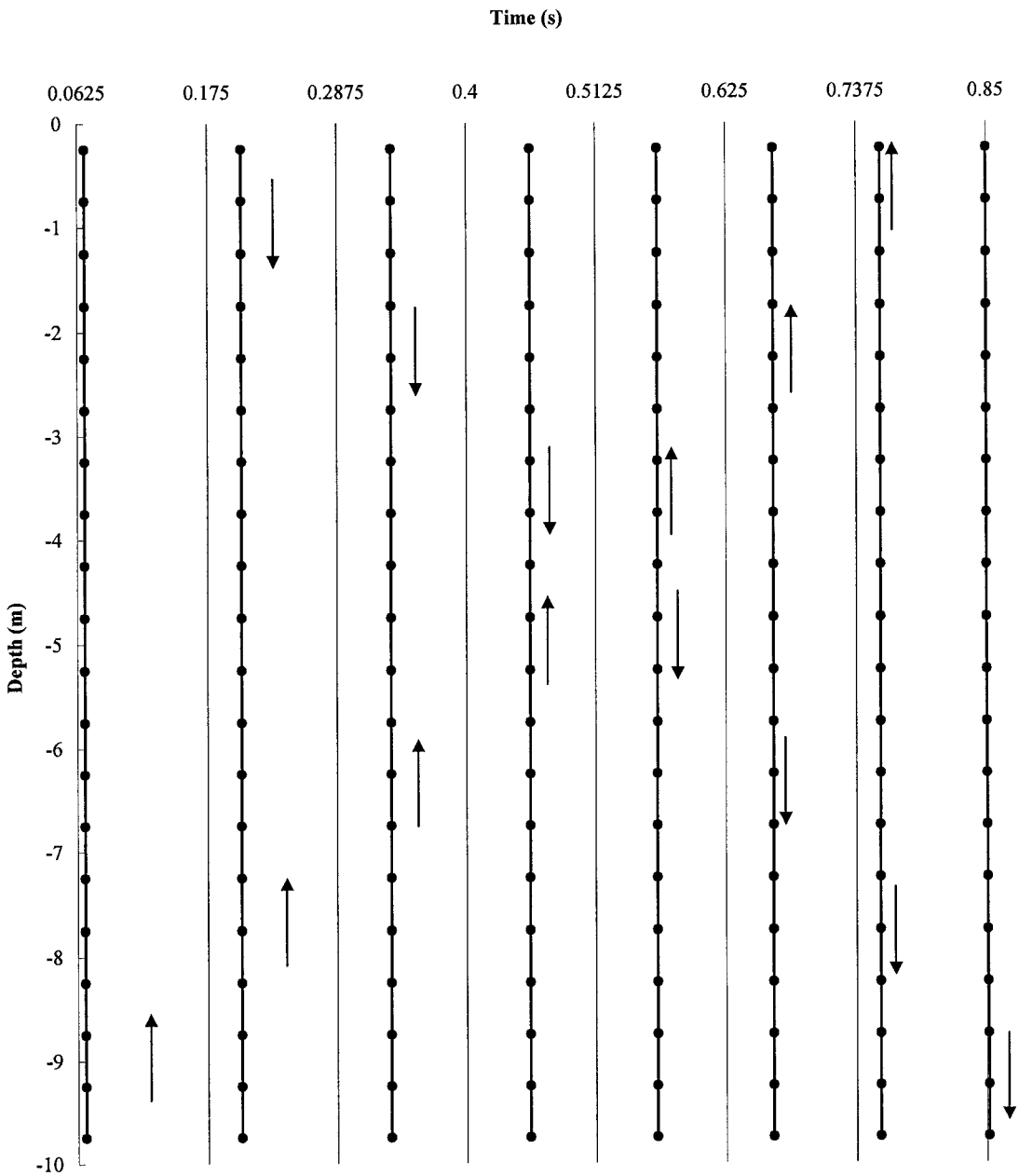

(b) V_s=280.0 m/s, T_g=0.8 s

Fig. 3.2 Movements of a vertically incident wave. (continued)

4. Energy flow in the system

The pile-soil-pile system starts to move when the incident wave propagates into the system. The incident wave energy is dissipated by nonlinear deformation of the soil during pile-soil-pile interaction (Trifunac, 2001).

The total energy transmitted into the system by the incident wave and the sum of all energies associated with the response of the pile-soil-pile system is illustrated in this chapter. The proportions of energy dissipated by nonlinear behavior of the soil near the piles and by the friction of soil blocks located between the piles are described for different pile-spacing ratios. Figure 4.1 shows the schematic illustration for motion of the total system caused by a vertically propagating wave.

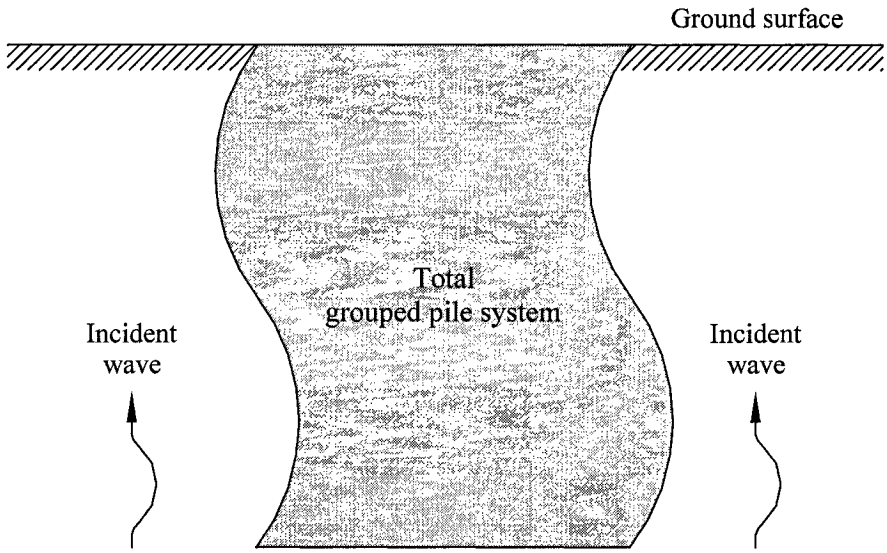

Fig. 4.1 Schematic illustration of motion of a grouped pile system caused by a vertically incident wave.

4.1 Transmitted energy and system energies

Figures 4.2 (a), (b), and (c) show the plot of the total system energies for a 6 x 6 grouped pile system placed in stiff ($V_s = 280.0$ m/s), medium ($V_s = 140.0$ m/s), and soft soil ($V_s = 70.0$ m/s). The grouped pile system is shaken by short input pulse ($T_g = 0.2$ s) and the pile spacing ratio is assumed to be 5.0 ($s/d = 5.0$).

The x axis shows the time in seconds, and y axis shows the energy in $\text{kN} \cdot \text{m}$. The first solid line next to the x axis represents the kinetic energy of the system ($E_K(t)$). The second solid gray line shows the sum of kinetic energy and strain energy of the piles ($E_K(t) + E_S^{pile}(t)$). The third solid line represents the sum of kinetic energy, strain energy of the pile, and energy dissipated by the nonlinear behavior of springs in the near field ($E_K(t) + E_S^{pile}(t) + E_S^{soil}(t)$). The fourth gray line from the bottom illustrates the sum of kinetic energy, strain energy of the pile, and the energy dissipated by springs and dashpots of the soil in the near field ($E_K(t) + E_S^{pile}(t) + E_S^{soil}(t) + E_D^{soil}(t)$). The fifth solid line from the x axis represents the total system energy, including energy dissipated by friction of the soil blocks located between the piles in the grouped pile system ($E_K(t) + E_S^{pile}(t) + E_S^{soil}(t) + E_D^{soil}(t) + E_F^{soil}(t)$). Finally, the thick gray line shows the total energy that gets into the system from the vertically incident wave ($E_I(t)$). This total system energy coincides with the energy dissipated by the system. Properties of the dissipated energy by components in the system (springs, dashpots, and soil blocks) are presented in section 4.2 for various types of grouped pile systems, pile-spacing ratios, and input waves.

The hysteretic energy is dissipated by nonlinear behavior of soil in the near field and by the friction forces of the soil blocks located between the piles. The strain energy of the pile does not participate in dissipating transmitted energy because the pile is assumed to behave in a linear elastic range. The oscillation is damped out quickly (around $t = 0.25$ s) in stiff soil, although it continues to $t = 1.25$ s in soft soil. Total system energy in stiff soil is about $234\,\mathrm{kN \cdot m}$, which is much smaller than the energy in soft soil $(12091\,\mathrm{kN \cdot m})$. The relative motion by wave passage is large in soft soil due to the low velocity of the incident wave ($V_s = 70.0\,\mathrm{m/s}$). This motion generates large energy and causes extensive deformation of the components in the system. However, because the relative motion between the top and bottom parts is not great compared with the system in soft soil, little energy can get into the system in stiff soil. This is a reason for the forming of the peak in total system energy as seen in Figure 4.2 (a). The lesser relative energy does not generate much nonlinear response in the system. Also, only a small amount of energy is dissipated by the springs because of high stiffness of soil in the near field.

Plots of total system energies for a 4 x 4 pile group foundation are presented in Appendix B. A similar tendency is seen in the results for the 4 x 4 pile group, but the amplitude of energy is small compared with the 6 x 6 pile group because of the different magnitude of total system.

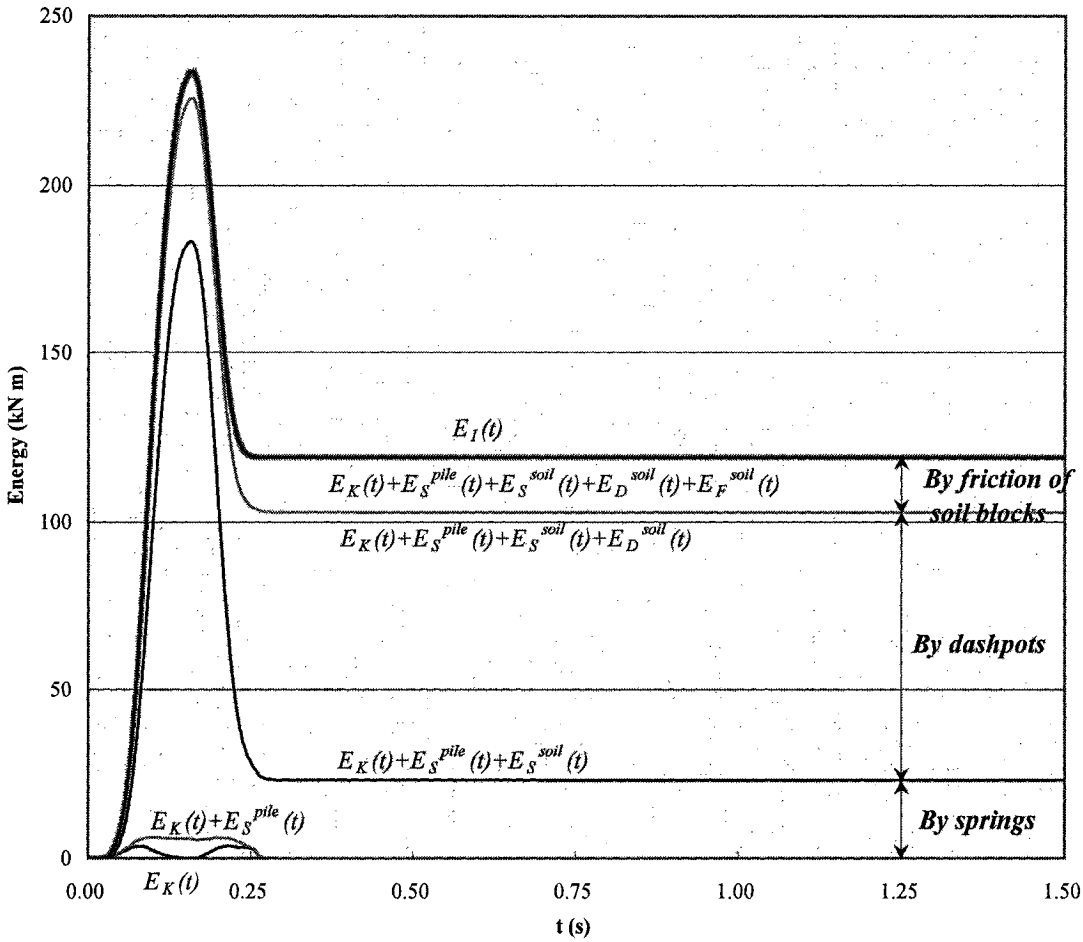

(a) Stiff soil (V_s = 280.0 m/s)

Fig 4.2 Total system energies for a 6 x 6 group pile cause by a short incident pulse (T_g = 0.2 s) when the pile-spacing raio is 5.0 (s/d = 5.0).

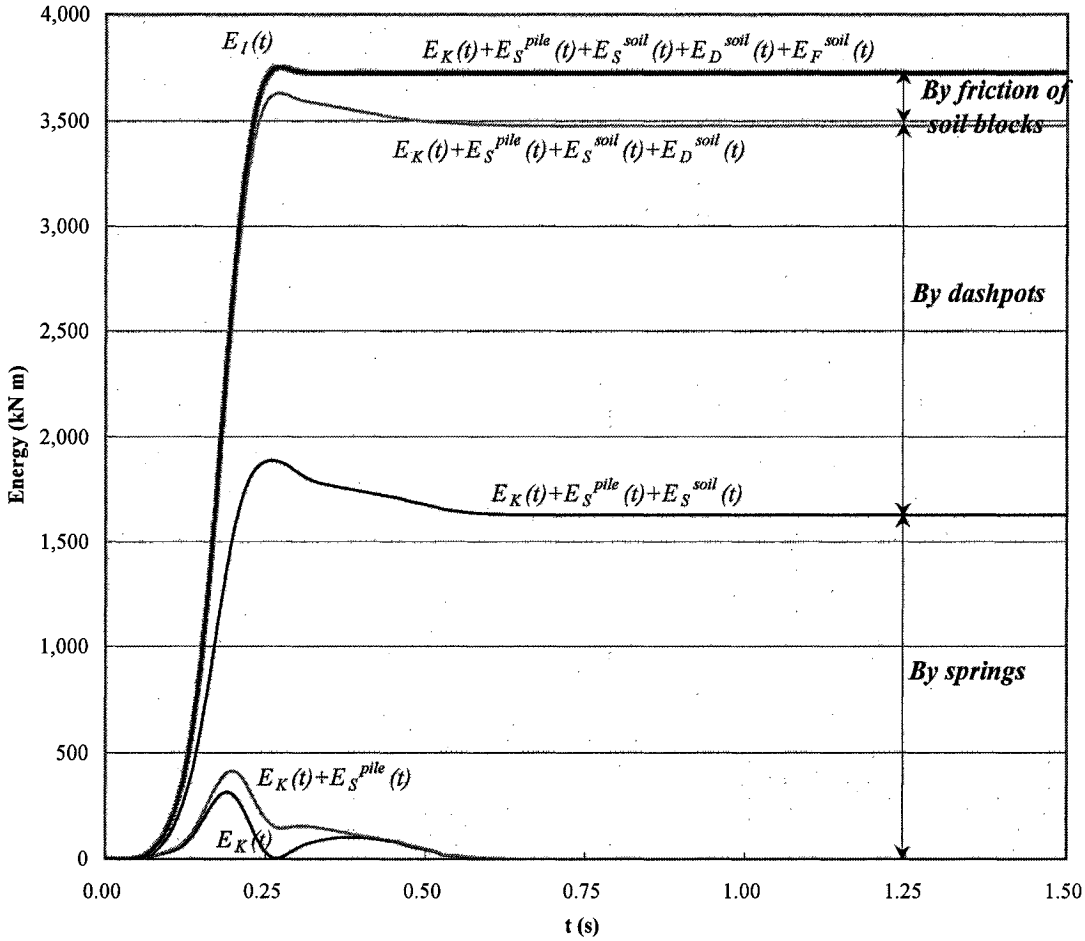

(b) Medium soil (V_s = *140.0* m/s)

Fig 4.2 Total system energies for a 6 x 6 group pile cause by a short incident pulse (T_g = *0.2* s) when the pile-spacing raio is 5.0 (s/d = 5.0). (continued)

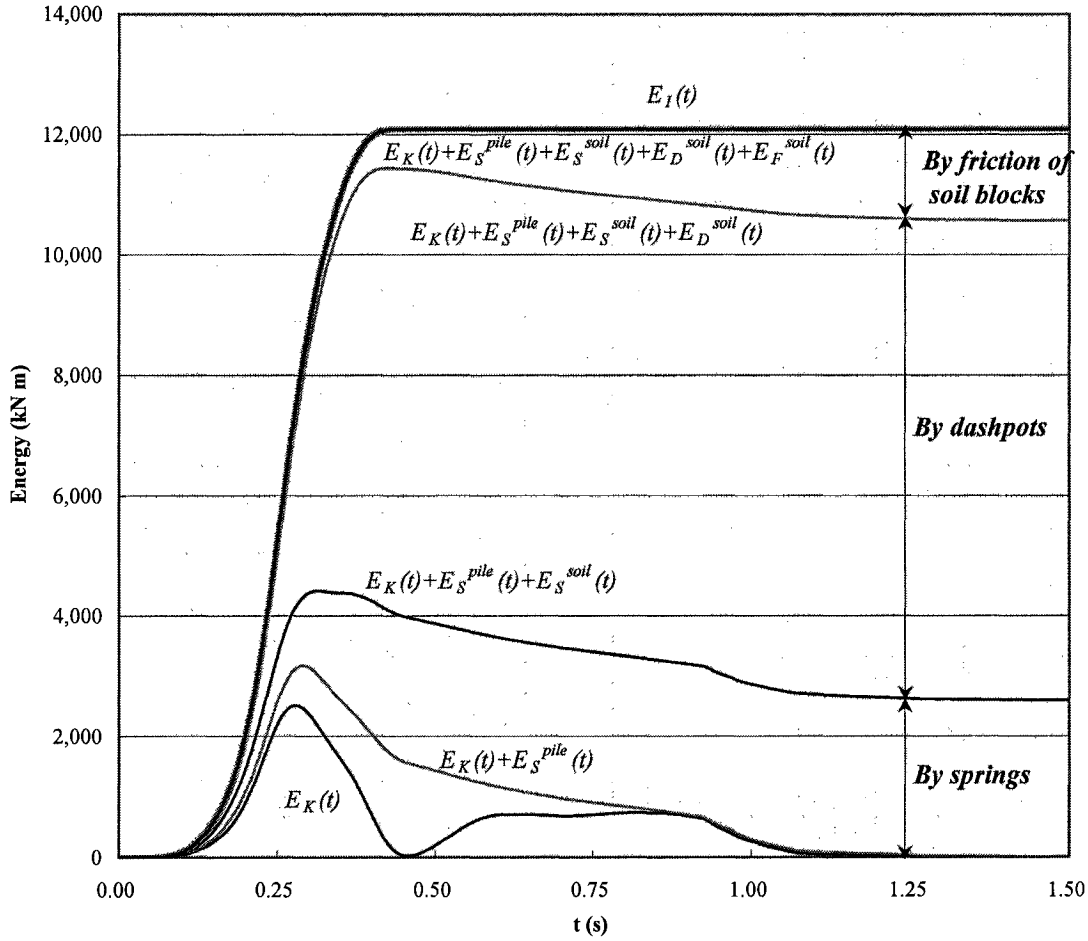

(c) Soft soil (V_s = *70.0* m/s)

Fig 4.2 Total system energies for a 6 x 6 group pile cause by a short incident pulse (T_g = *0.2* s) when the pile-spacing raio is 5.0 (s/d = 5.0). (continued)

4.2 Dissipated energy in the system

When a incident wave propagates into a group of piles, the energy is dissipated by the nonlinear behavior of the components in the system. Figures 4.3, 4.6, and 4.7 show the percentages of dissipated energy by springs and dashpots in the near field and by the friction of soil blocks located between the piles of the grouped pile system. The x axis shows the pile-spacing ratio ($s/d = 1.5 \sim 10.5$), and the y axis shows the percentage of dissipated energy by each component in the system. Solid line with full triangle represents the percentage of energy dissipated by the nonlinear behavior of springs in the near field (E_S^{soil}). The gray line with open circles shows the percentage of the sum of dissipated energy by springs and dashpots of the soil in the near field ($E_S^{soil} + E_D^{soil}$). The rest shows the energy dissipated by the friction of the soil blocks inside the foundation (E_F^{soil}).

When the short input pulse (T_g=0.2 s) propagates into the system, only a small portion of the energy is dissipated by the friction of the soil blocks located between the piles. Figure 4.3 (a) shows the percentages of dissipated energy by each of the components of the system for a 6 x 6 pile group system in medium soil ($V_s = 140.0$ m/s) when a short pulse ($T_g = 0.2$ s) shakes the system. The friction coefficient (μ), friction angle (ϕ), and damping factor (β) of the soil are assumed to be 0.5, 50°, and 0.02, respectively. The energy is dissipated mostly by the nonlinear behavior of the soil at the outer parts of the system.

Figure 4.4 shows the nonlinear hysteretic curve of springs at the ground level in a 6 x 6 pile group system, when a short input pulse propagates into the system. Part (a)

shows the hysteretic curve of the soil at the left side of the 1st pile and part (f) shows it at the right side of the 6th pile. The x axis represents the deformations of the soil adjacent to the piles, which are normalized to the maximum displacement of the input pulse (1.0 m). The y axis represents the reactive force in the springs. The area enclosed by a hysteretic curve represents the energy dissipated by the nonlinear behavior of springs in the near field. A large amount of energy is dissipated by the nonlinear springs when a short input pulse is transmitted into the system. Especially at the far right side of the system (part (f) in Figure 4.6), a considerable amount of energy is dissipated by large nonlinear motion of the soil.

Figure 4.3 (b) shows the percentage of dissipated energy by three components (springs, dashpots, and soil blocks) in the system when the input energy caused by a long pulse ($T_g = 0.8$ s) is transmitted into the grouped pile system. When the energy (generated by a long input pulse, $T_g = 0.8$ s) gets into the system, a large portion of this energy is dissipated by the friction of soil blocks. In this case, the behavior of springs in the near field remains in the linear range, because the deformation of soil is not great enough to exceed the yield deformation. Figure 4.5 shows the nonlinear hysteretic curve of springs when a long input pulse propagates into the system. The configuration of this figure is the same as in Figure 4.4. The nonlinear behavior of springs is found only at the right side of the 6th pile in the system, and the soil deformations adjacent to the 1st ~ 5th piles do not exceed the yield deformation. Therefore, the transmitted energy is dissipated only by the soil near the 6th pile. However, when the input energy is relatively large (short pulse, $T_g = 0.2$ s) and the pile-spacing ratio (s/d) is small, a large proportion of the input energy is dissipated by the springs and dashpots in the near field, as illustrated in Figure 4.4.

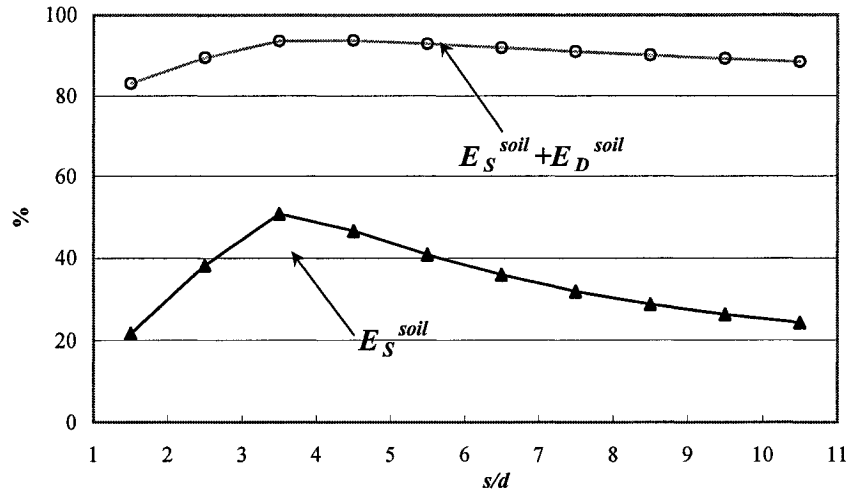

(a) $T_g = 0.2$ s

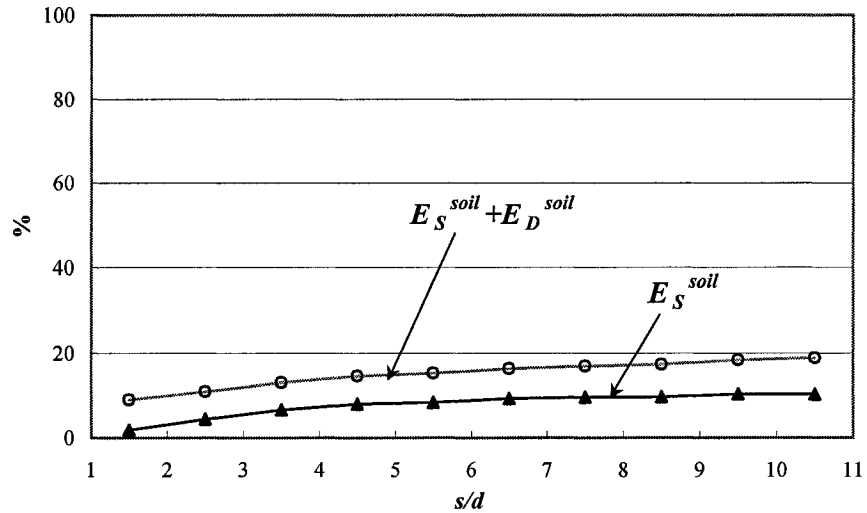

(b) $T_g = 0.8$ s

Fig. 4.3 Percentages of dissipated energy by springs, dashpots and soil blocks when a wave propagates into a 6 x 6 pile group in medium soil (V_s = 140 m/s).

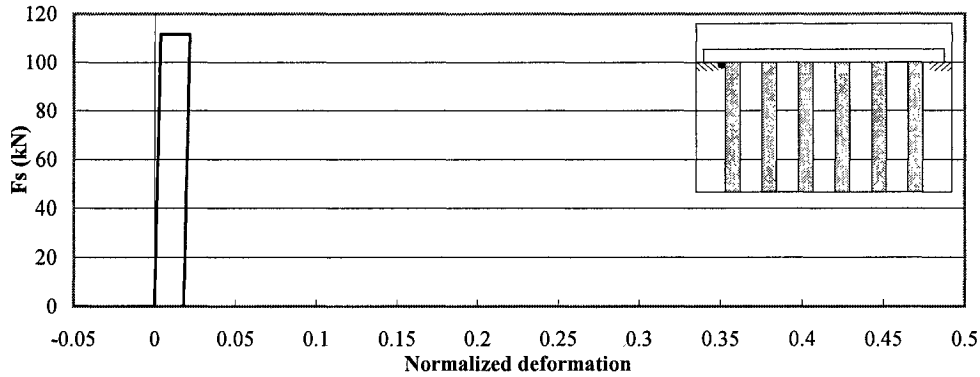

(a) At the left side of the 1st pile

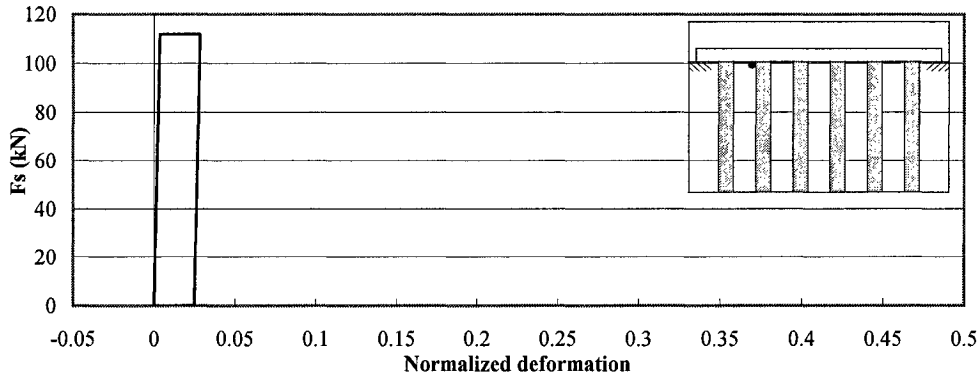

(b) At the left side of the 2nd pile

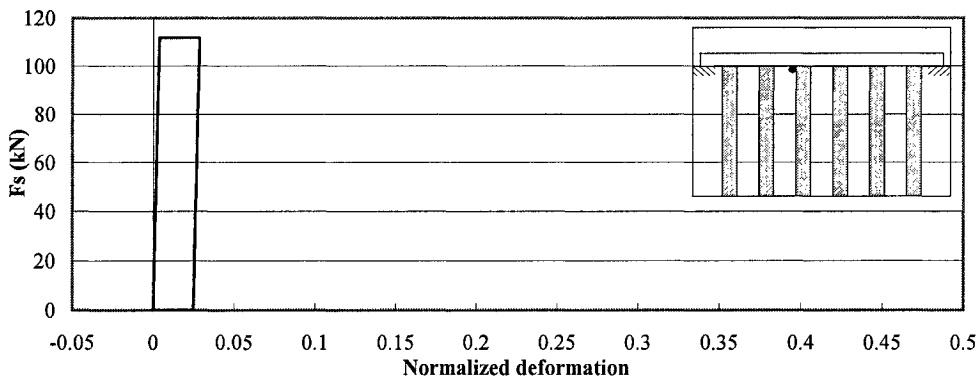

(c) At the left side of the 3rd pile

Fig. 4.4 Nonlinear hysteretic curve of springs in the 6 x 6 pile group at the ground level in medium soil (V_s = *140* m/s) caused by a short pulse (T_g = *0.2* s).

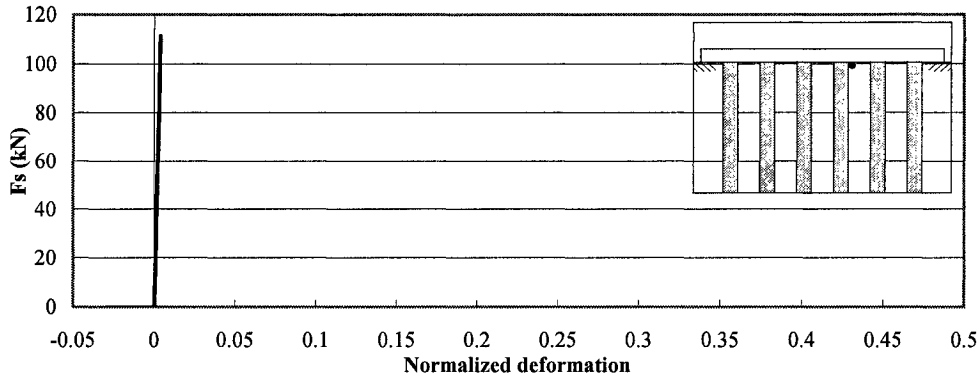

(d) At the right side of the 4th pile

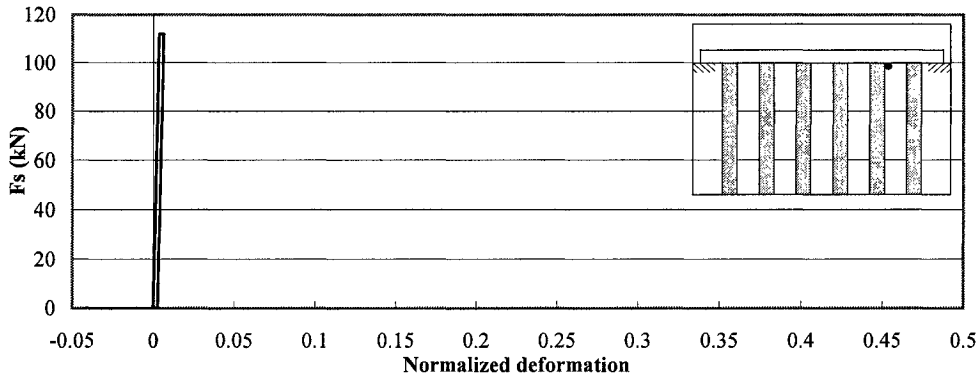

(e) At the right side of the 5th pile

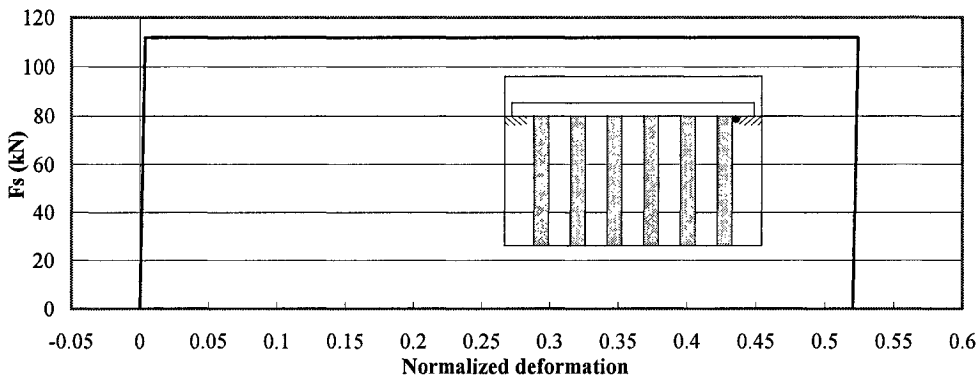

(f) At the right side of the 6th pile

Fig. 4.4 Nonlinear hysteretic curve of springs in the 6 x 6 pile group at the ground level in medium soil (V_s = *140* m/s) caused by a short pulse (T_g = *0.2* s). (continued)

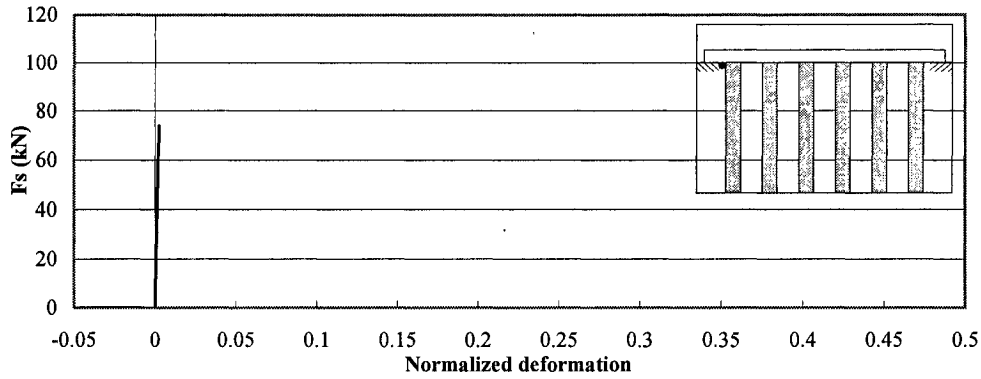

(a) At the left side of the 1st pile

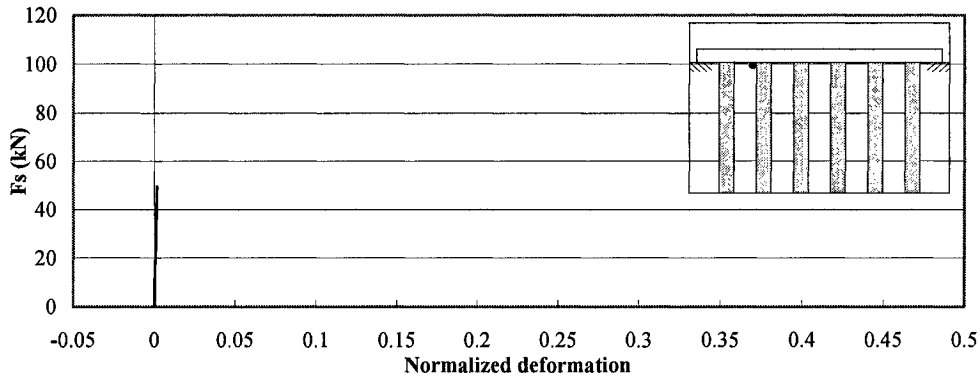

(b) At the left side of the 2nd pile

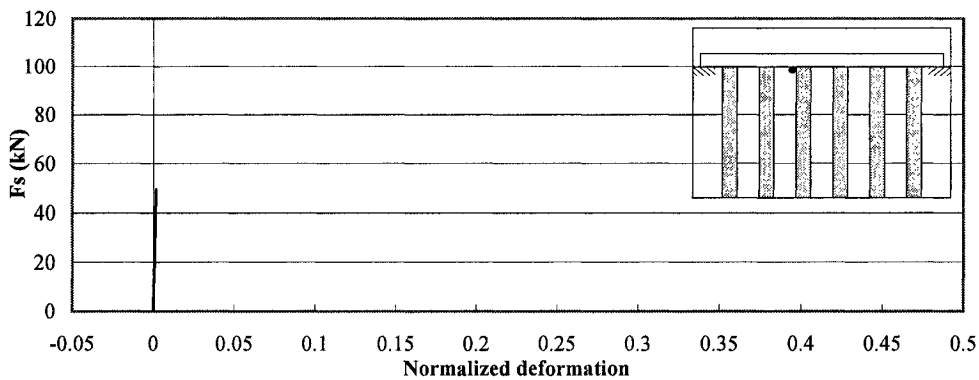

(c) At the left side of the 3rd pile

Fig. 4.5 Nonlinear hysteretic curve of springs in the 6 x 6 pile group at the ground level in medium soil (V_s = *140* m/s) caused by a long pulse (T_g = *0.8* s).

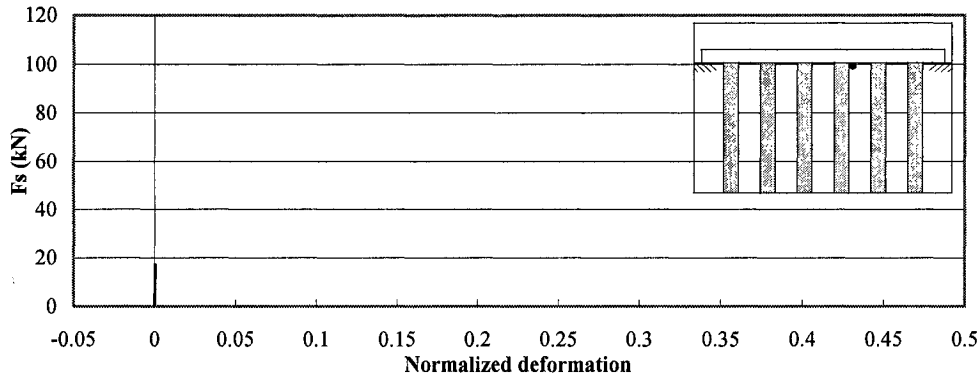

(d) At the right side of the 4th pile

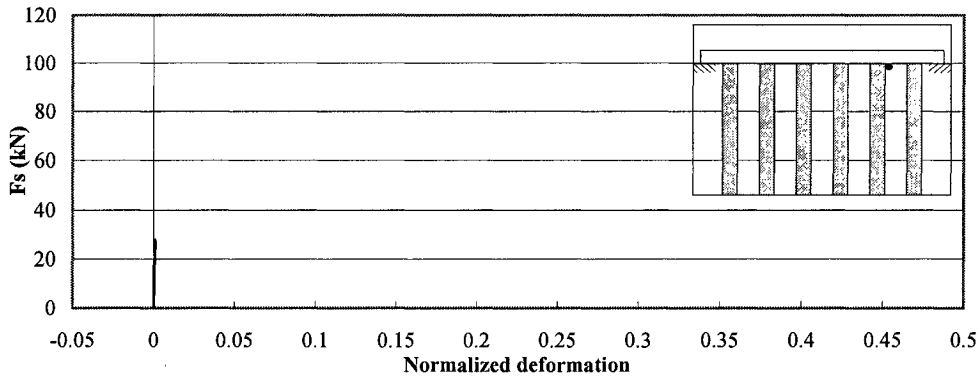

(e) At the right side of the 5th pile

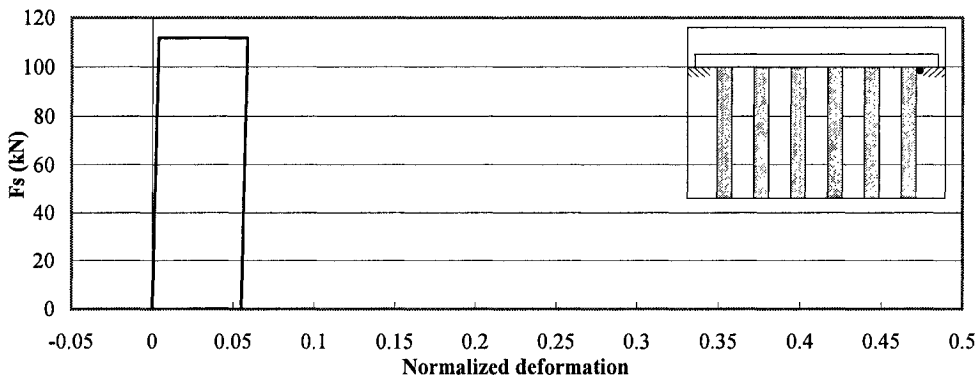

(f) At the right side of the 6th pile

Fig. 4.5 Nonlinear hysteretic curve of springs in the 6 x 6 pile group at the ground level in medium soil ($V_s = 140$ m/s) caused by a long pulse ($T_g = 0.8$ s). (continued)

Figure 4.6 (a) shows the percentage of energy dissipated for excitation by a short pulse (T_g = *0.2 s*) and for a 6 x 6 pile group foundation in stiff soil (V_s = *280.0 m/s*). When the pile spacing ratio is small (*s/d = 1.5 ~ 2.5*), the energy is not dissipated by the nonlinear hysteretic behavior of the springs at the soil-pile interface. Because the total energy is small, the resultant spring force does not exceed the ultimate resistance of the soil near the pile. As the total system energy increases by increasing the pile-spacing ratio (increasing the mass of the soil blocks), the portion of energy dissipated through the nonlinear behavior of the springs increases. However, if a closely spaced pile group is placed into soft soil (Figure 4.6 (b)), a relatively large portion of energy is dissipated by the response of the soil near the piles. The spring forces can exceed the ultimate resistance of the soil in the case of soft soil even when the system energy is small.

Figure 4.7 illustrates the response of a 6 x 6 pile group foundation in soft soil (V_s = *70.0 m/s*) for different friction coefficients and excited by a short input pulse (T_g = *0.2 s*). The pile-spacing ratio is 4.0 (*s/d = 4.0*), and the friction angle is 50° ($\phi = 50°$). Three kinds of damping factors are used in computation ($\beta = 0.02, 0.03, 0.04$).

Percentages of energy dissipated by the components in the system are shown in Figure 4.7 (a). The *x* axis shows the friction coefficient (μ = 0.2 ~ 0.7), and the *y* axis represents the percentage of energy dissipated. The energy dissipated by soil blocks increases as the friction coefficient of soil becomes larger. There are small differences in percentages of energy dissipated by the dashpots in the near field of soil for different values of damping factor. The energy dissipated by dashpots with $\beta = 0.04$ is slightly larger compared with that with $\beta = 0.02$, but the portion of energy dissipated by the soil blocks does not depend upon the damping factor of the soil.

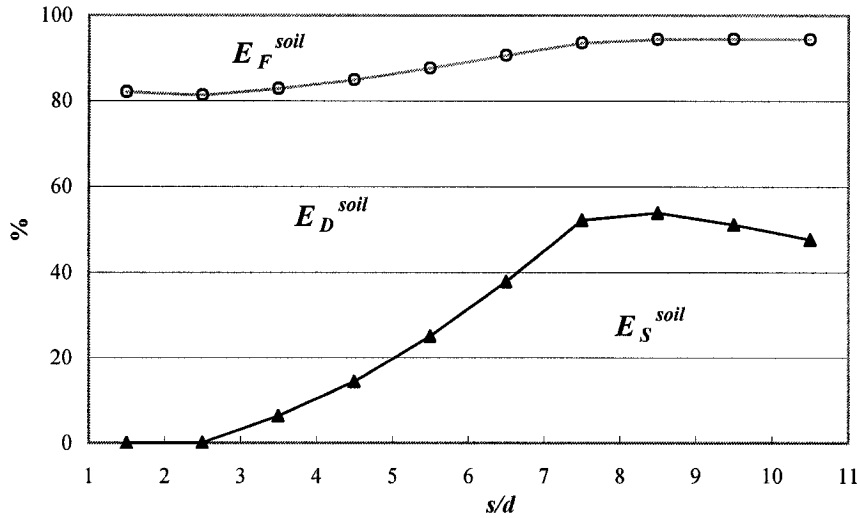

(a) In siff soil (V_s = *280.0* m/s)

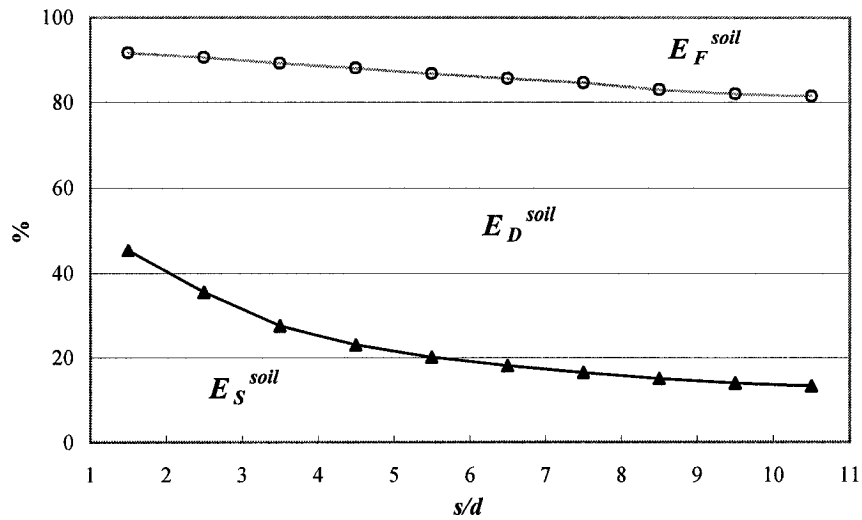

(b) In soft soil (V_s = *70.0* m/s)

Fig. 4.6 Percentages of energy dissipated by springs, dashpots, and soil blocks when a short pulse (T_g = *0.2* s) propagates into a 6 x 6 pile group.

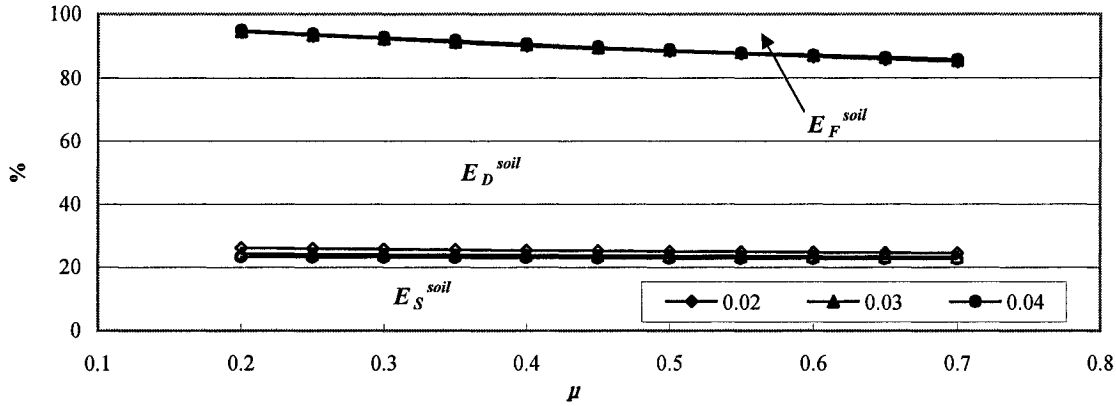

(a) Percentages of energy dissipated by components in the system

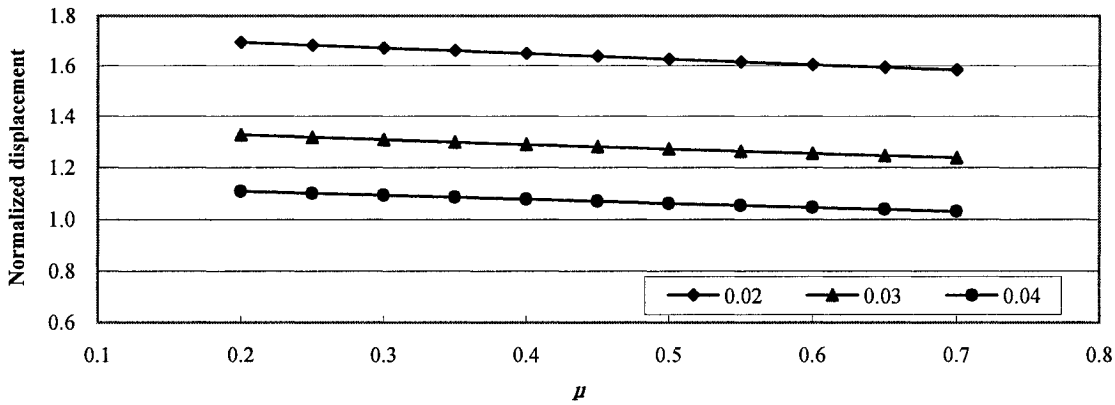

(b) Maximum displacements of pile top normalized to maximum displacement of pulse

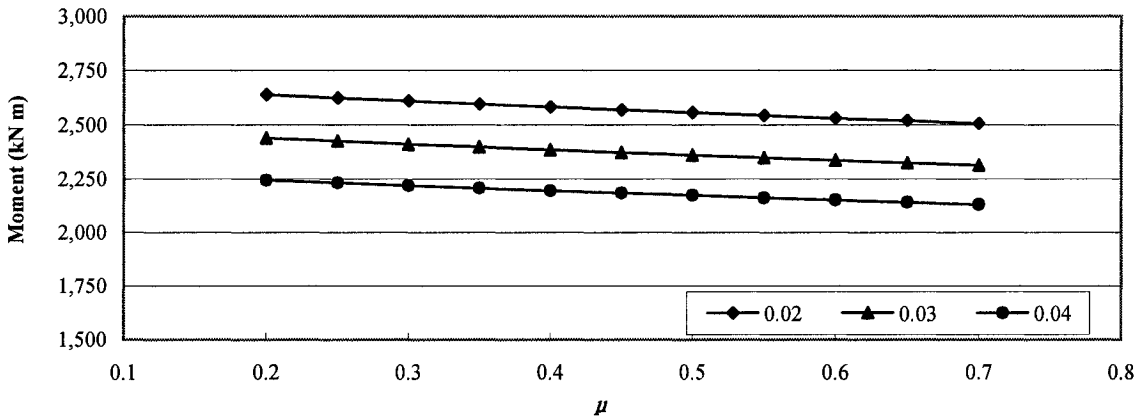

(c) Maximum bending moments of pile

Fig. 4.7 Response of a 6 x 6 pile group in soft soil (V_s = *70.0* m/s) cause by a short pulse (T_g = *0.2 s*) for various friction coefficients (μ).

Figures 4.7 (b) and (c) show maximum displacements and bending moments of a pile for different damping factors and for different friction coefficients in the soil. Displacements are normalized to the maximum displacement of the input pulse (1.0 m). Maximum displacements and bending moments of piles decrease with increasing friction coefficients of the soil blocks in the system. The damping factor of the soil in the near field also affects the displacements and bending moments of the piles.

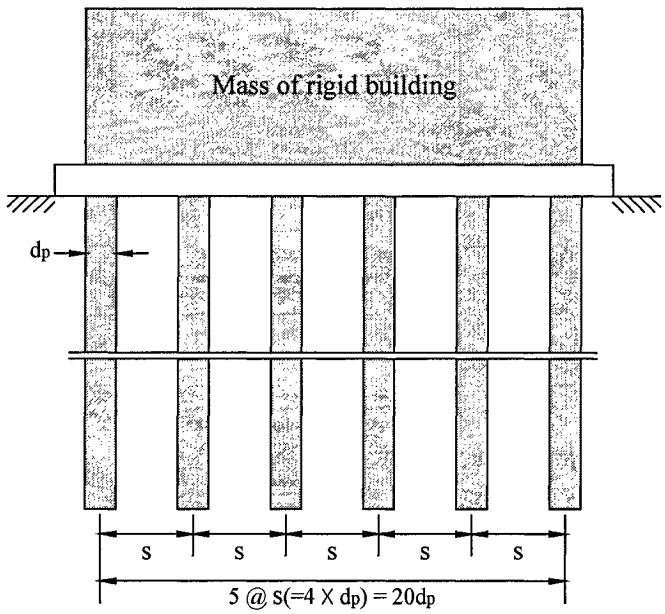

Fig. 4.8 A 6 x 6 pile group system with a mass of rigid building on the pile cap.

In the following, the changes in energy flow resulting from overall weight of the building and its the kinetic energy are illustrated for different values of friction angle in the soil. Figure 4.8 shows the 6 x 6 pile group system with a mass of building added

to the pile cap. To simplify dynamics and to maintain emphasis on the behavior of the pile, the building is assumed to be rigid and is allowed to translate only in the horizontal direction. Three "building" (1-story, 10-story, 30-story) are used in the analysis. The assumed mass of the building is 376.16 kg/m^3, which is calculated approximately for the Hollywood Storage Building in California (Trifunac et al., 2001). The system is placed on soft soil (V_s = *70.0* m/s) and is shaken by a short input pulse (T_g = *0.2* s) with an amplitude of 0.5m (U_{g0}=*0.5m*). The pile-spacing ratio is 4.0 (*s/d = 4.0*).

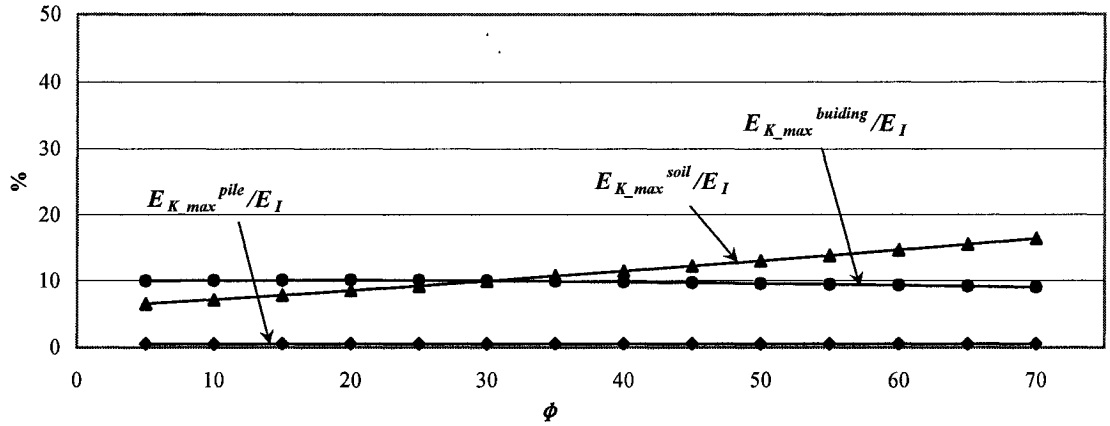

(a) 1-story

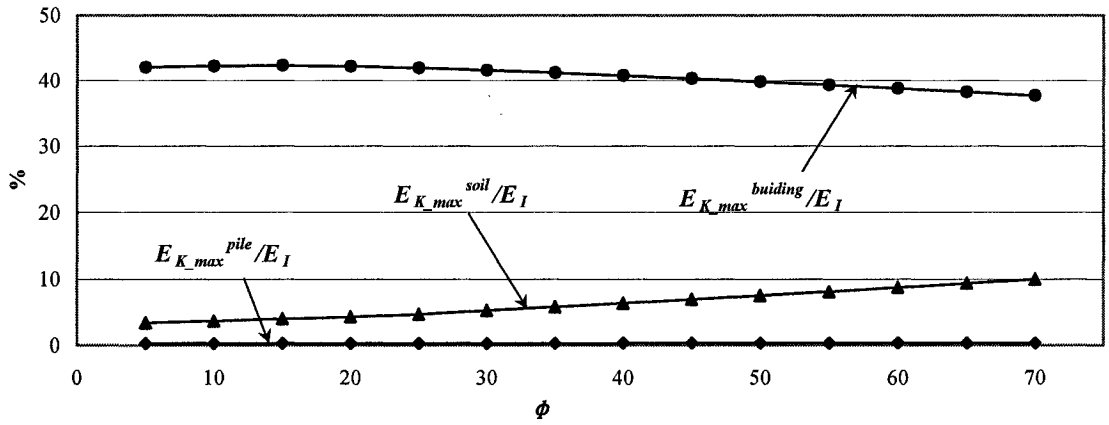

(b) 10-story

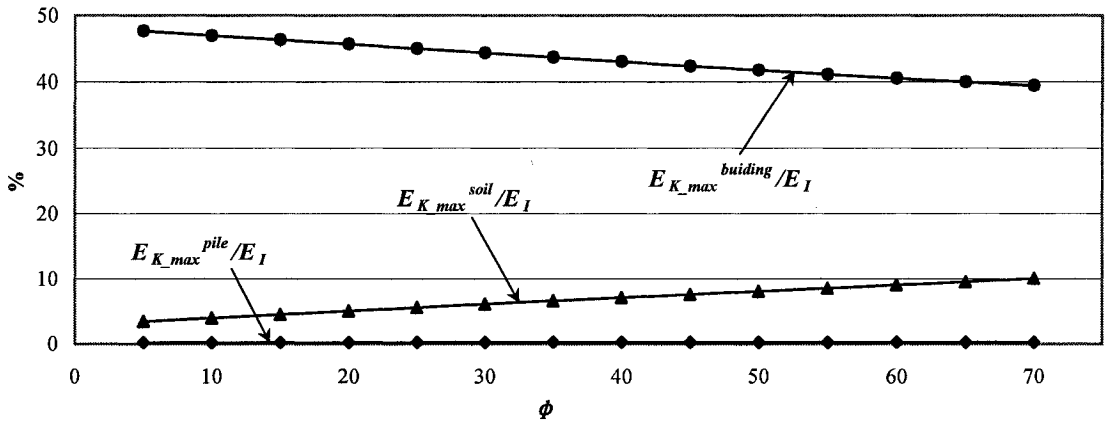

(c) 30-story

Fig. 4.9 Percentages of maximum kinetic energy to total system energy for various friction angles (Φ) of soil in a 6 x 6 pile group.

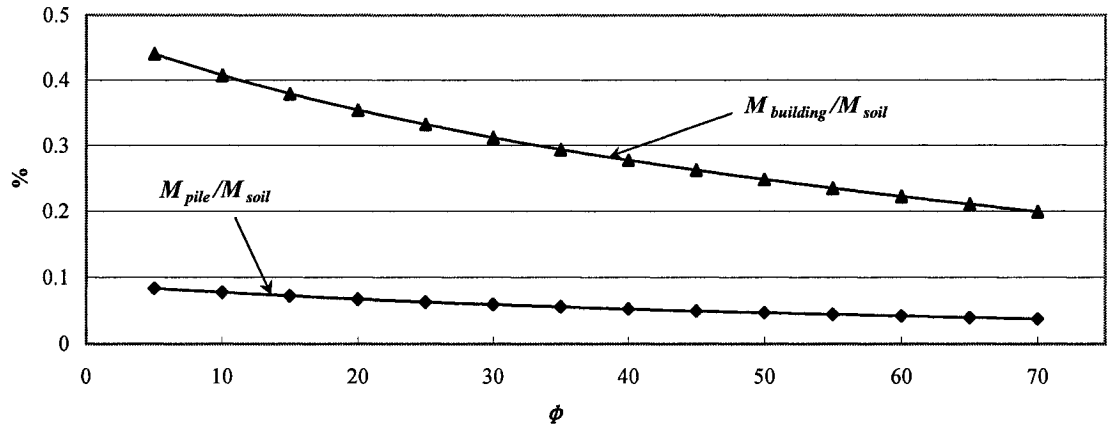

(a) 1-story

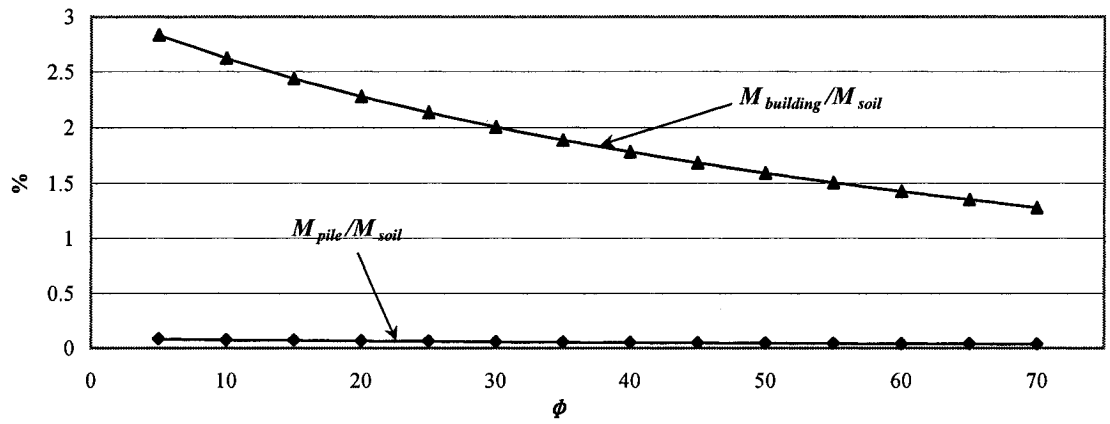

(b) 10-story

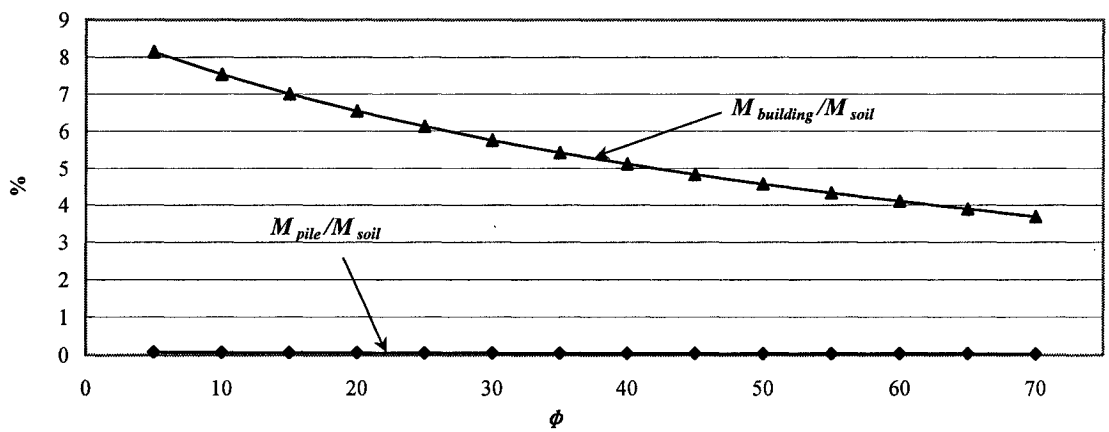

(c) 30-story

Fig. 4.10 Ratio of masses of building and pile to mass of soil in a 6 x 6 pile group for various friction angles of soil (Φ).

Figure 4.9 shows the percentages of maximum kinetic energy of the total system energy for three example "buildings". The friction angle is changed from 5° to 70°, and the friction coefficient is 0.5. The kinetic energy in the soil rises as the friction angle of the soil becomes larger, because the total mass of the soil increases. Figure 4.10 shows the ratio of the mass of building and piles to the mass of soil for different friction angles of soil. This ratio goes down as friction angles increase. The kinetic energy of the building decreases as the friction angle increases. The energy available to excite the building is reduced when a large portion of energy is dissipated in the foundation.

5. Response of piles in the system

The input energy associated with large pulse amplitudes causes nonlinear behavior of soil and is then dissipated by the nonlinear response. The piles embedded in the soil are affected by the nonlinear motion of the soil. In particular, the movement of soil blocks can cause irrecoverable, permanent deformation of the piles even though the pile material is assumed to respond in a linear elastic range. This chapter examines the movement of piles in groups when a vertically incident wave propagates into the system. The gaps caused by nonlinear behavior of the soil in soil-pile interface are computed for 6 x 6, 4 x 4, and 2 x 2 pile groups. The maximum bending moment and total displacement of piles are also presented. Finally, the effects of a group are investigated by analyzing the response of different pile groups with the same dimensions.

5.1 Movement of piles

Figures 5.1 and 5.2 show the relative displacements ($U_t - U_g$) of piles in a 6 x 6 pile group system for two types of vertically incident waves, ($T_g = 0.2\,\text{s}, 0.4\,\text{s}$) for 6 points in time. The foundation is placed in soft soil ($V_s = 70.0\,\text{m/s}$) and the pile spacing ratio is 2.5 ($s/d = 2.5$). In each figure, there are 6 graphs, which represent motions of 1st pile to 6th pile from left to right. The y axis represents the depth from ground surface.

Figure 5.1 shows the relative displacement of piles excited by a short pulse at 6 different times, t = *0.125* s, *0.25* s, *0.375* s, *0.5* s, *0.625* s, and *0.75* s. In the beginning (t=*0.125* s, *0.25* s), the motion of the piles is similar to the motion of the vertically propagating wave. At t = *0.125* s, the lower parts of piles begin to deform as the wave

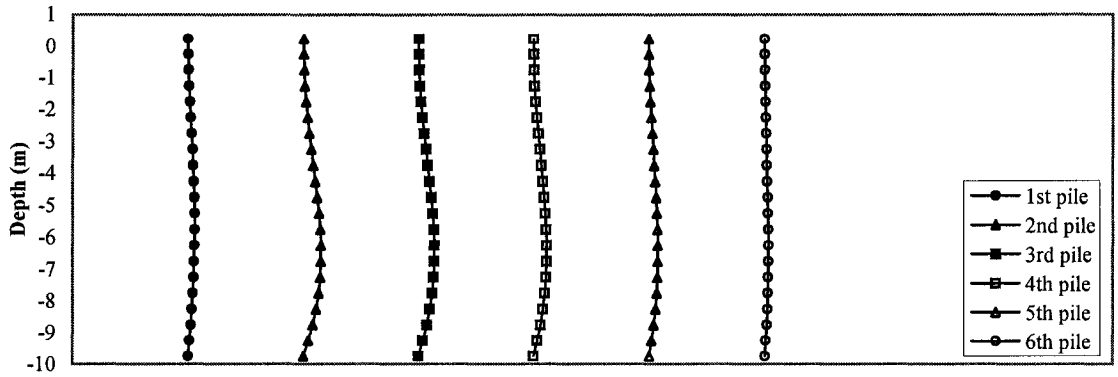

(a) t = 0.125 s

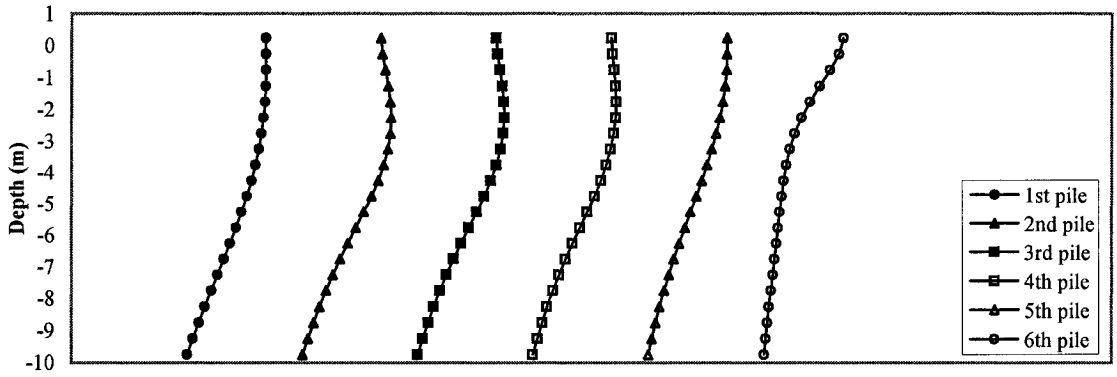

(b) t = 0.25 s

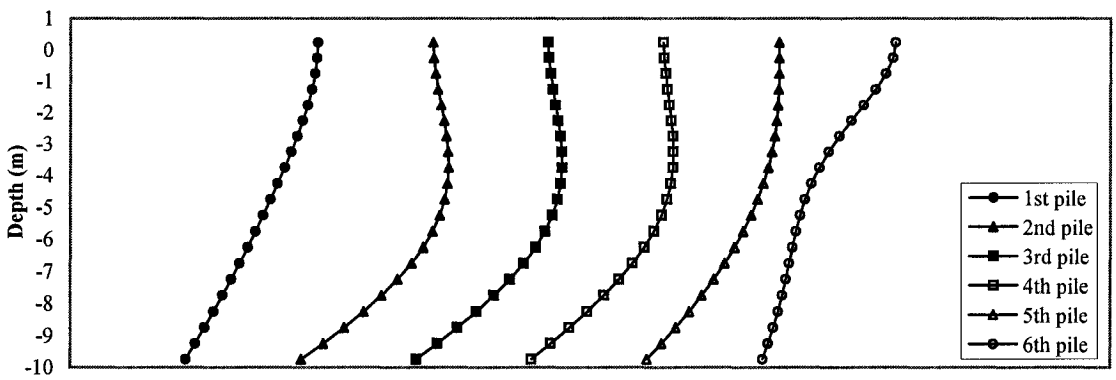

(c) t = 0.375 s

Fig. 5.1 Motion of a piles in 6 x 6 pile group in soft soil (V_s = *70.0* m/s) caused by a short incident pulse (T_g = 0.2 s).

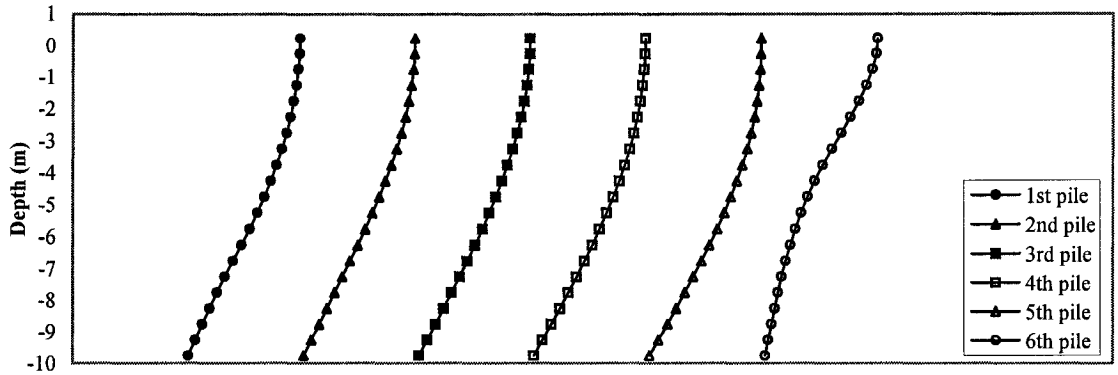

(d) t = 0.5 s

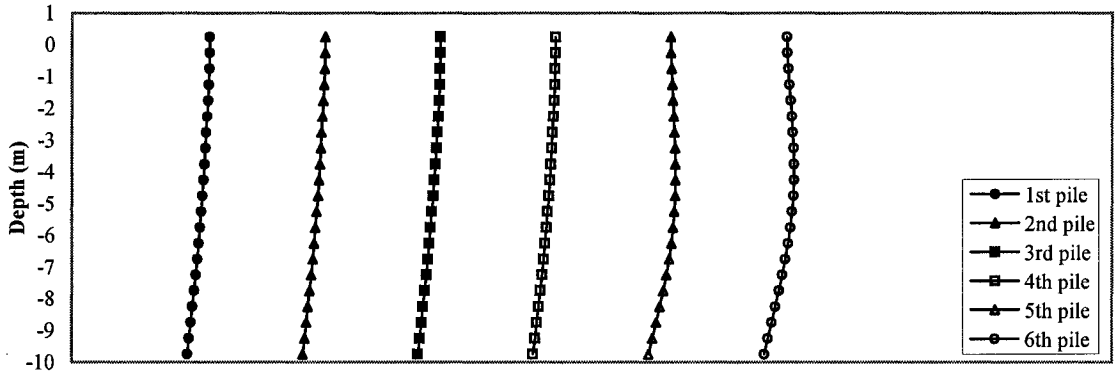

(e) t = 0.625 s

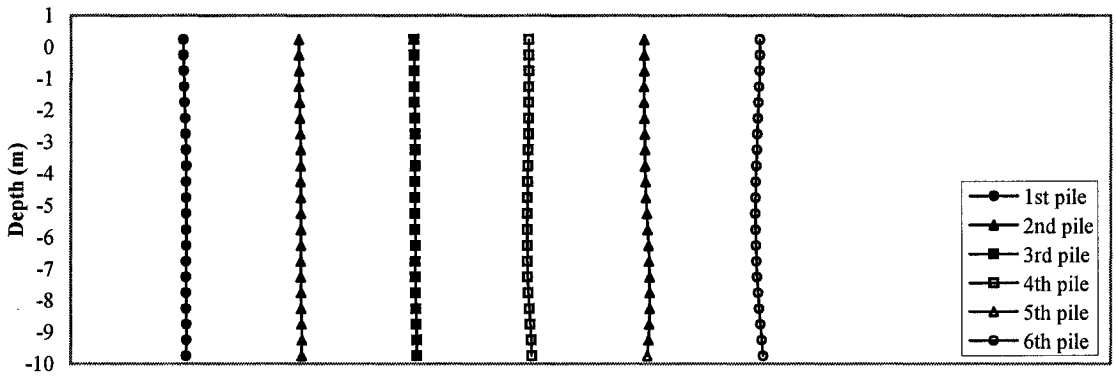

(f) t = 0.75 s

Fig. 5.1 Motion of a piles in 6 x 6 pile group in soft soil (V_s = *70.0* m/s) caused by a short incident pulse (T_g = 0.2 s). (continued)

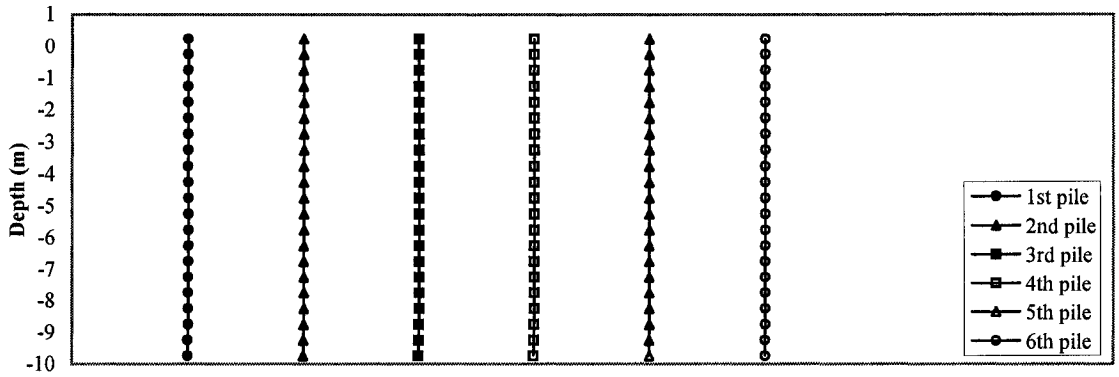

(a) t = 0.125 s

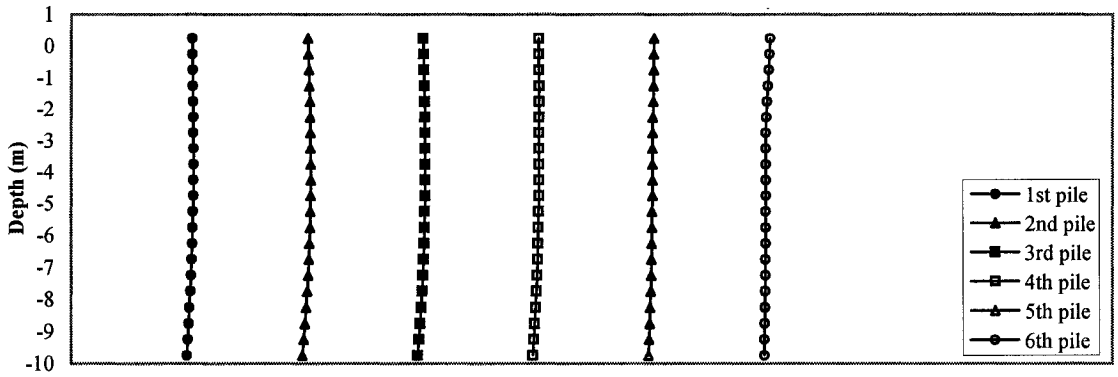

(b) t = 0.25 s

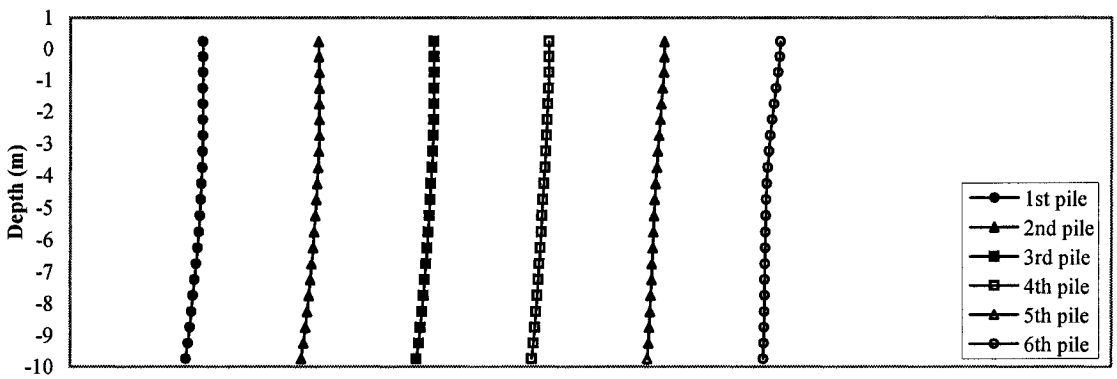

(c) t = 0.375 s

Fig. 5.2 Motion of piles in a 6 x 6 pile group in soft soil (V_s = *70.0* m/s) caused by a incident pulse with medium period (T_g = *0.4* s).

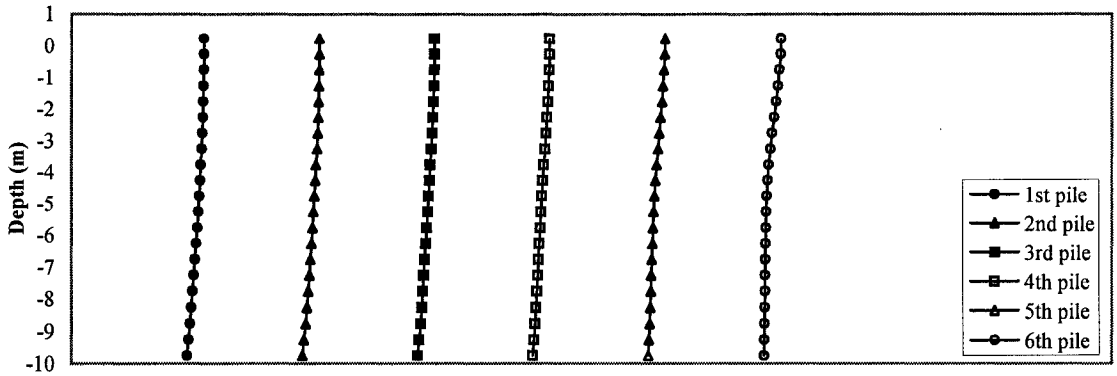

(d) t = 0.5 s

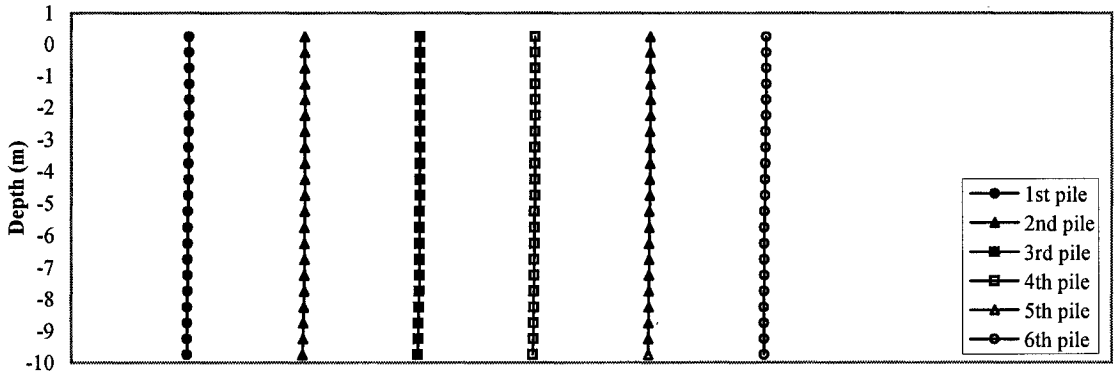

(e) t = 0.625 s

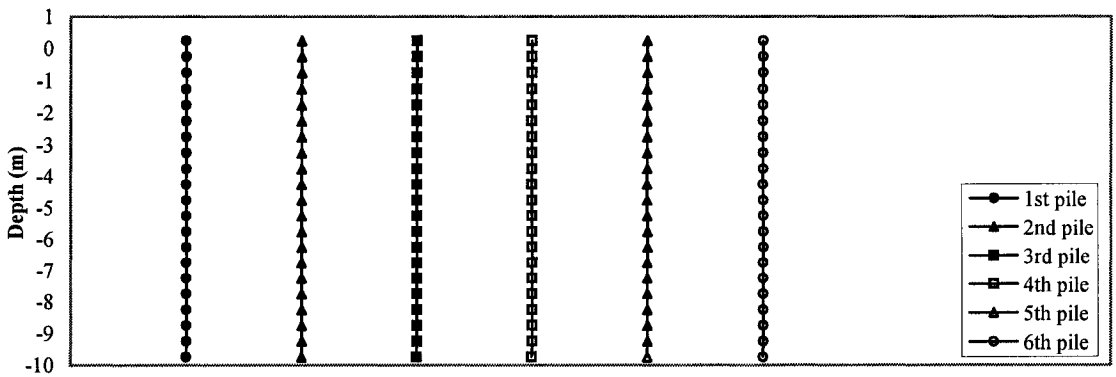

(f) t = 0.75 s

Fig. 5.2 Motion of piles in a 6 x 6 pile group in soft soil (V_s = *70.0* m/s) caused by a incident pulse with medium period (T_g = *0.4* s). (continued)

comes into the system. The second plot (t = *0.25* s) illustrates the motion of the piles when the amplitude of the incident wave is doubled at the ground surface due to the reflection of the incident wave. However, the motion of the piles becomes different from the movement of incident wave at t = *0.375* s, *0.5* s, *0.625* s, and *0.75* s because of the inertial forces from soil blocks that move between the piles. After the input wave goes out from the system, the piles continue to move until all the transmitted energy is dissipated. If a large energy has been transmitted into the system, the piles can have irrecoverable, permanent deformation, due to permanent displacement of soil blocks.

Figure 5.2 shows the relative displacements of piles caused by a vertically propagating pulse with a medium period ($T_g = 0.4\,\mathrm{s}$). A relatively small motion is generated by a relatively long incident wave. The magnitude of input energy is not great enough to cause nonlinear deformations in this case. The motion of piles follows the passage of the propagating wave and returns to the original position when all vibrations are damped out.

The motion of piles in 4 x 4 and 2 x 2 pile group foundations is presented in Appendix B. It is also plotted at six time steps and for two durations of a vertically incident wave ($T_g = 0.2\,\mathrm{s}, 0.4\,\mathrm{s}$). Similar trends are found for these pile groups. However, the amplitudes of motion are relatively small compared with the present example for a 6 x 6 pile group foundation, and therefore little influence from the movement of soil blocks is present.

5.2 Gaps opening adjacent to piles

When a pile embedded in soil is subjected to lateral loading, it is often observed that gaps are formed between the pile shaft and the surrounding soil (Pender and Pranjoto, 1996). In this study, gaps are computed by using the nonlinear springs that represent soil and that are presented in section 2.2. The deformations of piles and the creation of gaps, which are caused by the nonlinear behavior at the soil-pile interaction, are considered in the following.

Figure 5.3 shows the absolute displacements of piles and gaps in adjacent soil at the ground level in soft soil ($V_s = 70.0$ m/s) when the short pulse ($T_g = 0.2$ s, $U_{g0} = 0.5$ m) shakes the 6 x 6 grouped pile system. Deformations are normalized to the maximum displacement of the input pulse (1.0 m). Parts (a), (b), (c), (d), (e), and (f) show the displacements of piles and gaps adjacent to the 1st, 2nd, 3rd, 4th, 5th, and 6th piles, respectively. The x axis shows the time in seconds, and the y axis shows the normalized displacement and gaps. The solid line shows the absolute displacement of a pile. The thin solid line and the dotted line represent gaps at the left side and right side in the near-field soil adjacent to the pile. The separation between pile and soil remains open when the amplitude of transmitted energy is large enough to cause nonlinear behavior in the soil. The gap is generated by soil compression with large stress, and the largest gap is formed in the soil at the right side of the 6th pile, which is located at far right side of the 6 x 6 pile group system.

Figure 5.4 shows the same results in medium soil ($V_s = 140.0$ m/s), with all other parameters remaining same as for the case shown in Figure 5.3. The gaps at the soil-pile interface are not found in the soil adjacent to the 2nd, 3rd, 4th, or 5th piles, which are

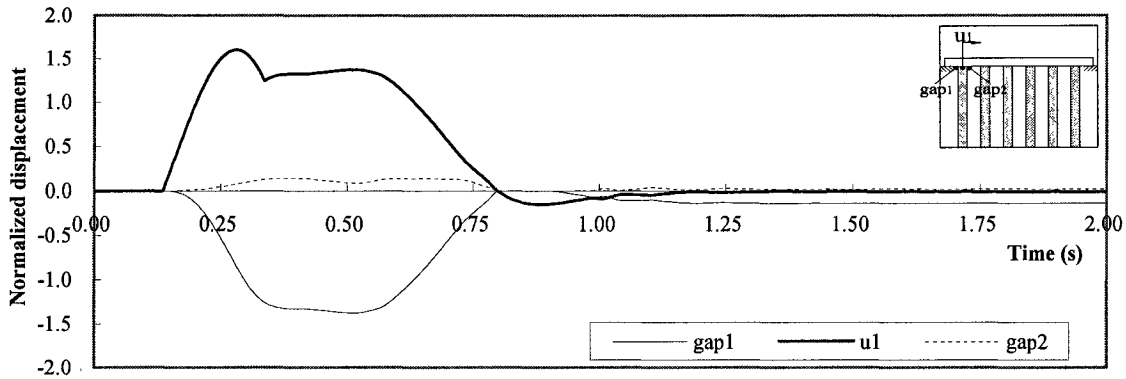

(a) 1st pile and gap1, gap2

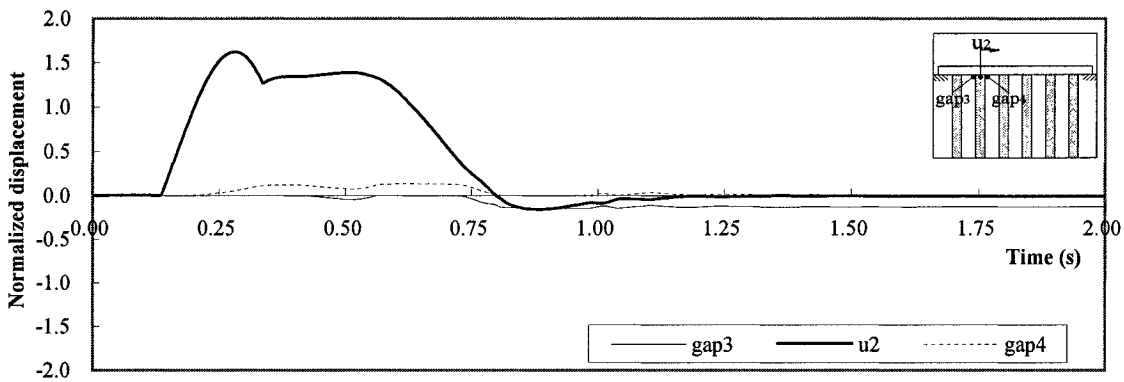

(b) 2nd pile and gap3, gap4

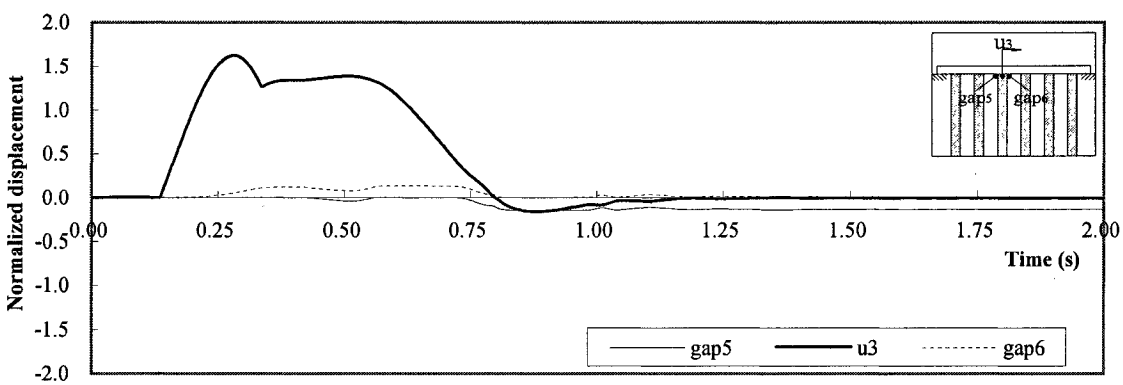

(c) 3rd pile and gap5, gap6

Fig. 5.3 Displacements of piles and gaps at the ground level when a short pulse (T_g = *0.2* s) propagates into a 6 x 6 pile group in soft soil (V_s = *70.0* m/s).

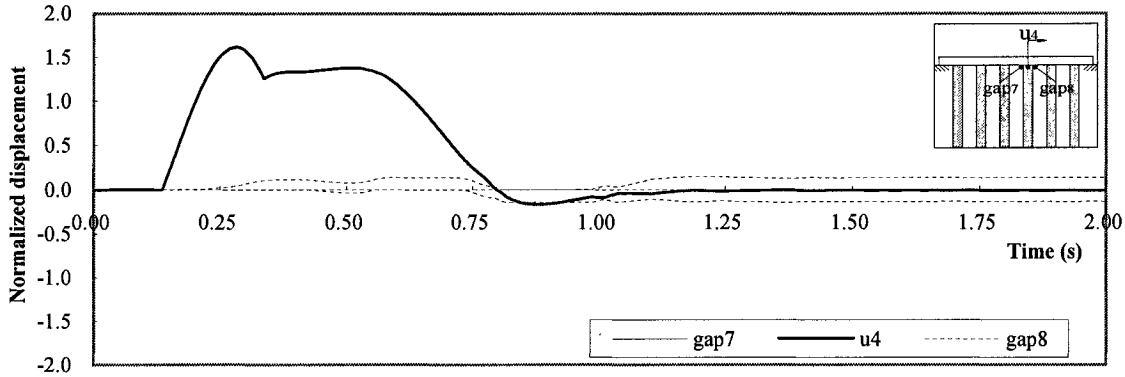

(d) 4th pile and gap7, gap8

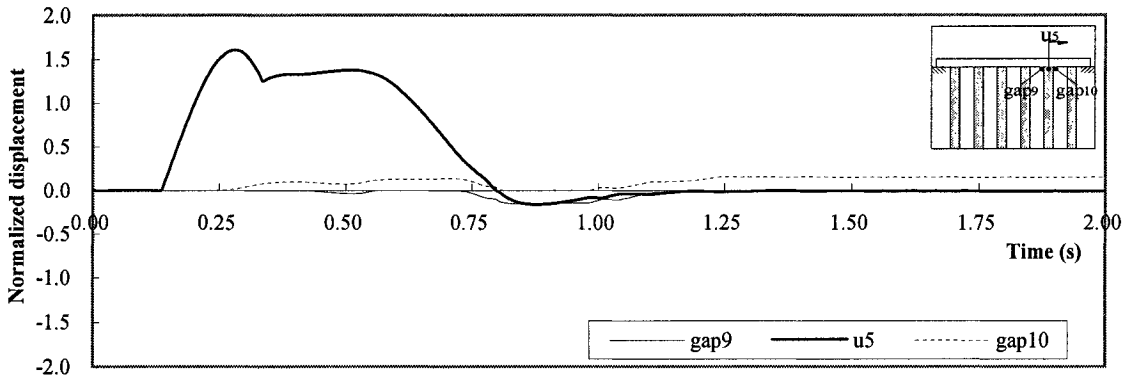

(e) 5th pile and gap9, gap10

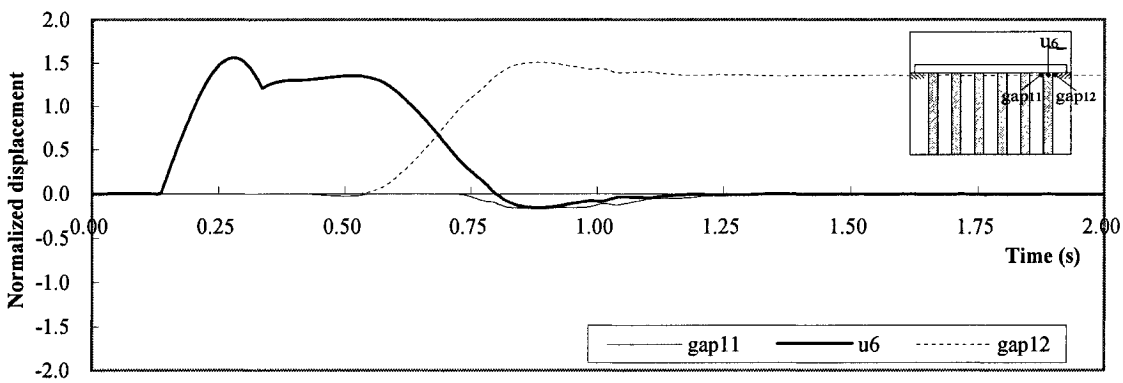

(f) 6th pile and gap11, gap12

Fig. 5.3 Displacements of piles and gaps at the ground level when a short pulse (T_g = *0.2* s) propagates into a 6 x 6 pile group in soft soil (V_s = *70.0* m/s). (continued)

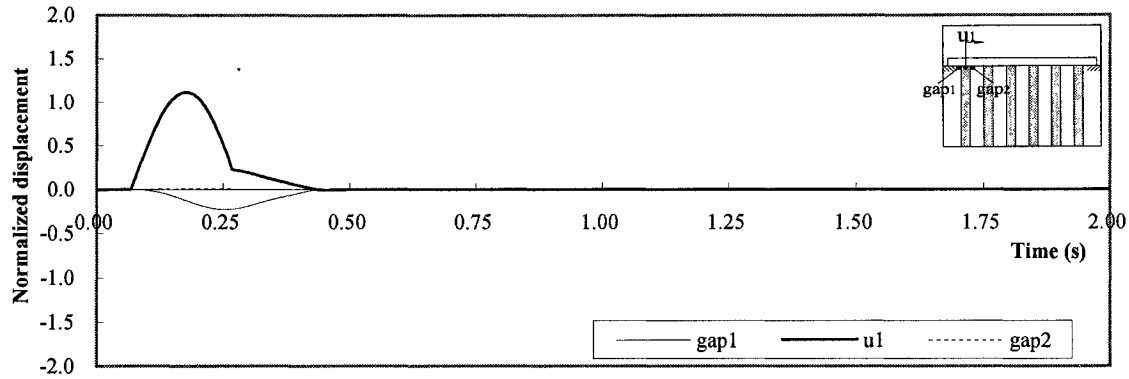

(a) 1st pile and gap1, gap2

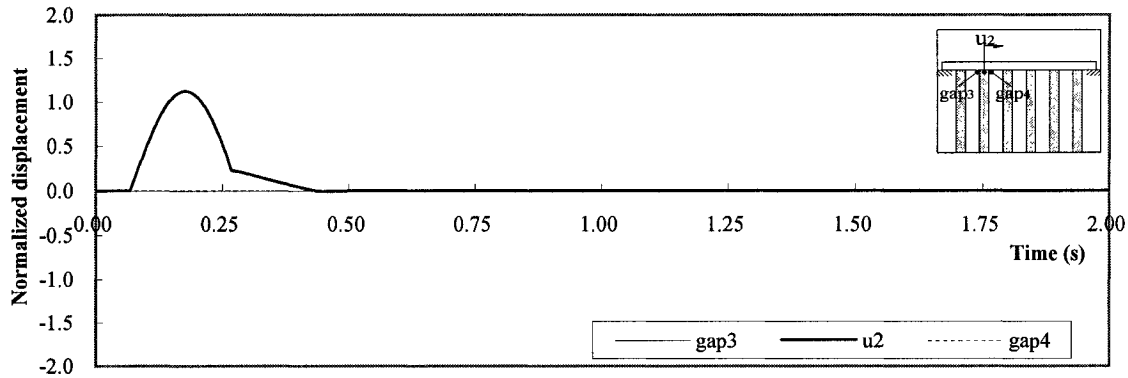

(b) 2nd pile and gap3, gap4

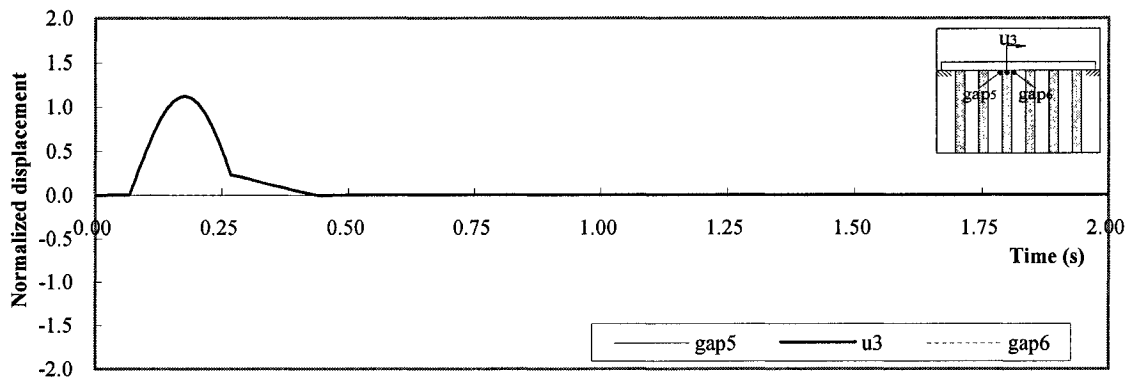

(c) 3rd pile and gap5, gap6

Fig. 5.4 Displacements of piles and gaps at the ground level when a short pulse (T_g = *0.2* s) propagates into a 6 x 6 pile group in medium soil (V_s = *140.0* m/s).

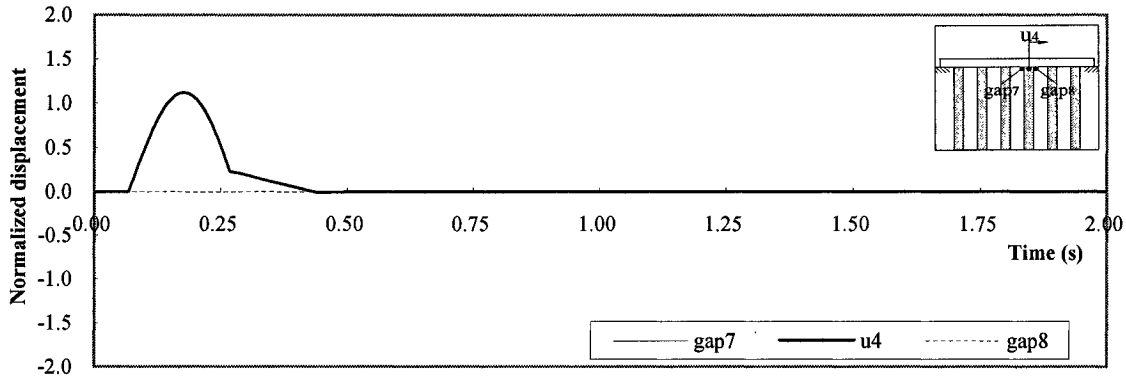

(d) 4th pile and gap7, gap8

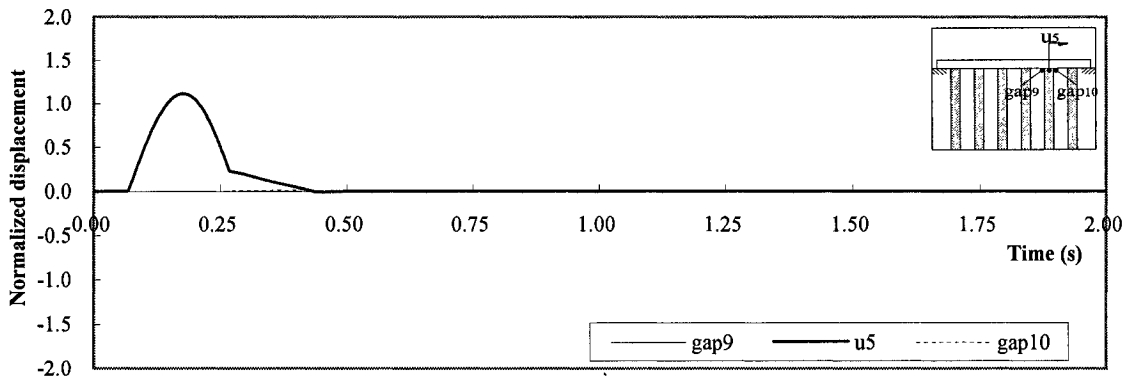

(e) 5th pile and gap9, gap10

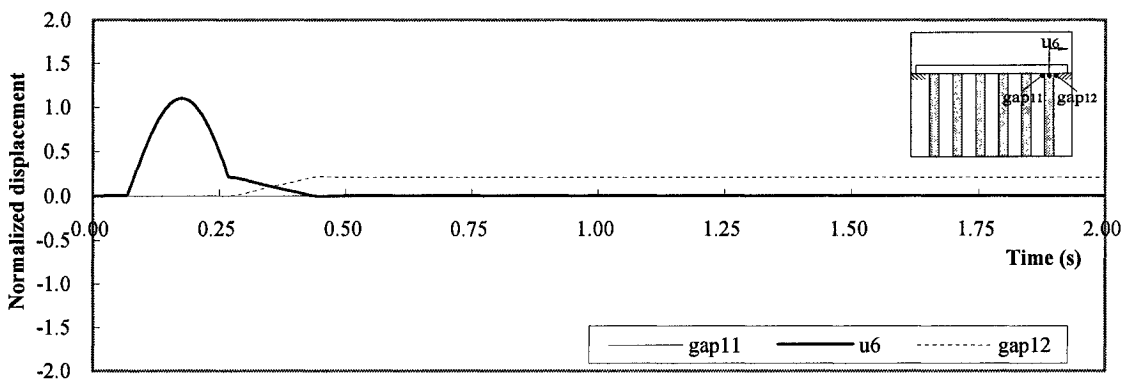

(f) 6th pile and gap11, gap12

Fig. 5.4 Displacements of piles and gaps at the ground level when a short pulse (T_g = *0.2* s) propagates into a 6 x 6 pile group in medium soil (V_s = *140.0* m/s). (continued)

placed inside the 6 x 6 pile group. The separation between pile and soil remains open only in the soil at the right side of the 6th pile.

A larger gap is formed when the wave propagates into a group of piles placed in soft soil. This is illustrated in Figures 5.3 (soft soil) and 5.4 (stiff soil). Nonlinear behavior is more frequent in soft soil due to its low stiffness, and the relative motion is greater because of wave amplification.

Figure 5.5 shows the gaps and absolute displacements of piles in soft soil for a vertically incident pulse with medium period ($T_g = 0.4$ s), and for a 6 x 6 pile group system. Gaps remain open in the soil at the right side of 6th pile and in the soil at the left side of the 1st pile. The amplitudes of these gaps are small compared with the case when shorter pulse ($T_g = 0.2$ s) propagates into the system (Figure 5.3). However, piles do not go back to their original positions even after all vibrations are damped out in this case (Figure 5.4). Although the pile behaves in a linear elastic range, irrecoverable, permanent deformation is created due to the movement of the soil blocks between the piles.

Figure 5.6 shows the permanent deformation of piles and of soil blocks in a 6 x 6 pile group system in soft soil excited by a vertically incident wave ($T_g = 0.4$ s, $U_0 = 0.5$ m), at time $t = 2.0$ s. The solid lines represent the permanent deformations of piles, and thick gray lines represent the residual displacements of soil blocks. The thin solid lines from left to right represent the original positions of the 1st pile and soil blocks in the 1st column to soil blocks in the 5th column and the 6th pile. Almost all components in the system remain at right relative to their initial positions. In particular, large permanent deformations are found at the top layers of the soil blocks. The elastic piles

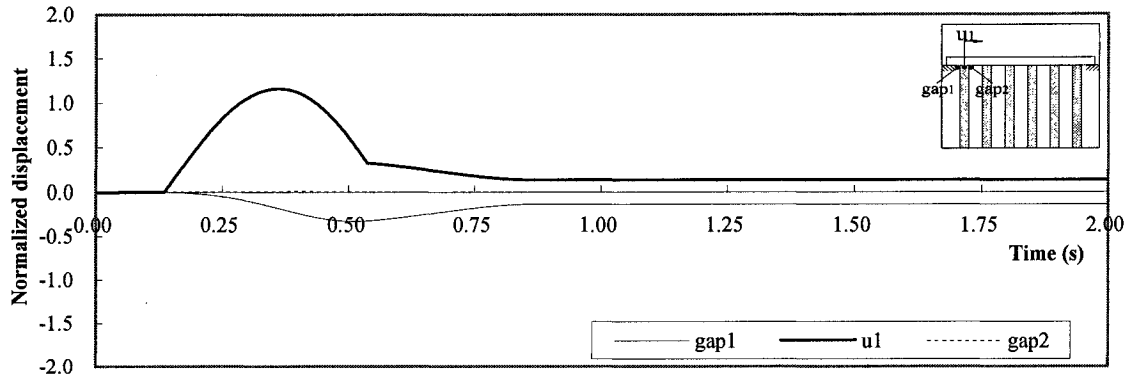

(a) 1st pile and gap1, gap2

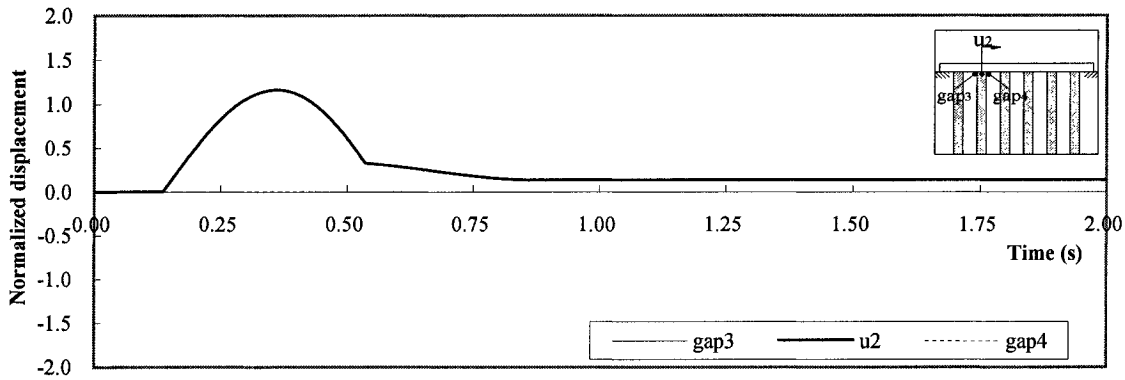

(b) 2nd pile and gap3, gap4

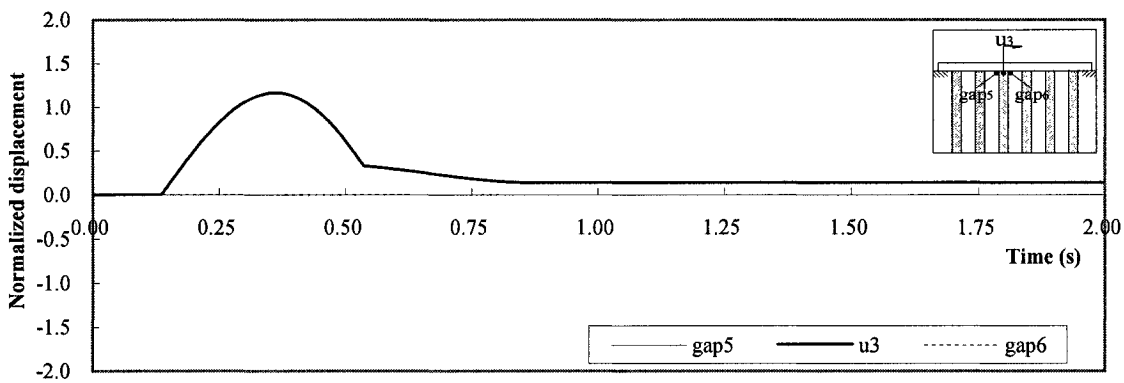

(c) 3rd pile and gap5, gap6

Fig. 5.5 Displacements of piles and gaps at the ground level when a pulse with medium period (T_g = *0.4* s) propagates intoa 6 x 6 pile group in soft soil (V_s = *70.0* m/s).

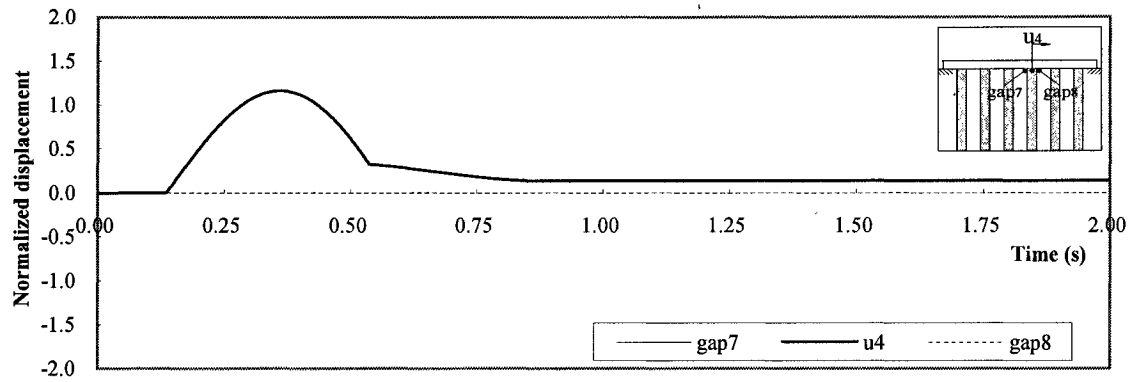

(d) 4th pile and gap7, gap8

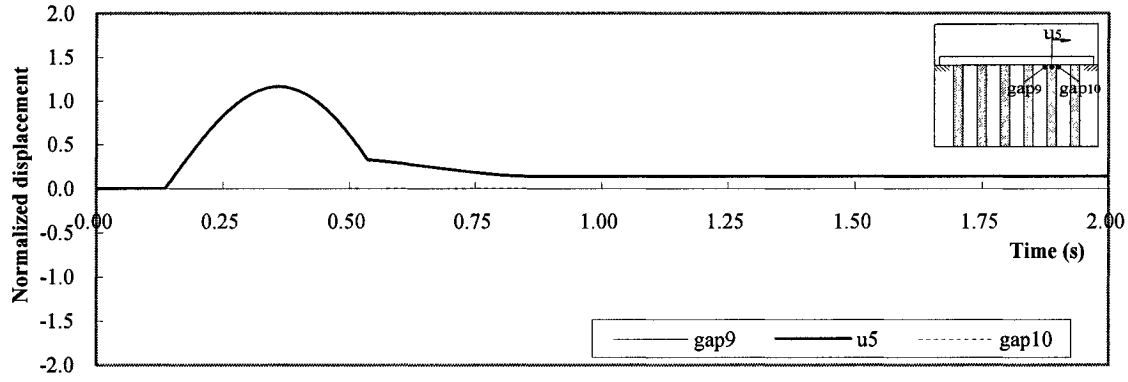

(e) 5th pile and gap9, gap10

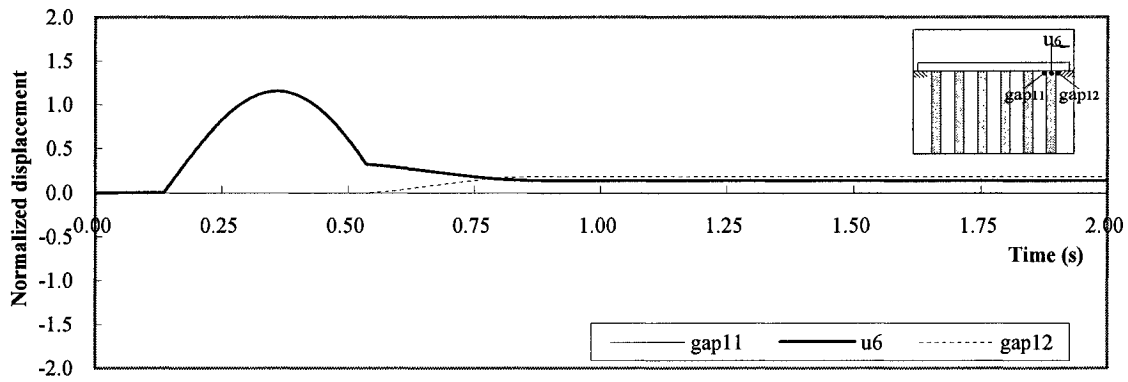

(f) 6th pile and gap11, gap12

Fig. 5.5 Displacements of piles and gaps at the ground level when a pulse with medium period (T_g = *0.4* s) propagates intoa 6 x 6 pile group in soft soil (V_s = *70.0* m/s). (continued)

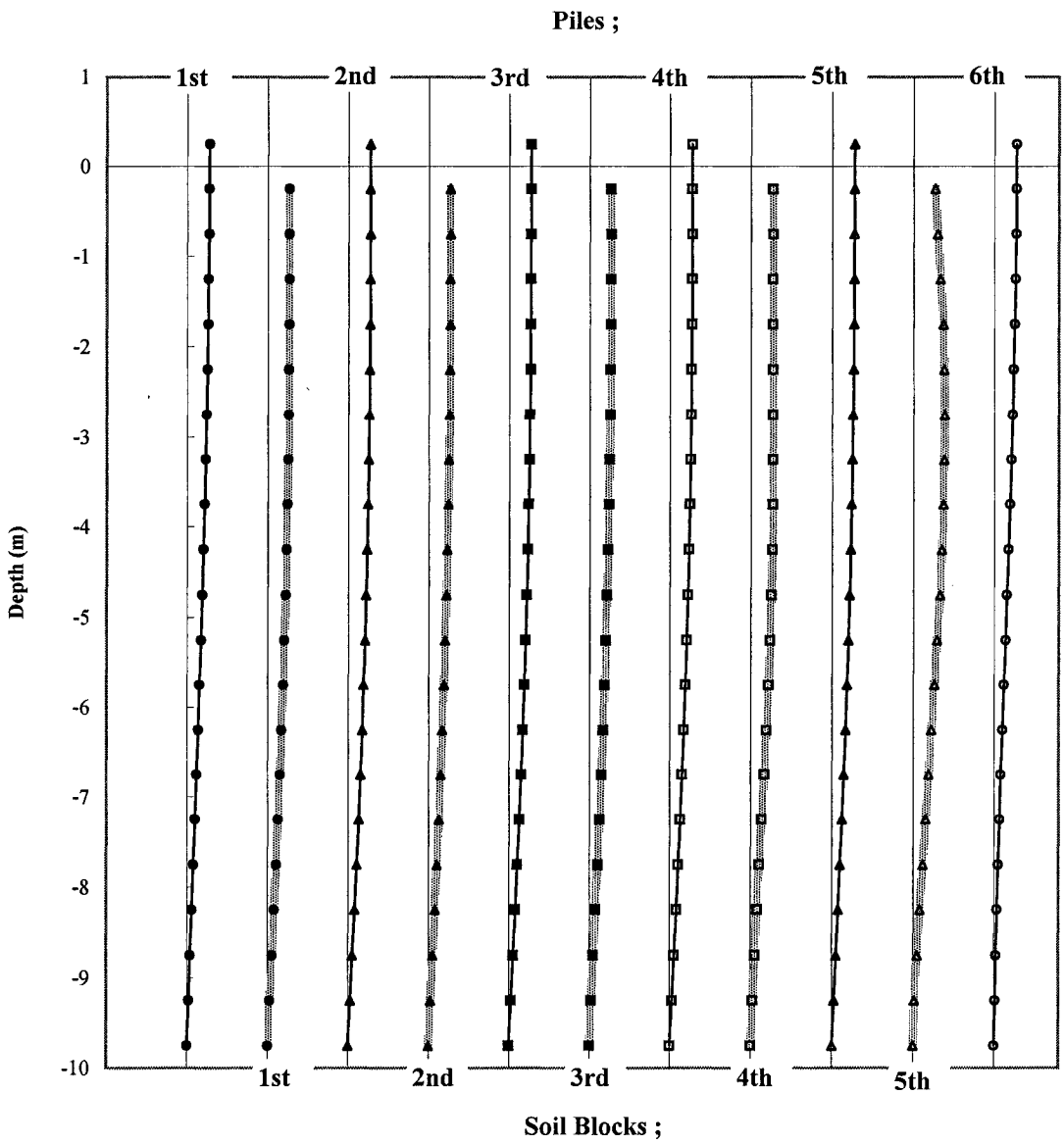

Fig. 5.6 Permanent deformations of piles and soil blocks of a 6 x 6 pile group in soft soil (V_s = *70.0 m/s*) caused by a vertically incident pulse with medium period (T_g *=0.4 s,* U_{g0} *=0.5 m*).

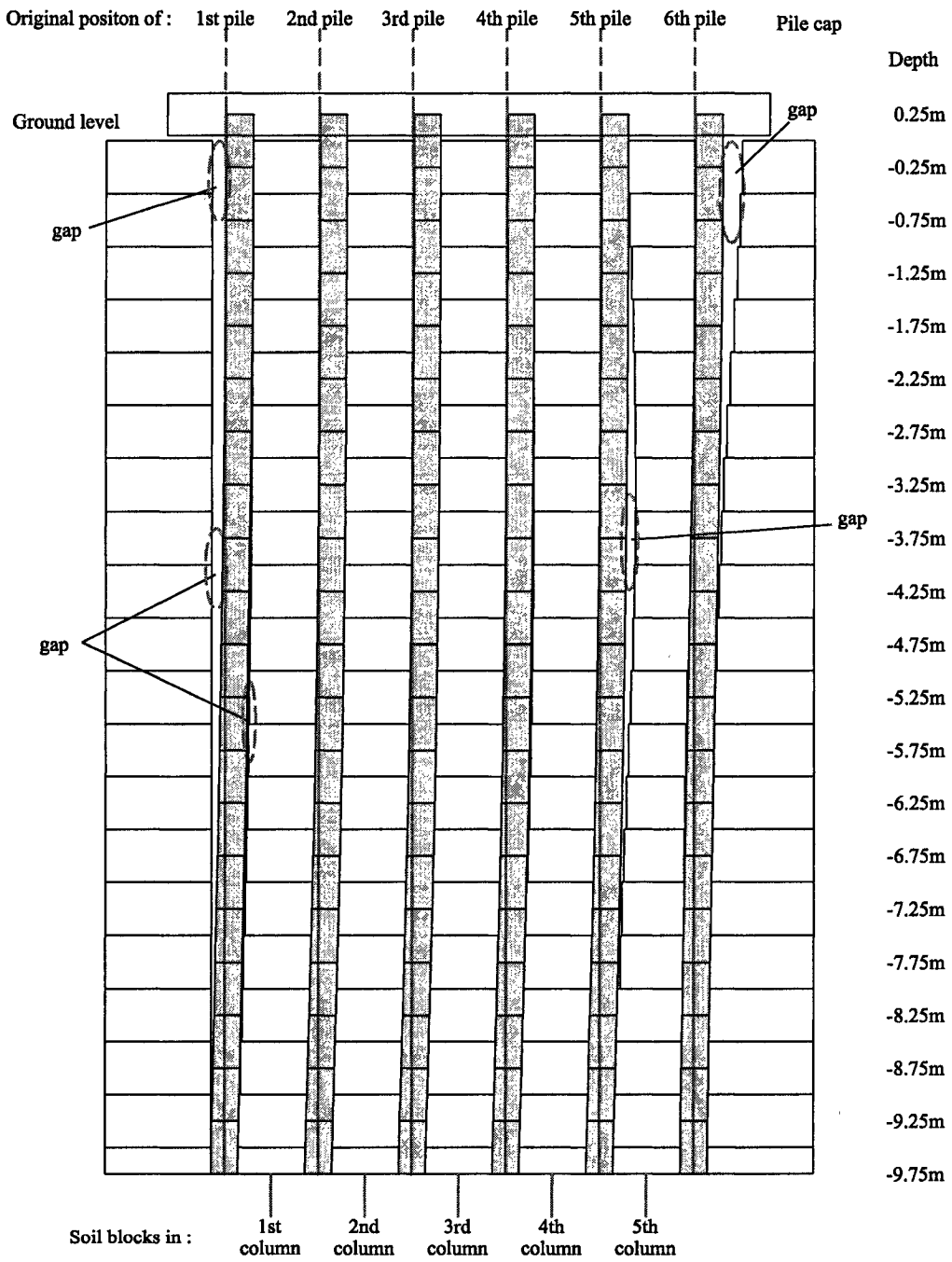

Fig. 5.7 Schematic illustration of permanent deformation of a system in soft soil caused by a vertically incident pulse with medium period (V_s=*70.0* m/s, T_g=*0.4* s).

also have residual deformation due to the forces from the soil blocks, which are generated by their permanent deformations. The recoverable forces of the piles do not exceed the friction forces of soil blocks when all movements of the system are damped out. Because piles are connected by a rigid pile cap, the 1st pile also has irrecoverable deformation even though it does not have contacts or forces exerted on it by soil blocks.

Figure 5.7 illustrates schematically the permanent deformation of the system, including irrecoverable deformation of piles and the gaps in the soil at the soil-pile interface. A large gap is formed at the right side of the 6th pile. As the vertically incident wave shakes the system from left to right, the significant deformation is found at the right part of the system, and gaps are formed mainly at the top parts of the system.

The absolute displacements of piles and the gaps for the 6 x 6 pile group foundation in stiff soil are presented in Appendix B. No separations between pile and soil are found in this case because of the greater stiffness of stiff soil. The results for 4 x 4 and 2 x 2 pile group foundations are also presented in Appendix B.

5.3 Bending moment and deformation of piles

The maximum deflection and bending moment of piles are important for an engineer designing a pile foundation for lateral loads (Hsiung, 2003). The maximum deflection is related to the safety of the super-structure supported by piles. The piles will be overstressed when the bending moment exceeds the allowable moment of the pile materials. Therefore, the maximum bending moment and deformation of piles in a group are analyzed in the following.

Figure 5.8 shows the maximum absolute bending moments and maximum displacements of piles in a 6 x 6 pile group system placed in medium soil ($V_s = 140.0$ m/s). The maximum displacement of the piles is normalized by the maximum displacement of the input pulse (1.0 m). The responses of the piles are computed for short a incident pulse ($T_g = 0.2$ s) and for a long incident pulse ($T_g = 0.8$ s). The pile-spacing ratio and amplitude of input pulse are assumed to be 4.0 ($s/d = 4.0$) and 0.5m ($U_{g0} = 0.5$ m).

The plot in the left part of Figure 5.8 shows the maximum absolute bending moment of piles in the system. The x axis shows the maximum bending moment in kN-m and the y axis shows the depth below the ground surface. The solid lines with full circles and open circles represent the responses of the 1st pile and 6th pile, respectively, which are at the outer ends of the group. The gray lines show the responses of piles located inside of the group. The maximum bending moment occurs at the tops of the piles where they are connected to the rigid pile cap. A short input pulse ($T_g = 0.2$ s) generates a large bending moment at the tops of the piles. Particularly, the pile at the far

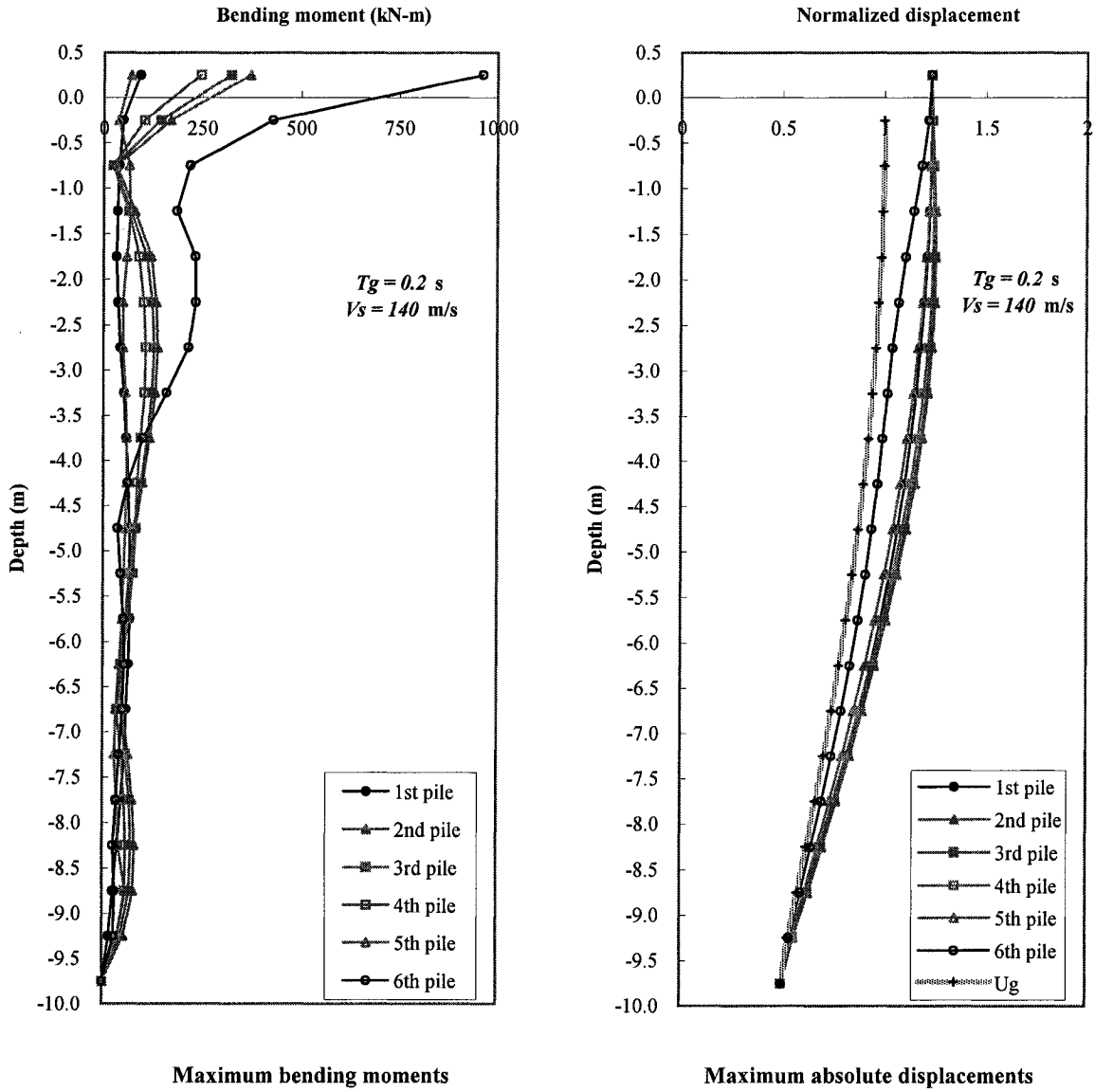

(a) By a short incident pulse ($T_g = 0.2\ s$)

Fig. 5.8 Maximum absolute bending moments and maximum displacements of piles of a 6 x 6 pile group in medium soil ($V_s = 140.0$ m/s).

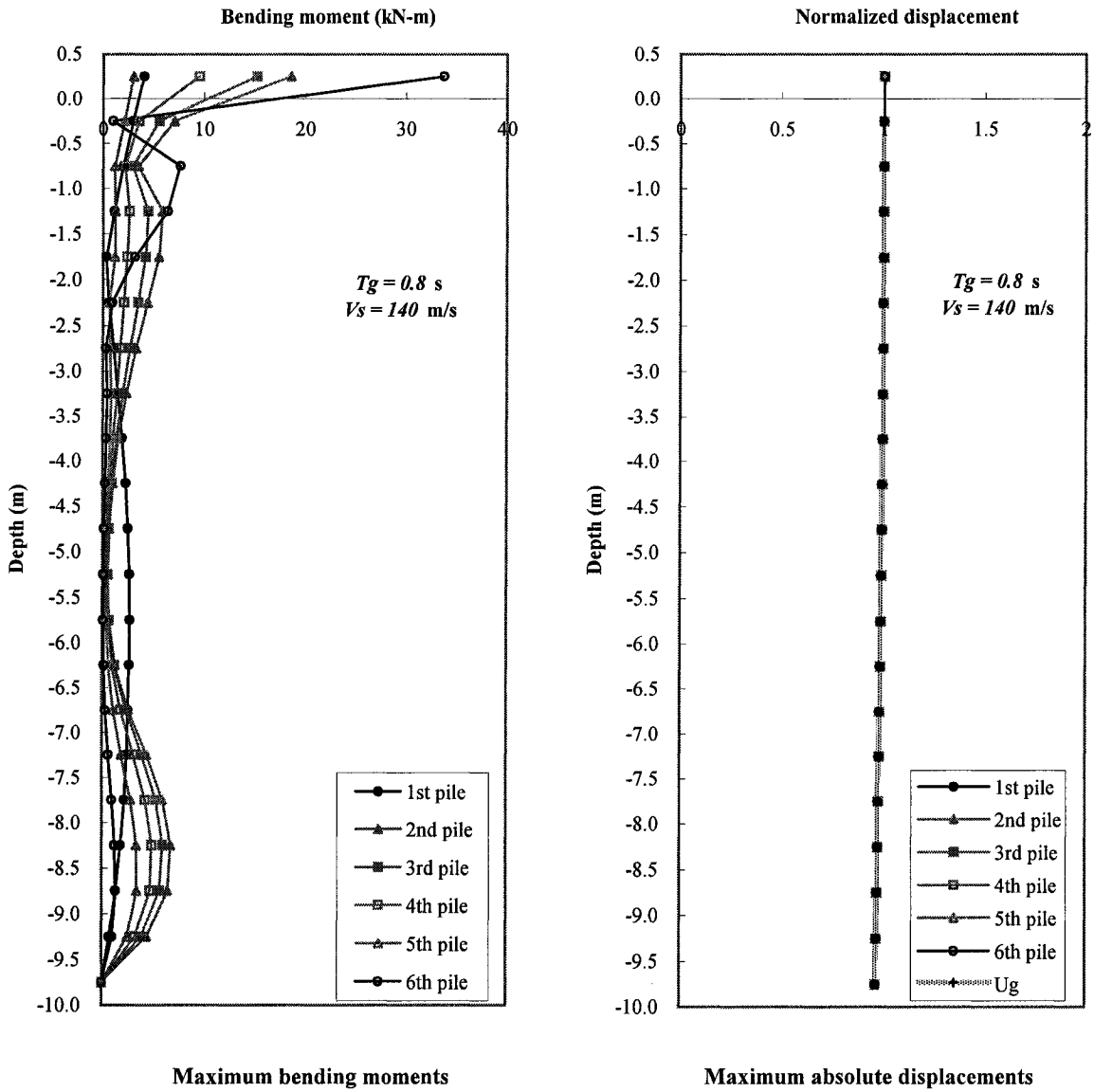

(b) By a long incident pulse (T_g = *0.8 s*)

Fig. 5.8 Maximum absolute bending moments and maximum displacements of piles of a 6 x 6 pile group in medium soil (V_s = *140.0* m/s). (continued)

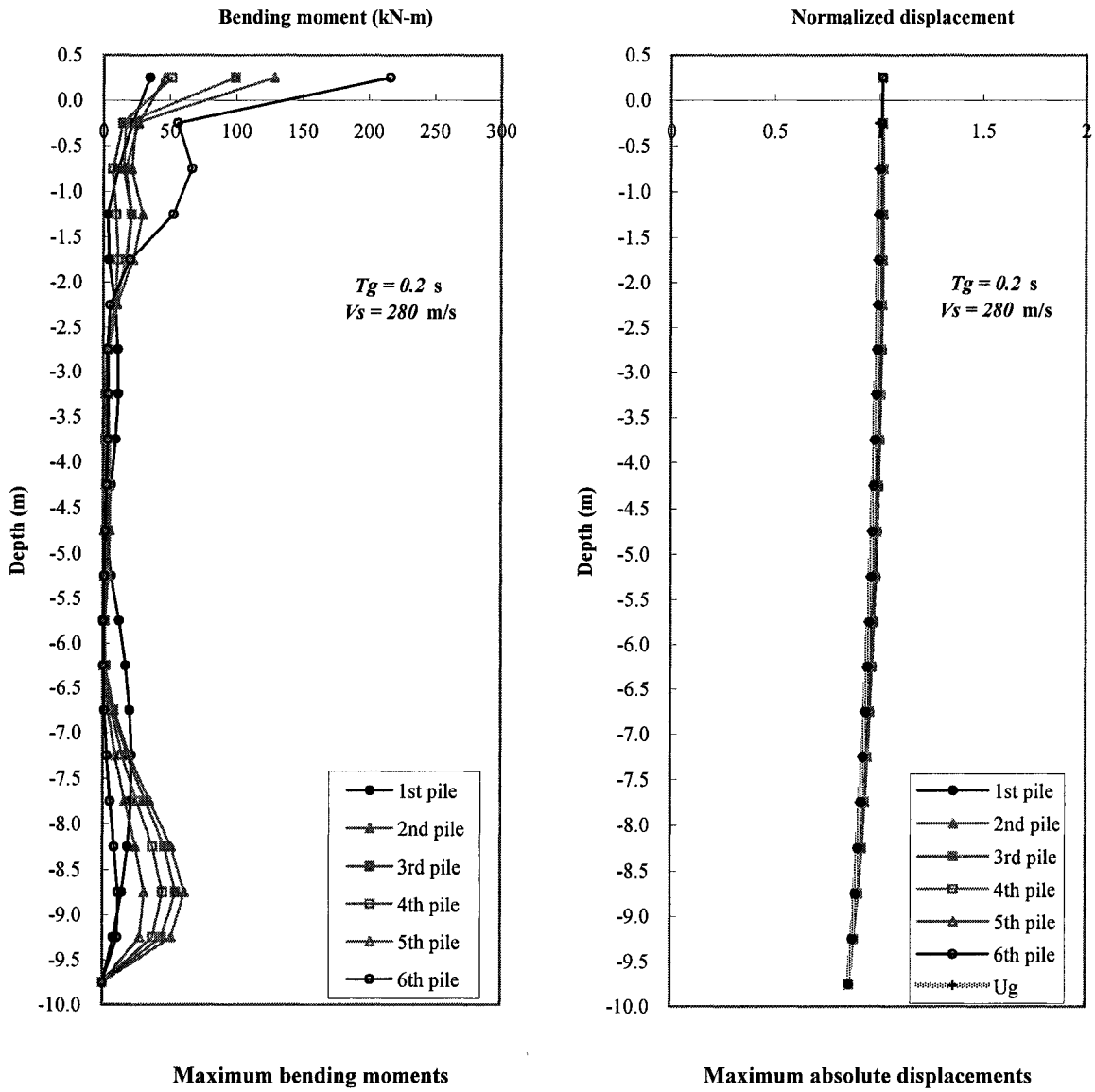

(a) In stiff soil (V_s = *280.0* m/s)

Fig. 5.9 Maximum absolute bending moments and maximum displacements of piles of a 6 x 6 pile group by short incident pulse (T_g = *0.2* m/s).

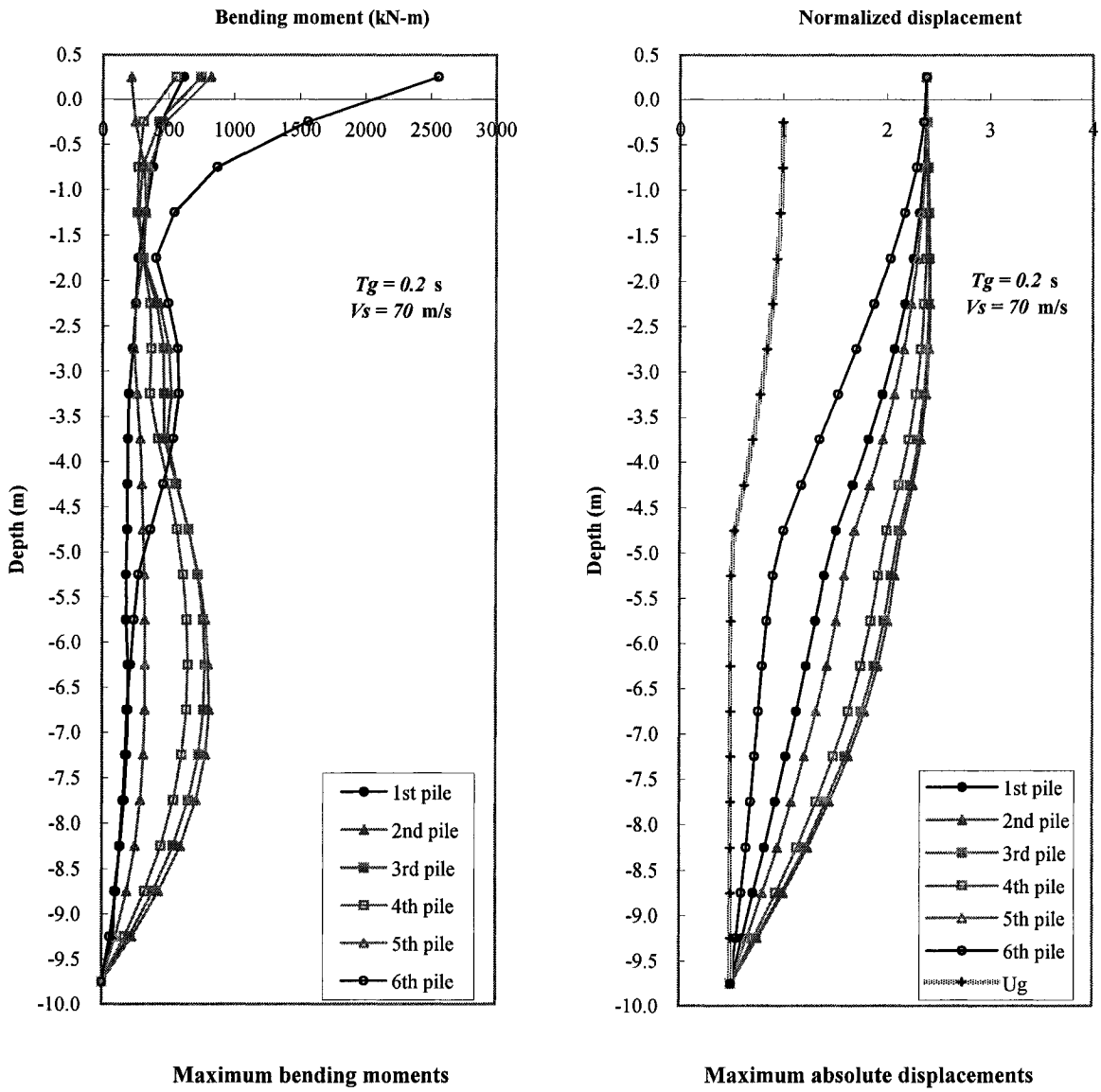

(b) In soft soil (V_s = *70.0* m/s)

Fig. 5.9 Maximum absolute bending moments and maximum displacements of piles of a 6 x 6 pile group by short incident pulse (T_g = *0.2* m/s). (continued)

right side of the system experiences a large bending moment at the top (1st and 6th piles in 6 x 6 pile group system, 1st and 4th piles in 4 x 4 system). Because of the effects of the movement of soil blocks, relatively large bending moments are generated at the mid-height of the piles that are located inside the system.

The plot in the right part of Figure 5.8 shows the maximum total displacement ($U+U_g$) of each pile and the maximum displacement of the incident wave. The x axis represents the normalized displacement, and the y axis shows the depth. Solid lines and gray lines represent the displacements of piles in the group. The thick gray line with crosses represents the maximum displacement of the vertically incident input pulse. There is considerable difference between the maximum displacement of piles and wave amplitude near the top of the piles for a short pulse ($T_g = 0.2\,\mathrm{s}$), which causes permanent gaps in the soil-pile interfaces near the ground surface. The piles and the soil move almost simultaneously when excited by a long input pulse ($T_g = 0.8\,\mathrm{s}$), which generates no separation between piles and soil.

Figures 5.9 (a) and (b) illustrate the response of piles in stiff soil ($V_s = 280.0\,\mathrm{m/s}$) and in soft soil ($V_s = 70.0\,\mathrm{m/s}$) when a short input pulse ($T_g = 0.2\,\mathrm{s}$) shakes the 6 x 6 pile group. The other conditions are the same as in the case shown in Figure 5.8. The maximum absolute moment and total displacement are greater when the system is placed in soft soil, due to amplification of response and low stiffness of soil in the near field of the piles. A greater bending moment is generated in the mid-height of the piles in soft soil relative to the system placed in stiff soil. A large difference between the total displacement of the piles and the input pulse is found for the pile foundation placed in soft soil, which forms large gap openings in the soil-pile interfaces, as seen in

section 5.2. However, the movements of the piles relative to the incident pulse are small in stiff soil due to the high stiffness of the soil. The maximum absolute bending moment is relatively small compared with the response determined when a short pulse shakes the system in soft soil.

The maximum bending moments and displacements of piles for excitation by a pulse with intermediate duration ($T_g = 0.4\,\mathrm{s}$) are presented in Appendix B. The results for 4 x 4, and 2 x 2 pile groups are also shown in Appendix B. The same trends as for the 6 x 6 pile group are found in these cases.

5.4 Investigation of group pile effects

In the following, the group effects are investigated by analyzing different types of pile foundations with the same dimensions. Figure 5.10 illustrates five types of pile group systems schematically. The pile-spacing ratios are 10.0 (*s/d = 10.0*) in a 2 x 2 pile group foundation and 2.0 (*s/d = 2.0*) in a 6 x 6 pile group foundation. The total length from the 1st pile to the last pile is the same, $10.0 \cdot d_p$, where d_p is the diameter of a pile. The friction angle and friction coefficient of the soil are assumed to be $50°$ and 0.5 ($\phi = 50°$, $\mu = 0.5$). The mass of the rigid building is add to the pile cap. Three kinds of "building" (1-story, 10-story, and 30-story) are used for computation, which have unit mass of $376.16 kg/m^3$ (as shown in Chapter 4).

Figure 5.11 shows the percentages of maximum kinetic energy of the total system energy for various types of pile groups with rigid "building" on the top. The *x* axis shows the number of piles (2 ~ 6), and the *y* axis presents the percentage of energy. The kinetic energy of the building grows as the number of piles increases. A relatively small portion of energy is dissipated in the foundations with a large number of piles, but the percentage of kinetic energy of the soil to total system energy decreases as piles are added to the foundation. The amount of total mass of the soil is small in foundations with a large number of piles, with a small pile-spacing ratio. Figure 5.12 shows the ratio of the masses of building and piles to the mass of soil in the foundation.

Maximum displacements of piles normalized with the maximum displacement of the incident wave are shown in Figure 5.13 (a). Relatively large displacements are generated in the system with a small number of piles because the foundation does not

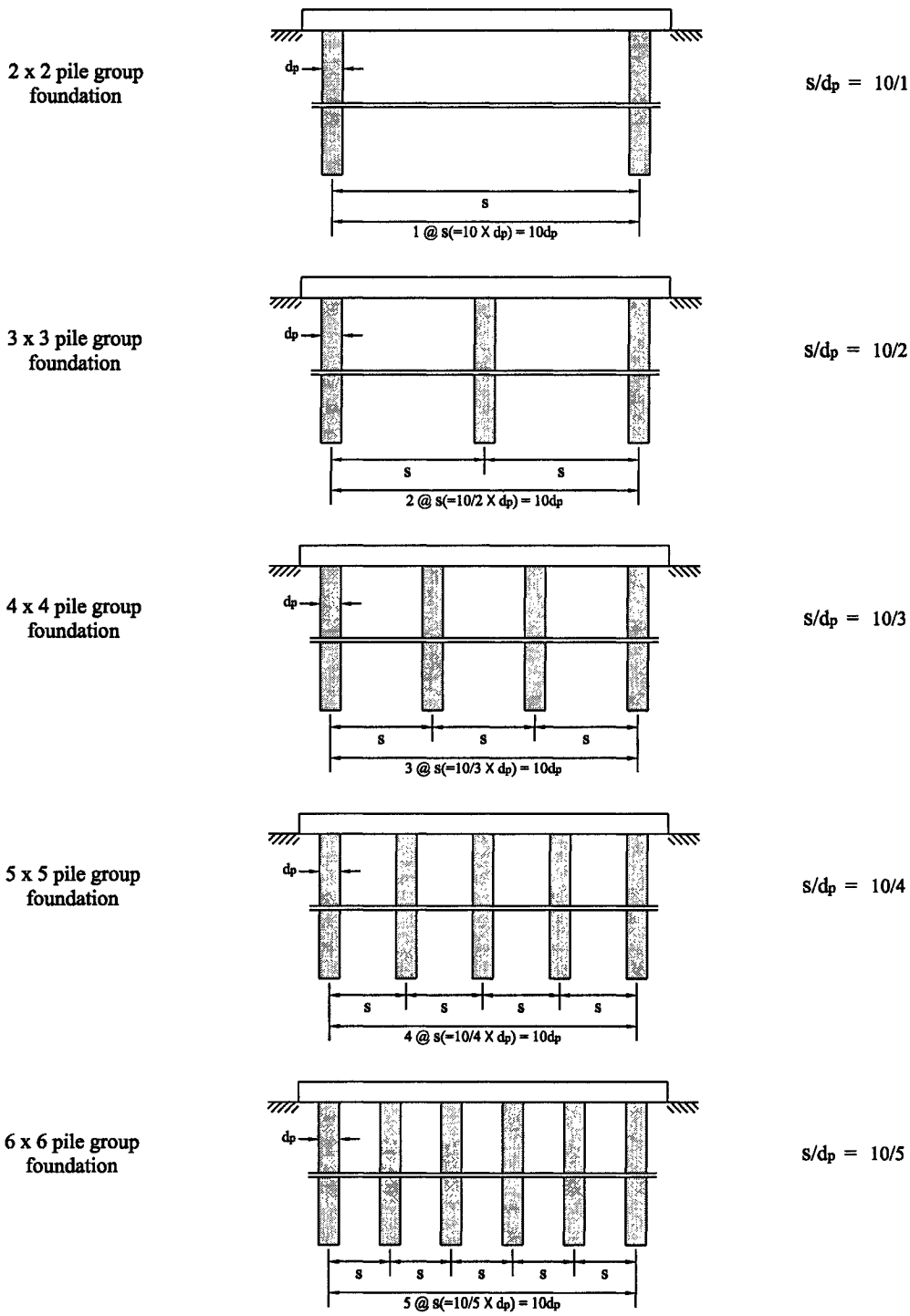

Fig. 5.10 Five types of pile group foundations with the same dimensions.

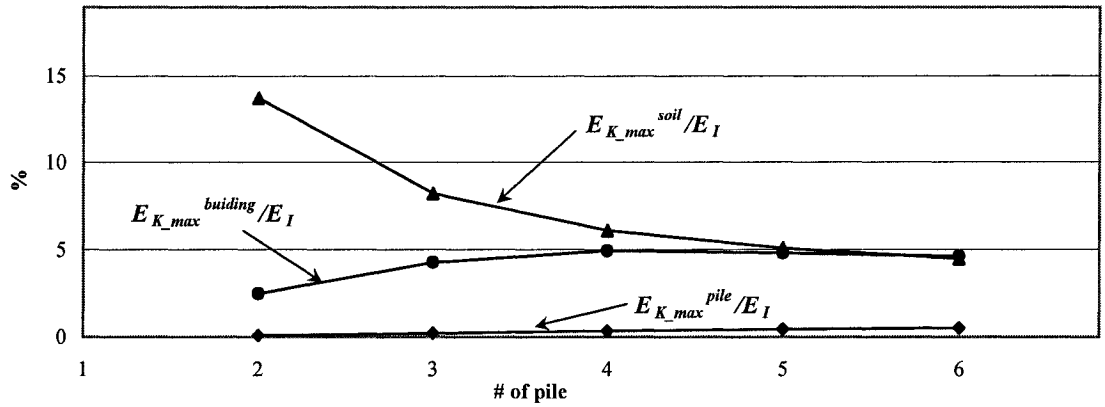

(a) 1-story

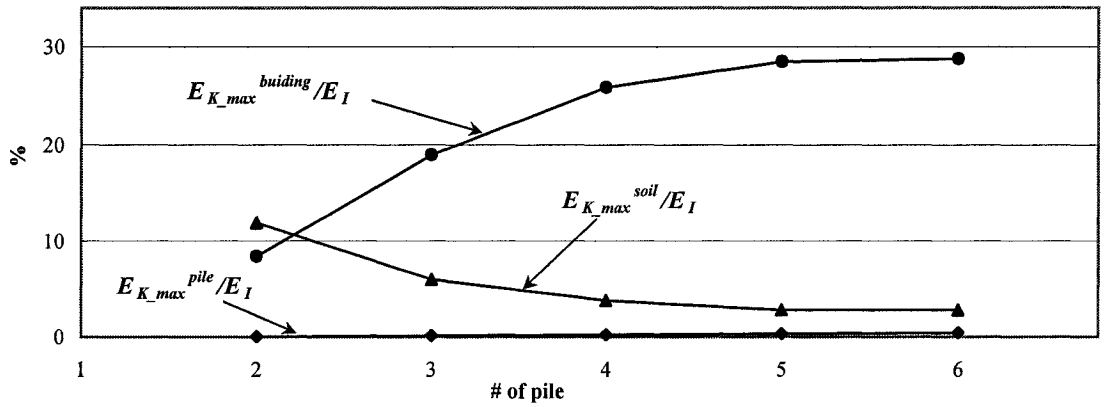

(b) 10-story

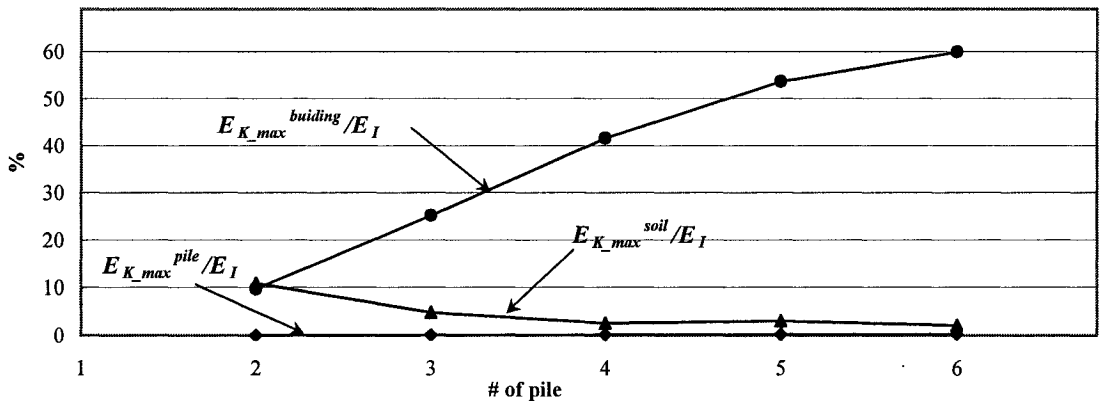

(c) 30-story

Fig. 5.11 Percentages of maximum kinetic energy to total system energy for various types of pile groups.

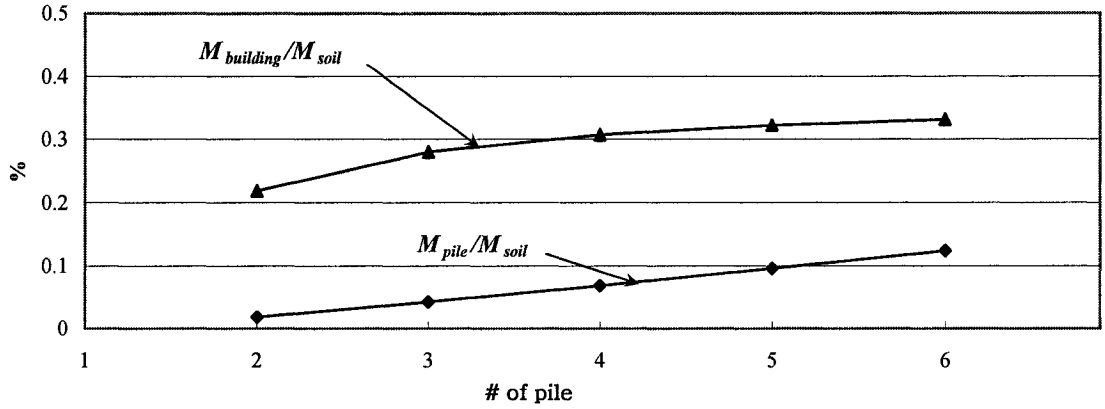

(a) 1-story

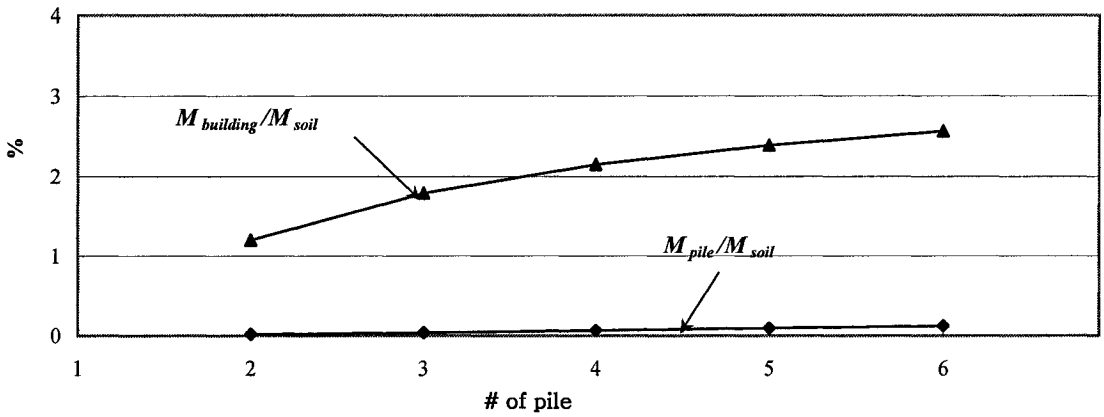

(b) 10-story

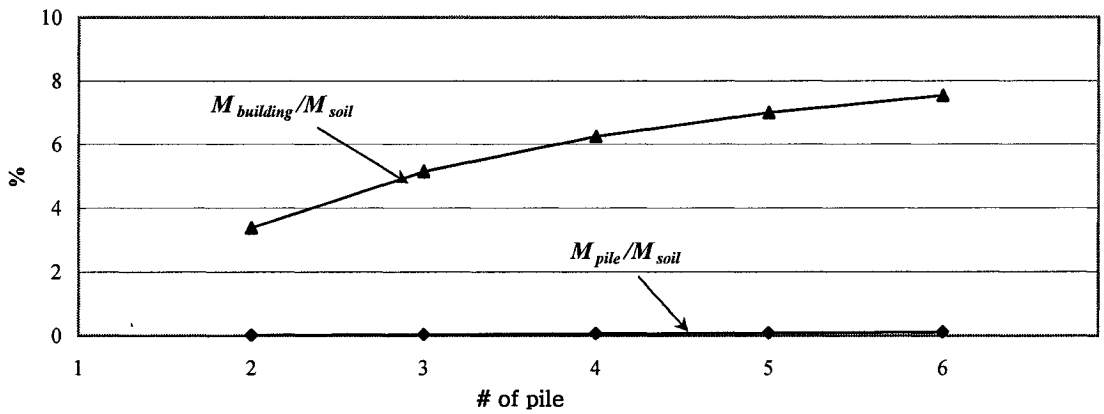

(c) 30-story

Fig. 5.12 Ratio of masses of buildings and piles to mass of soil for various types of pile groups.

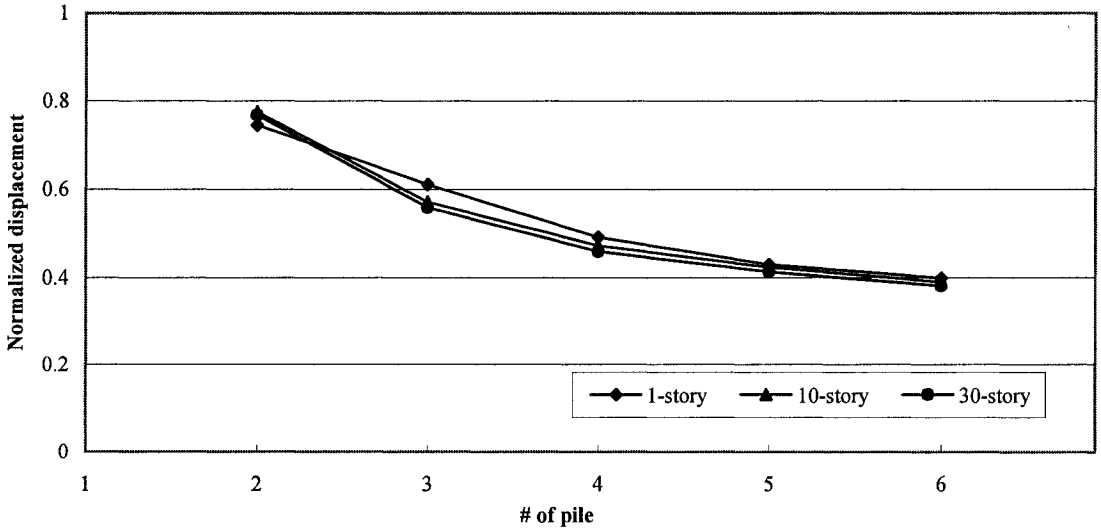

(a) Maximum displacements of pile top normalized to maximum displacement of pulse

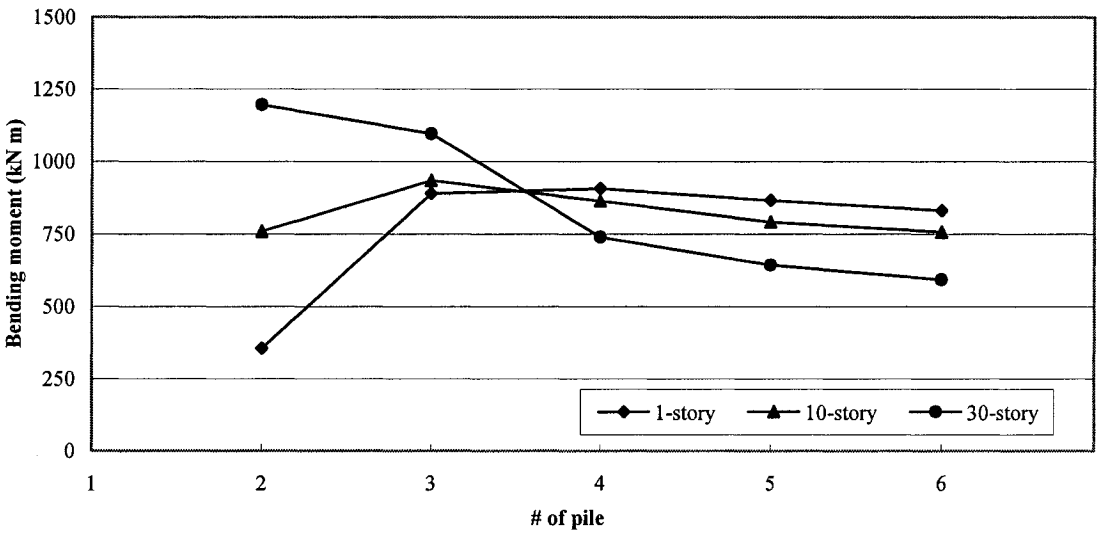

(b) Maximum bending moment of pile

Fig. 5.13 Response of various types of pile group foundations with rigid buildings in soft soil (V_s = *70.0* m/s) caused by a short pulse (T_g = *0.2* s).

offer much resistance to horizontal translation. Figure 5.13 (b) shows the maximum bending moments for piles in different pile groups.

It can be seen that small horizontal displacements and bending moments in piles are generated in foundations with a greater number of piles. However, a large portion of incident wave energy is then transferred to the super structure. This energy excites the building and can damage it. In contrast, relatively littel energy gets into the building at the foundation with a small number of piles, although a large displacement and bending moment of the piles may occur in this type of foundation. This can be critical for piles and the stability of the foundation.

6. Summary and Conclusions

In this study, a simple pile-soil-pile model for the lateral response is investigated, considering nonlinear behavior of the soil and grouped effects on the piles. The grouped pile effects are developed via interaction force of the soil blocks. The general excitation and response of a foundation subjected to a non-vertically incident wave are presented briefly.

The properties of the proposed model are studied by comparison with compliance functions for horizontal oscillation of a rigid disc placed on an elastic half-space. The compliance function of the group pile system is very close to the results found by of Luco et al. (1971, 1972) in a linear range. As the amplitudes of force become greater, the real part of compliance increases significantly, and the peak shifts toward a value of low frequency, which is seen in a stiffness-softening system.

Pile-soil-pile interactions may change the motion of the ground and the response of total foundation system. These interactions depend upon the properties of soil, the pile group, and input motions. The pile-soil-pile interactions dissipate and can significantly reduce the input energy, which can excite and damage the superstructures.

Considerable energy is imparted into the system by a short input pulse with low velocity (in soft soil) due to large relative deformation caused by the wave passage. The incident wave energy can cause nonlinear behavior of the soil in the system and is dissipated by this response during pile-soil-pile interaction. Large input motions cause big bending moments in piles and create gaps at the soil-pile interface. Piles located at the outer ends of groups experience the greatest bending moments and separations

(gaps) from the adjacent soil, and the frictional movements of soil blocks can cause permanent deformation of piles even though the pile material is assumed to respond in a linear elastic range. Larger gaps and bending moments are generated when a group of piles is placed in soft soil. When soil-pile interaction remains in a linear range of deformation, the energy is dissipated only by the friction of the soil blocks.

Studies of the examples show that the number of piles and the pile-spacing ratio also effect the interactions in the pile foundation. The designer should search for appropriate parameters to reduce the energy transferred into the building, while maintaining suitable safety factors in the design of piles and foundations.

References

1. Achenbach, J. D., *Wave Propagation in Elastic Solids*, Elsevier Science Publishing Company Inc., New York, New York. (1973)

2. American Petroleum Institute, Recommended Practice for Planning, Designing and Constructing Fixed Offshore Platforms, API Recommended Practice 2A (RP 2A), 19th Edition, Washington, D.C. (1991)

3. Ashour, M., Norris, G., and Pilling, P., 'Lateral loading of a pile in layered soil using the strain wedge model', *Journal of Geotechnical and Geoenvironmental Engineering,* Vol. 124, No. 4, pp 303-315. (1998)

4. Ashour, M., Norris, G., and Pilling, P., 'Strain wedge model capability of analyzing behavior of laterally loaded isolated piles, drilled shafts, and pile groups', *Journal of Bridge Engineering,* Vol. 7, No. 4, pp 245-254. (2002)

5. Ashour, M., Pilling, P., and Norris, G., 'Lateral behavior of pile group in layered soils', *Journal of Geotechnical and Geoenvironmental Engineering,* Vol. 130, No. 6, pp 580-592. (2004)

6. Avilés, J., Suárez, M., and Sánchez-Sesma, F. J., 'Effects of wave passage on the relevant dynamic properties of structures with flexible foundation', *Earthquake Engineering and Structural Dynamics*, Vol. 31, pp 139-159. (2002)

7. Biot, M. A., 'Bending of an infinite beam on elastic foundation', *Journal of Applied Mechanics, Transactions, ASCE*, Vol. 59, pp A1-A7. (1937)

8. Blaney, G. W., and O'Neill, M. W., 'Measured lateral response of mass on single pile in clay', *Journal of Geotechnical Engineering*, Vol. 112, No. 4, pp 443-457. (1986)

9. Blaney, G. W., and O'Neill, M. W., 'Analysis of dynamics laterally loaded pile in clay', *Journal of Geotechnical Engineering*, Vol. 112, No. 9, pp 827-840. (1986)

10. Bowles, J. E., *Foundation analysis and design*, McGraw-Hill, New York, NY. (1982)

11. Brown, D. A., Reese, L. C., and O'Neill, M. W., 'Cycle lateral loading of a large-scale pile group', *Journal of Geotechnical Engineering*, Vol. 113, No. 11, pp 1326-1343. (1987)

12. Brown, D. A., Morrison, C., and Reese, L. C., 'Lateral load behavior of pile group in sand', *Journal of Geotechnical Engineering*, Vol. 114, No. 11, pp 1261-1276. (1988)

13. Cai, Z., and Bathurst, R. J., 'Deterministic sliding block methods for estimating seismic displacements of earth structures', *Soil Dynamics and Earthquake Engineering*, 15, 4, pp 255-268. (1996)

14. Chopra, A. K., and Zhang, L, 'Earthquake-induced base sliding of concrete gravity dams', *Journal of Structural Engineering*, Vol. 117, No. 12, pp 3698-3719. (1992)

15. Craig, R. F., *Soil Mechanics*, E & FN Spon, 6th Edition, New York, NY. (1997)

16. Curras, C. J., Boulanger, R. W., Kutter, B. L., and Wilson, D. E., 'Dynamic experiments and analyses of a pile-group-supported structure', *Journal of Geotechnical and Geoenvironmental Engineering,* Vol. 127, No. 7, pp 585-596. (2001)

17. Das, B. M., *Principles of Foundation Engineering*, PWS-KENT Publishing Company, 2nd Edition, Boston, Massachusetts. (1990)

18. Dorby, R., and Gazetas, G., 'Simple method for dynamic stiffness and damping of floating pile groups', *Geotechnique*, 38, No. 4, pp 557-574. (1988)

19. El Naggar, M. H., and Novak, M., 'Nonlinear lateral interaction in pile dynamics', *Soil Dynamics and Earthquake Engineering*, 14, 2, pp 141-157. (1995)

20. El Naggar, M. H., and Novak, M., 'Nonlinear analysis for dynamic lateral pile response', *Soil Dynamics and Earthquake Engineering*, 15, 4, pages 233-244. (1996)

21. El Sharnouby, B., and Novak, M., 'Static and low-frequency response of pile groups', *Canadian Geotechnical Journal*, Vol. 11, pp 79-94. (1985)

22. Essebier, S., and Baker, G., 'Computational techniques for nonlinear dynamics of continuous systems', *Journal of Engineering Mechanics*, Vol. 121, No. 11, pp 1193-1199. (1995)

23. Gazetas, G., 'Dynamic compliance matrix of rigid strip footing bonded to viscoelastic cross anisotropic halfspace', *International Journal of Mechanical Sciences*, Vol. 23, No. 9, pp 547-559. (1981)

24. Gazetas, G., 'Analysis of machine foundations: state of the art', *Soil Dynamics and Earthquake Engineering*, Vol. 2, No. 1, pp 1-42. (1983)

25. Gazetas, G., and Dorby, R., 'Simple radiation damping model for piles and footings', *Journal of Engineering Mechanics*, Vol. 110, No. 6, pp 937-956. (1984)

26. Gazetas, G., and Dobry, R., 'Horizontal response of piles in layered soils', *Journal of Geotechnical Engineering,* Vol. 110, No. 1, pp 20-40. (1984)

27. Gazetas, G., Fan, K., and Kaynia, A., 'Dynamic response of pile groups with different configurations', *Soil Dynamics and Earthquake Engineering*, Vol. 12, pp 239-257. (1993)

28. Gazetas, G., and Uddin, N., 'Permanent deformation of preexisting sliding surface in dams', *Journal of Geotechnical Engineering*, Vol. 120, No. 11, pp 2041-2061. (1994)

29. Han, Y., and Novak, M., 'Dynamic behaviour of single piles under strong harmonic excitation', *Canadian Geotechnical Journal*, 25, 3, pp 523-534. (1988)

30. Hao, T-Y, 'Investigation of energy flow in earthquake response of structures', Thesis

presented to the University of Southern California, Los Angeles, California, in partial fulfillment of the requirements for the degree of Doctor of Philosophy. (2002)

31. Han, Y., and Vaziri, H., 'Dynamic response of pile groups under lateral loading', *Soil Dynamics and Earthquake Engineering*, Vol. 11, pp 87-99. (1992)

32. Hsiung, Y. M., 'Theoretical elastic-plastic solution for laterally loaded piles', *Journal of Geotechnical and Geoenvironmental Engineering,* Vol. 129, No. 6, pp 475-480. (2003)

33. Hundal, M. S., 'Response of a base excited system with Coulomb and viscous friction', *Journal of Sound and vibration*, Vol. 64, No. 3, pp 371-378. (1979)

34. Ivanović, S. S., Trifunac, M. D., Novikava, E. I., Gladkov, A. A., and Todorovska, M. I., 'Ambient vibration tests of a seven-story reinforced concrete building in Van Nuys, California, Damaged by the 1994 Northridge Earthquake', *Soil Dynamics and Earthquake Engineering*, Vol. 19, No. 6, pp 391-411. (2000)

35. Jacobsen, L. S., and Ayre, R. S., *Engineering Vibrations*, McGraw-Hill Company, Inc, New York, NY. (1958)

36. Kagawa, T., and Kraft, L. M., 'Soil-pile-structure interaction of offshore structures during an earthquake', *Proceedings 12th Annual Offshore Technology Conference*, Vol. 3, pp 235-245. (1980)

37. Kaynia, A. M., and Mahzooni, S., 'Forces in pile foundations under seismic loading', *Journal of Engineering Mechanics,* Vol. 122, No. 1, pp 46-53. (1996)

38. Kishida, H., and Nakai, S., 'Analysis of a laterally loaded pile with non-linear subgrade reaction', *Transactions of the Architectural Institute of Japan*, 281, pp 41-55. (1979)

39. Kramer, S. L., *Geotechnical Earthquake Engineering*, Prentice Hall, Upper Saddle River, New Jersey. (1996)

40. Kutter, B. L., and Wang, S., 'A bounding surface model for dynamic soil-pile interaction', *Structural Engineering World Wide 1998*, Elsevier Science Ltd., Oxford, England, Paper T143-3. (1998)

41. Luco, J. E., 'Dynamic interaction of a shear wall with the soil', *Journal of the Engineering Mechanics Division, ASCE,* Vol. 95, No. EM2, pp 333-346. (1969)

42. Luco, J. E., and Westmann, R. A., 'Dynamic response of Circular Footings', *Journal of the Engineering Mechanics Division, ASCE,* Vol. 97, No. EM5, pp 1381-1395. (1971)

43. Luco, J. E., and Westmann, R. A., 'Dynamic response of a rigid footing bonded to an elastic half space', *Journal of Applied Mechanics,* Vol. 39, No. , pp 527-534. (1972)

44. Luco, J. E., Wong, H. L. and Trifunac, M. D., 'A note on the dynamic response of rigid embedded foundations', *Earthquake Engineering and Structural Dynamics*, Vol. 4, pp 119-127. (1975)

45. Luco, J. E., Trifunac, M. D., and Wong, H. L., 'Soil structure interaction effects on forced vibration tests', *Report No. 86-05*, Department of Civil Engineering, University of Southern California, Los Angeles, California. (1986)

46. Makris, N., and Gazetas, G., 'Dynamic pile-soil-pile interaction. Part 2: Lateral and seismic response', *Earthquake Engineering and Structural Dynamics*, Vol. 21, pp 145-162. (1992)

47. Makris, N., 'Soil-pile interaction during the passage of Rayleigh waves: An analytical solution', *Earthquake Engineering and Structural Dynamics*, Vol. 23, pp 153-167. (1994)

48. Matlock, H, 'Corrections for design of laterally loaded piles in soft clay', *Proceedings 2th Annual Offshore Technology Conference*, Vol. 1, pp 577-588. (1970)

49. McVay, M., Zhang, L., Molnit, T., and Lai, P., 'Centrifuge testing of large laterally loaded pile groups in sands', *Journal of Geotechnical and Geoenvironmental Engineering,* Vol. 124, No. 10, pp 1016-1026. (1998)

50. Meirovitch, L., *Elements of Vibration Analysis*, McGraw-Hill, 2nd Edition, Boston, Massachusetts. (1986)

51. Mori, M., and Hasegawa, M., 'Seismic response analysis of pile-supported buildings considering material nonlinearity and pile-soil separation', *12th World Conference on Earthquake Engineering*, New Zealand Society for Earthquake Engineering, Upper Hutt, New Zealand, 2000, Paper No. 1774. (2000)

52. Mylonakis, G., Nikolaou, A., and Gazetas, G., 'Soil-pile-bridge seismic interaction: Kinematic and inertial effects. Part 1: Soft soil', *Earthquake Engineering and Structural Dynamics*, Vol. 26, pp 337-359. (1997)

53. Newmark, N. M., 'Effects of earthquakes on dams and embankments', *Geotechnique*, 15, No. 2, pp 139-160. (1965)

54. Nogami, T., and Novak, M., 'Resistance of soil to a horizontally vibrating pile', *Earthquake Engineering and Structural Dynamics*, 5, 3, pp 249-261. (1977)

55. Nogami, T., 'Flexural responses of grouped piles under dynamic loading', *Earthquake Engineering and Structural Dynamics*, Vol. 13, pp 321-336. (1985)

56. Nogami, T., and Konagai, K., 'Time domain flexural response of dynamically loaded single piles', *Journal of the Engineering Mechanics Division, ASCE*, Vol. 114, pp 1512-1525. (1988)

57. Nogami, T., Otani, J., Konagai, K., and Chen, H-L, 'Nonlinear soil-pile interaction model for dynamic lateral motion', *Journal of Geotechnical Engineering,* Vol. 118, No. 1, pp 89-106. (1992)

58. Novak, M., 'Dynamic stiffness and damping of piles', *Canadian Geotechnical Journal*, 11, 4, pp 574-598. (1974)

59. Novak, M., and Nogami, T., 'Soil-pile interaction in horizontal vibration', *Earthquake Engineering and Structural Dynamics*, 5, 3, pp 263-281. (1977)

60. Novak, M., and Aboul-Ella, F., 'Impedance functions of piles in layered media', *Journal of the Engineering Mechanics Division, ASCE*, Vol. 104, pp 643-661. (1978)

61. Novak, M., Nogami, T., and Aboul-Ella, F., 'Dynamic soil reactions for plane strain case', *Journal of the Engineering Mechanics Division, ASCE*, Vol. 104, pp 953-959. (1978)

62. Novak, M., and Sheta, M., 'Approximate approach to contact effects of piles', *Proceedings of a session sponsored by the Geotechnical Engineering Division at the ASCE National Convention, Dynamic Response of Pile Foundations: Analytical Aspects*, pp 53-79. (1980)

63. Novak, M., and Han, Y. C., 'Impedance of soil layer with boundary zone', *Journal of Geotechnical Engineering*, Vol. 116, No. 6, pp 1008-1014. (1990)

64. O'Rourke, M. J., and Dobry, R., 'Spring and dashpot coefficient for machine foundations on piles', *Proceedings American Concrete Institute International Symposium on Foundation for Equipment and Machinery,* Mar., Milwaukee, Wisconsin. (1979)

65. Pender, M. J., and Pranjoto, S., 'Gapping effects during cyclic lateral loading of piles in clay', *Proceedings Eleventh World Conference on Earthquake Engineering*, Pergamon, Elsevier Science Ltd., Oxford, England, Disc 2, Paper No. 1007. (1996)

66. Penzien, J., Scheffley, C. F., and Parmelee, F. A., 'Seismic analysis of bridges on long piles', *Journal of Engineering Mechanics*, ASCE, Vol. 90, No. EM3, pp 3953. (1964)

67. Poulos, H. G., and Davis, E. H., *Pile foundation analysis and design*, John Wiley and Sons, New York, NY. (1980)

68. Pratt, T. K., and Williams, R., 'Non-linear analysis of stick/slip motion', *Journal of Sound and Vibration*, Vol. 74, No. 4, pp 531-542. (1981)

69. Rathje, E. M., and Bray, J. D., 'Nonlinear coupled seismic sliding analysis of earth structures', *Journal of Geotechnical and Geoenvironmental Engineering,* Vol. 126, No. 11, pp 1002-1014. (2000)

70. Ruesta, P. F., and Townsend, F. C., 'Evaluation of laterally loaded pile group at Roosevelt Bridge', *Journal of Geotechnical and Geoenvironmental Engineering,* Vol. 123, No. 12, pp 1153-1161. (1997)

71. Shaw, S. W., 'On the dynamic response of a system with dry friction', *Journal of Sound and Vibration*, Vol. 108, No. 2, pp 305-325. (1986)

72. Todorovska, M. I., and Trifunac, M. D., 'Radiation damping during two-dimensional building-soil interaction', *Report No. 91-01*, Department of Civil Engineering,

University of Southern California, Los Angeles, California. (1991)

73. Trifunac, M. D., 'Zero baseline correction of strong-motion accelerograms', *The Bulletin of the Seismological Society of America*, Vol. 61, No. 5, pp 1201-1211. (1971)

74. Trifunac, M. D., Ivanović, S. S., Todorovska, M. I., Novikova, E. I., and Gladkov, A. A., 'Experimental evidence for flexibility of a building foundation supported by concrete friction piles', *Soil Dynamics and Earthquake Engineering*, Vol. 18, No. 3, pp 169-187. (1999)

75. Trifunac, M. D., Ivanović, S. S., and Todorovska, M. I., 'Apparent periods of a building, Part I: Fourier analysis', *Journal of Structural Engineering*, Vol. 127, No. 5, pp 517-526. (2001)

76. Trifunac, M. D., Ivanović, S. S., and Todorovska, M. I., 'Apparent periods of a building, Part II: Time-frequency analysis', *Journal of Structural Engineering*, Vol. 127, No. 5, pp 527-537. (2001)

77. Trifunac, M. D., Hao, T-Y, and Todorovska, M. I., 'On energy flow in earthquake response', *Report No. 01-03*, Department of Civil Engineering, University of Southern California, Los Angeles, California. (2001)

78. Uang, C. M., and Bertero, V. V., 'Use of energy as a design criterion in earthquake-resistant design', *Report No. UCB/EERC-88/18*, Earthquake Engineering Research Center, University of California, Berkeley, California. (1988)

79. Velez, A., Gazetas, G., and Krishnan, R., 'Lateral dynamic response of constrained-head piles', *Journal of Geotechnical Engineering*, Vol. 109, No. 8, pp 1063-1081. (1983)

80. Vesic, A. B., 'Bending of beams resting on isotropic solid', *Journal of the Engineering Mechanics Division, ASCE*, Vol. 87, No. 2, pp 35-53. (1961)

81. Vesic, A. B., 'Model studies of beams resting on a silt subgrade', *Journal of the Soil Mechanics and Foundation Division, ASCE*, Vol. 89, No. SM1, pp 1-31. (1963)

82. Waas, G., and Hartmann, H. G., 'Seismic analysis of pile foundations including pile-soil-pile interaction', *Proceedings of the eighth world conference on Earthquake Engineering,* Prentice-Hall, Inc., Englewood Cliffs, New Jersey, Vol. 5, pp 55-62. (1984)

83. Westermo, B., and Udwadia, F., 'Periodic response of a sliding oscillator system to harmonic excitation', *Earthquake Engineering and Structural Dynamics*, Vol. 11, pp 135-146. (1983)

84. Wolf, J. P., and von Arx, G. A., 'Impedance function of a group of vertical piles', *Proceedings of Geotechnical Engineering Division at the ASCE Special Conference on Earthquake Engineering and Soil Dynamics,* pp 1024-1041. (1978)

85. Wolf, J. P., and Von Arx, G. A., 'Horizontally traveling waves in a group of piles taking

pile soil-pile interaction into account', *Earthquake Engineering and Structural Dynamics*, Vol. 10, pp 225-237. (1982)

86. Wolf, J. P., *Dynamic soil-structure interaction*, Printice-Hall, Inc., Englewood Cliffs, N.J. (1985)

87. Wu, G., and Finn, W. D. L., 'Dynamic elastic analysis of pile foundations using finite element method in the frequency domain', *Canadian Geotechnical Journal*, 34, 1, pp 34-43. (1997)

88. Wu, G., and Finn, W. D. L., 'Dynamic nonlinear analysis of pile foundations using finite element method in the time domain', *Canadian Geotechnical Journal*, 34, 1, pp 44-52. (1997)

89. Zeng, X., and Steedman, R. S., 'Rotating block method for seismic displacement of gravity walls', *Journal of Geotechnical and Geoenvironmental Engineering,* Vol. 126, No. 8, pp 709-717. (2002)

Appendix A

1. Stiffness of the soil in the near field

It is assumed that the contact pressure at any point is proportional to deflection at the same point of the beam as

$$p = K \cdot u, \tag{A1}$$

where

$p =$ contact pressure

$K =$ modulus of subgrade reaction

$u =$ deflection.

The differential equation of bending of a beam of flexural stiffness is obtained by introducing equation (A1) as follow

$$E_b I_b \frac{d^4 u}{dx^4} + K \cdot u = 0, \tag{A2}$$

where $E_b I_b$ is flexural stiffness of the beam. By substituting $u = e^{mx}$ in equation (A2), we obtain the characteristic equation

$$m^4 = -\frac{K}{E_b I_b}. \tag{A3}$$

The roots are

$$m_1 = \sqrt[4]{\frac{K}{4E_b I_b}}(1+i) = \lambda(1+i), \qquad m_2 = \sqrt[4]{\frac{K}{4E_b I_b}}(-1+i) = \lambda(-1+i),$$

$$m_3 = \sqrt[4]{\frac{K}{4E_b I_b}}(-1-i) = \lambda(-1-i), \qquad m_4 = \sqrt[4]{\frac{K}{4E_b I_b}}(1-i) = \lambda(1-i),$$

$$\lambda = \sqrt[4]{\frac{K}{4E_b I_b}}\ , \tag{A4}$$

where

$\lambda =$ characteristic of the system

The general solution of equation (A2) is

$$u = A_1 \cdot e^{m_1 x} + A_2 \cdot e^{m_2 x} + A_3 \cdot e^{m_3 x} + A_4 \cdot e^{m_4 x}, \tag{A5}$$

where

A_1, A_2, A_3, A_4 = constants.

By using

$$e^{i\lambda x} = \cos\lambda x + i\sin\lambda x$$

$$e^{-i\lambda x} = \cos\lambda x - i\sin\lambda x$$

and λ, we can get general form of equation (A5) as

$$u = e^{\lambda x}\left(C_1 \cos \lambda x + C_2 \sin \lambda x\right) + e^{-\lambda x}\left(C_3 \cos \lambda x + C_4 \sin \lambda x\right) , \qquad \text{(A6)}$$

where

C_1, C_2, C_3, C_4 = new constants.

Vesic(1961) presented rigorous analysis for a beam of infinite length by extending Biot's solution. He assumed that the subgrade behaves as an homogenous, isotropic, elastic solid, characterized by a Young's modulus and Poisson's ratio of soil. The integration was solved by interpolation and approximation.

The characteristic of system by Vesic is

$$\lambda' = \frac{0.689}{b}\left(\frac{b}{c}\right)^{0.813} , \qquad \text{(A7)}$$

$$c = \left[1.10\left(1-\nu_s\right)^2 \frac{E_b I_b}{E_s}\right]^{1/3} , \qquad \text{(A8)}$$

where

ν_s = Poisson's ratio of soil

E_s = Young's modulus of soil

b = half width of beam.

Vesic(1961) demonstrated that the two approaches are equivalent if the beam is sufficiently long. Then, the relation can be obtained between the modulus and the soil

characteristics, flexural rigidity and width of the beam, by equating equation (A4) to equation (A7).

$$K = \left(\frac{0.65}{B}\right) \cdot \sqrt[12]{\frac{E_s B^4}{E_b I_b}} \cdot \left(\frac{E_s}{1-\upsilon_s{}^2}\right) \quad , \tag{A9}$$

where

K = modulus of subgrade reaction

E_s = Young's modulus of the soil

$E_b I_b$ = flexural stiffness of the beam

B = width of the beam $= 2b$.

2. Ultimate resistance of soil

For clay, the resistance is given as a strength per unit length of the soil layer by (American Petroleum Institute, 1991)

$$P_U = 3c_u d + \gamma' z d + J c_u z, \; z \le z_r \tag{A10}$$

$$P_U = 9c_u d, \qquad z \le z_r,$$

where

c_u = undrained shear strength

γ' = effective unit weight of the soil

J = dimensionless empirical constant

$z =$ depth below soil surface

$d =$ pile diameter

$z_r = \dfrac{6d}{\dfrac{\gamma' d}{c_u} + J} =$ the depth of the reduced resistance zone.

Dimensionless empirical constant, J, with values ranging from 0.25 to 0.5 has been determined by field test. Lateral bearing capacities of sand at shallow depth P_{us} and at large depth P_{ud} are recommended (American Petroleum Institute, 1991) as

$$P_{us} = (C_1 \cdot H + C_2 \cdot D) \cdot \gamma' \cdot H \qquad \text{(A11)}$$

$$P_{ud} = C_3 \cdot D \cdot \gamma' \cdot H ,$$

where

$\gamma' =$ effective unit weight of the soil

$H =$ depth

$D =$ average pile diameter from surface to depth

C_1, C_2, C_3 = coefficient determined as ϕ'

$\phi' =$ angle of internal friction.

Appendix B

The movements caused by the vertically incident waves for 9 cases ($V_s = 280.0\,\text{m/s}$, $140.0\,\text{m/s}$, $70.0\,\text{m/s}$, and $T_g = 0.2\,\text{s}$, $0.4\,\text{s}$, $0.8\,\text{s}$) are summarized in Figure B.1. Figure B.2 shows the total system energy for a 4 x 4 pile group. The motions of the piles in 4 x 4 and 2 x 2 pile group foundations are presented in Figures B.3 through B.6. It is plotted at 6 time steps and for 2 durations of vertically incident waves ($T_g = 0.2\,\text{s}, 0.4\,\text{s}$).

The absolute displacements of the piles and the gaps for a 6 x 6 pile group in stiff soil are presented in Appendix B. The results for 4 x 4 and 2 x 2 pile group foundations are also presented in Figures B.8 through B.13. The maximum bending moments and displacements of the piles for excitation by a pulse with intermediate duration ($T_g = 0.4\,\text{s}$) are shown in here. The results of 4 x 4, and 2 x 2 pile groups are also shown in Appendix B.

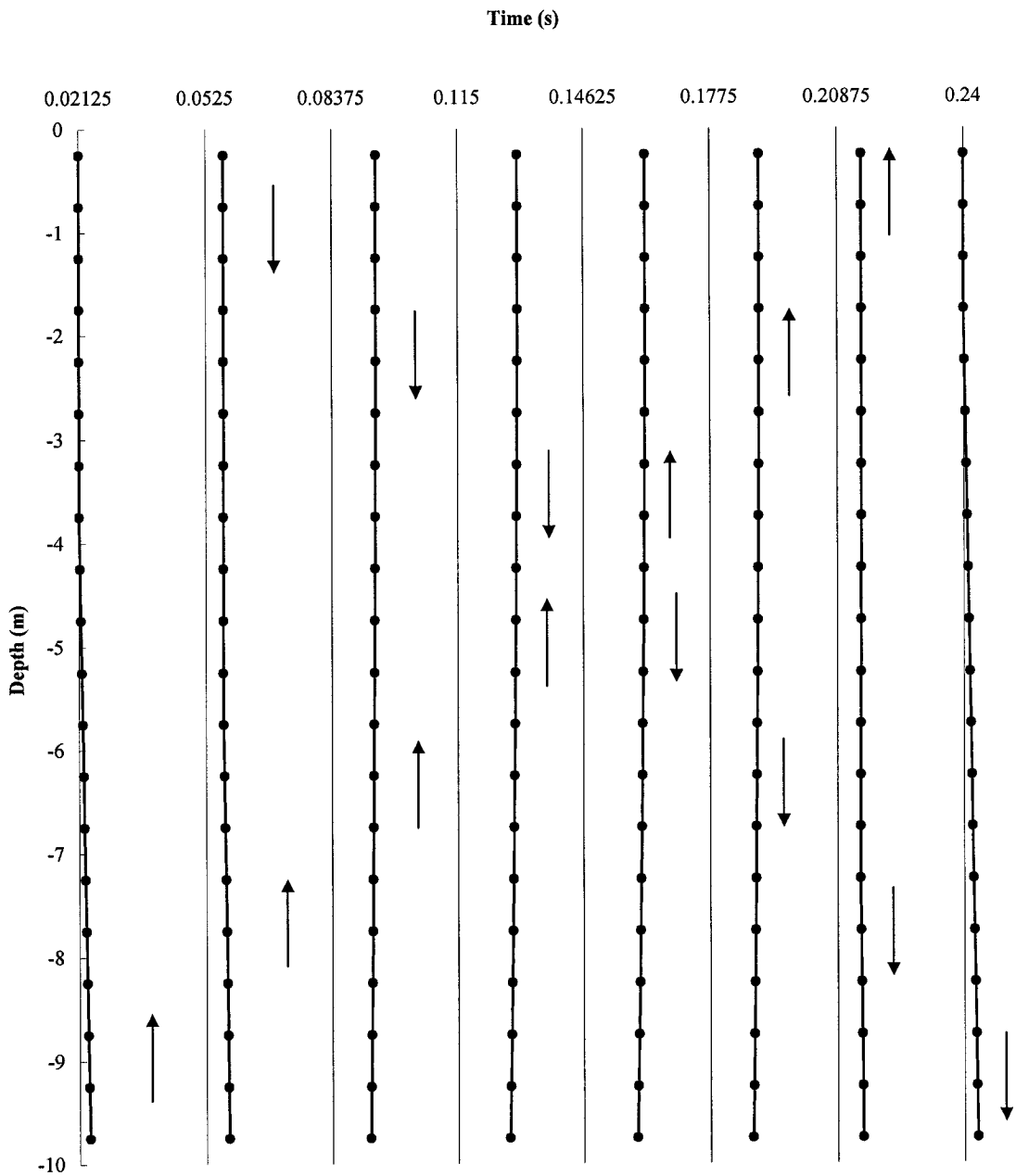

(a) V_s=280.0 m/s, T_g=0.2 s

Fig. B.1 Movements of a vertically incident wave.

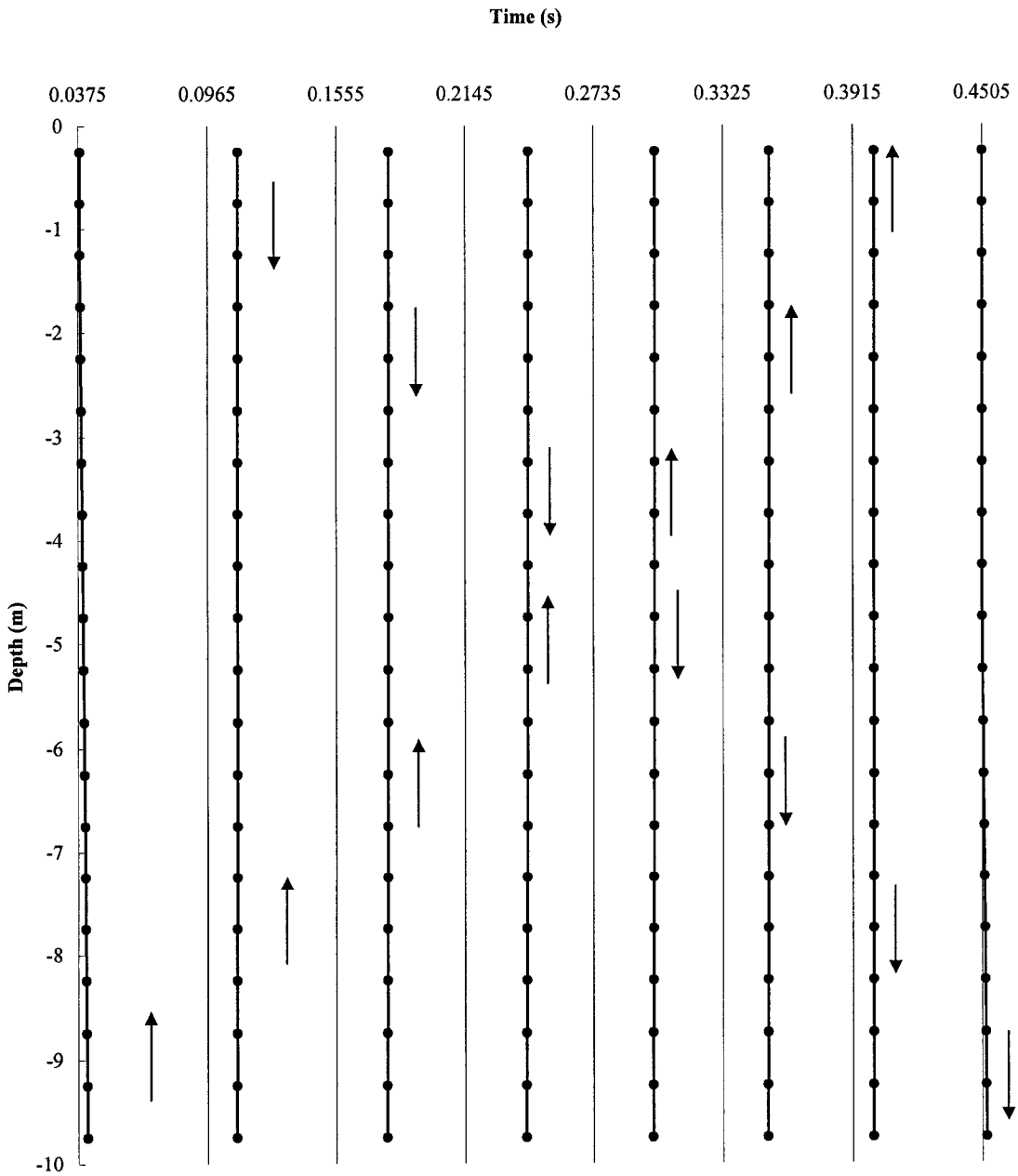

(b) V_s=280.0 m/s, T_g=0.4 s

Fig. B.1 Movements of a vertically incident wave. (continued)

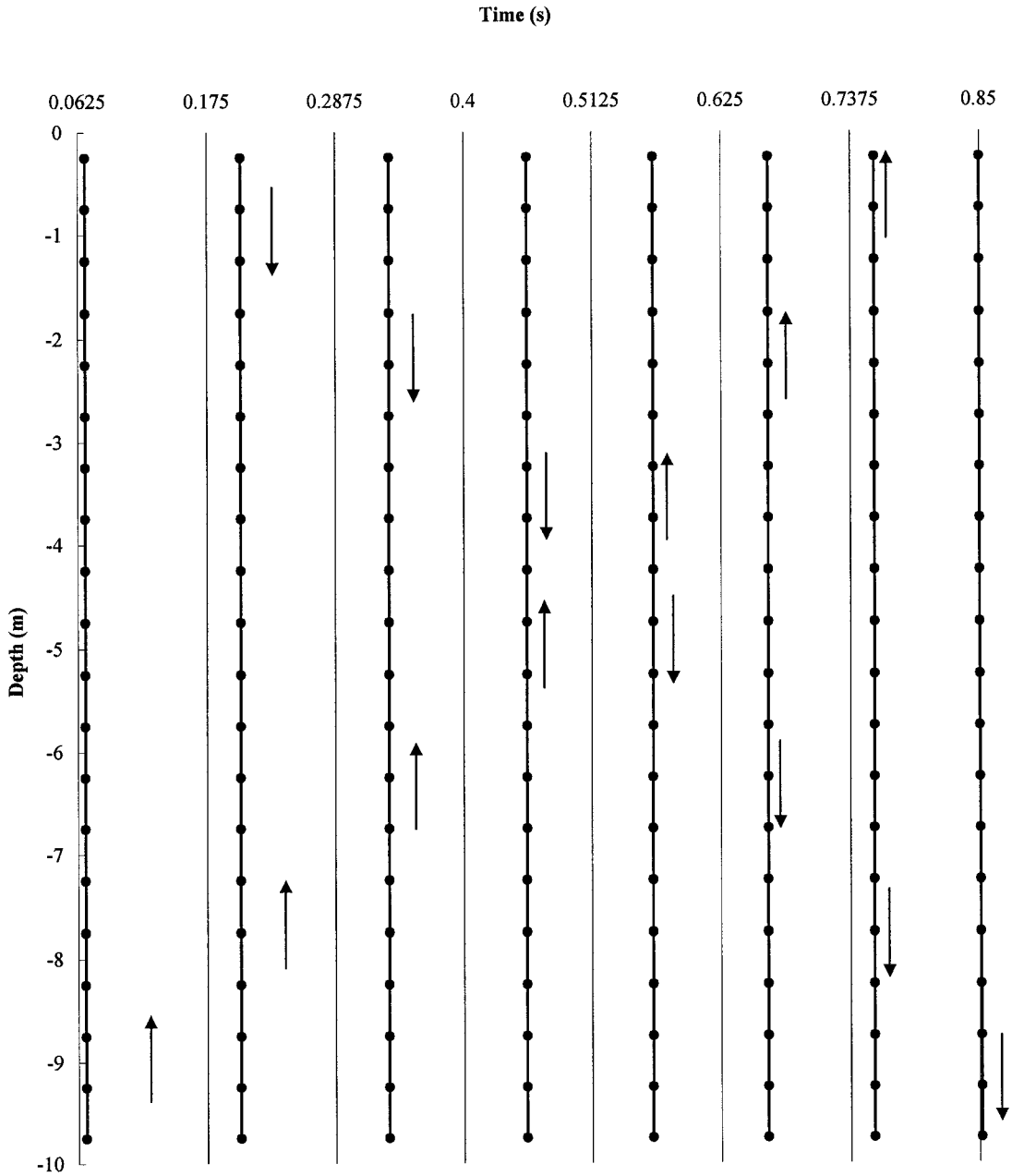

(c) V_s=280.0 m/s, T_g=0.8 s

Fig. B.1 Movements of a vertically incident wave. (continued)

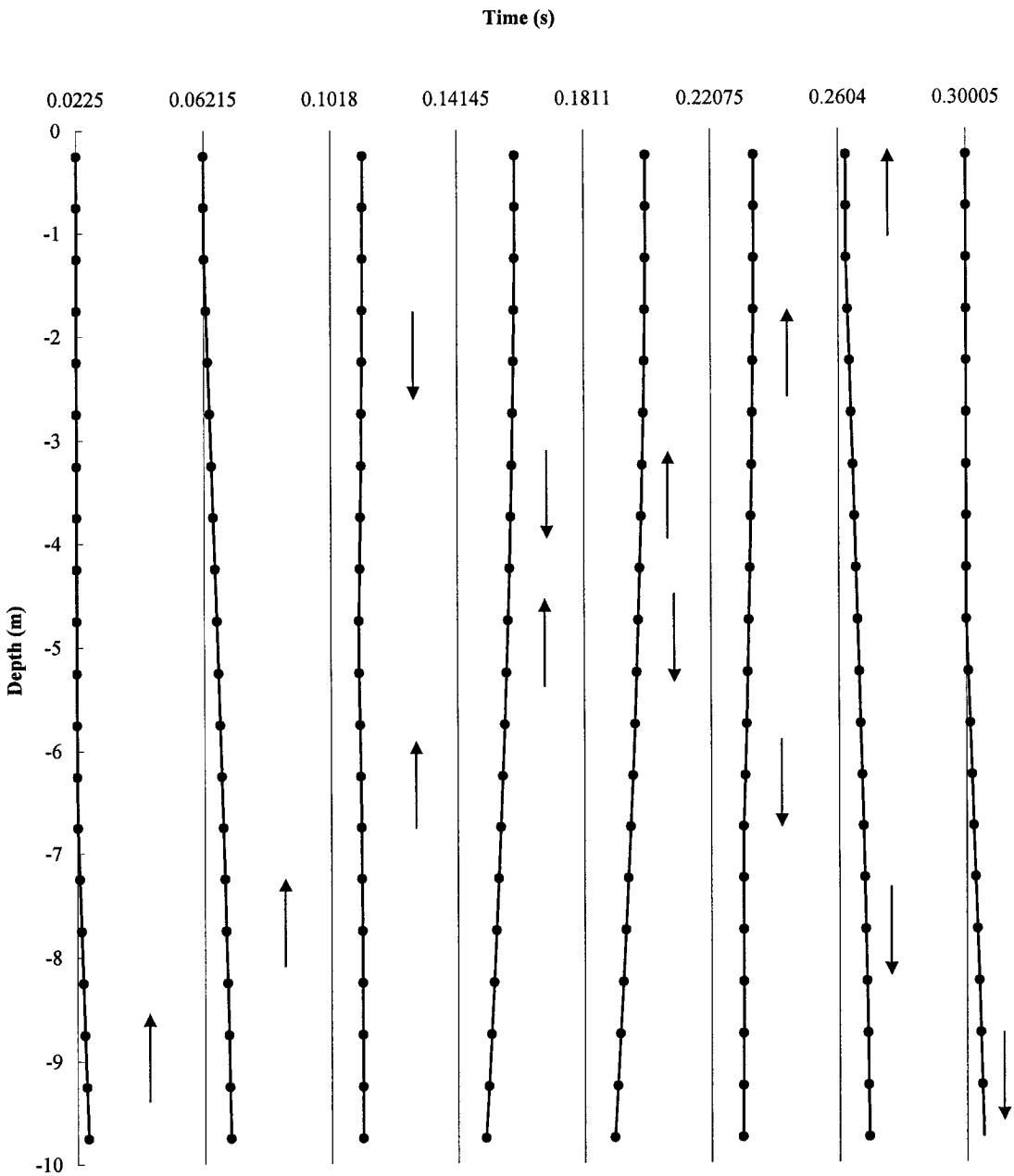

(d) V_s=*140.0* m/s, T_g=*0.2* s

Fig. B.1 Movements of a vertically incident wave. (continued)

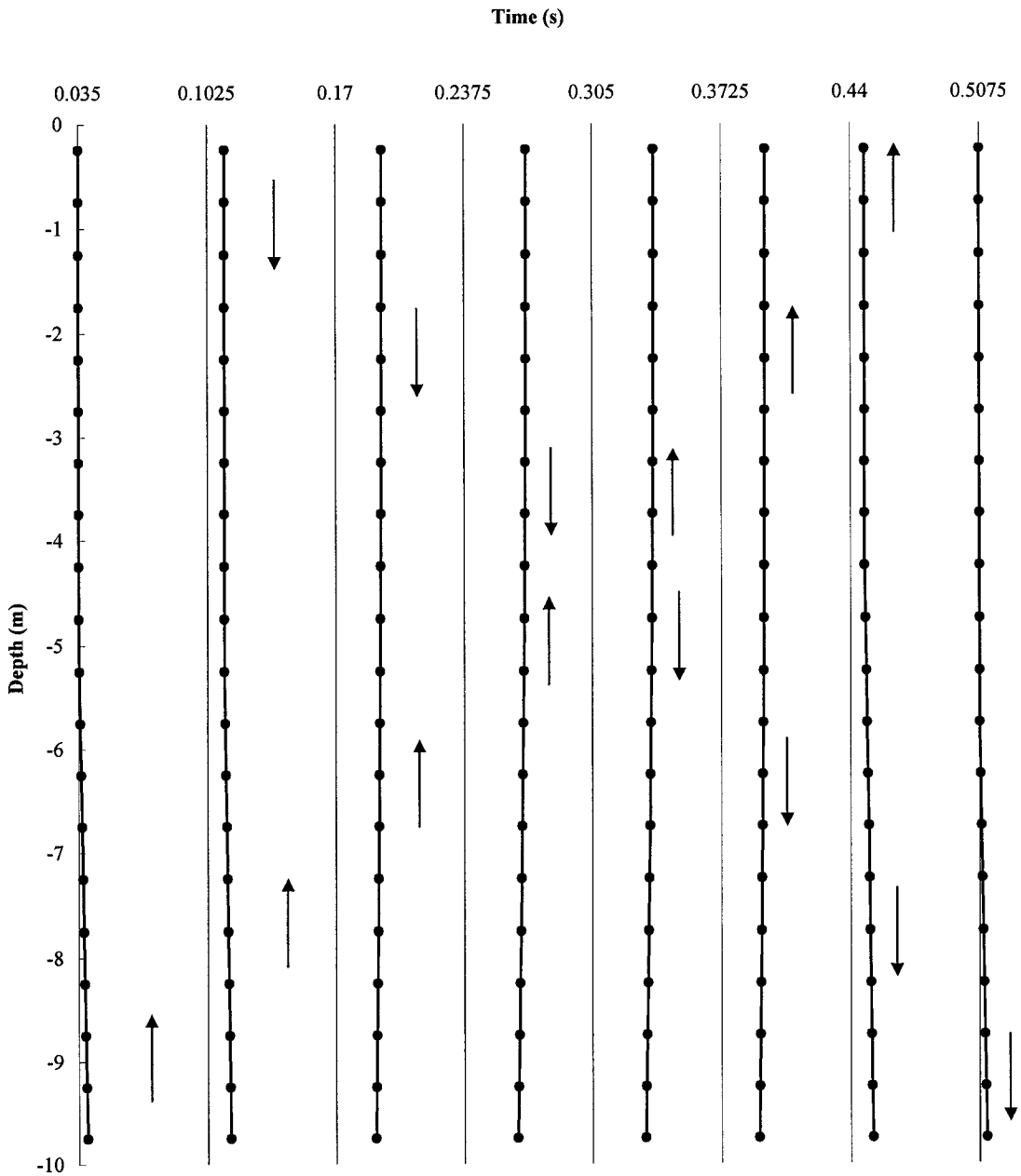

(e) V_s=140.0 m/s, T_g=0.4 s

Fig. B.1 Movements of a vertically incident wave. (continued)

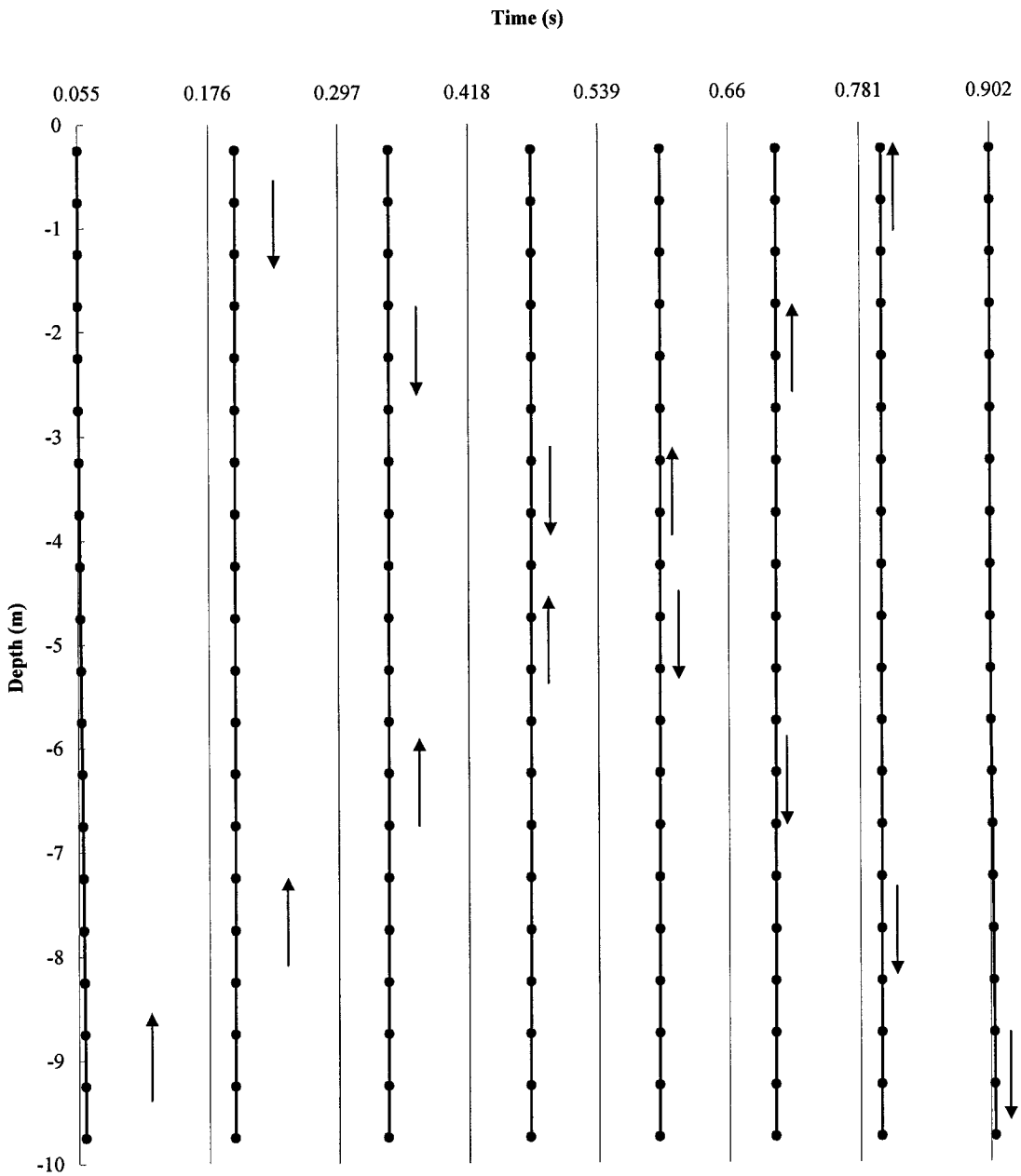

(f) V_s=140.0 m/s, T_g=0.8 s

Fig. B.1 Movements of a vertically incident wave. (continued)

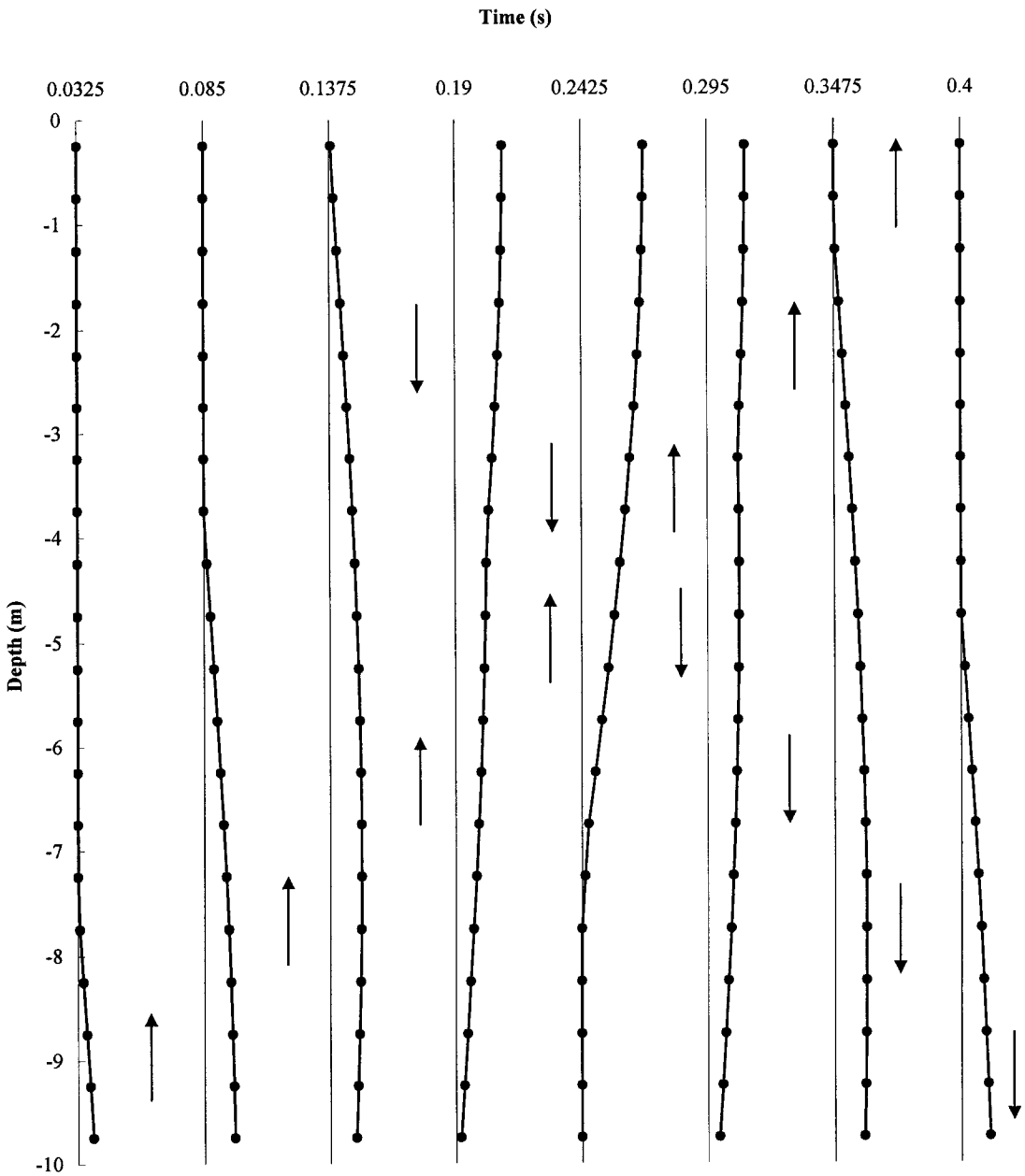

(g) V_s=*70.0* m/s, T_g=*0.2* s

Fig. B.1 Movements of a vertically incident wave. (continued)

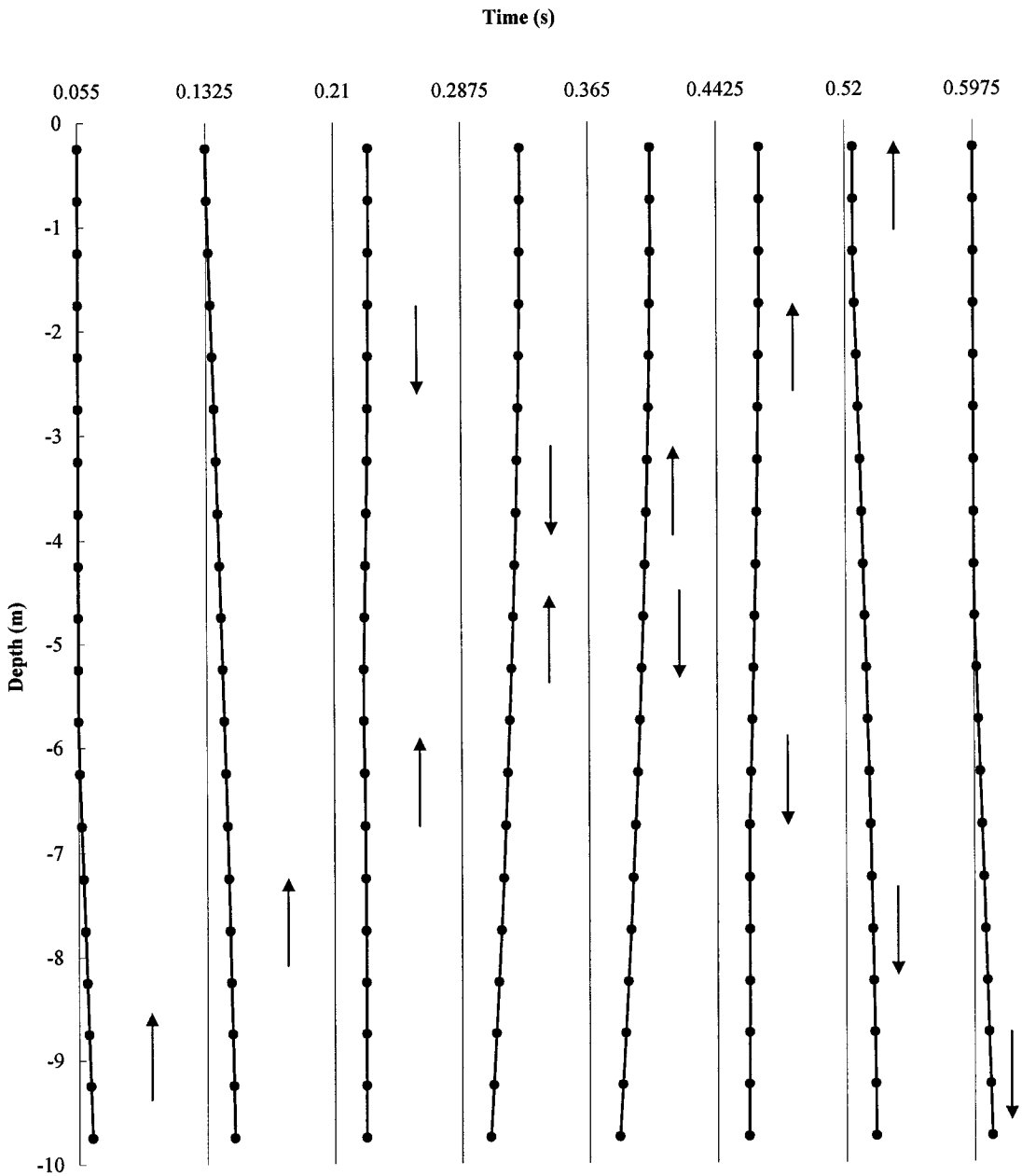

(h) V_s=*70.0* m/s, T_g=*0.4* s

Fig. B.1 Movements of a vertically incident wave. (continued)

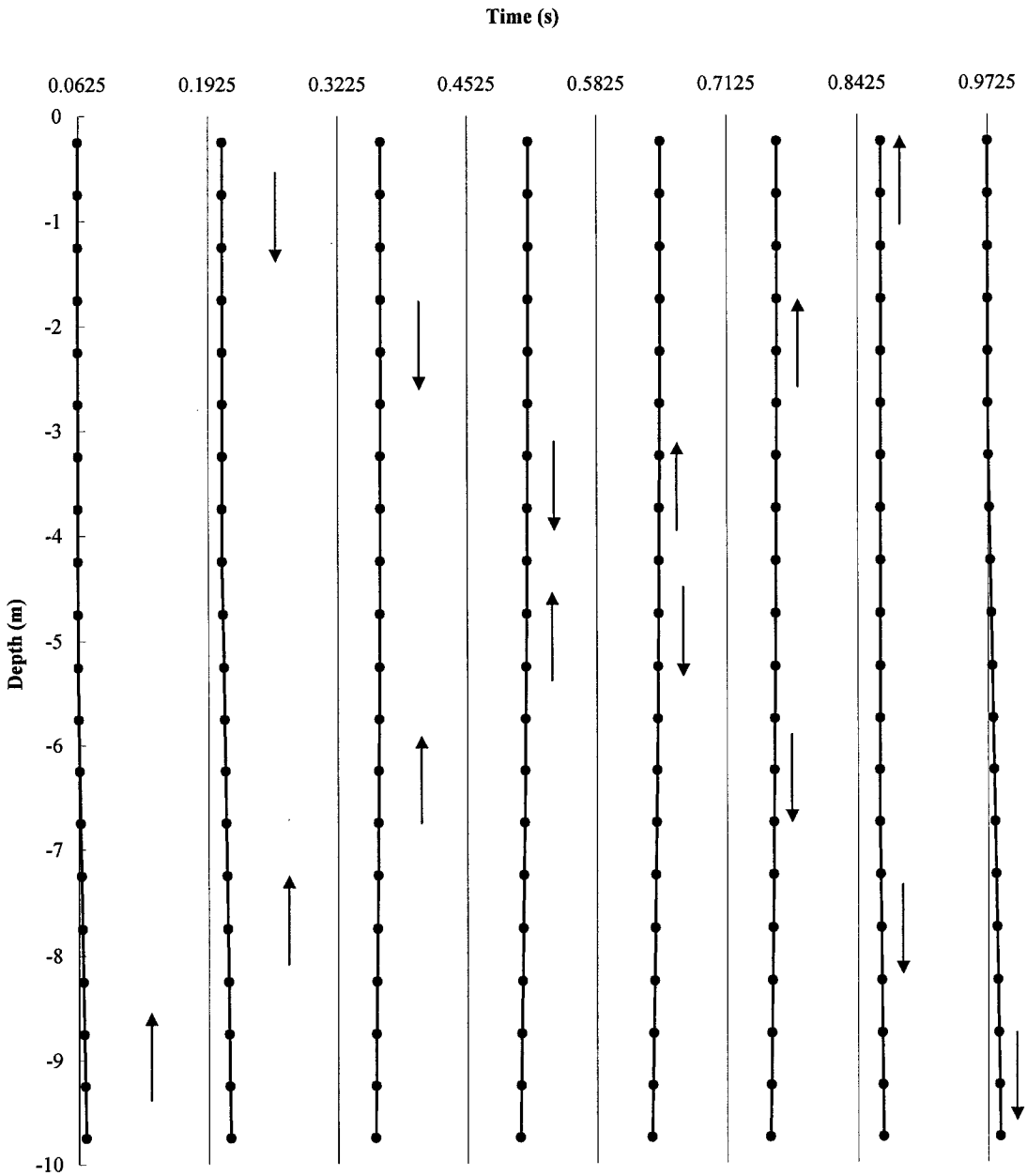

(i) V_s=*70.0* m/s, T_g=*0.8* s

Fig. B.1 Movements of a vertically incident wave. (continued)

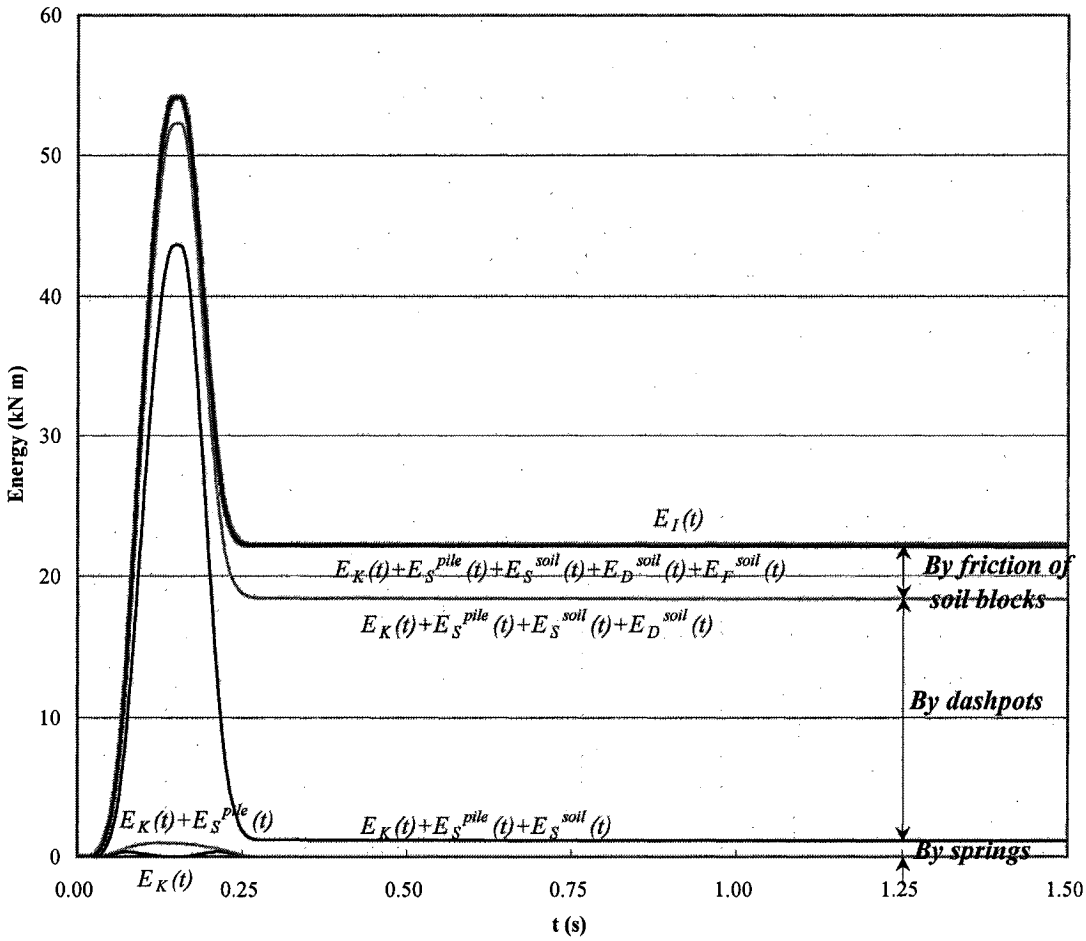

(a) Stiff soil (V_s = *280.0* m/s)

Fig B.2 Total system energies for a 4 x 4 group pile caused by a short incident pulse (T_g = *0.2* s) when the pile-spacing raio is 5.0 (s/d=5.0).

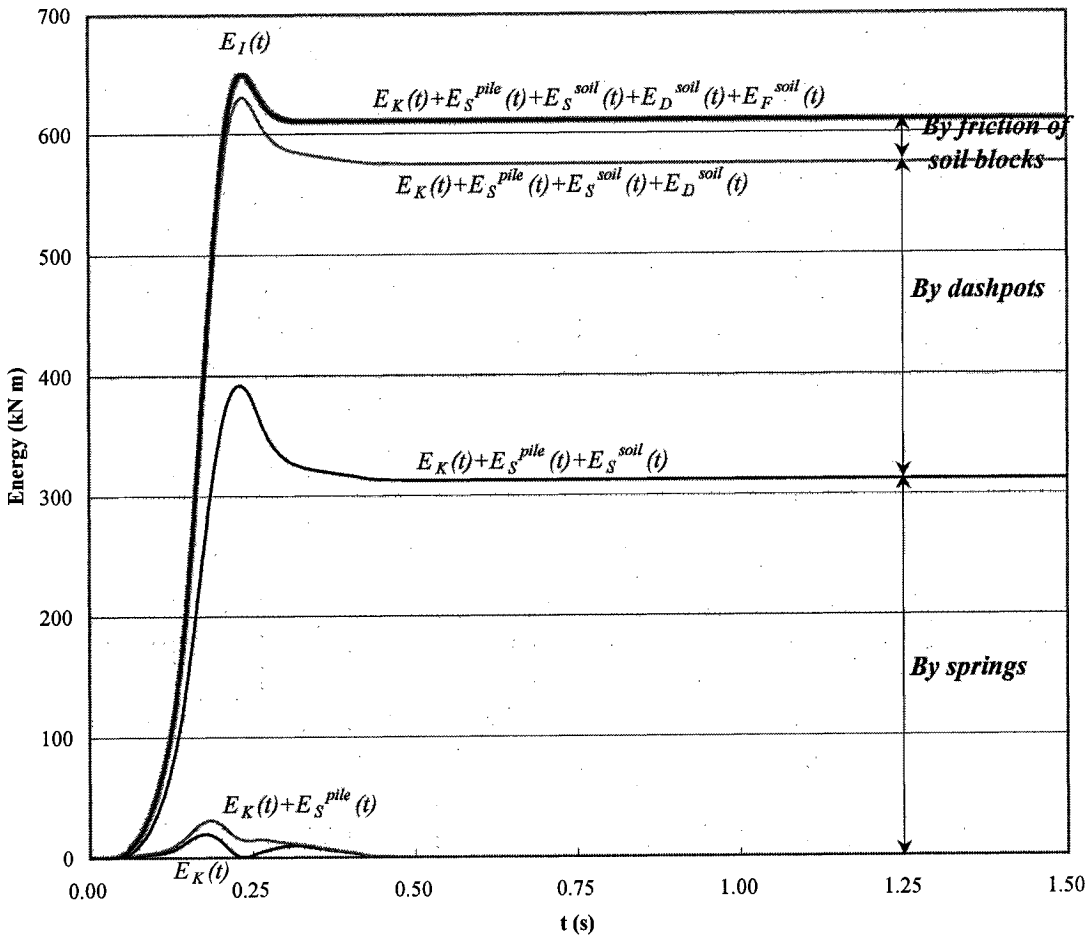

(b) Medium soil (V_s = *140.0* m/s)

Fig B.2 Total system energies for a 4 x 4 group pile caused by a short incident pulse (T_g = *0.2* s) when the pile-spacing raio is 5.0 (s/d=5.0). (continued)

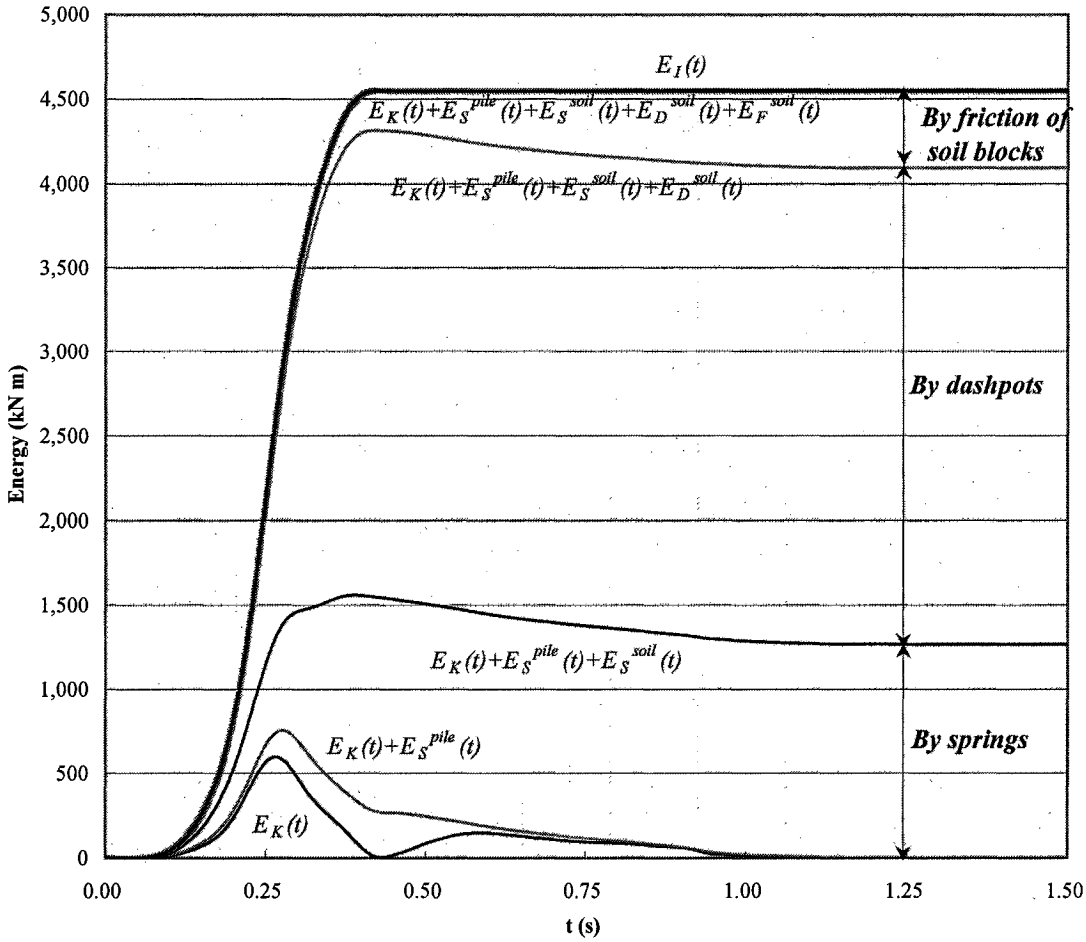

(c) Soft soil (V_s = *70.0* m/s)

Fig B.2 Total system energies for a 4 x 4 group pile caused by a short incident pulse (T_g = *0.2* s) when the pile-spacing raio is 5.0 (s/d=5.0). (continued)

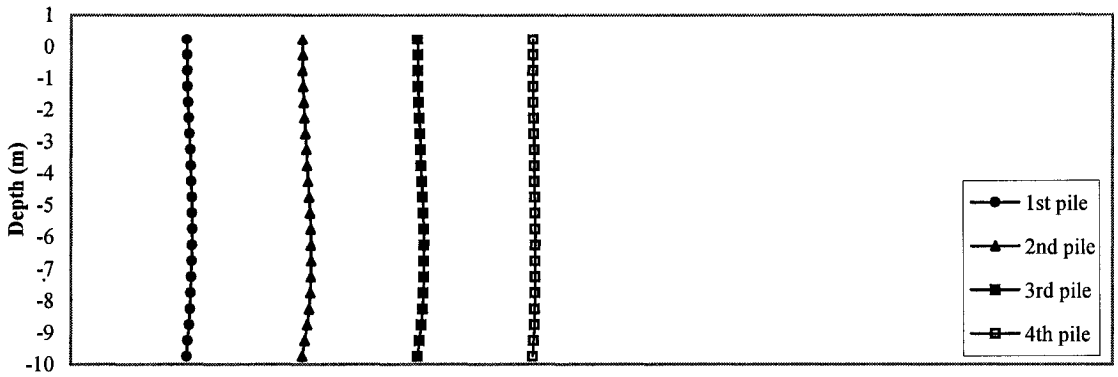

(a) t = 0.125 s

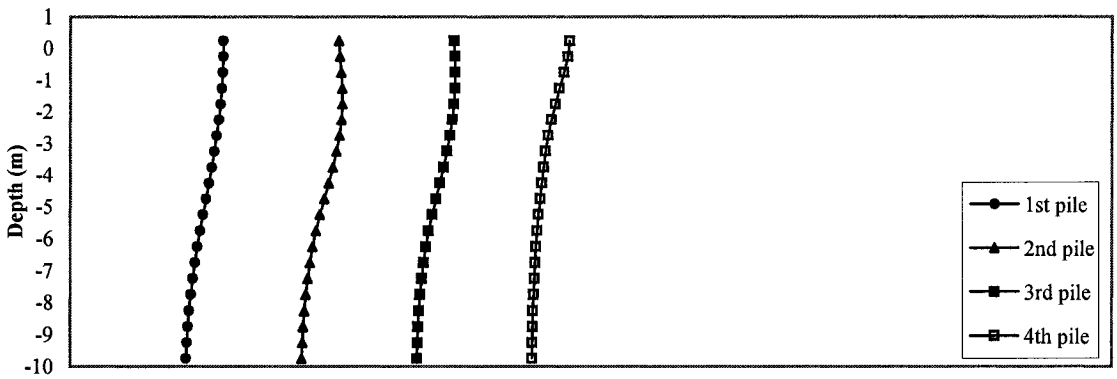

(b) t = 0.25 s

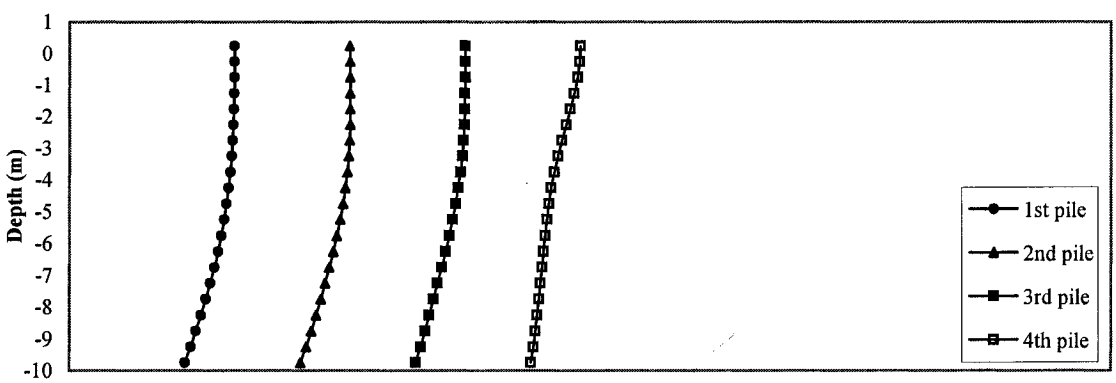

(c) t = 0.375 s

Fig. B.3 Motion of piles in a 4 x 4 pile group in soft soil (V_s = *70.0* m/s) caused by a short incident pulse (T_g = *0.2* s).

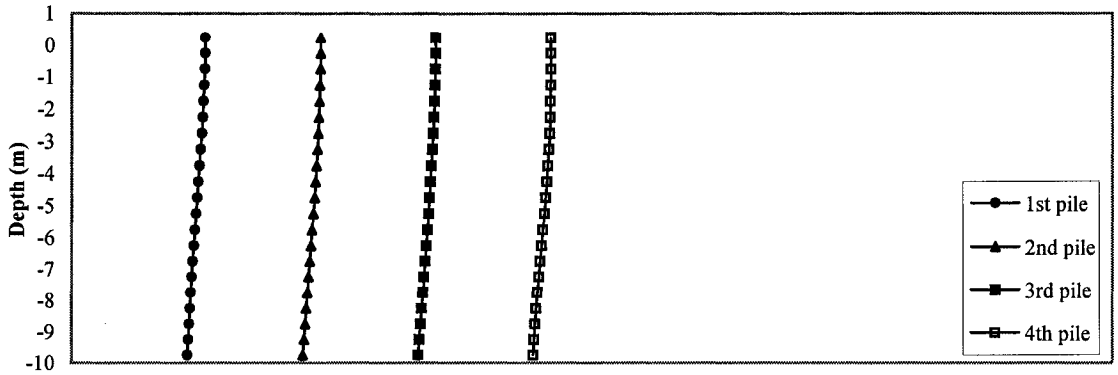

(d) t = 0.5 s

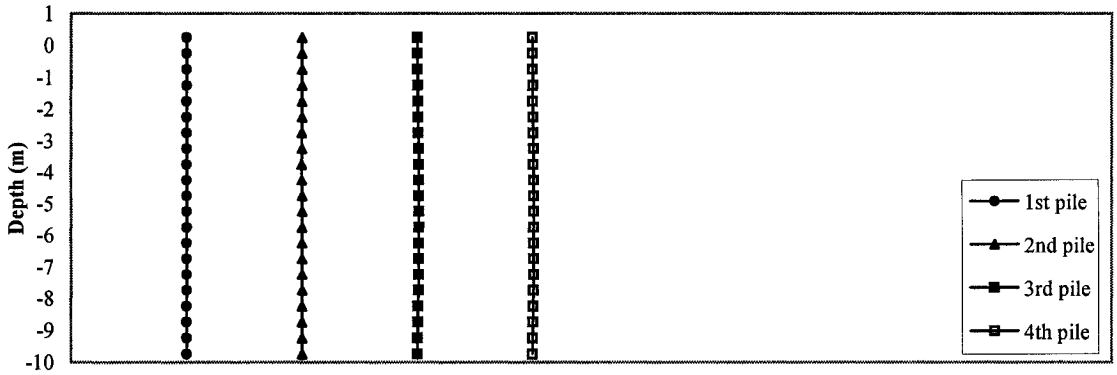

(e) t = 0.625 s

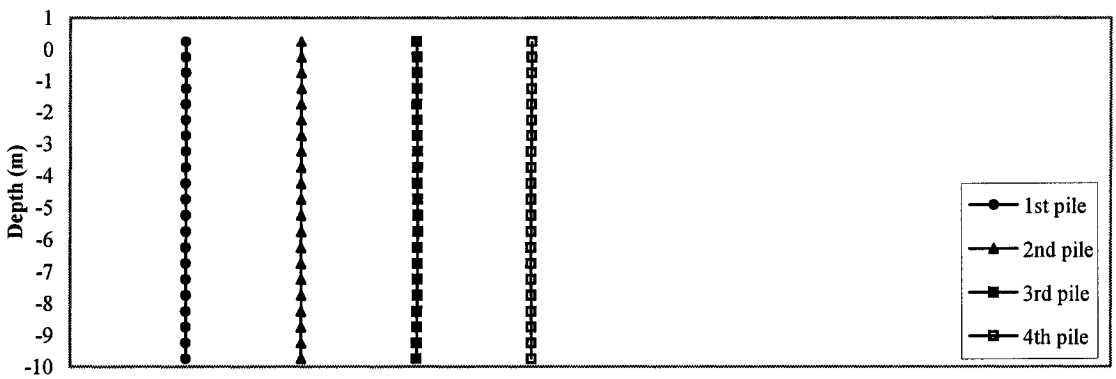

(f) t = 0.75 s

Fig. B.3 Motion of piles in a 4 x 4 pile group in soft soil (V_s = *70.0* m/s) caused by a short incident pulse (T_g = *0.2* s). (continued)

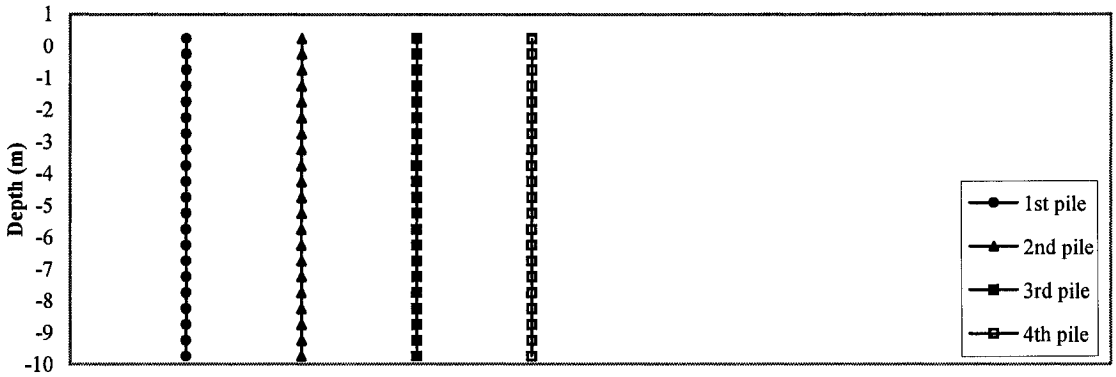

(a) t = 0.125 s

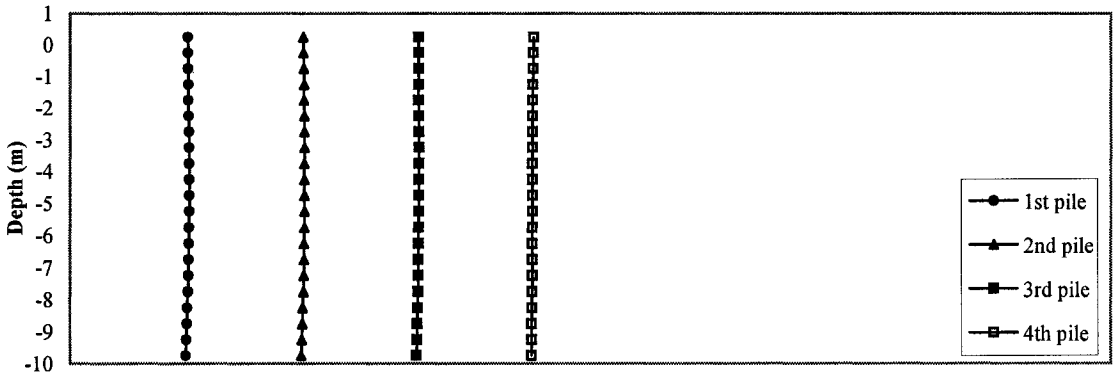

(b) t = 0.25 s

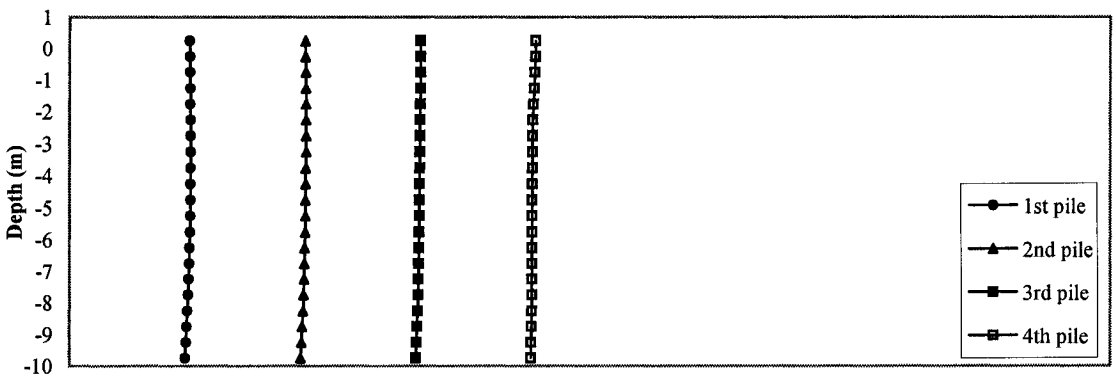

(c) t = 0.375 s

Fig. B.4 Motion of piles in a 4 x 4 pile group in soft soil (V_s = *70.0* m/s) caused by a incident pulse with medium period (T_g = *0.4* s).

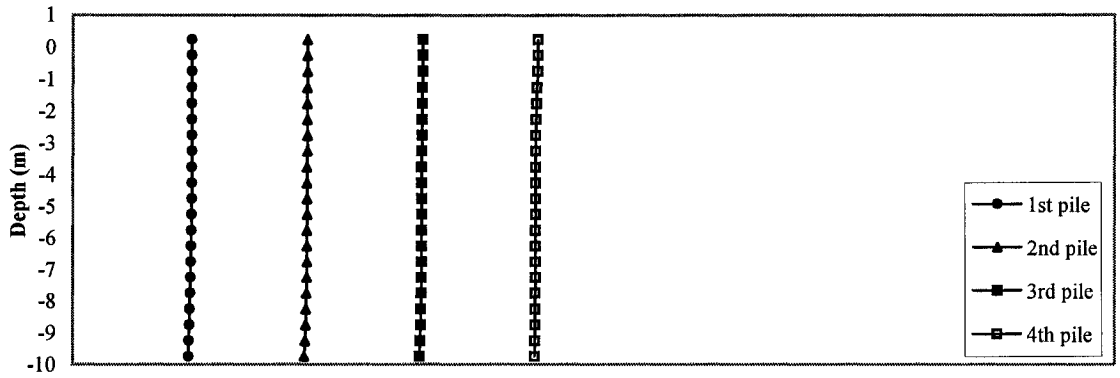

(d) t = 0.5 s

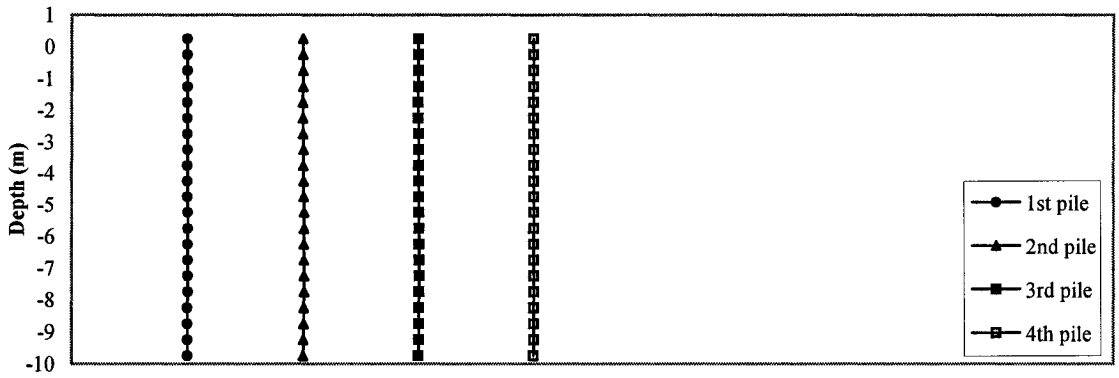

(e) t = 0.625 s

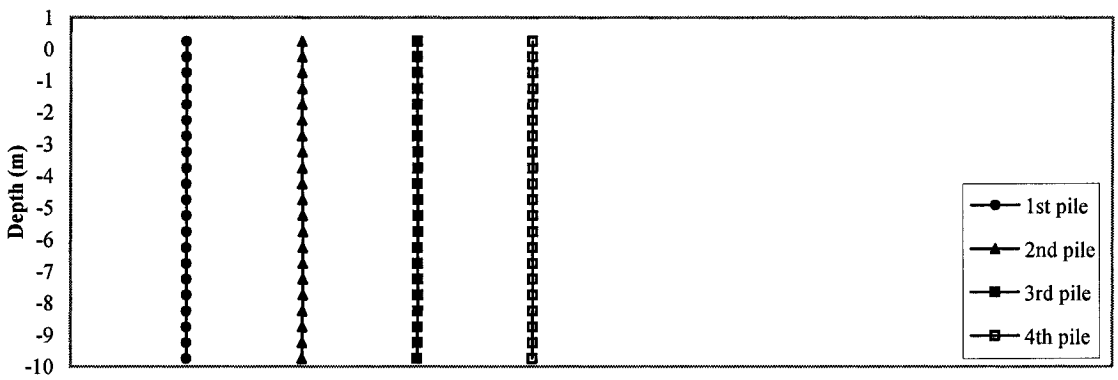

(f) t = 0.75 s

Fig. B.4 Motion of piles in a 4 x 4 pile group in soft soil (V_s = *70.0* m/s) caused by a incident pulse with medium period (T_g = *0.4* s). (continued)

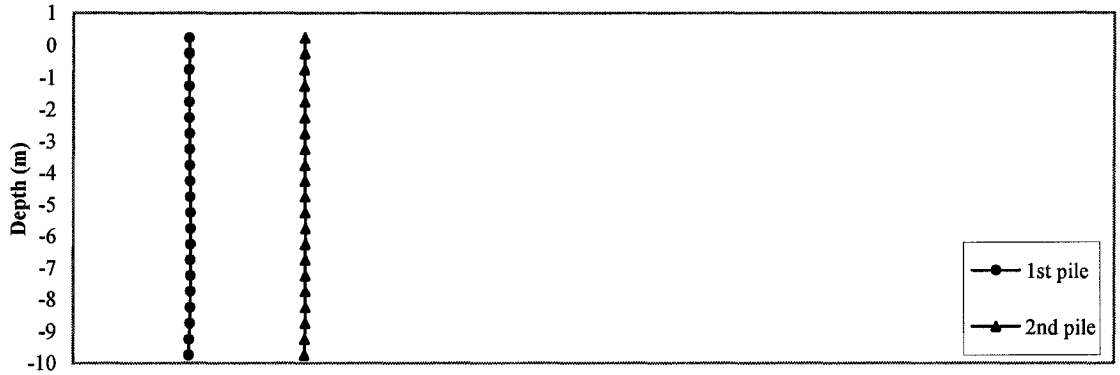

(a) t = 0.125 s

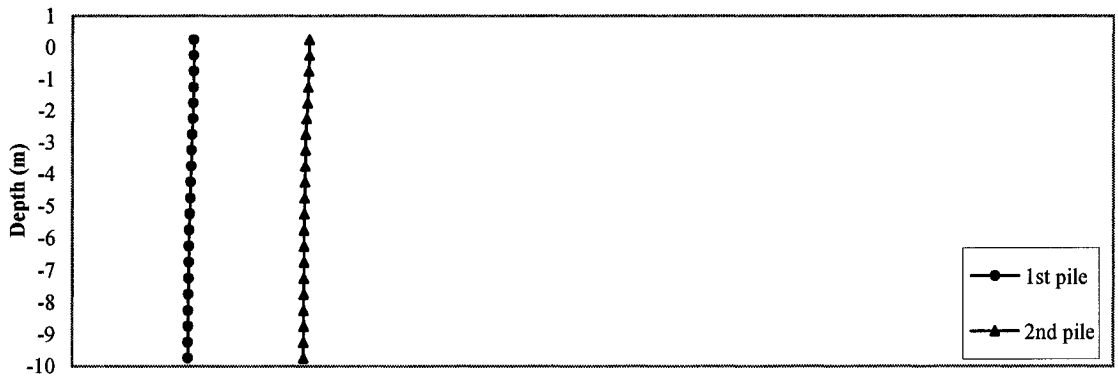

(b) t = 0.25 s

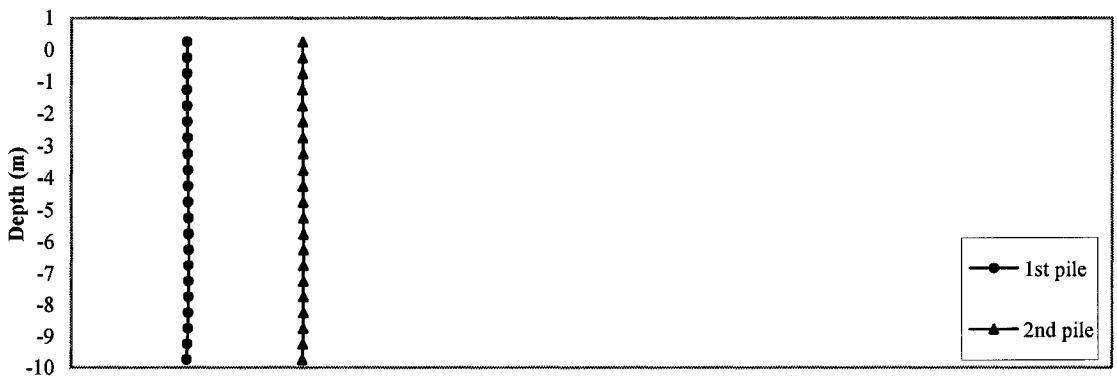

(c) t = 0.375 s

Fig. B.5 Motion of piles in a 2 x 2 pile group in soft soil (V_s = *70.0* m/s) caused by a short incident pulse (T_g = *0.2* s).

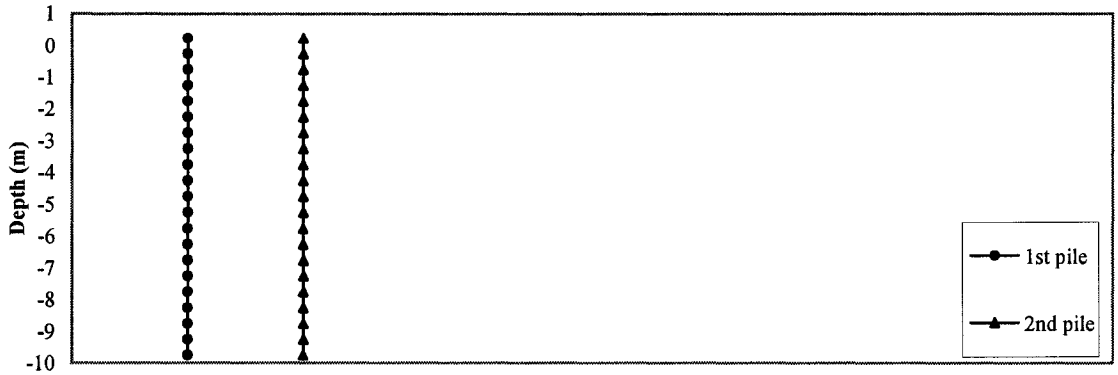

(d) t = 0.5 s

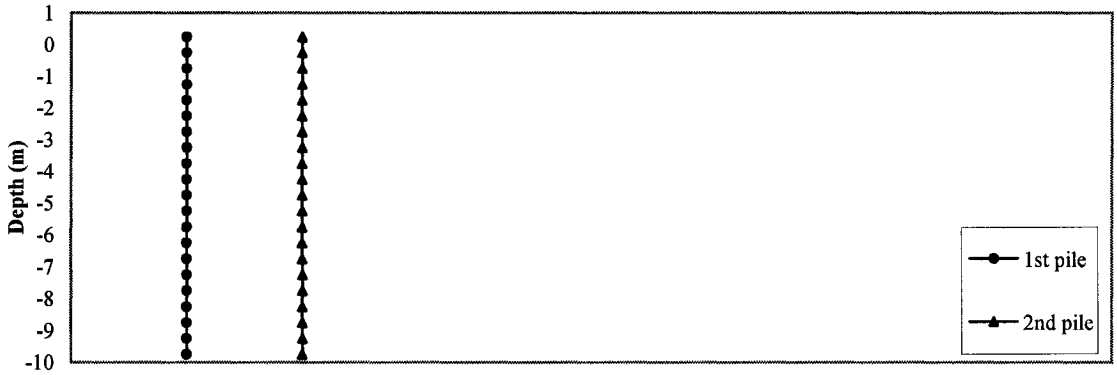

(e) t = 0.625 s

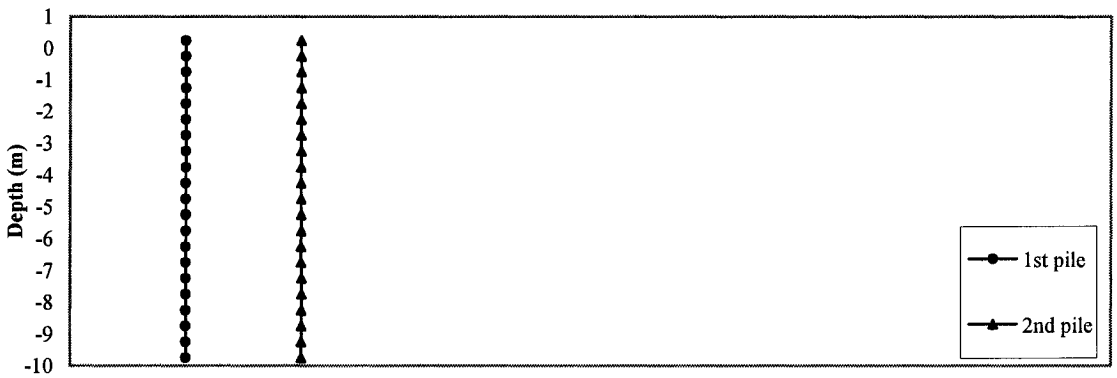

(f) t = 0.75 s

Fig. B.5 Motion of piles in a 2 x 2 pile group in soft soil (V_s = *70.0* m/s) caused by a short incident pulse (T_g = *0.2* s). (continued)

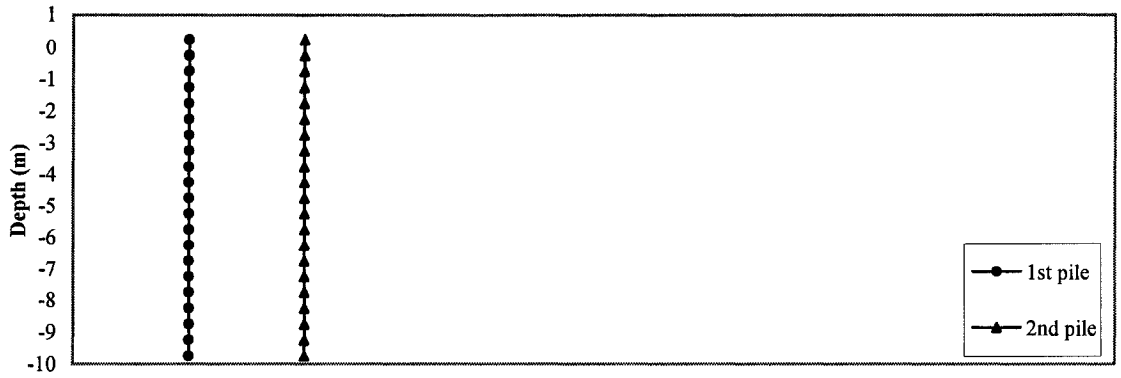

(a) t = 0.125 s

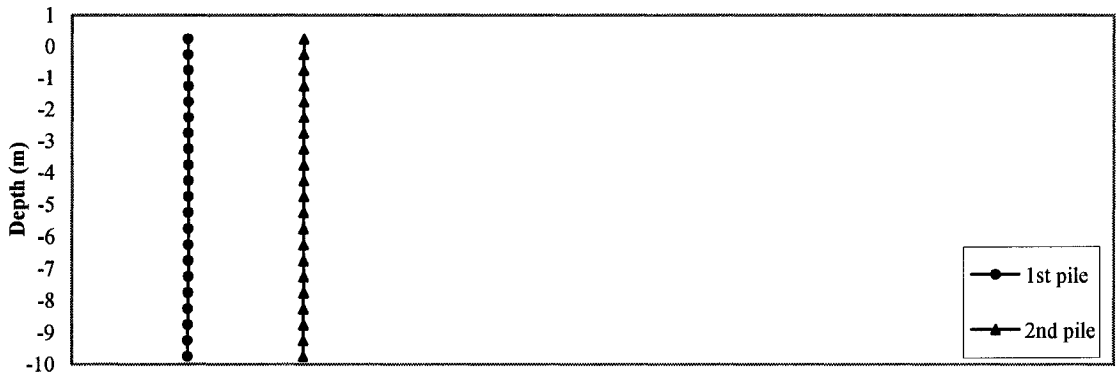

(b) t = 0.25 s

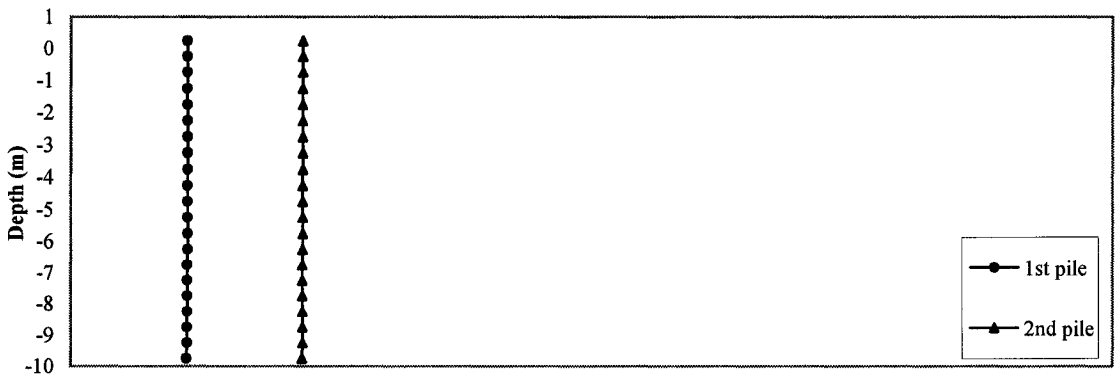

(c) t = 0.375 s

Fig. B.6 Motion of piles in a 2 x 2 pile group in soft soil (V_s = *70.0* m/s) caused by a incident pulse with medium period (T_g = *0.4* s).

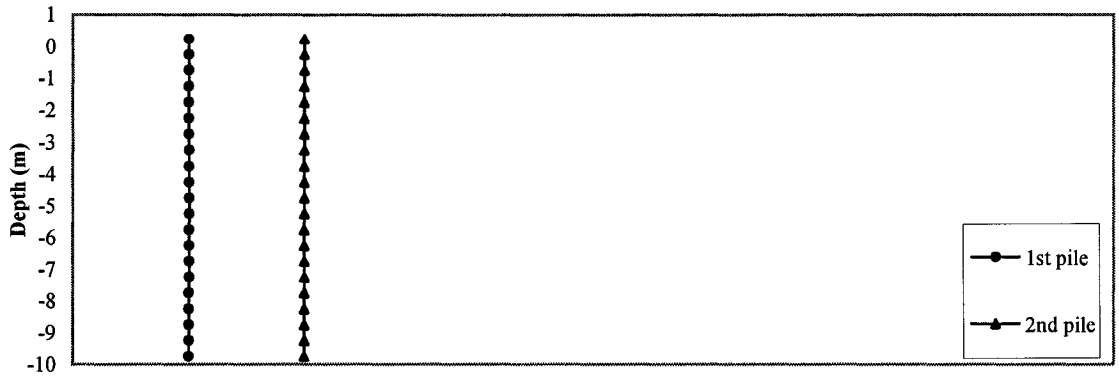

(d) t = 0.5 s

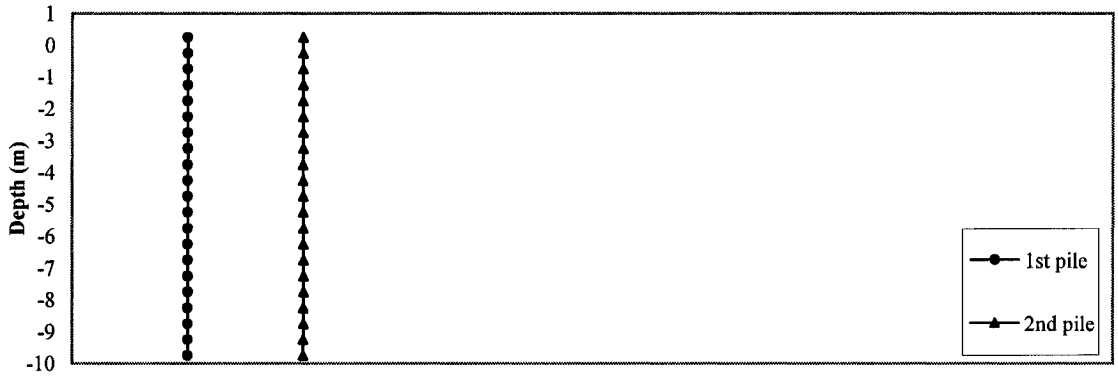

(e) t = 0.625 s

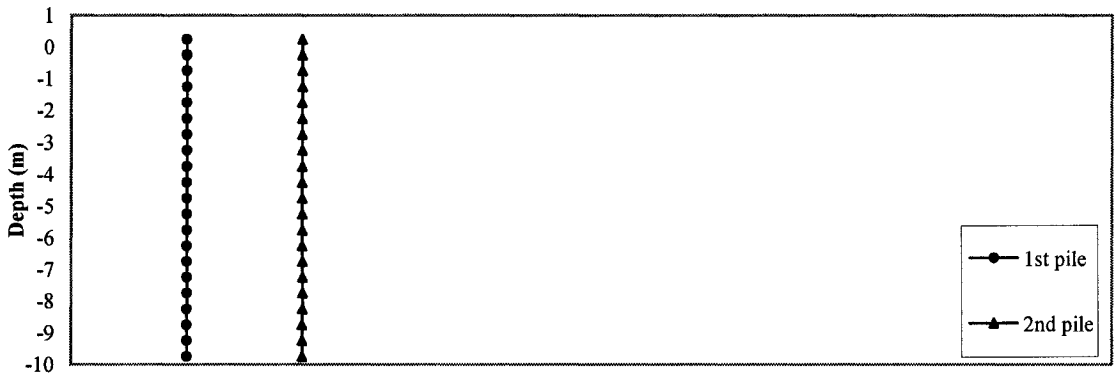

(f) t = 0.75 s

Fig. B.6 Motion of piles in a 2 x 2 pile group in soft soil (V_s = *70.0* m/s) caused by a incident pulse with medium period (T_g = *0.4* s). (continued)

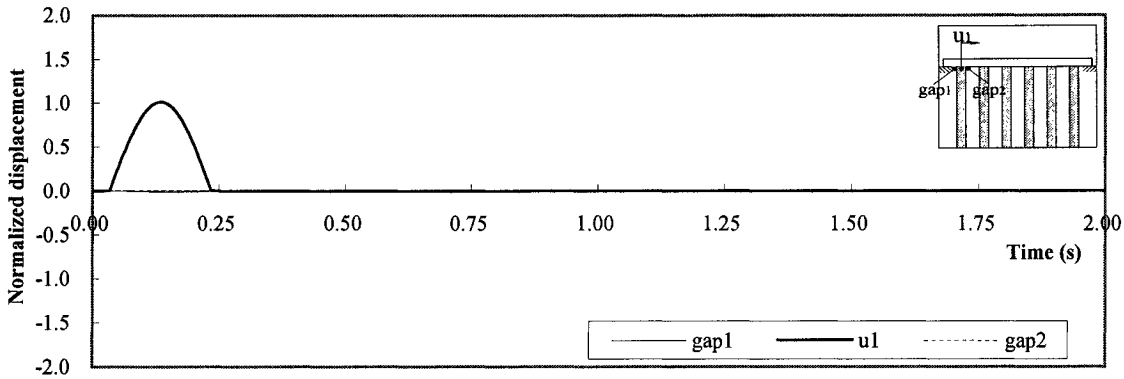

(a) 1st pile and gap1, gap2

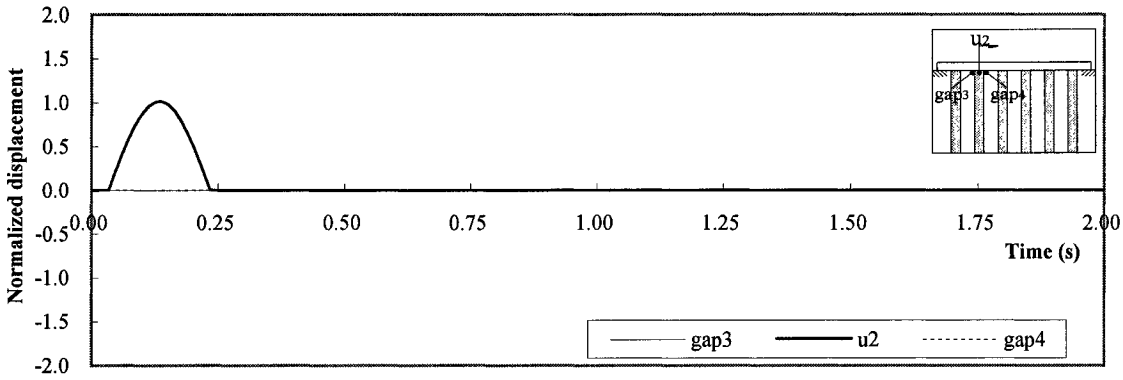

(b) 2nd pile and gap3, gap4

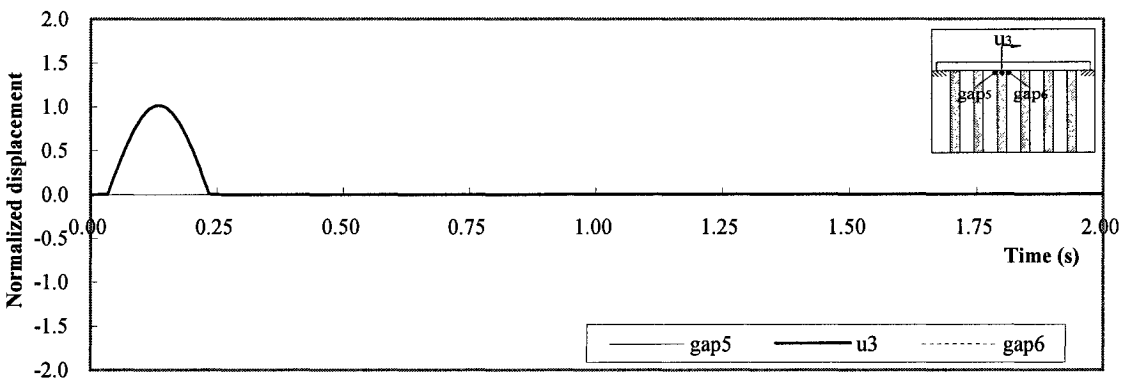

(c) 3rd pile and gap5, gap6

Fig. B.7 Displacements of piles and gaps at the ground level when a short pulse (T_g = *0.2* s) propagates into a 6 x 6 pile group in stiff soil (V_s = *280.0* m/s).

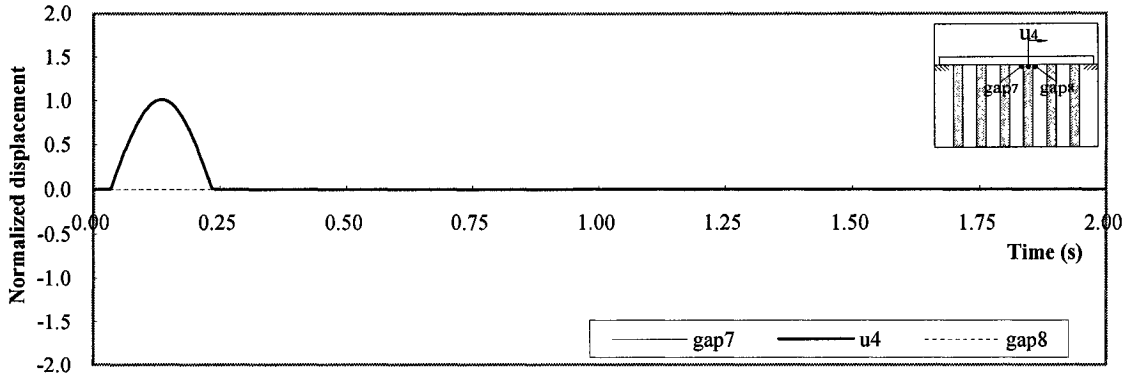

(d) 4th pile and gap7, gap8

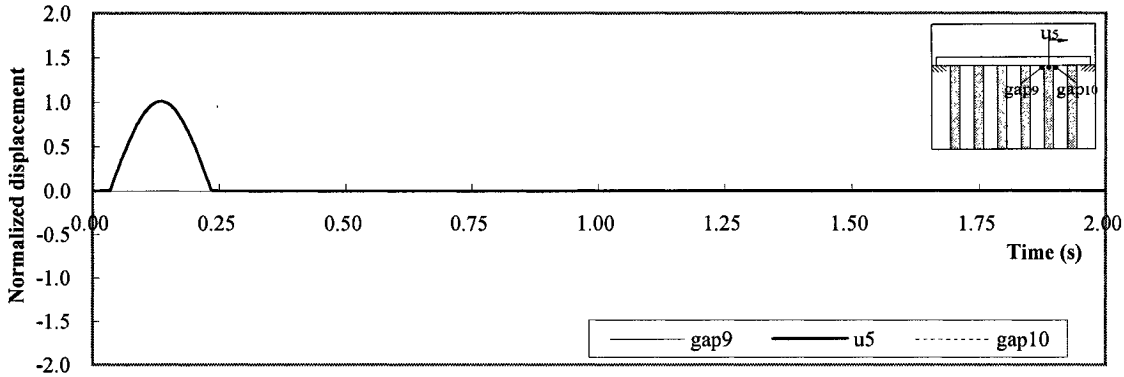

(e) 5th pile and gap9, gap10

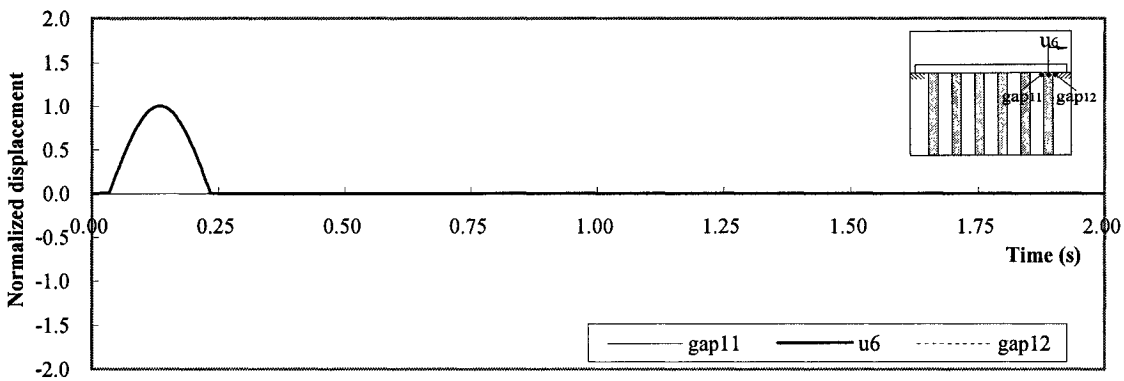

(f) 6th pile and gap11, gap12

Fig. B.7 Displacements of piles and gaps at the ground level when a short pulse ($T_g = 0.2$ s) propagates into a 6 x 6 pile group in stiff soil ($V_s = 280.0$ m/s). (continued)

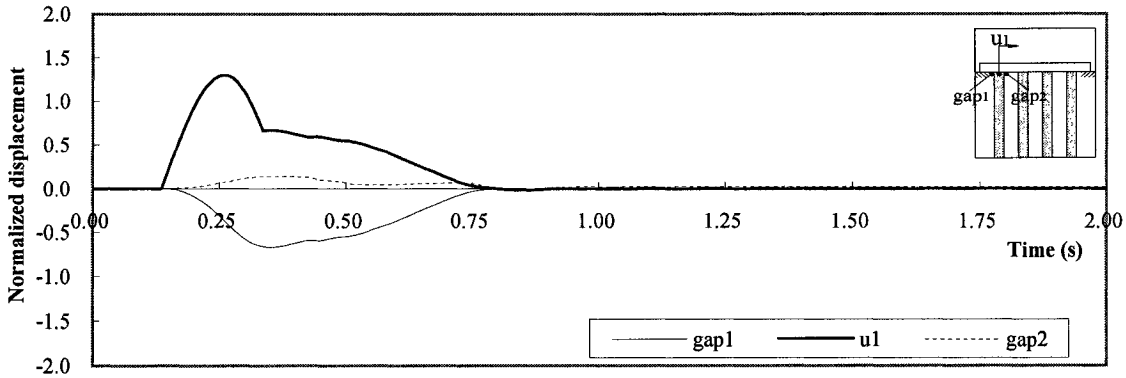

(a) 1st pile and gap1, gap2

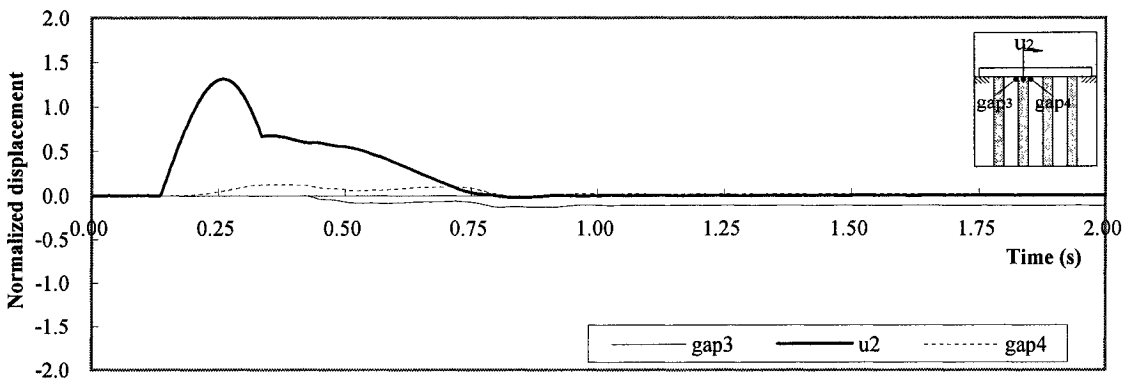

(b) 2nd pile and gap3, gap4

Fig. B.8 Displacements of piles and gaps at the ground level when a short pulse (T_g = *0.2* s) propagates into a 4 x 4 pile group in soft soil (V_s = *70.0* m/s).

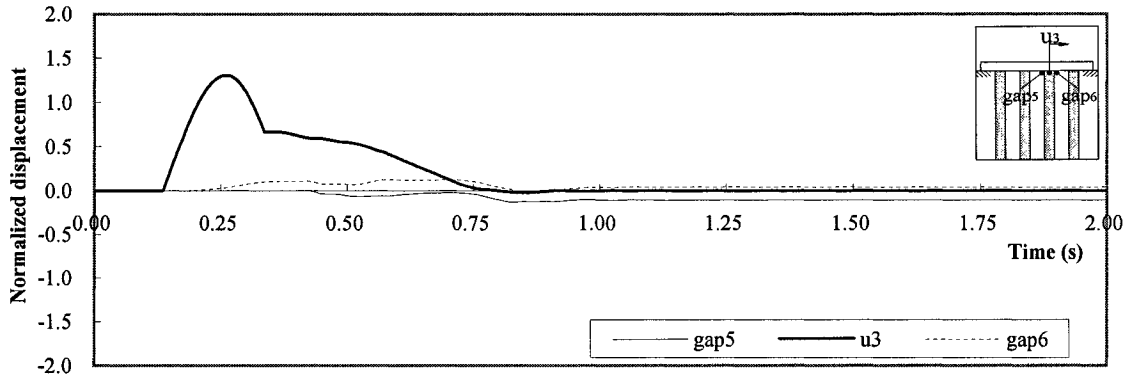

(c) 3th pile and gap5, gap6

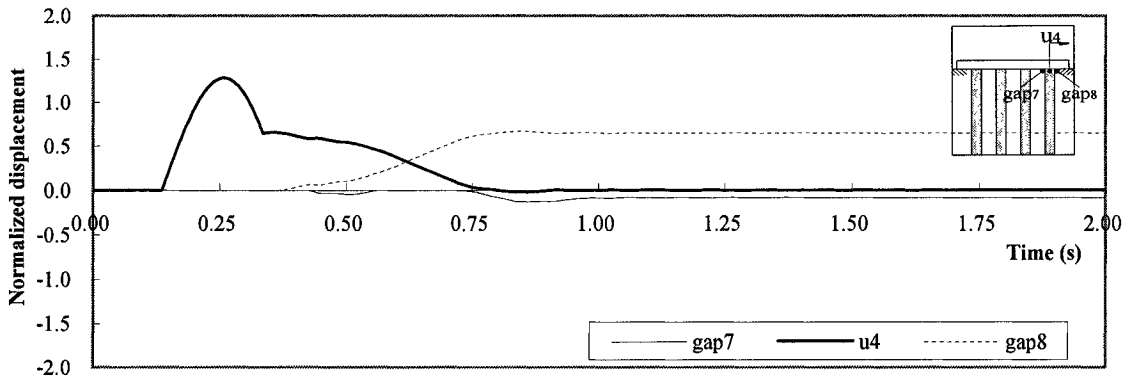

(d) 4th pile and gap7, gap8

Fig. B.8 Displacements of piles and gaps at the ground level when a short pulse (T_g = *0.2* s) propagates into a 4 x 4 pile group in soft soil (V_s = *70.0* m/s). (continued)

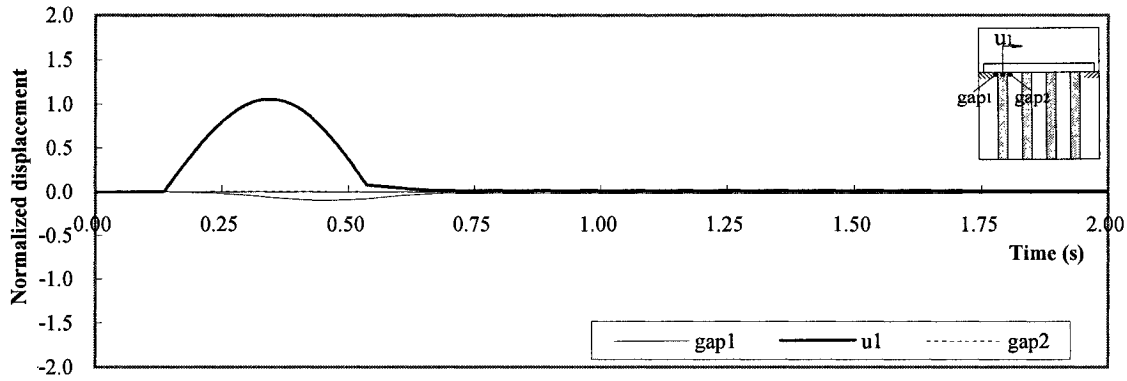

(a) 1st pile and gap1, gap2

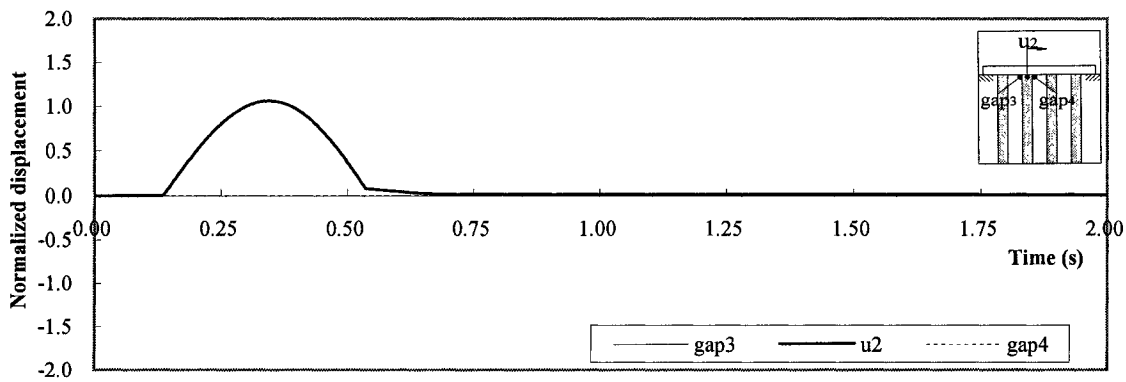

(b) 2nd pile and gap3, gap4

Fig. B.9 Displacements of piles and gaps at the ground level when a medium pulse (T_g = *0.4* s) propagates into a 4 x 4 pile group in soft soil (V_s = *70.0* m/s).

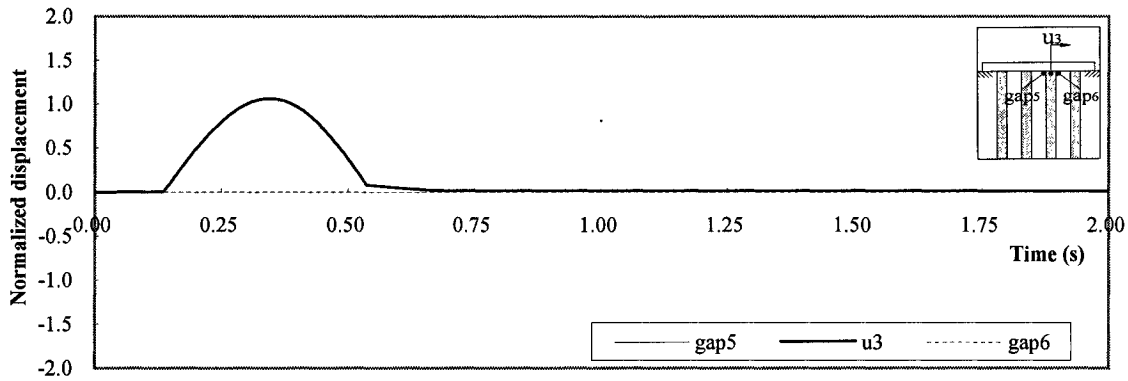

(c) 3th pile and gap5, gap6

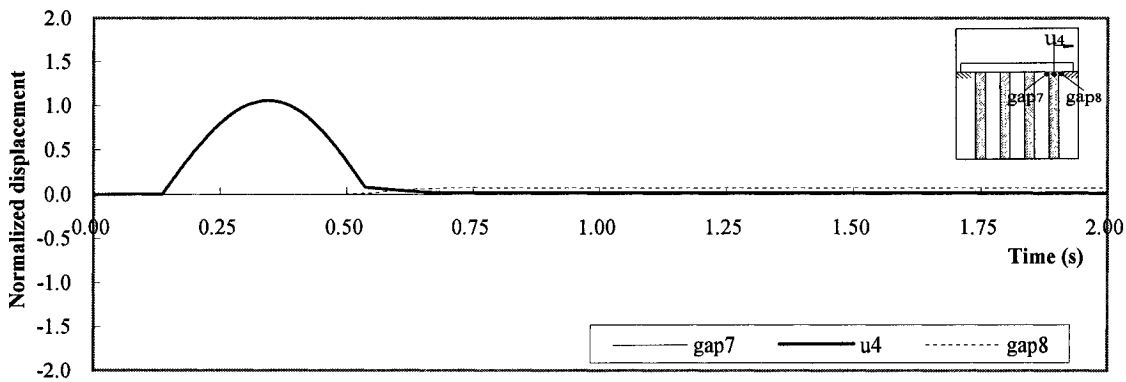

(d) 4th pile and gap7, gap8

Fig. B.9 Displacements of piles and gaps at the ground level when a medium pulse (T_g = *0.4* s) propagates into a 4 x 4 pile group in soft soil (V_s = *70.0* m/s). (continued)

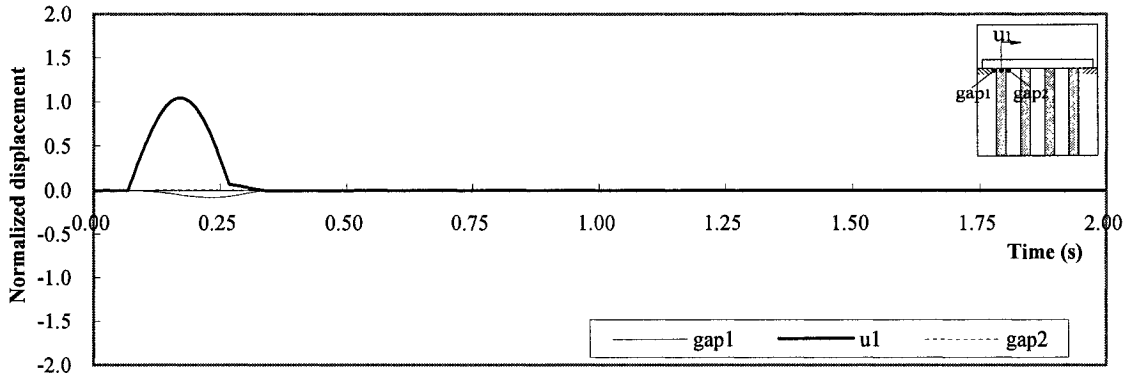

(a) 1st pile and gap1, gap2

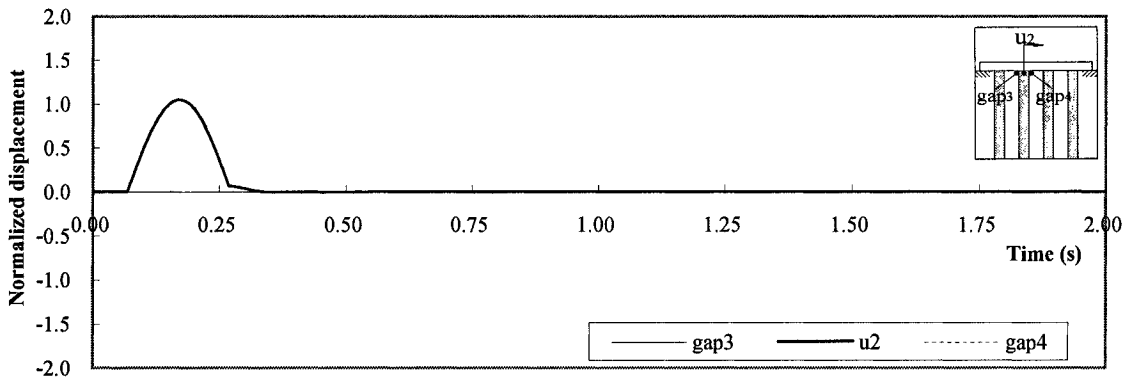

(b) 2nd pile and gap3, gap4

Fig. B.10 Displacements of piles and gaps at the ground level when a short pulse (T_g = *0.2 s*) propagates into a 4 x 4 pile group in medium soil (V_s = *140.0* m/s).

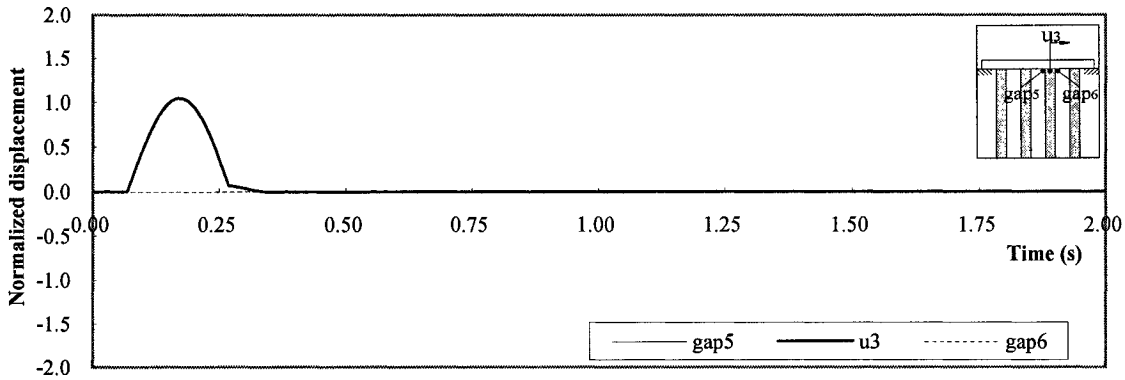

(c) 3th pile and gap5, gap6

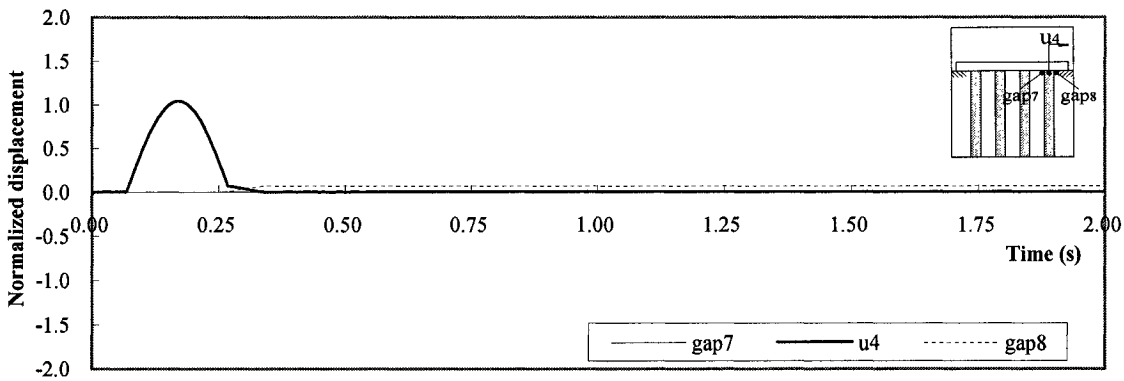

(d) 4th pile and gap7, gap8

Fig. B.10 Displacements of piles and gaps at the ground level when a short pulse (T_g = *0.2 s*) propagates into a 4 x 4 pile group in medium soil (V_s = *140.0* m/s). (continued)

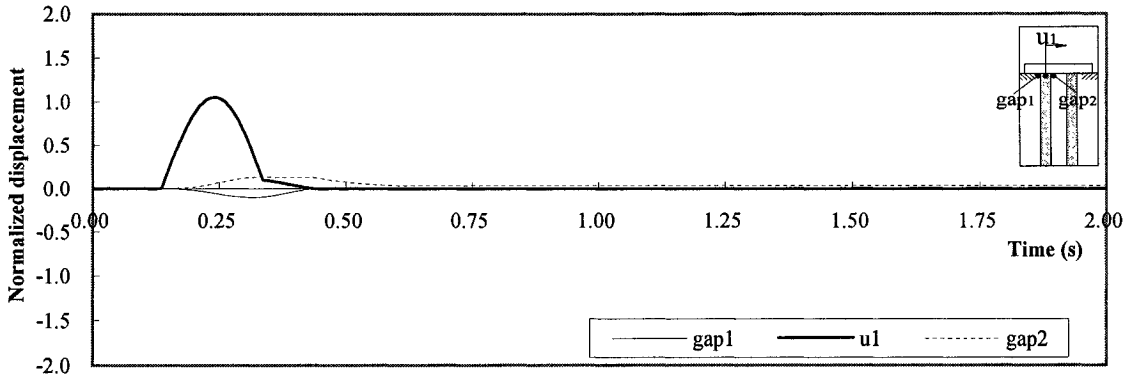

(a) 1st pile and gap1, gap2

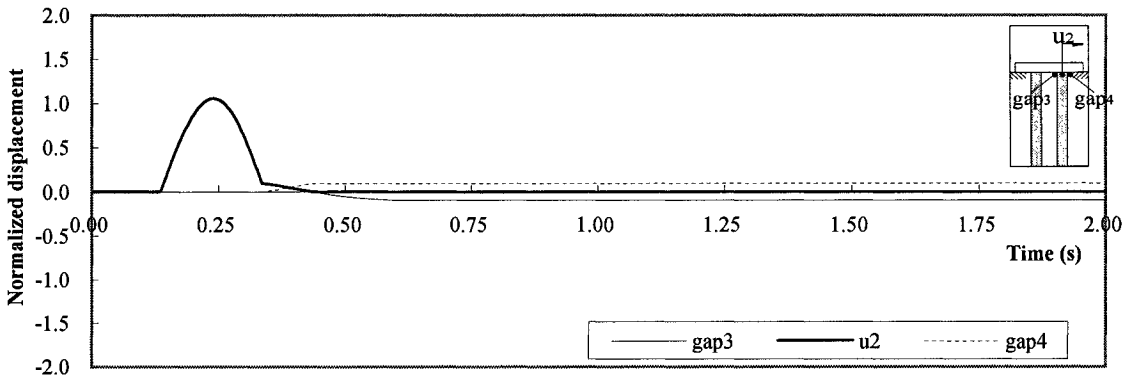

(b) 2nd pile and gap3, gap4

Fig. B.11 Displacements of piles and gaps at the ground level when a short pulse (T_g = *0.2* s) propagates into a 2 x 2 pile group in soft soil (V_s = *70.0* m/s).

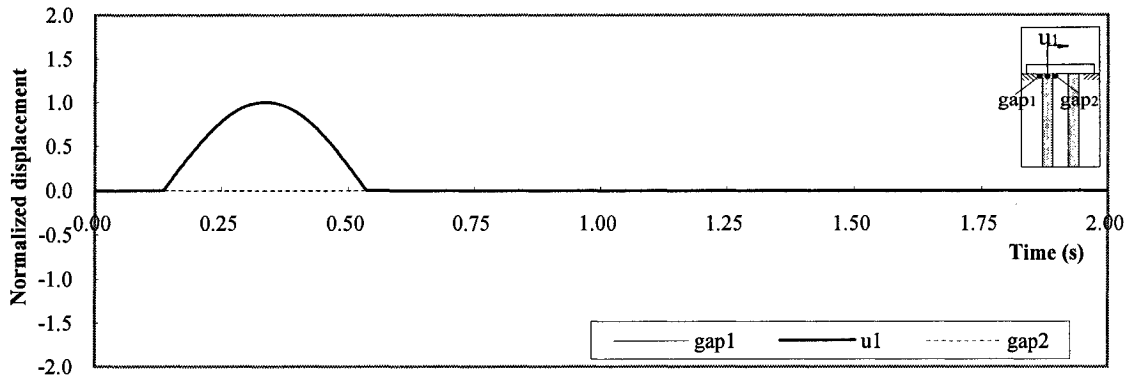

(a) 1st pile and gap1, gap2

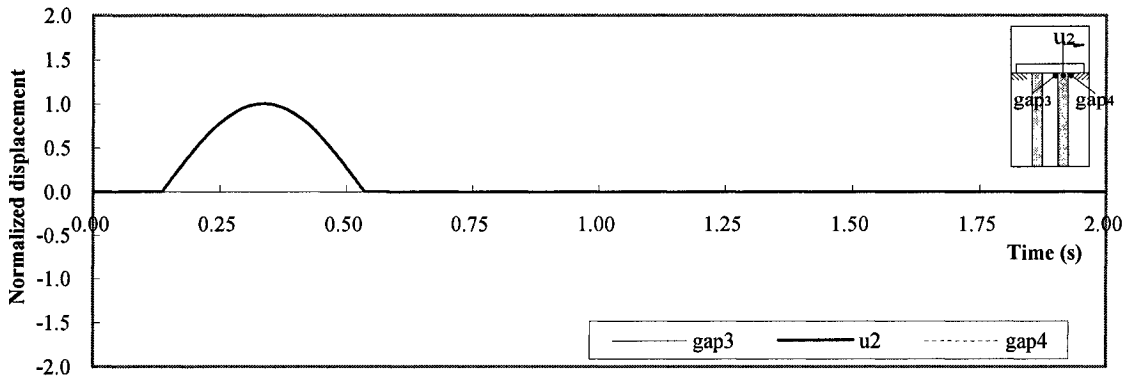

(b) 2nd pile and gap3, gap4

Fig. B.12 Displacements of piles and gaps at the ground level when a medium pulse (T_g = *0.4 s*) propagates into a 2 x 2 pile group in soft soil (V_s = *70.0* m/s).

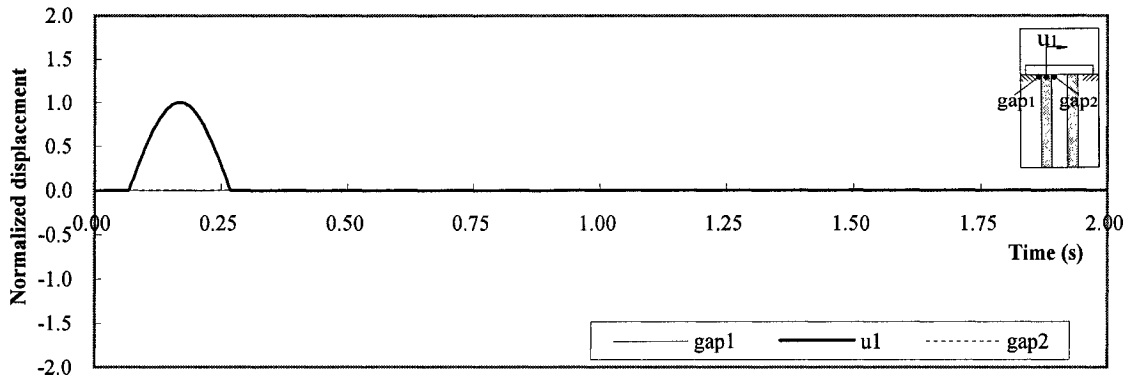

(a) 1st pile and gap1, gap2

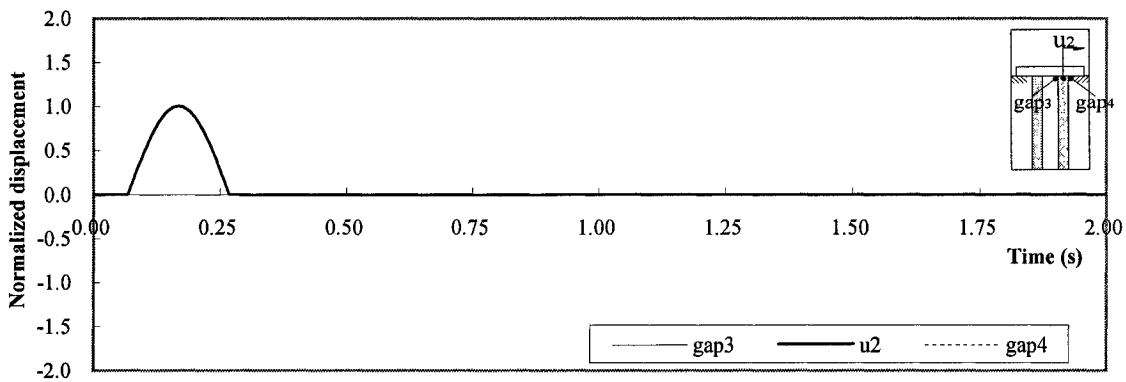

(b) 2nd pile and gap3, gap4

Fig. B.13 Displacements of piles and gaps at the ground level when a short pulse (T_g = *0.2 s*) propagates into a 2 x 2 pile group in medium soil (V_s = *140.0* m/s).

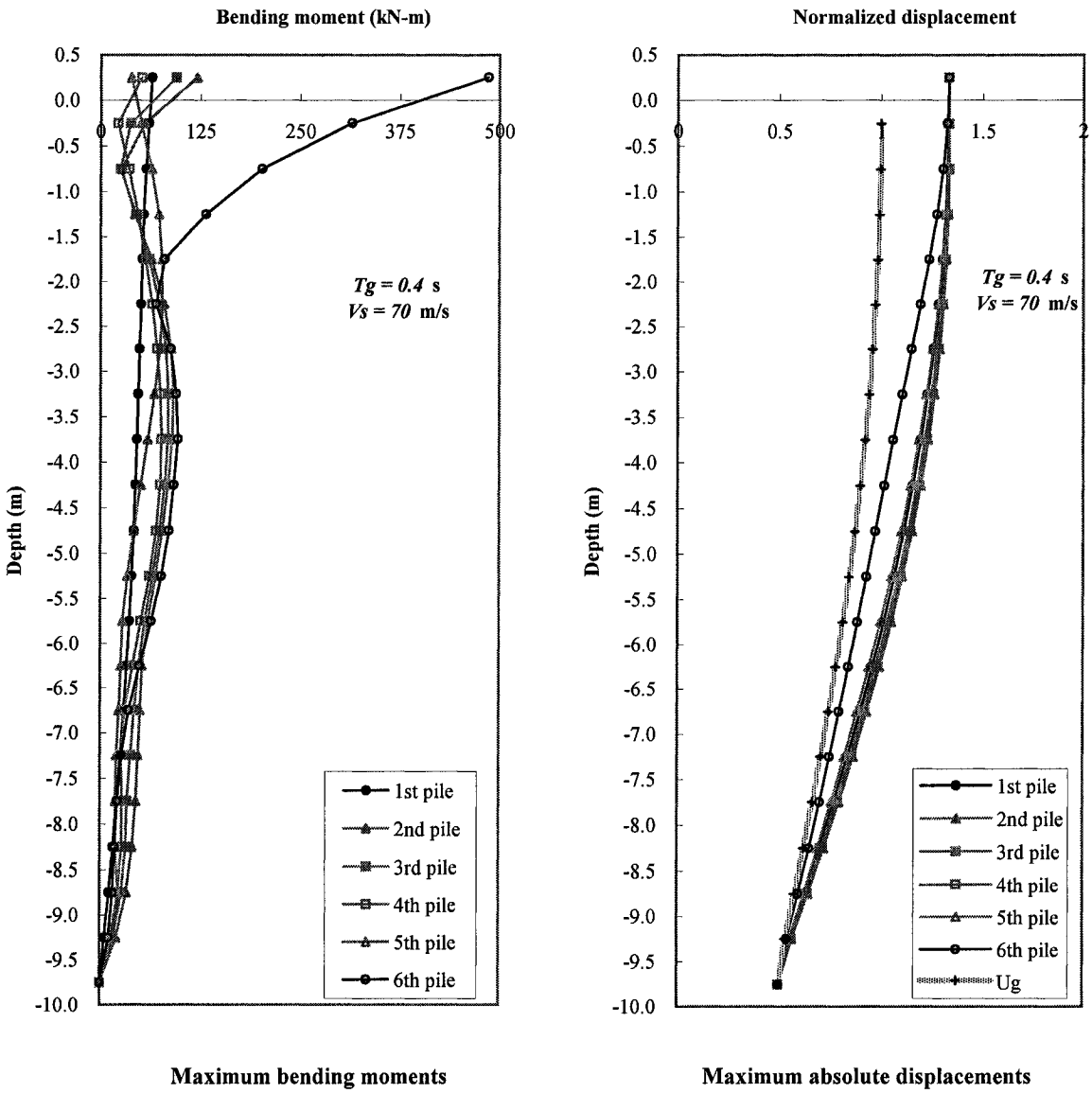

(a) In a 6 x 6 pile group system

Fig. B.14 Maximum absolute bending moments and maximum displacements of piles of group pile in soft soil (V_s = *70.0* m/s) by a vetically incident pulse (T_g = *0.4* s).

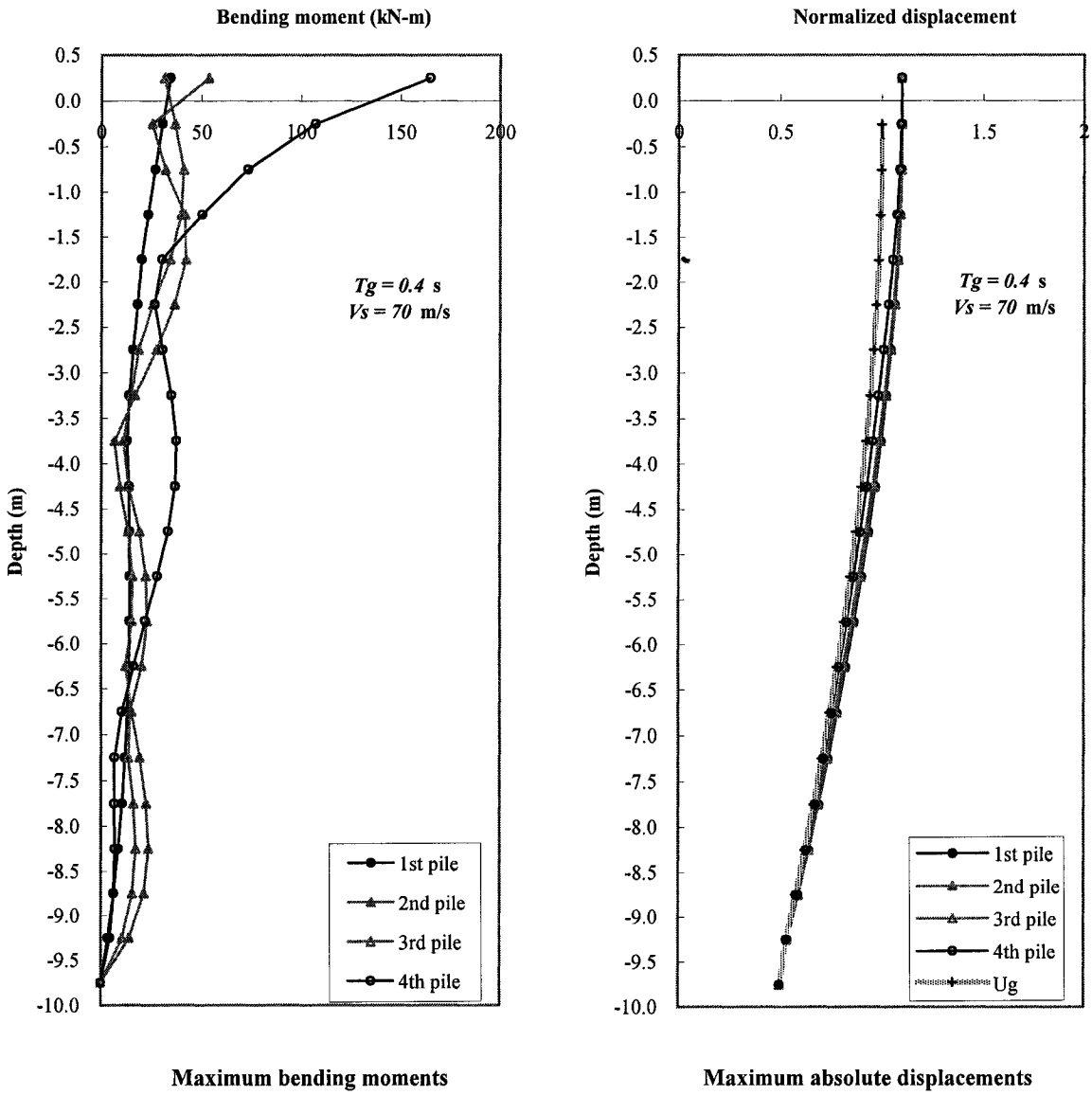

(b) In a 4 x 4 pile group system

Fig. B.14 Maximum absolute bending moments and maximum displacements of piles of group pile in soft soil (V_s = *70.0* m/s) by a vetically incident pulse (T_g = *0.4* s). (continued)

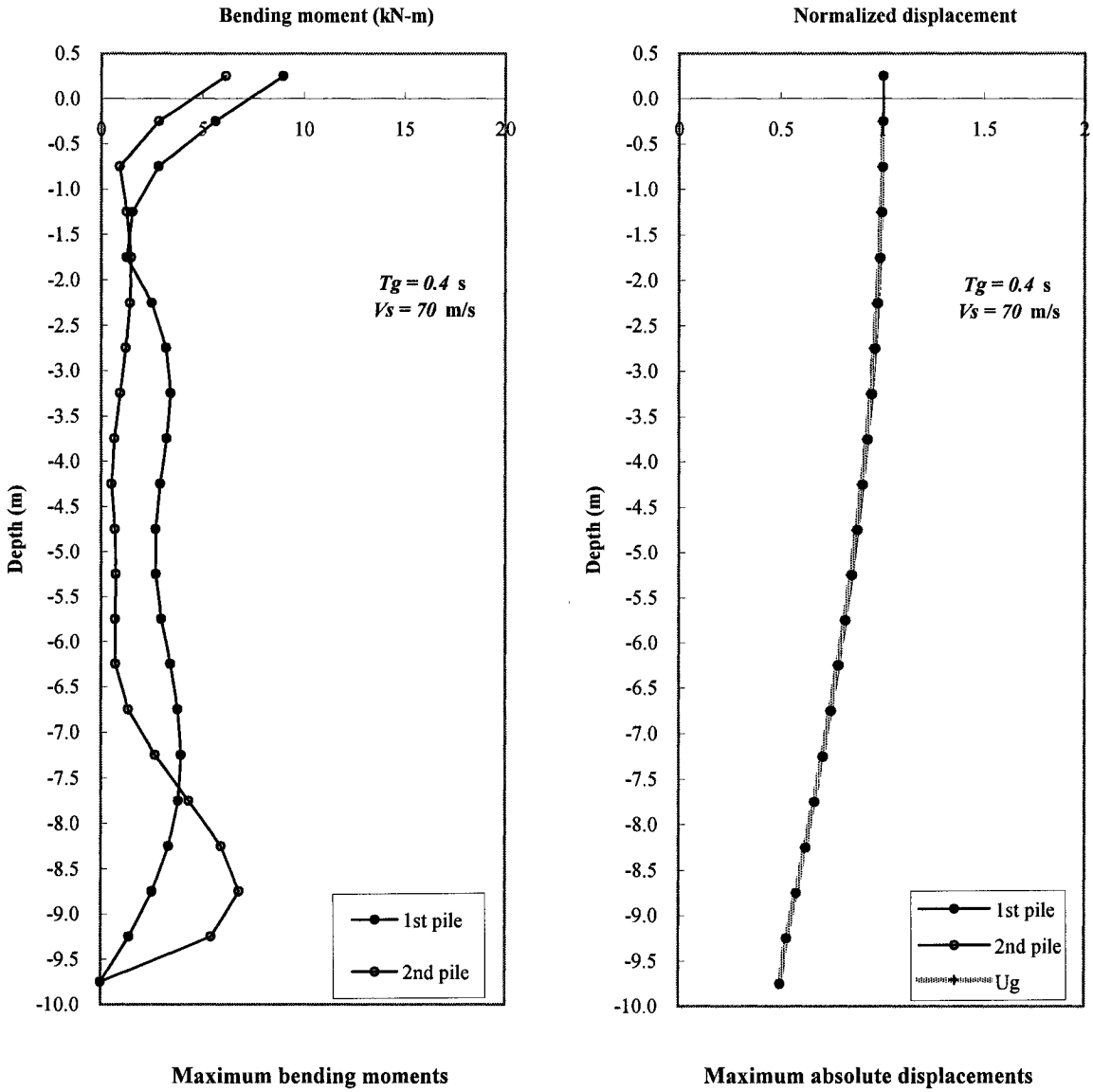

(c) In a 2 x 2 pile group system

Fig. B.14 Maximum absolute bending moments and maximum displacements of piles of group pile in soft soil (V_s = 70.0 m/s) by a vetically incident pulse (T_g = 0.4 s). (continued)

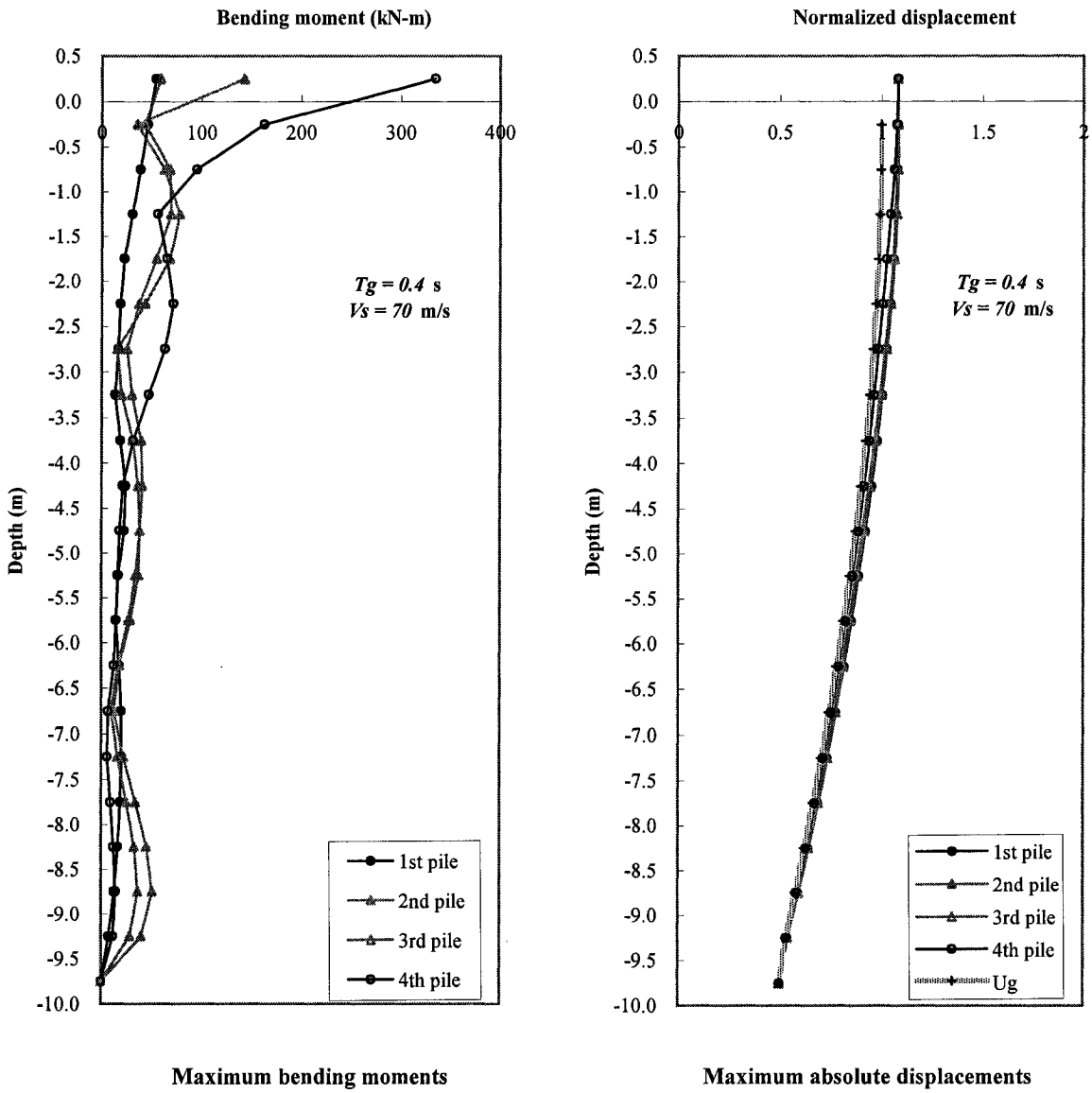

(a) By a short incident pulse ($T_g = 0.2\ s$)

Fig. B.15 Maximum absolute bending moments and maximum displacements of piles of a 4 x 4 pile group in medium soil ($V_s = 140.0$ m/s).

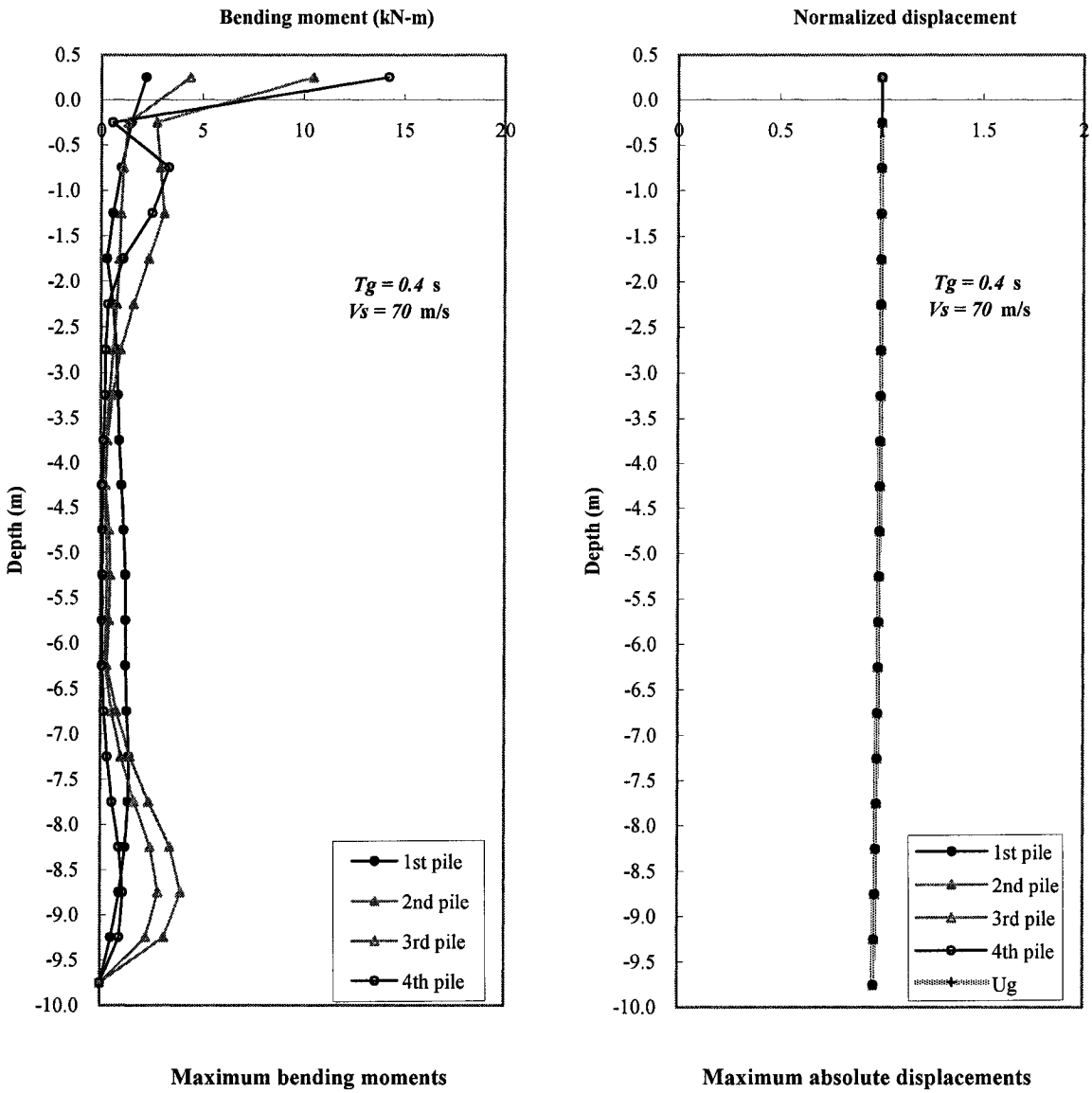

(b) By a long incident pulse (T_g = 0.8 s)

Fig. B.15 Maximum absolute bending moments and maximum displacements of piles of a 4 x 4 pile group in medium soil (V_s = 140.0 m/s). (continued)

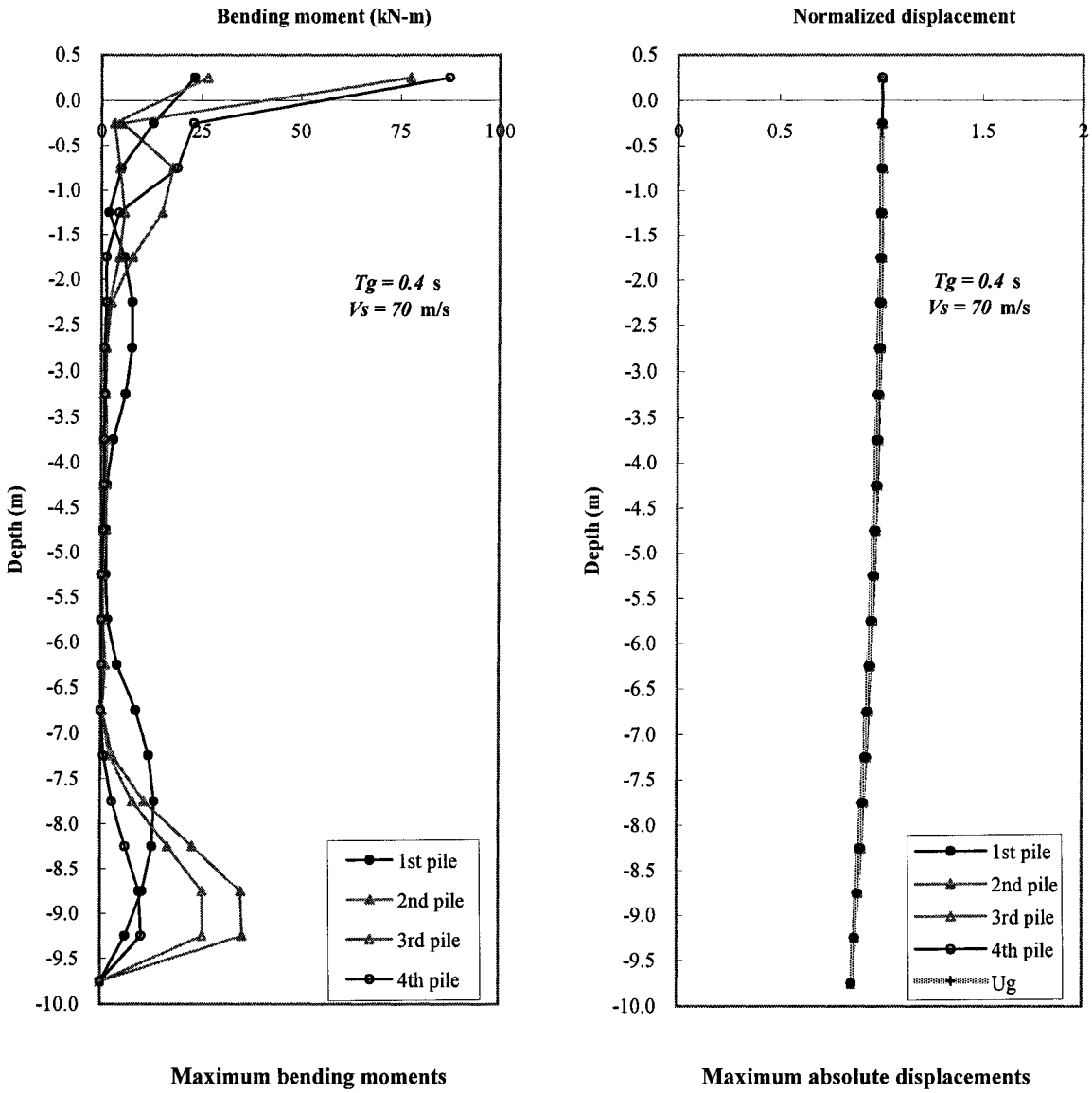

(a) In stiff soil (V_s = *280.0 m/s*)

Fig. B.16 Maximum absolute bending moments and maximum displacements of piles of a 4 x 4 pile group by a short incident pulse (T_g = *0.2* m).

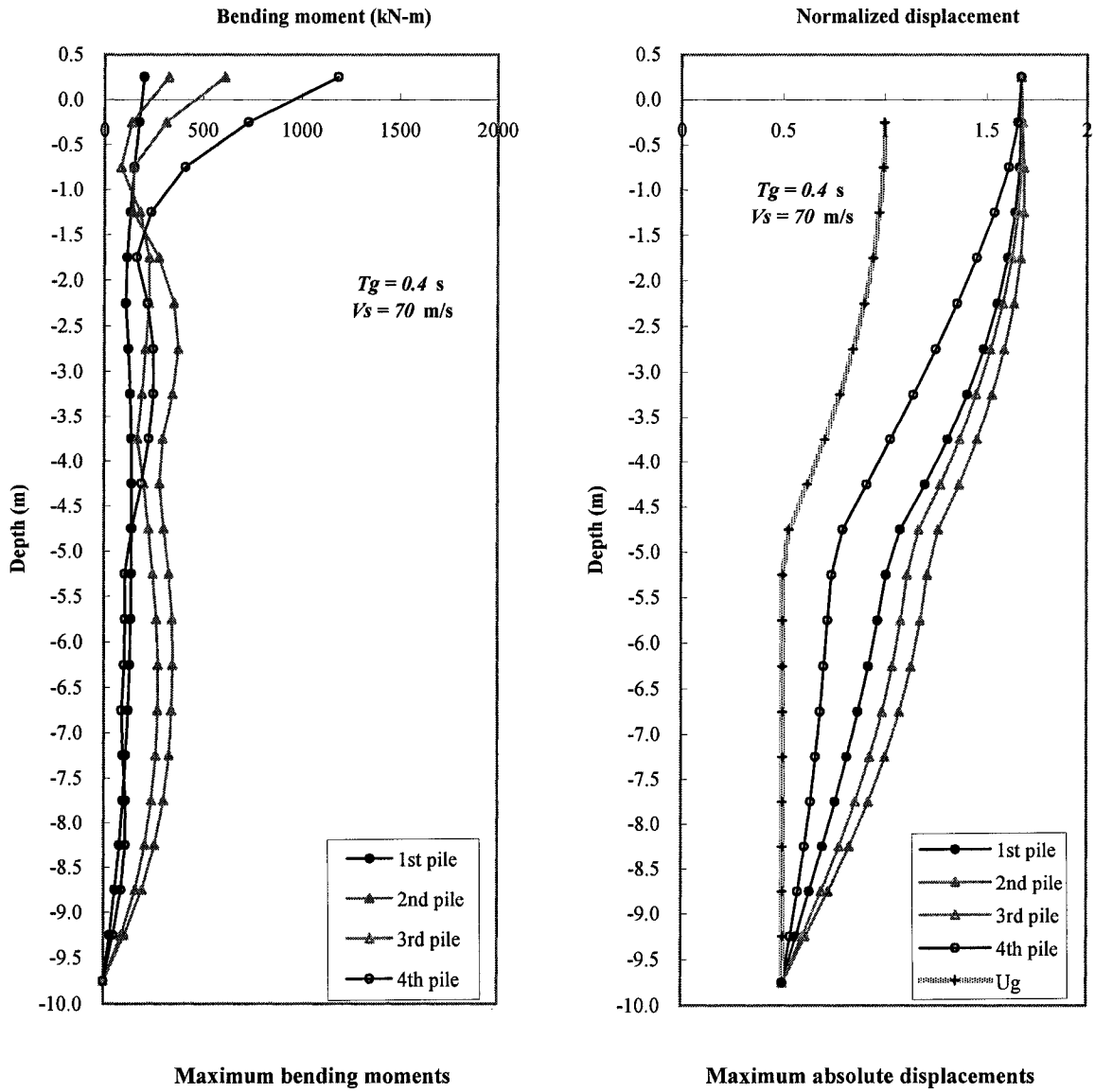

(b) In soft soil (V_s = *70.0* m/s)

Fig. B.16 Maximum absolute bending moments and maximum displacements of piles of a 4 x 4 pile group by a short incident pulse (T_g = *0.2* m). (continued)

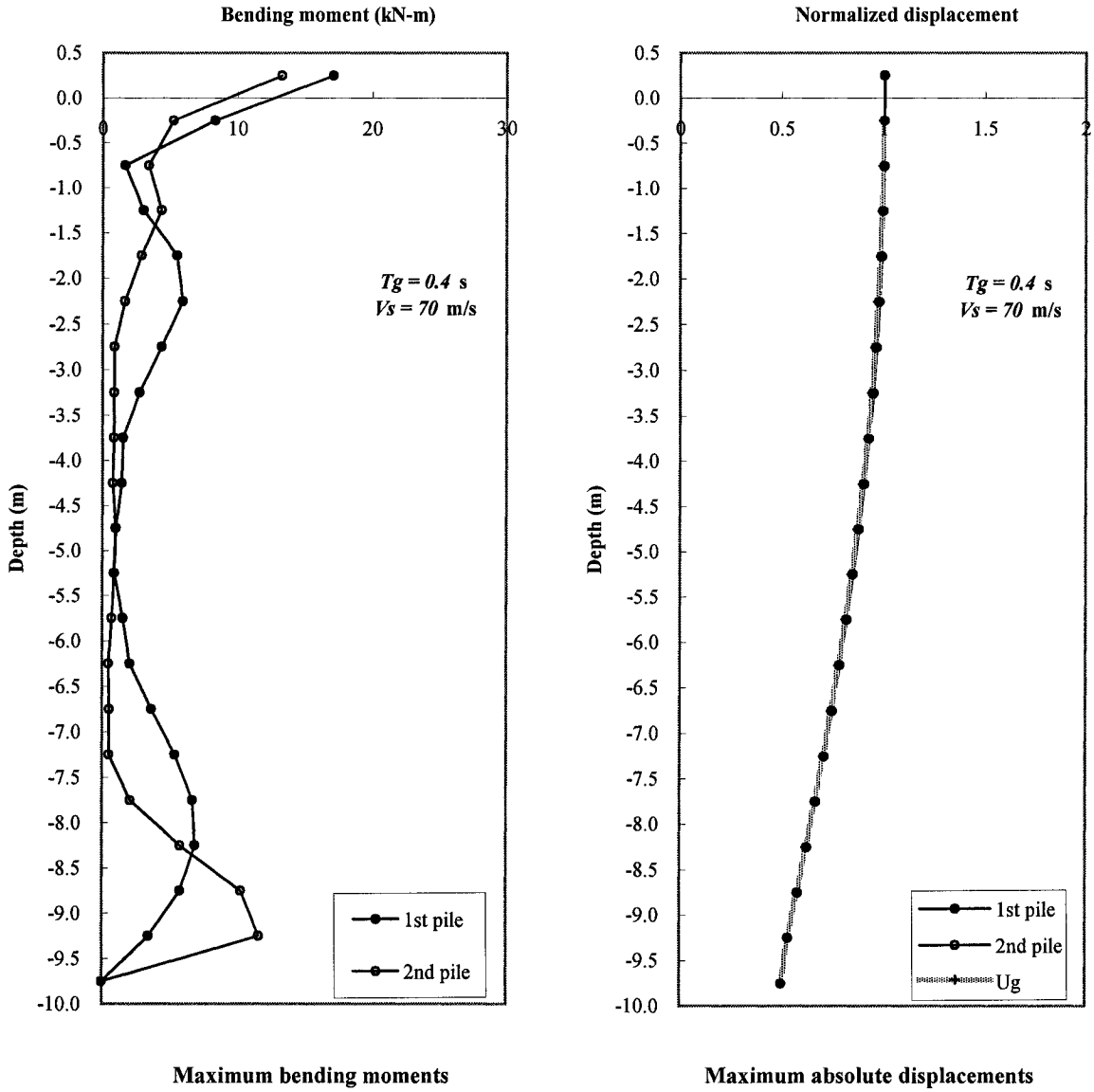

(a) By a short incident pulse (T_g = *0.2 sec*)

Fig. B.17 Maximum absolute bending moments and maximum displacements of piles of a 2 x 2 pile group in medium soil (V_s = *140.0* m/s).

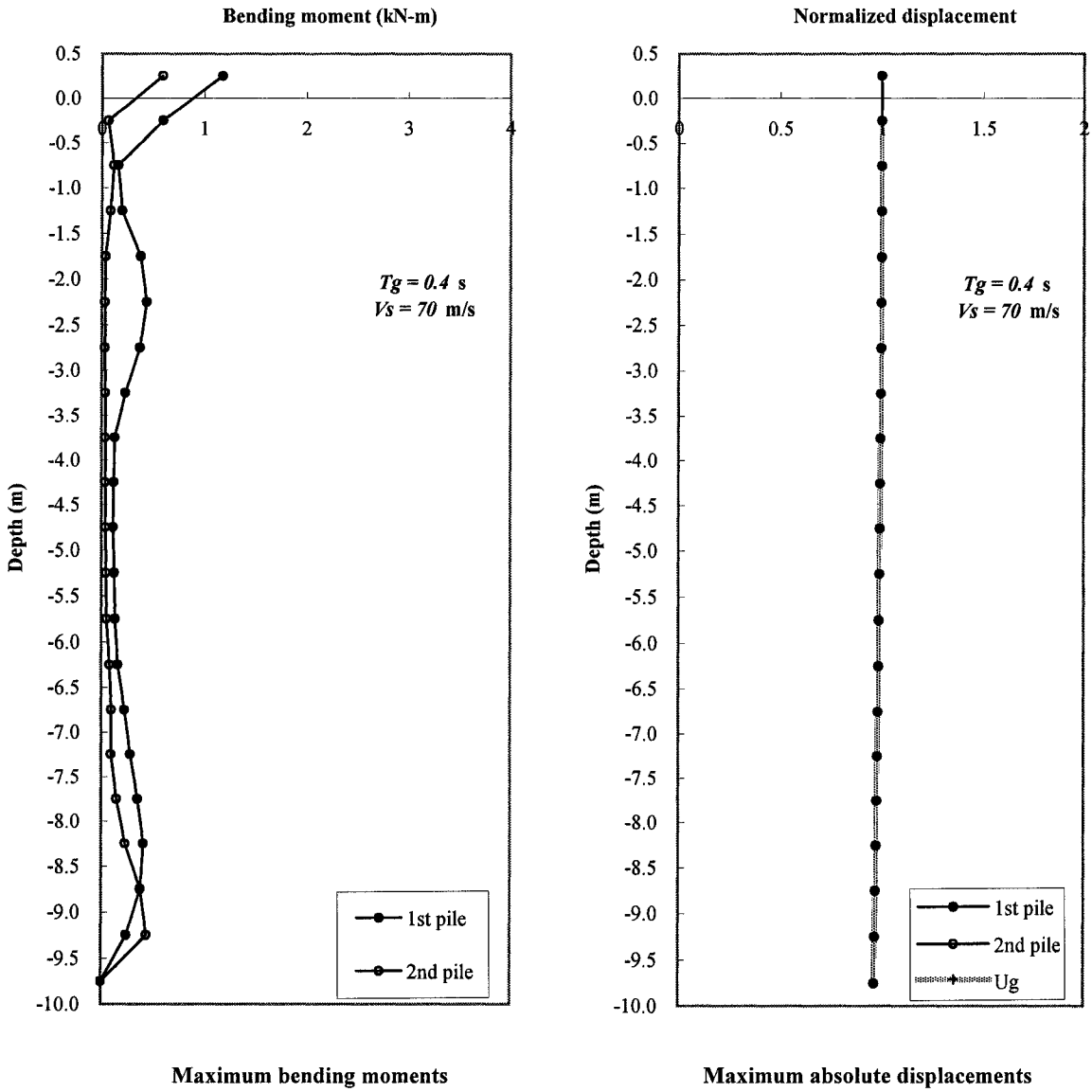

(b) By a long incident pulse (T_g = *0.8 s*)

Fig. B.17 Maximum absolute bending moments and maximum displacements of piles of a 2 x 2 pile group in medium soil (V_s = *140.0* m/s). (continued)

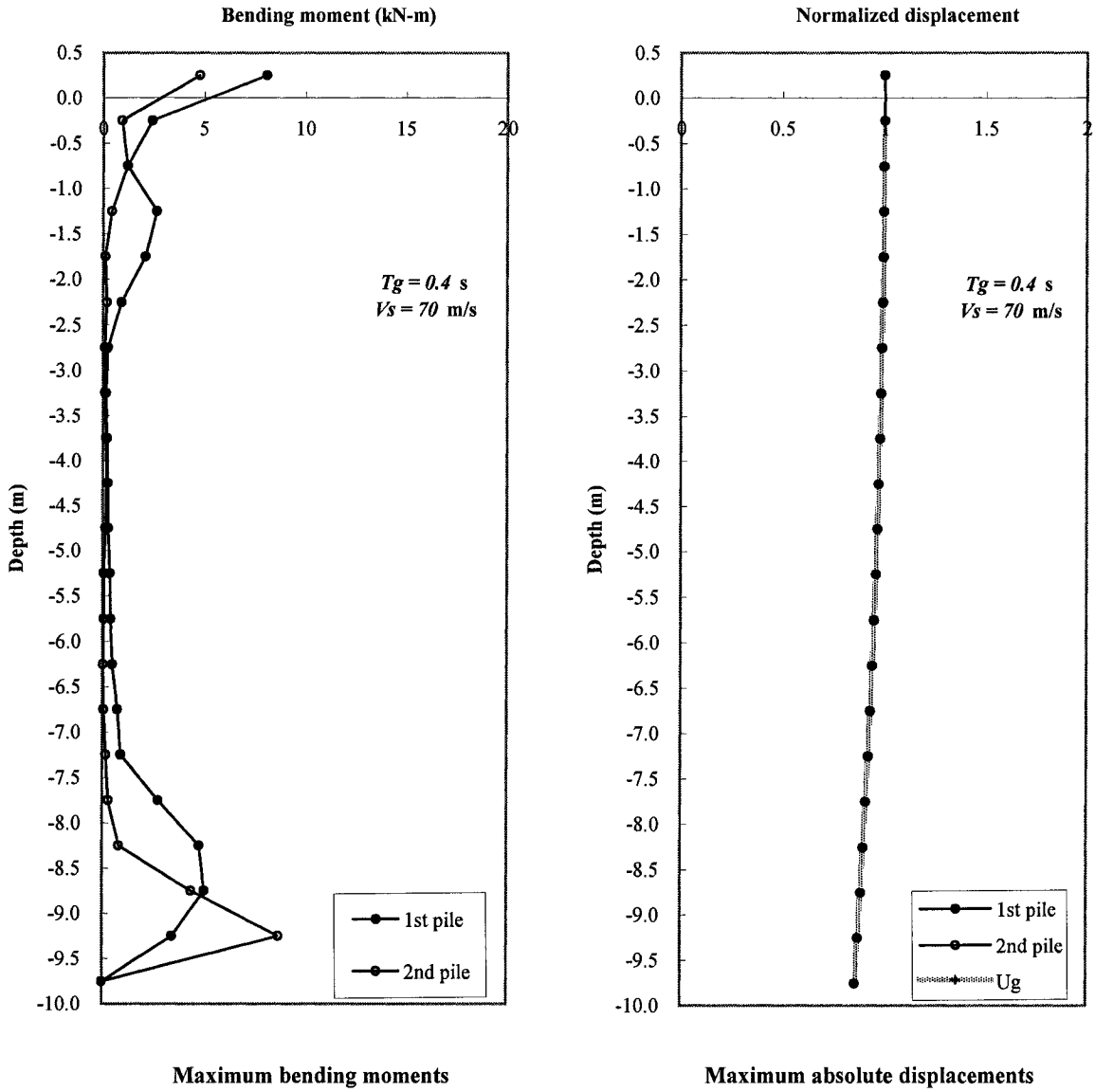

(a) In stiff soil (V_s = *280.0* m/s)

Fig. B.18 Maximum absolute bending moments and maximum displacements of piles of a 2 x 2 pile group by short incident pulse (T_g = *0.2* m).

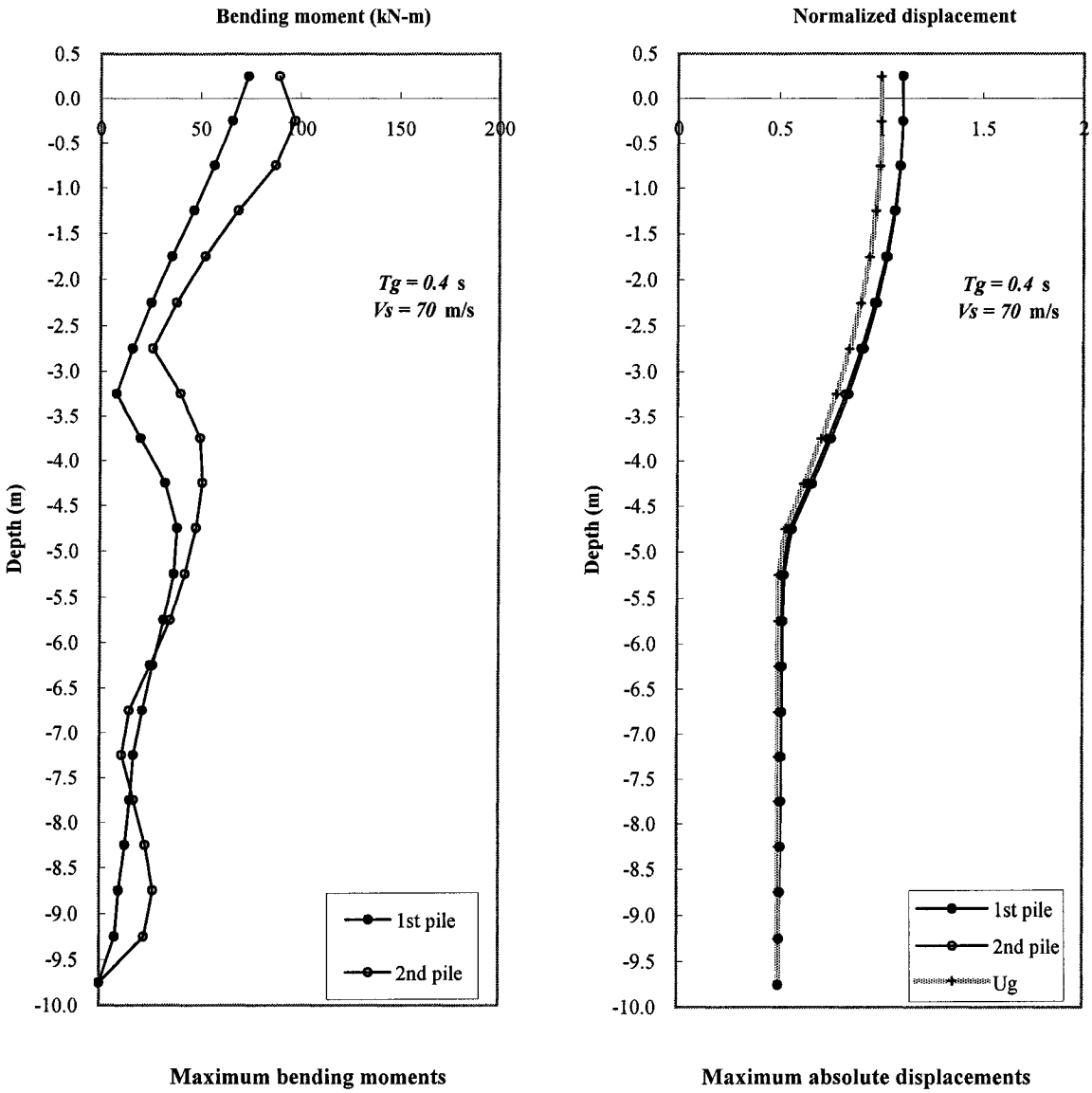

(b) In soft soil (V_s = *70.0* m/s)

Fig. B.18 Maximum absolute bending moments and maximum displacements of piles of a 2 x 2 pile group by short incident pulse (T_g = *0.2* m). (continued)